Steering Nanoparticle-Placenta Interactions: Impact of Particle Properties and Functionalization on Placental Uptake, Penetration and Biological Effects

---

Dissertation

zur

Erlangung der naturwissenschaftlichen Doktorwürde
(Dr. sc. nat.)

vorgelegt der

Mathematisch-naturwissenschaftlichen Fakultät

der

Universität Zürich

von

Carina Muoth

aus

Brigels GR

Promotionskomitee

Prof. Dr. Hanspeter Nägeli (Vorsitz)
Prof. Dr. Michael Arand
Prof. Dr. Jörg Huwyler
Dr. Peter Wick (Leitung der Dissertation)

Zürich, 2016

to my family

Summary

Engineered nanoparticles (NPs) possess unique biological, physical and chemical properties, which make them particularly interesting for the development of novel nanomedical therapies and diagnostics. As such, their small size facilitates intracellular uptake, their high surface-area-to-volume-ratio leads to an increased drug loading capacity and specific targeting ligands can be linked to the NP surface in order to target different tissues. In particular during pregnancy, advances in nanomedicine may help to design targeted therapies to specifically treat the mother, the placenta or the fetus with reduced side effects as compared to conventional therapies. On the other hand, exposure of pregnant women to NPs may also pose risks to the development and growth of the vulnerable fetus. Indeed, there is evidence that certain NPs can cross the placental barrier and harm the developing fetus. Therefore, both intentional and unintentional exposure to NPs in pregnancy is conceivable. However, knowledge on NP-placenta interactions is very limited and concepts how to steer placental translocation are essentially lacking. This thesis aims to establish the groundwork towards the systematic understanding of NP uptake mechanisms and biological effects at the human placental barrier in dependence of NP properties. Providing this knowledge is imperative for the development of effective and site-specific drug delivery carriers as well as for safety by design approaches in industry. Since the placenta is the most species-specific mammalian organ, findings from *in vivo* animal studies cannot be simply translated to humans. Thus, we developed advanced human placenta models and employed them to assess mechanistic aspects of NP uptake, accumulation, penetration and toxicity at the human placental barrier.

In the introductory review of this thesis, the current literature on NP translocation across the placental barrier was summarized and first conclusions were drawn on the possibility to steer translocation in dependence of different physico-chemical properties. Moreover, the suitability of available placenta models to study NP transfer was discussed and strategies were suggested on how to improve their *in vivo* predictability. This review provided the basis for the design of advanced placenta models and for the choice of appropriate NPs to verify the models and to control particle-placenta interactions.

In the first part of this thesis, a simplified placenta *in vitro* model was established using the microcontact printing technique. This approach allowed studying the impact of different actin structures on endocytic uptake and intracellular distribution of polystyrene nanoparticles (PS NPs). In detail, BeWo cells were physically constrained on micropatterns of four different geometries on which they exhibited significantly different organizations of the actin cytoskeleton. Single cell analysis of intracellular distribution and internalized amount of 80 nm, 240 nm and carboxylate 300 nm PS NPs were assessed.

In the second part of this thesis, we developed, characterized and verified a novel 3D *in vitro* co-culture microtissue (MT) model resembling the human placental barrier tissue. Highly reproducible co-culture MTs were obtained with the hanging drop technology consisting of a core of placental fibroblasts surrounded by a layer of BeWo cells. Moreover, we showed that this model is suitable to study acute toxicity and adverse effects on placental functionality using different NPs including quantum dots, titanium dioxide and copper oxide NPs.

In the third part of this thesis, we showed that the co-culture MT model can provide predictive results on NP localization, penetration and uptake mechanisms at the human placental barrier. MTs were exposed to PEGylated or carboxylate gold (Au) NPs with diameters of 3-4 or 13-14 nm and uptake was analyzed using different qualitative and quantitative methods.

To conclude, we pioneered the development of a co-culture MT model that depicts important characteristics of the human placental tissue. For the first time, mechanistic studies on NP uptake, accumulation, penetration and biological effects can be performed in a highly reproducible tissue-like microenvironment. Furthermore, we provided novel insights in how NP uptake and penetration into the placental tissue can be steered via particle properties and surface functionalization, paving the way towards the development of targeted therapies in pregnancy.

Zusammenfassung

Durch die Herstellung von synthetischen Nanopartikeln (NP) mit speziellen biologischen, physikalischen und chemischen Eigenschaften eröffnen sich neue Möglichkeiten für die Entwicklung nanomedizinischer Anwendungen. Verglichen zu Mikropartikeln führt beispielsweise die Grösse der NP zu einer vereinfachten Aufnahme in die Zellen und ihr grosses Oberfläche-zu-Volumen-Verhältnis ermöglicht eine erhöhte Ladekapazität von verschiedenen Medikamenten. Zudem kann ihre Oberfläche mit spezifischen Liganden funktionalisiert werden. Durch einen solchen zielgerichteten Ansatz könnten die Dosen und damit einhergehende Nebenwirkungen im Vergleich zu konventionellen Medikamenten massgeblich reduziert werden. Vor allem während der Schwangerschaft bietet die Nanomedizin eine vielversprechende Möglichkeit, um die Mutter, die Plazenta oder den Fötus unabhängig voneinander zu behandeln. Andererseits besteht durch die Exposition der Mutter gegenüber NP aber auch eine mögliche Gefährdung des Fötus, dessen Wachstum und Entwicklung. Es gibt durchaus Studien, die beweisen, dass bestimmte NP die Plazentabarriere passieren und dem Fötus schaden. Fundiertes Wissen über die Interaktion verschiedener NP mit der menschlichen Plazentabarriere ist jedoch nur begrenzt vorhanden und Konzepte um diese plazentale Translokation zu steuern existieren bisher nicht. Das Ziel dieser Arbeit war, die Basis für ein systematisches Verständnis der NP Aufnahme, Mechanismen, Translokation und biologischer Effekte zu schaffen. Diese Grundlage ist unerlässlich für die Entwicklung von wirksamen und spezifischen Drug Delivery Carriers in der Nanomedizin und ‘safety by design‘ Methoden in der Industrie. Da die strukturellen und funktionellen Eigenschaften der Plazenta unter den Säugetieren signifikant verschieden sind, ist eine Extrapolation von Tierstudien auf den Menschen problematisch. Daher wurden in dieser Arbeit fortschrittliche menschliche *in vitro* Plazentamodelle entwickelt und angewendet, um mechanistische Aspekte der NP Aufnahme, Akkumulation, Penetration und Toxizität an der menschlichen Plazentabarriere zu untersuchen.

In der Einleitung wurde die aktuelle Literatur zur Translokation verschiedener NP durch die Plazentabarriere in einem Review zusammengefasst. Erste Schlüsse wurden gezogen, ob die Translokation über die verschiedenen physiko-chemischen Eigenschaften der NP gesteuert werden kann. Ausserdem wurde diskutiert, inwiefern

die bestehenden Plazentamodelle für NP Translokationsstudien geeignet sind und mit welchen Strategien ihre *in vivo* Relevanz verbessert werden könnte. Basierend auf diesem Review wurde das Design der Plazentamodelle definiert und die Wahl geeigneter NP für die Verifizierung des Modells und die Steuerung der NP-Plazenta Interaktion getroffen.

Im ersten Teil dieser Arbeit wurde die Mikrokontaktprinting-Technik für die Entwicklung eines 2D Plazenta-Modells verwendet. Bei dieser Technik wurden BeWo Zellen auf Micropatterns mit vier unterschiedlichen Geometrien kultiviert, welche zu signifikant verschiedenen Aktinstrukturen der BeWo Zellen führten. Dadurch konnte der Einfluss dieser Strukturen auf die endozytotische Aufnahme und intrazelluläre Verteilung von 80 nm, 240 nm und carboxylierten 300 nm Polystyrol NP in Einzelzellen untersucht werden.

Im zweiten Teil wird die Entwicklung und Charakterisierung eines 3D *in vitro* Mikrogewebe-Modells (MT) der menschlichen Plazenta vorgestellt. Mittels Hanging Drop Technologie gelang es, reproduzierbare Co-Kultur MT zu erzeugen, die aus einem Kern aus plazentalen Fibroblasten, umgeben von einer Schicht aus BeWo Zellen bestehen. Ausserdem wird gezeigt, dass dieses Modell für die Untersuchung verschiedener NP (Quantum Dots, Titandioxid und Kupferoxid NP) bezüglich ihrer akuten Toxizität und Effekte auf plazenta-spezifische Funktionalität geeignet ist.

Im dritten Teil wurde das Co-Kultur MT Modell angewendet, um die Penetration, Lokalisation und Aufnahmemechanismen verschiedener NP zu untersuchen. Die MTs wurden mit PEGylierten oder carboxylierten Gold (Au)NP mit Durchmessern von 3-4 oder 13-14 nm inkubiert. Deren Aufnahme in die MTs wurde mit verschiedenen qualitativen und quantitativen Methoden analysiert.

Zusammenfassend kann man sagen, dass wir die Vorreiter der Entwicklung eines Co-Kulturen MT Modells sind, welches die wichtigen Eigenschaften der menschlichen Plazentabarriere widerspiegelt. Zum ersten Mal können mechanistische Studien zu NP Aufnahme, Akkumulation, Penetration und biologischen Effekten in einer hoch reproduzierbaren gewebeähnlichen Mikroumgebung durchgeführt werden. Zudem erbringen wir neue Erkenntnisse wie die NP Aufnahme und Penetration in die Plazenta über die Eigenschaften und Oberflächenfunktionalisierungen der NP gesteuert werden können und bahnen so den Weg in Richtung Entwicklung von gezielten Therapien während der Schwangerschaft.

Table of Contents

List of Abbreviations

ATP	Adenosine triphosphate
Au	Gold
BSA	Bovine serum albumin
CK	Cytokeratin
CLSM	Confocal laser scanning microscopy
CSK	Cytoskeleton
CTB	Cytotrophoblast
CuO	Copper Oxide
Cyto D	Cytochalasin D
DAPI	4’,6-diamidino-2-phenylindole
DD	Double distilled
DLS	Dynamic light scattering
DMEM	Dulbeccos’s Modified Eagle Medium
DMSO	Dimethylsulfoxide
DNA	Deoxyribonucleic acid
Dox	Doxorubicin
ECM	Extracellular matrix
EDX	Energy-dispersive X-ray spectroscopy
EGF	Epithelial growth factor
ELISA	Enzyme-linked immunosorbent assay
ENM	Engineered nanomaterial
FCS	Fetal calf serum
FGM	Fibroblast growth medium
hCG	Human chorionic gonadotropin
HE	Hematoxylin and eosin
HLA	Human leukocyte antigen
HPLC-MS	Liquid chromatography - mass spectrometry
hr	Hour
IBM	Ion beam microscopy
ICP-MS	Inductively coupled plasma mass spectrometry
Ig	Immunoglobulin

LA-ICP-MS	Laser ablation inductively coupled plasma mass spectrometry
µCP	Microcontact Printing
min	Minutes
MT	Microtissue
NM	Nanomaterials
NP	Nanoparticle
PBS	Phosphate buffered saline
PEG	Polyethylene glycol
PFA	Paraformaldehyde
PS	Polystyrene
Pst2	Pitstop 2
Qdot	Quantum Dots
ROS	Reactive oxygen species
RT	room temperature
SD	standard deviation
SEM	Standard error of the mean
SEM	Scanning electron microscope
STB	Syncythiotrophoblast
TEM	Transmission electron microscope
TiO_2	Titanium Dioxide
Tf	Transferrin
TUNEL	Terminal deoxynucleotidyl transferase dUTP nick end labeling
RNA	Ribonucleic acid

Chapter 1

Introduction

1.1 The placenta

The placenta is a highly specialized materno-fetal organ with an intrauterine existence of nine months during which it is responsible for the normal growth, development and protection of the fetus (Burton and Fowden 2015). Importantly, uptake and exchange of various substances to and from the fetus take place via the placenta, which makes it a particularly interesting conduit for fetal drug administration.

1.1.1 Development and anatomy of the human placenta

After fertilization, the oocyte (fertilized egg) undergoes cell division and enters the morula stage, which is a mass of 16 to 32 cells (blastomeres). On day four, the morula separates into the embryoblast (inner cell mass) with a fluid filled cavity and the trophoblast (outer cells). The embryo arises from the embryoblast whereas the trophoblast is the primary source for the development of the placenta and fetal membranes. At this stage, the morula is transformed into a blastocyst. Around six days after fertilization, the blastocyst starts to implant into the uterus via a complex interaction between trophoblastic cells and the maternal uterine epithelium (Aplin and Kimber 2004). As the implantation into the uterus proceeds, the trophoblast undergoes a spatially and temporally regulated differentiation. Specifically, undifferentiated cytotrophoblasts (CTBs) that derive from the trophoblast differentiate towards the villous and the extravillous pathway. In the villous pathway, CTBs fuse into a multinucleated syncytiotrophoblast (STB) that forms the epithelial layer of the fetal chorionic villi and produces a variety of different hormones (see Chapter 1.1.2). Throughout pregnancy, a part of these CTBs remain undifferentiated and acts as stem cells that provide growth to the overlying STB through continuous proliferation and subsequent fusion. In the extravillous pathway, CTBs differentiate into anchoring trophoblasts that form (anchoring) villi and attach to the uterine wall. After the blastocyst has implanted, two trophoblastic subpopulations detach from these anchoring villi namely the interstitial trophoblasts that invade the uterine endometrium and the inner third of the myometrium and the endovascular trophoblasts that infiltrate lumens and uterine spiral arteries through which maternal blood will enter the placenta (Gude et al. 2004, Knofler 2010, Verma and Verma 2013). However, since placental and fetal tissues are sensitive to oxidative stress, a low oxygen environment is essential to protect their development from damage by oxygen-free

radicals during the first trimester. To limit maternal blood flow to the fetus, uterine spiral arterioles are plugged by aggregates of endovascular trophoblasts (Jauniaux et al. 2003).

After complete implantation of the blastocyst into the endometrium (Figure 1.1A), the development of the placenta begins. Between day 11 and day 13, the formation of primary chorionic villi is initiated by the invasion of the STB, which contains a core of CTBs, into the lacunae (Figure 1.1B). At the end of pregnancy, these lacunae will fuse and form the intervillous space. Secondary villi arise from primary villi and contain an inner core of embryonic mesoderm. After three weeks, the embryonic mesoderm starts to differentiate into blood vessels, which then connect to vessels of the umbilical cord finally forming tertiary villi (Verma and Verma 2013) (www.embryology.ch, access date: 2nd of May 2016).

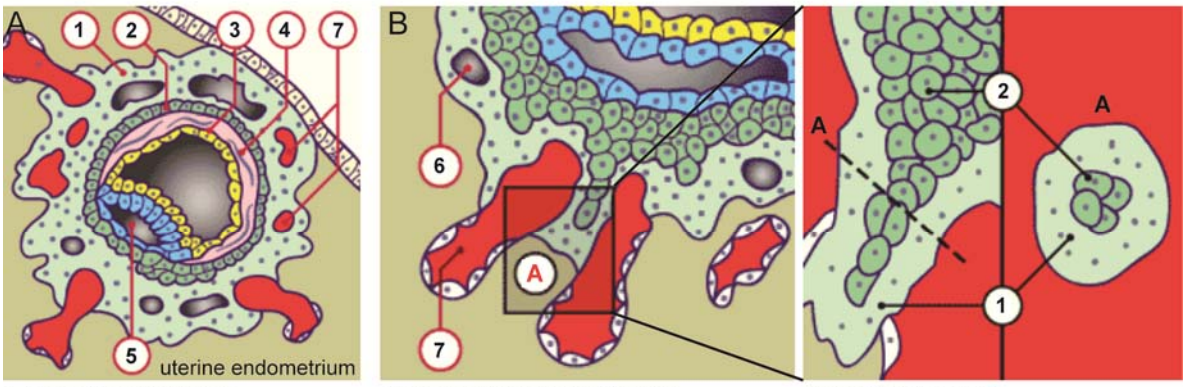

Figure 1.1. A) Complete implantation of the blastocyst into the endometrium around 9 to 10 days after fertilization. **B)** Formation of primary chorionic villi with CTBs that started to penetrate into the cords of the STB. Figure adapted from www.embryology.ch (access date: 2nd of May 2016).

After 10-12 weeks, the placental barrier is formed and maternal blood flow to the interstitial space is established. At the same time, oxygen tension rises from < 20 mmHg to > 50 mmHg that plays an essential role in further development of the placenta and the fetus (Jauniaux et al. 2000). The placenta consists of a maternal part that is called basal plate and chorionic plate which belongs to the fetal side (Figure 1.2A) (Gude et al. 2004). The functional vascular units of the placenta are called cotyledons of which each contains one fetal villous tree (branched fetal villi)

that gets into direct contact with maternal blood in the intervillous space (Figure 1.2B). These villous trees are responsible for the specific barrier function of the placenta and the separation of the maternal and fetal blood stream. In the first and second trimester, all nutrients, gases, and other substances have to cross four different layers of the fetal villi before they reach the fetal bloodstream: STB, CTBs, fetal stroma, and the fetal capillary endothelium. Specifically, the fetal side of the intervillous space is lined with the STB that forms a continuous multinucleated cell barrier without intercellular borders. Underneath, there are single CTBs that support growth and regeneration of the STB as described above. A basement membrane separates these trophoblasts from the stroma of the villous trees containing Hofbauer cells (macrophages), mesenchymal fibroblasts, reticular cells, and fetal blood vessels (Figure 1.2C) (Kaufmann et al. 1977).

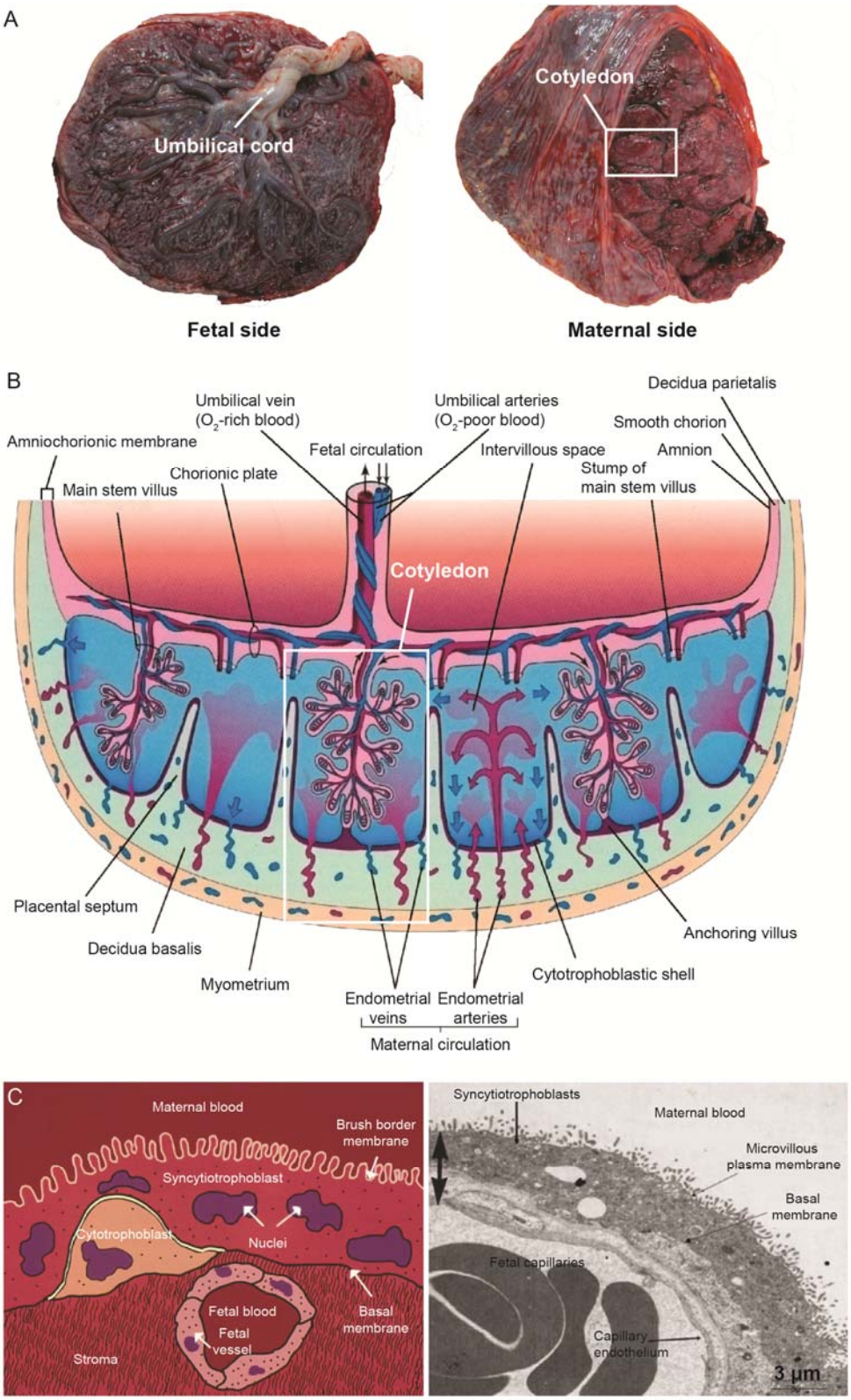

Figure 1.2. Anatomical structure of the human term placenta. **A)** The macroscopic images show the fetal side of a placenta with the umbilical cord and the chorionic plate and the maternal side with numerous cotyledons. A cross-section of the human term placenta is shown in **B)** with a detailed scheme of a villous tree membrane and the corresponding TEM image *in vivo* depicted in **C)**. Both schemes were adapted from Saunders et al. (Saunders 2009) and TEM micrograph was adapted from Sibley et al. (Sibley 2009).

To facilitate the exchange of nutrients for the rapidly growing fetus, the placental barrier structure changes over time. In the first weeks, the placental barrier is twice the thickness of its final size in the second trimester in order to protect developmental processes (i.e. embryogenesis and organogenesis) (Figure 1.3A). At this stage, the embryo is nourished through simple diffusion, which is replaced by the utero-placental blood circulation at a later stage. After the first trimester, the barrier becomes thinner and in the term placenta, a distinct STB layer remains, whereas only few CTBs are left (Figure 1.3B). Moreover, the exchange area of the placenta is enlarged from 5 m^2 to roughly 12 m^2 (Larsen et al. 2002), which is enabled through 20-30 cotyledons that consist of highly branched villous trees and a syncytial layer with a brush border membrane. In addition, the number of fetal capillaries increases and they get adjacent to the STB such that the maternal and fetal blood get closer to each other (approximately 2-4 µm). In this way, a rapid exchange of gases and metabolites between the mother and the fetus is ensured to support rapid fetal growth at the end of pregnancy (Gude et al. 2004).

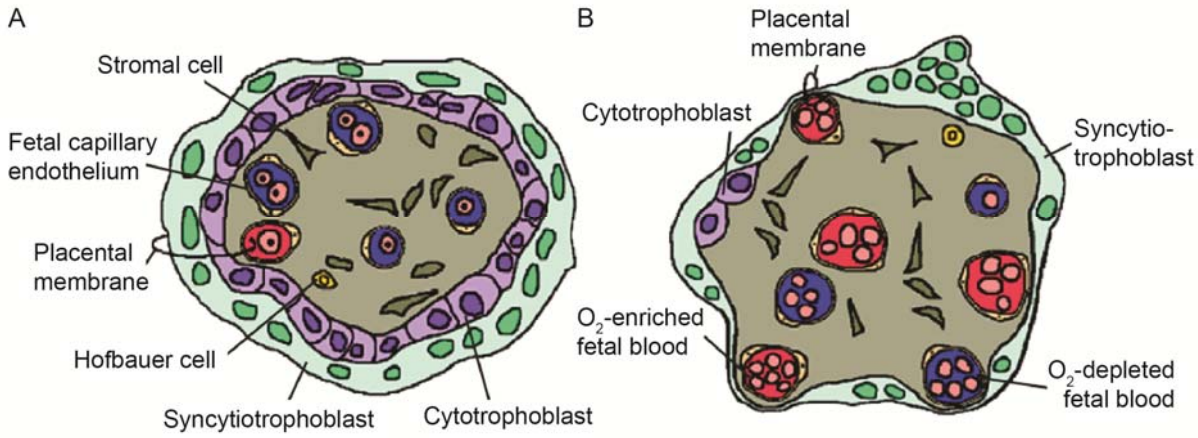

Figure 1.3. Placental barrier structure at approximately 10 weeks **(A)** and at full term **(B)**. Figure adapted from Gude et al. (Gude et al. 2004).

1.1.2 Functions of the human placenta

The main functions of the placenta include the transport of gases (oxygen (O_2)/carbon dioxide (CO_2)), water and nutrients to the fetus, removal of waste products from the fetus, protection against various diseases and xenobiotics, providing maternal tolerance and the release of hormones to support pregnancy, metabolism and fetal development among others (Verma and Verma 2013).

Transport function

During the first trimester, nutrition of the embryo is histiotrophic and includes trophoblast phagocytosis of glycoproteins that are secreted from uterine glands until at least week 10 of pregnancy, where maternal blood flow to the fetal chorionic villi is being established (hemotrophic nutrition) (Burton et al. 2002). Three major mechanisms are involved in the placental exchange including passive, active and vesicular transport.

Passive transport (energy independent) includes simple diffusion, osmosis and simplified transport. Specifically, non-polar (e.g. O_2, CO_2) and lipophilic molecules (e.g. free fatty acids, glycerol) but also alcohol and most drugs cross the placental barrier following concentration gradients (simple diffusion). Especially for respiratory gases, the placental membrane allows a rapid diffusion since it is highly permeable to O_2 and CO_2. Transfer of gases is also favored by a higher maternal partial pressure of O_2 and a higher fetal partial pressure of CO_2. Moreover, fetal hemoglobin exerts a higher affinity for O_2 and a lower affinity for CO_2 as compared to the mother. The transport of soluble substances occurs via osmosis. For water and lipid-insoluble molecules, it is suggested that transtrophoblastic channels in the plasma membrane of the STB may have a supporting role in their transfer, which is possibly regulated through pressure-dependent dilatation and closure of the channels (Benirschke and Driscoll 1967, Stulc 1997, Maroun et al. 2014). However, the existence of these channels is controversially discussed. Simplified transport also follows a concentration gradient but additionally involves transport molecules. Glucose, the main source of carbohydrates for the fetus, is transported via protein-mediated facilitated diffusion with the help of specific glucose transporters (GLUTs) that are located in the STB and fetal endothelial cells (Illsley 2000).

In contrast, active transport (energy-dependent) occurs against a concentration gradient, which, among others, requires the involvement of Na^+/K^+ or Ca^{2+} transport, ATPases or Na^+/H^+ exchangers, that are found in the microvillus plasma membrane of the STB and the basal membranes (Sibley 2009). Active transport of amino acids, which are necessary for the fetus to synthesize proteins, includes specific amino acid transporter proteins of many different isoforms and is further facilitated via hormones such as growth or thyroid stimulating hormones (Galan et al. 2009). Other examples for actively transported substances across the placenta comprise vitamins, potassium, magnesium, calcium, and phosphate (Gude et al. 2004).

Transplacental transfer of maternal transferrin (Tf) and maternal immunoglobulin G (IgG) occurs via vesicular transport (endocytosis/exocytosis) by the STB. Fc receptors are involved in IgG transfer, which is especially important to provide passive immunity to the fetus (Verma and Verma 2013). Tf receptors participate in active Tf transfer that has an essential role in iron transport from the maternal to the fetal side (Tawada et al. 1985).

Barrier function

Besides the physical barrier of the placenta with its villous tree membrane, the expression of different transporters in the STB plays a key role not only in transplacental transport but also in the protective function of the placenta. As described above, the STB exhibits a polarized morphology with a microvillus brush border on its apical side facing maternal blood and a basolateral membrane facing towards the fetal blood vessels (Sibley 2009). Both sides of the membrane express numerous uptake and efflux transporters such as the ATP-binding cassette (ABC) or the solute carrier (SLC) family of transporters (Vahakangas and Myllynen 2009, Staud et al. 2012).

Among the ABC transporters, P-glycoproteins (Pgp) (encoded by the multidrug resistance 1 (MDR1) gene), multidrug resistance-associated proteins 1 and 2 (MRPs) and breast cancer resistance proteins (BCRPs) are of particular importance for the active transport of substrates out of the cells. Specifically, Pgp, MRP2 and BCRP are located at the apical side of the STB where they protect the fetus from maternal toxins by transferring them out of the syncytium (Figure 1.4) (Staud et al. 2012). MRP1 is located at the basolateral side of the STB and the fetal endothelium in order to actively pump substrates into the fetal blood vessels (St-Pierre et al. 2000). Evseenko et al. compared the expression and activity of ABC transporters in primary CTBs, whole placentas, BeWo, and Jar cell lines. Gene expression of MDR1, MDR3, MRP1, MRP2, and BCRP was confirmed for all cell types and placentas. In BeWo cells, expression of MDR1 and MRP2 were lower and expression of BCRP and MRP1 were higher as compared to primary trophoblasts and placentas. Except for large differences in MDR1 expression between the different cell types and placentas, variations of gene expression for the other investigated ABC transporters were modest (Evseenko et al. 2006).

SLC transporters comprise over 300 members that are present in various tissues. There are either substrate-specific transporters for the transport of endogenous

substances (e.g. sugars, amino acids) or transporters with wide substrate specificity, which are important for the elimination of drugs. In the placenta, several SLC transporters have been identified such as organic anion, cation, carnitine, serotonin, and noradrenalin transporters (Vahakangas and Myllynen 2009, Staud et al. 2012). Their main function is to facilitate energy-independent uptake of charged or hydrophilic substrates into the STB (Staud et al. 2012). In BeWo cells, several studies confirmed the presence of organic anion (Zhou et al. 2007) and carnitine transporters (Hirano et al. 2008, Rytting and Audus 2008).

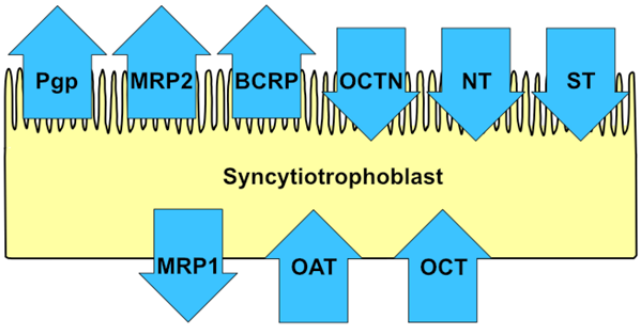

Figure 1.4. Localization of the main importer and exporter proteins in the STB of a human placental barrier at term. Abbreviations: BCRP, breast cancer resistance protein; MRP, multidrug resistance-associated protein; NT, noradrenalin transporter; OAT, organic anion transporter; OCT, organic cation transporter; OCTN, organic carnitine transporter; Pgp, P-glycoproteins; ST, serotonin transporter.

Most importantly, chemical inhibitors are available to block most of these transporters, which is important to reveal whether they are involved in nanoparticle uptake into trophoblast cells *in vitro* (Vahakangas and Myllynen 2009).

In addition to these transporters, the villous stroma contains Hofbauer cells, which function as macrophages of the placenta and additionally contribute to the barrier function of the placenta through their pinocytotic and phagocytic activities (Seval et al. 2007).

Endocrine function

To ensure maintenance of pregnancy and proper growth of the fetus, the placenta (mainly the STB) produces many different hormones throughout pregnancy. These hormones can be divided into two classes: peptide and steroid hormones. Human chorionic gonadotropin (hCG), human placental lactogen (hPL), placental growth hormone (PGH), corticotropin releasing hormones, insulin-like growth factors, vascular endothelial growth factors, and placental growth factors belong to peptide

hormones whereas estrogen, progesterone and glucocorticoids, belong to steroid hormones.

hCG is a glycoprotein composed of an α-subunit common for all glycoprotein hormones and a placenta-specific β-subunit. hCG is produced by the STB and is one of the earliest products secreted after conception with peak levels at about week 8-10 followed by a decline and a second rise in late pregnancy. It has several functions such as to enhance CTB differentiation into the STB (Yang et al. 2003), the promotion of progesterone production by the corpus luteum (Cole 2010) and an angiogenic function that is important for placental development (Zygmunt et al. 2002). Due to its pleiotropic functions, hCG is an important marker to assess the functionality of *ex vivo* or *in vitro* placental tissue in particular after the exposure to harmful xenobiotics or nanoparticles (NPs).

hPL is mainly produced by the STB throughout pregnancy with peak levels close to the end. The main function of hPL together with PGH is to ensure fetal nutrition through the decrease of maternal insulin sensitivity and glucose utilization finally resulting in a higher maternal blood glucose level. At the same time, hPL induces lipolysis in the mother whereby free fatty acids are released and can be used as an energy source to compensate for the loss of glucose (Handwerger and Freemark 2000).

Progesterone is produced by the placenta and the corpus luteum and is an important hormone to maintain pregnancy. It inhibits uterine contraction through the decrease of uterine smooth muscle contractility (Gude et al. 2004). By the end of the first trimester, the corpus luteum degenerates and its function is completely taken over by the placenta.

Estrogen is mainly produced by the ovaries, corpus luteum and the placenta. It is an important growth hormone for the mother and targets several reproductive organs (breast, uterus, cervix, vagina) (Page 1993).

Immunologic function

From an immunological point of view, the fetus is a “semi-allograft” in the uterus of the mother since fetal human leukocyte antigen (HLA), a combination of maternal and paternal genes, is seen as “non-self” by the maternal immune system. However, besides the physical barrier of the placenta, several immunological mechanisms account for the survival of the fetus. One major mechanism is the limited expression of classical HLA-A, -B and -C antigens on the apical membrane of trophoblasts

facing the maternal blood, which may protect the fetus from maternal cytotoxic T-cells (Erlebacher et al. 2007). On the other hand, trophoblasts express the nonclassical HLA-G antigens, which inhibit fetal cell lysis by decidual natural killer cells (Rouas-Freiss et al. 1997). In addition, HLA-G antigen, pregnancy hormones and the release of cytokines by regulatory T-cells (e.g. TGF-β, IL-10) contribute to maternal immunosuppression (La Rocca et al. 2014).

Metabolic function

The placenta fulfills a series of different metabolic functions in order to supply nutrient substrates to the fetus. It takes over many tasks of the adult liver such as handling of bile acids, biliary pigments and detoxification of xenobiotics via metabolizing enzymes (e.g. cytochrome P450) (Marin et al. 2003).

Furthermore, it is involved in the synthesis of glycolipids and cholesterol (Gude et al. 2004) and in activities such as protein synthesis, oxidation and interconversion of amino acids among others (Verma and Verma 2013).

Even though mammalian placentas perform the same basic function, there are striking interspecies differences in placental structure, organization and function. Since *in vivo* placenta studies are based on the use of animals, a clear understanding of these species-specific differences is important to better estimate the relevance of such studies for humans.

1.1.3 Species-specific differences in placental structure and function

The placenta is the most species-specific mammalian organ with essential differences in structure and function. Three main types can be distinguished: the epitheliochorial (e.g. sheep, pig, horse), the endotheliochorial (e.g. cat, dog, elephant) and the hemochorial placenta (rabbit, rodent, human) (Furukawa et al. 2011). Their classification is based according to the number and types of layers between the fetal trophoblast and maternal blood, which are either uterine epithelial cells of the endometrium (epitheliochorial placenta), a layer of maternal endothelial cells (endotheliochorial placenta) or direct contact of the fetal trophoblast with maternal blood (hemochorial placenta) (Enders and Blankenship 1999). Since most *in vivo* animal studies on nanotoxicity, translocation and biodistribution are performed in rodents, the focus is set on the differences between human and rodent placentas.

Hemochorial placentas are further classified into hemomonochorial (human), hemodichorial (rabbits) and hemotrichorial placentas (rodents) that are composed of

one, two or three trophoblast layers, respectively (Furukawa et al. 2011). The main structural differences between the latter and human placentas are the organization into a junctional zone and a labyrinth in rodents, while in humans, there is an intervillous space where fetal chorionic villi are bathed in maternal blood (see Chapter 1.1.1) (Figure 1.5). In rodents, exchange takes place in the labyrinth, which contains maternal blood sinuses and fetal blood vessels that are arranged in a labyrinth-like structure (Georgiades et al. 2002). The three trophoblast layers include one mononuclear trophoblast and two STB layers. The spongiotrophoblast, the trophoblastic giant cells (similar to human CTBs) and glycogen cells belong to the junctional zone, which is responsible for the endocrine function of the placenta. In contrast to rodent placentas, the STB layer of the human placenta conducts both, feto-maternal exchange and endocrine functions (Malassine et al. 2003).

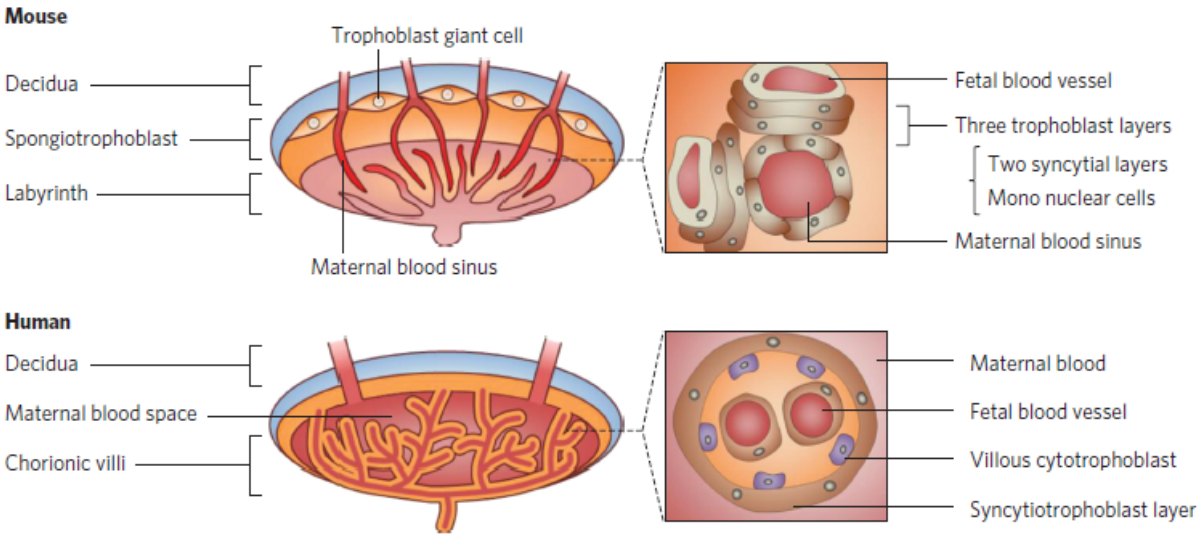

Figure 1.5. Hemotri- and hemomonochorial structure of a mouse and human placenta, respectively. Figure taken from Yamashita et al. (Yamashita et al. 2011).

Moreover, the yolk sac placenta in humans is essential for the fetal survival and development during the first 9 weeks of pregnancy after which it starts to degenerate, whereas in rodents its activity is retained throughout gestation (Jollie 1990, Freyer and Renfree 2009). Other differences comprise the gestation period (9 months for humans, approximately 3 weeks for rats and mice) and the number of cotyledons (20-30 in human, one in rodents) and embryos (one in human, up to 12 in rodents) (Rossant and Cross 2001) (http://placentation.ucsd.edu, access date: 16th of June 2016).

Keeping all these structural and functional differences between human and rodent placentas in mind, questions arise in how far data from *in vivo* animal studies of NPs or other xenobiotics can be extrapolated to humans. However, given the tragedy of thalidomide-induced birth defects in the 1960's, administration of thalidomide into pregnant rats did not significantly interfere with fetal development, while in humans, it induced severe birth defects (Schumacher et al. 1968). This is one of the most prominent examples showing that *in vivo* animal studies are often of low clinical relevance for human applications. To avoid such disasters in future, and to provide human-relevant data for NP- or drug-placenta interactions, it is indispensable to develop and use reliable models of human placental origin.

1.2 Human placenta models

In pregnant women, there is the possibility to monitor transplacental transfer rates of substances by collecting human maternal and umbilical cord blood (e.g. during labor or after an accident). However, this method does not provide information on placental drug metabolism as well as on drug distribution and accumulation (Prouillac and Lecoeur 2010). Moreover, access to such samples is limited to substances intentionally administered during pregnancy but is not realistic for NPs in the near future.

In general, inclusion of pregnant women in biomedical research is of high ethical concern since there is evidence that NPs could seriously harm the development and growth of the vulnerable fetus. Therefore, current knowledge on effects, uptake and translocation of different NPs through the human placental barrier is based on findings from human *ex vivo* or *in vitro* models.

1.2.1 *Ex vivo* placenta tissue models

Ex vivo placenta perfusion

Human placentas are obtained directly after delivery and single cotyledons are perfused *ex vivo* (Panigel et al. 1967, Schneider et al. 1972). This model system is widely used to study the transfer of drugs, NPs or other xenobiotic with a high predictability for *in vivo* transfer (Grafmueller et al. 2013). Drawbacks of this model are a low success rate, genetic variability and limited perfusion time.

Placental tissue explants

Placental explants are obtained from human placentas and can be cultured *in vitro* to study, among other functions, metabolism, endocrine function, enzyme function, proliferation, differentiation, toxicology, and disease processes. The main advantage of this system is that it preserves the natural co-culture of the STB with different cell types. Disadvantages comprise genetic variability and the difficulty to distinguish individual activities of all involved cell types (Miller et al. 2005).

1.2.2 Acellular *in vitro* models

Placental membrane vesicles

Membrane vesicles can be isolated from the microvillus surface or the basal membrane of the STB from human term placentas (Bissonnette 1982). Such vesicles were used to study the expression and functionality of different transporters in both membranes. However, since intracellular constituents are completely lacking in this model system, it does not recapitulate the physiological *in vivo* situation very well (Glazier and Sibley 2006).

1.2.3 Cell-based *in vitro* models

Human primary cells

Primary mononuclear CTBs can be isolated from human placentas (Kliman et al. 1986) and are used to study uptake, efflux, metabolism and hormone secretion (Bode et al. 2006). In culture, these cells spontaneously differentiate into a syncytium but it is difficult to obtain a tight monolayer since primary CTBs syncytialize into aggregates with large intercellular spaces.

Human cell lines

Several human placental cell lines are available including the choriocarcinoma cell lines BeWo, Jeg-3 and Jar that possess characteristics of villous trophoblasts, and cell lines that are derived from the first trimester trophoblasts (i.e. HTR-8/SVneo) (Orendi et al. 2011).

BeWo cell line: Originally, BeWo cells were isolated from a human cerebral metastasis of a malignant trophoblast cancer (choriocarcinoma). During 8 years, Hertz et al. serially transplanted these cancer cells to the cheek pouch of hamsters (Hertz 1959). Afterwards, the BeWo choriocarcinoma cell line was successfully established through their isolation from the hamsters and their subsequent co-culture

with human decidual tissue from the endometrium of a normal pregnancy (Pattillo and Gey 1968). Most importantly, it was shown that BeWo cells display many of the characteristics of primary human villous trophoblasts such as the secretion of placental hormones (hCG, hPL, progesterone, and estrogens) (Pattillo et al. 1971) and a polarized monolayer with different apical and basolateral morphology as well as expression of specific transporters and marker enzymes (Liu et al. 1997, Zhao and Hundal 2000). In contrast to primary trophoblasts, BeWo cells continuously proliferate, they exhibit a low fusion rate and do not spontaneously differentiate into a multinucleated syncytium. Nevertheless, differentiation can be induced by forskolin or cyclic-adenosine monophosphate (cAMP) among others (Wice et al. 1990). Briefly, forskolin activates adenylyl cyclase, which results in increased levels of intracellular cAMP. Augmented cAMP activates protein kinase A (PKA) (Knerr et al. 2005) with subsequent activation of the transcription factor glial cell missing 1 (GCM1). In turn, GCM1 upregulates the classical cell fusion peptide syncytin-1 (ERVWE1), which is supposed to be involved in trophoblast fusion (Mi et al. 2000). As a result of cell fusion, the expression of specific proteins such as β-hCG, placental protein 13 (LGALS13/PPT13) or syncytin-1 and syncytin-2 (Vargas et al. 2009) is upregulated and they are commonly accepted as biochemical markers of BeWo cell fusion. However, Orendi et al. demonstrated that inhibition of PKA with H89 in the presence of forskolin significantly decreased protein and mRNA expression of LGALS13 but did not affect hCG protein expression. Therefore, it was proposed that hCG is not necessarily related to BeWo cell fusion and that there must be a second, PKA-independent pathway of hCG protein expression. Consequently, an additional marker to hCG levels may be helpful to properly assess BeWo syncytialization (e.g. LGALS13 expression or visualization of cell membranes) (Orendi et al. 2010). Since BeWo cells possess many of the morphological and physiological characteristics of villous trophoblasts, they are widely used in human placenta *in vitro* models to study nanoparticle uptake, translocation and cellular effects (e.g. using Transwell® inserts).

Jar and Jeg-3 cell lines: Like BeWo cells, Jar and Jeg-3 cell lines were derived from choriocarcinoma cells and were used to study differentiation, invasion, oxidative stress responses, endocrinology, and immunological reactions. Even though Jeg-3 cells produce placental hormones (e.g. progesterone, hCG, steroids) (Chou 1982, Kato and Braunstein 1991) and express different enzymes (Tremblay et al. 1999), they do not differentiate into a syncytium after forskolin treatment (Al-Nasiry et al.

2006). Jar cells also secrete a number of different placental hormones (Kato and Braunstein 1991) and express transporter proteins (Pgp, MDR3, BCRP) but they are more similar to mononucleated, undifferentiated CTBs than to syncytiotrophoblastic cells (Evseenko et al. 2006). Due to the cytotrophoblastic character of both, Jeg-3 and Jar cell lines, they are not suitable for transplacental transfer studies. Recently, Lee et al. demonstrated for the first time the development and characterization of a placenta-on-a-chip model using Jeg-3 cells in order to mimic structural and functional characteristics of the human placental barrier (Lee et al. 2015).

HTR-8/SVneo cell line: HTR-8/SVneo was derived from first trimester extravillous trophoblasts transduced with the gene encoding for simian virus 40 large T antigen (Graham et al. 1993). This invasive cell line has been used to study trophoblast migration and invasion.

Even though these model systems are well-established, there is a large gap to fill between human *in vitro* and *ex vivo* placenta models. On the one hand, 2D cell cultures offer convenient handling and analysis, high-throughput compatibility and low costs. On the other hand, these systems are highly artificial as cells grow on flat and rigid plastic or glass substrates, become flat and elongated, undergo extensive division, and often lose their differentiated phenotype. *Ex vivo* placenta models better recapitulate the *in vivo* tissue structure and response, which is, among other benefits, important for the validation of *in vitro* models. However, they are limited in their availability, throughput, exposure time, and suitability for NP assessments. A promising approach to bridge the gap between simplified 2D cell cultures and *ex vivo* placenta tissues is the development of organoid-like placenta models (Pampaloni et al. 2007).

1.3 3D cell culture models

1.3.1 Advantages of 3D cell culture models

In the body, cells are embedded within a complex environment that comprises an extra cellular matrix (ECM) containing many different proteins (e.g. collagens, integrins, laminin, and fibronectin) and cell types (Baker and Chen 2012). 3D cell culture models provide such an environment and enable close cell-cell and cell-ECM interactions, which essentially affect cell shape, proliferation, apoptosis, metabolism,

and differentiation (Yamada and Cukierman 2007, Baker and Chen 2012, Shamir and Ewald 2014).

Already in 1982, Benya and Shaffer showed that dedifferentiated chondrocytes only re-expressed their differentiated phenotype and synthesized high levels of type II collagen and proteoglycan when grown in a 3D agarose gel (Benya and Shaffer 1982). In 3D mammary epithelial microtissues (MTs), integrin-induced apical-basal polarity significantly increased their resistance to apoptosis while non-polarized structures remained sensitive to apoptosis-inducing agents (Weaver et al. 2002).

Today, the most prominent 3D *in vitro* models are multicellular tumor spheroids that closely mimic the complex tumor microenvironment with its gradients of proliferating cells, nutrients and gases. These factors highly influence therapeutic outcome and thus render 3D cancer MT models a useful platform to investigate cellular toxicity, tissue distribution and penetration kinetics of anti-cancer drugs (Markovitz-Bishitz et al. 2010, Ong et al. 2010, Rimann and Graf-Hausner 2012, Longati et al. 2013, Falkenberg et al. 2016). For liver and heart MTs, morphological and functional characterization showed that MTs better reflect the *in vivo* situation than 2D cell cultures (Abu-Absi et al. 2002, Kratschmar et al. 2013, Messner et al. 2013, Mueller et al. 2014, Ramaiahgari et al. 2014, Beauchamp et al. 2015, Mathur et al. 2015). For example, in liver MTs of hepatocytes several studies confirmed the formation of bile canaliculi-like structures, the upregulation of functional enzyme activities and high levels of protein production as compared to 2D cell cultures (Abu-Absi et al. 2002, Kratschmar et al. 2013, Messner et al. 2013, Mueller et al. 2014, Ramaiahgari et al. 2014). In addition, these MTs remain viable for several days, which allow acute and long-term hepatotoxicity testing of different drugs (e.g. acetaminophen, diclofenac (Messner et al. 2013), aflatoxin B1, amiodarone, valproic acid, and chlorpromazine (Mueller et al. 2014)) with an improved predictability of toxic responses as compared to 2D monocultures. Heart MTs generated from induced pluripotent stem cells (iPSCs) comparably find increasing application in drug screening (Wang et al. 2014, Tzatzalos et al. 2016). Recently, spontaneous contractions of a 3D MT model consisting of iPSC-derived human cardiomyocytes could be monitored for at least one month and MTs were sensitive to electrical, pharmacological and physical stimuli (Beauchamp et al. 2015). Mathur et al. developed a cardiac MT of well aligned human iPSC-derived cardiomyocytes, which were exposed to a microcirculation mimicking the *in vivo* transport of gases, nutrients or drugs. Moreover, effects on the

MT beat rate and its IC_{50} values after treatment with Verapamil were shown to be in better agreement with results of animal studies and clinical observations as 2D cell culture models (Mathur et al. 2015).

These studies nicely show that 3D MT models were engineered to recapitulate a variety of different tissues and to address specific questions. In order to develop a tissue model that best meets the desired criteria (e.g. structural organization), it is important to carefully select the appropriate strategy for its generation.

1.3.2 Methods to generate 3D cell cultures

Today, a large variety of different 3D cell culture systems are commercially available either using scaffold/matrix-based or scaffold-free systems (Rimann and Graf-Hausner 2012).

Scaffold/matrix-based systems

Scaffold/matrix material may be of biological (e.g. gels containing laminin, collagen IV, entactin, and heparin sulfate proteoglycans as found in Matrigel™ (BD Bioscience) or Cultrex® (Trevigen)) or synthetic origin (e.g. polyethylene glycol (Qgel), polycaprolactone (3D Biotek)). To generate spheroids, cells are either seeded directly onto an acellular 3D matrix or dispersed in a liquid hydrogel that later polymerizes (Rimann and Graf-Hausner 2012, Edmondson et al. 2014).

Both, synthetic and biological gels provide an *in vivo* like structural support to the cells. Natural gels are highly biocompatible, bioactive and their composition can be optimized according to the experimental needs by adding e.g. specific growth factors or adjusting levels of ECM proteins and other molecules. Drawbacks of natural gels include batch-to-batch variations in ECM composition, high costs for large-scale production and large variations in spheroid sizes (Tibbitt and Anseth 2009, Hughes et al. 2010, Breslin and O'Driscoll 2013). On the other hand, synthetic gels are easy to produce, highly reproducible and have controllable mechanical properties. However, such gels mainly provide structural support since they lack endogenous factors and thus remain biologically inert (Tibbitt and Anseth 2009).

Scaffold-free systems

Scaffold-free systems comprise forced-floating, agitation-based approaches and the hanging drop technology (Figure 1.6). In the forced-floating method, round or conical bottomed 96-well plates are coated prior to cell seeding in order to prevent cell attachment. Cell-cell interactions are facilitated by centrifugation. This method is

simple, inexpensive and single spheroids are easy accessible, which renders it suitable for high-throughput analysis. In order to avoid time-consuming plate-coating steps, pre-coated plates are commercially available (e.g. from Sumitomo Bakelite or NOF Corporation) (Breslin and O'Driscoll 2013). Agitation-based approaches can be classified into spinner flask bioreactors or rotating cell culture bioreactors. The principle is the same for both systems: either the cell suspension is stirred (spinner flask) or the whole container is rotated (rotating cell culture). Continuous motion of the cell suspension avoids adherence to the container wall thereby inducing spheroid formation. Agitation-based methods are simple and allow for large-scale production of spheroids, lacking, however, control over the size of the spheroids (Breslin and O'Driscoll 2013). In the hanging drop technology, cells settle down to the bottom of the drop and form a spheroid at the air-liquid interface due to gravity-enforced cell assembly (one spheroid/drop). With this technique, spheroids of highly reproducible sizes are generated. Moreover, it is compatible with small volumes and cell numbers as well as with high-throughput systems (Kelm and Fussenegger 2004, Tung et al. 2011). The main disadvantage of this technique is its high costs.

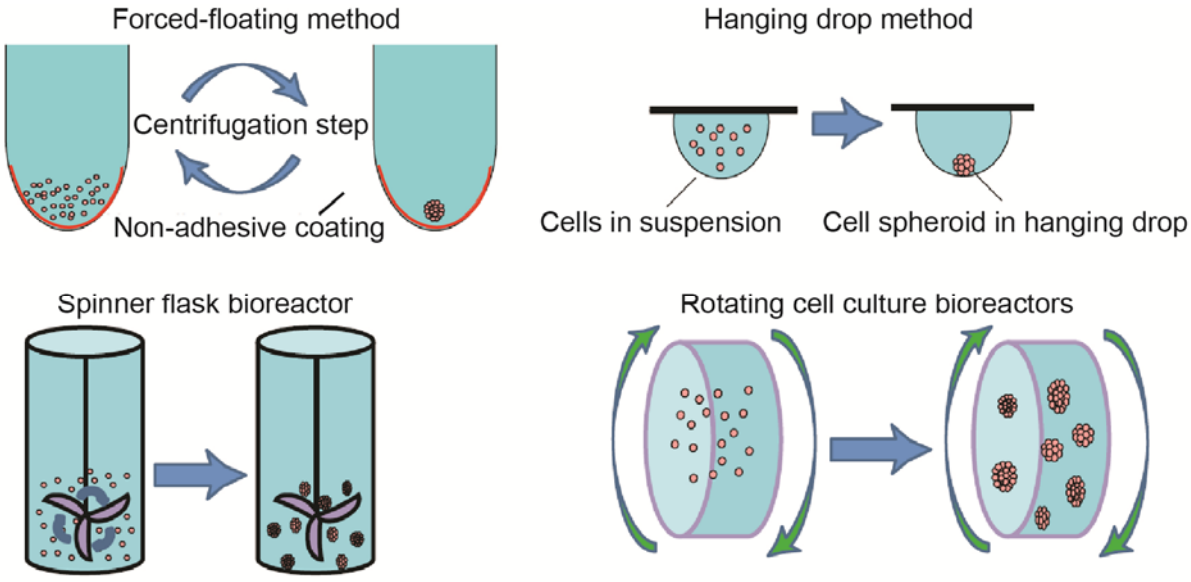

Figure 1.6. Scaffold-free methods to generate 3D spheroids. Figure adapted from Lin et al. (Lin and Chang 2008).

Scaffold-free methods are highly attractive to study NP-tissue interactions because there is no interference of NPs with the scaffold material, which may lead to misleading results and to further restrictions or limitations of the model. Among these approaches, the hanging drop technology is an interesting option to generate well-

structured core/shell MTs as cell numbers can be precisely controlled and additional cell types can be individually added to the MTs at different time points.

1.4 Nanomaterials

1.4.1 Definition

The term “nanos” arises from the Greek language and stands for “dwarf”. According to the recommendation of the *European Commission*, nanomaterials (NMs) are defined as materials containing particles where at least one dimension of 50 % or more of the particles in the number size distribution are in the size range between 1-100 nm (http://ec.europa.eu/environment/chemicals/nanotech/faq/definition_en.htm, access date: 15th of February 2016). The definition of the *International Organization for Standardization* (ISO/TS 80004-2:2015) distinguishes between the shapes of NMs. Thereby, nanoparticles (NPs) are defined as particles where all three external dimensions are < 100 nm, nanofibers with two and nanoplates with one external dimension in the nanoscale. In nanomedicine, a cut-off size of 100 nm did not cover all NMs with beneficial physico-chemical properties or physiological interactions. Therefore, it was suggested to include NMs with at least one dimension up to 300 nm (Etheridge et al. 2013). In contrast to bulk material (> ~1 µm, no size-dependent changes in physico-chemical properties), NMs have a very high surface-area-to-volume-ratio, which results in unique chemical and physical properties such as an increased chemical reactivity (Goesmann and Feldmann 2010).

Depending on their origin, NMs can be divided into three categories, namely naturally occurring, incidental or engineered nanomaterials (ENMs). Natural NMs include for instance the dust of volcanoes or forest fires whereas unintentional by-products from different processes such as diesel exhaust, polishing or smoking derived particles belong to incidental NMs. ENMs are developed for specific purposes in various industrial, commercial and biomedical applications that benefit from their adjustable physico-chemical properties and surface functionalization (Figure 1.7) (Stern and McNeil 2008, Ryan and Brayden 2014).

Figure 1.7. Different types of nanomaterials. Figure adapted from Tinkle et al. (Tinkle et al. 2014).

1.4.2 Applications of nanoparticles

NPs are integrated into various commercially available products (e.g. cosmetics, textiles, sports or car industry) but their use is also being explored for the development of novel industrial or medical applications.

The most prominent example of a commercial product is the incorporation of TiO_2 into sunscreens. Nanoparticulate TiO_2 (< 50 nm) has UV light absorbing properties while it remains transparent on the skin to the human eye. In contrast, larger TiO_2 NPs (approximately 200 nm) are added to white paints due to their beneficial whitening properties (reviewed by (Stark et al. 2015)). NPs are also popular additives for surface coatings since they enable a thin and thus cost attractive coating. For example, self-cleaning glasses for windows or cars are coated with TiO_2 NPs that induce a cleaning mechanism based on photocatalysis and hydrophilicity. After the exposure to UV light, free radicals are generated from the NPs to oxidize dirt, which

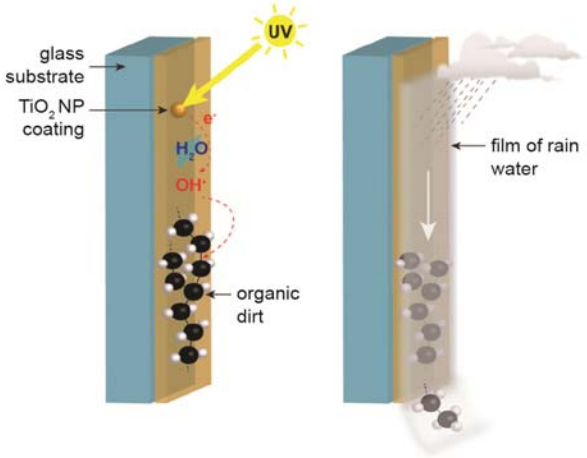

Figure 1.8. Example of TiO_2 NPs in a commercial product. The principle of self-cleaning windows is based on a photocatalytic coating with TiO_2 NPs that oxidize dirt and a hydrophilic surface in order to easily remove the dirt by rain water. Figure adapted from Stark et al. (Stark et al. 2015).

is finally removed by an even layer of rainwater on the hydrophilic surface (Pilkington Active™) (Figure 1.8). The use of copper oxide (CuO) NPs has been explored for antimicrobial coatings (Ren et al. 2009) and to improve power conversion efficiency of solar cells due to their good solar spectral absorption (Wanninayake et al. 2015), among others.

In addition to industrial applications, the implementation of NPs in the development of novel medical devices, therapies and diagnostics substantially contributed to

advances in the medical field. Today, approximately 80 applications received FDA approval including devices and therapeutics (Etheridge et al. 2013). Among the devices, major categories are *in vitro* testing and *in vivo* imaging followed by coating devices and bone substitutes. For instance, gold (Au) NPs are widely used as scaffolds for chemical and biological sensors. Their unique properties (e.g. surface functionalization, optical properties) allow the development of sensors with improved stability and selectivity to detect for instance small molecules, proteins, nucleic acids or cells (Wilson 2008, Saha et al. 2012). A well-known example is pregnancy test strips based on a lateral flow immunoassay. The pregnancy hormone human chorionic gonadotropin specifically binds to antibody-conjugated AuNPs, which in turn bind to immobilized capture antibodies on the strip, that finally result in a strong red color signal (Figure 1.9) (reviewed by (Stark et al. 2015)).

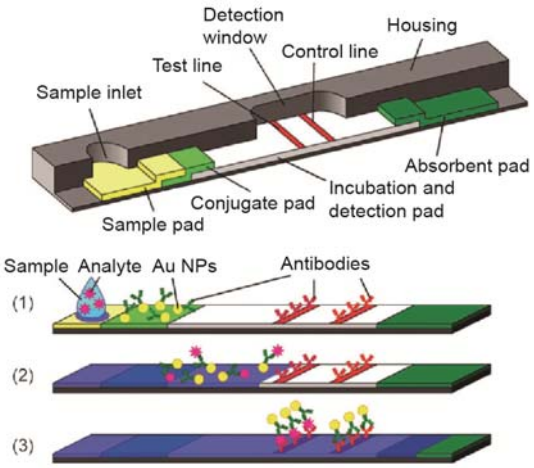

Figure 1.9 Example of AuNPs in a nanomedical product. Lateral flow immunoassay in a pregnancy test: the analyte containing the pregnancy hormone flows on the pad **(1)** and binds to AuNPs conjugated with specific antibodies **(2)**. NPs with antigens bind to the test line whereas NPs without antigens bind to the control line **(3)**. Figure adapted from Stark et al. (Stark et al. 2015).

Other examples include the use of ferrofluidic NPs to track and separate circulating tumor cells (CellTracks®, Janssen Diagnostics, USA), silicone-coated superparamagnetic iron oxide NPs as gastrointestinal contrast agents in MRI (Lumirem™, Guerbet Ltd., France), antimicrobial silver NPs as wound dressings (Acticoat®, Smith & Nephew, UK), and calcium-phosphate (Vitoss®, Stryker, USA) and hydroxyapatite nanocrystals as bone substitutes (OSTIM®, Heraeus Kulzer Int., Germany). Among nanomedical therapeutics, anti-cancer treatments are the most

widespread applications. In 1995, Doxil® was the first NP-based anti-cancer therapy that received FDA approval. The formulation contains Doxorubicin (Dox) encapsulated within PEGylated liposomes, which in the case of a Kaposi's sarcoma, results in an improved drug biodistribution, extended circulation half-life and thus in an enhanced drug accumulation in the tumor tissue (Simpson et al. 1993). Other examples are Abraxane®, which is based on the attachment of paclitaxel to the serum protein albumin to treat metastatic breast cancers (Miele et al. 2009) and iron oxide NPs for the hyperthermia therapy of brain tumors (NanoTherm®, Magforce AG, Germany) (Mura et al. 2013).

However, the application of different multifunctional particles as targeted drug delivery systems and simultaneously as tracking agents for diagnostic purposes is still under investigation. For example, intravenous injection of magnetic Au-PEG NPs loaded with Dox into Ehrlich tumors of mice and the presence of an external magnetic field resulted in an active targeting of the tumor tissue. Moreover, it markedly reduced further tumor growth as well as side effects to healthy tissues (Elbialy et al. 2015). Similarly, Zhang et al. conjugated Dox to ultra-small AuNPs and effectively treated melanoma in mice with minimal systemic toxicity after intratumoral injection (Zhang et al. 2015). Another interesting approach was shown by Patra et al. where Gemcitabine loaded AuNPs were additionally bound to Cetuximab in order to specifically target epidermal growth factor receptors, which are known to be overexpressed in pancreatic cancer cells. This combination increased tumor growth inhibition from 30 % using Gemcitabine alone to > 80 % (Patra et al. 2008). Quantum dot (Qdot) NPs also hold great potential as multifunctional NPs due to their small size (< 10 nm) that allows biological interactions at the near atomic scale and their broad absorption and emission spectra (Volkov 2015). To reduce their intrinsic toxicity, new classes of Qdots were introduced with different types of core, shell and surface chemistry (Kamila et al. 2016). For example, carbon Qdots were conjugated with the anti-cancer drug Oxaliplatin. Their intralesional injection into hepatocarcinoma 22 xenografts in mice showed a reduction of 82 % in tumor volume after 3 days and tracking of the drug was possible during the whole process due to fluorescence of the carbon Qdots. It was stated that the complex becomes activated only in the reductive environment found in tumor tissue but remains stable in blood circulation (Zheng et al. 2014).

These examples demonstrate the great potential of NPs as drug delivery systems to specifically and effectively treat diseased tissues. However, there is still a large knowledge gap regarding unforeseen side-effects of such medical or industrial NPs. Especially for the treatment of pregnant women, it is of particular importance to ensure the use of safe NPs in order to avoid devastating damage to the developing fetus.

1.4.3 Adverse effects of nanoparticles in pregnancy

The application of several NPs in daily products is expected to lead to an increased exposure of pregnant women to such materials, which raised major concerns about potential teratogenic effects to the vulnerable fetus.

So far, most studies on teratogenic effects of NPs were conducted in pregnant rodents after inhalation or injection of different NPs (Chu et al. 2010, Pietroiusti et al. 2011, Yamashita et al. 2011, Blum et al. 2012, Campagnolo et al. 2013). For example, daily inhalation of 230 µg/m^3 Qdots by pregnant mice led to a reduction in pregnancy rate, restricted fetal growth and altered placental weight (Blum et al. 2012). Another study confirmed that tail vein injection of CdS core/shell Qdots into pregnant mice reduced the survival rate of pups in dependence of Qdot size and surface coating (MPA < PEG < SiO_2) (Chu et al. 2010).

Pietroiusti et al. investigated the effect of pristine or oxidized single-wall carbon nanotubes (SWCNTs) after intravenous injection into pregnant mice. At concentrations of 3 or 30 µg/mouse, all types of SWCNTs induced fetal malformations, abnormal placental development and swollen uteri (Pietroiusti et al. 2011). Interestingly, even low-dose treatment (100 ng/mouse) resulted in embryotoxic effects (Pietroiusti et al. 2011) whereas intravenous injection of up to 10 µg/mouse of amino-functionalized PEG-SWCNT did not induce any adverse effects (Campagnolo et al. 2013). Only at a dose of 30 µg PEG-SWCNT/mouse occasional fetal malformations such as a delayed development of the paws or head abnormalities were observed (Campagnolo et al. 2013). Exposure of pregnant mice to 10 mg/kg hydroxyl-functionalized CNTs significantly increased the resorption rate, and fetal morphological and skeletal deformations (Philbrook et al. 2011). Similar malformations were observed after the exposure to multi-wall CNTs (Fujitani et al. 2012), which in addition resulted in brain malformations and reduced fetal bodyweight (Huang et al. 2014), a higher abortion rate and reduced placental vasculature among others (Qi et al. 2014).

After treatment of pregnant mice with silica NPs, higher resorption rates, smaller fetuses, and structural and functional abnormalities in the placenta were observed (Yamashita et al. 2011). Furthermore, injection of iron oxide NPs into pregnant mice resulted in increased fetal deaths and resorptions (Di Bona et al. 2014).
Inhalation of CuO NPs during pregnancy resulted in pulmonary inflammations in the pregnant mice, and reduced survival rate and increased numbers of macrophages in the bronchoalveolar lavage fluid of the pups. In contrast, total Cu level in fetuses and placentas as well as histopathological evaluation of placentas did not significantly differ between exposed or control groups (Adamcakova-Dodd et al. 2015).
However, it is difficult to directly compare these *in vivo* animal studies due to differences in the study design or lack of information regarding NP characterization. Moreover, only if we start to understand the underlying mechanisms of NP toxicity at the placental barrier, we will be able to estimate the risks and side-effects but also the chances of such NPs for human applications. The first step in understanding how toxic effects are exerted that are directly caused by NPs, rather than by released ions, starts with revealing their cellular uptake pathways.

1.4.4 Cellular uptake of different nanoparticles

In order to successfully develop safe and site-specific nanomedical applications, it is inevitable to understand how NPs interact and how they are taken up by different cell types or tissues (Petros and DeSimone 2010). Once NPs have entered the body either via the lung, skin, gastrointestinal tract or via intravenous injections, they are able to rapidly reach different targets via the blood stream. Since most NPs are in the same size range as many macromolecules, they may enter cells via the same uptake pathways (Kettiger et al. 2013). Several *in vitro* studies concluded that most NPs entered cells via energy-dependent endocytosis (Canton and Battaglia 2012) or as seen in the case of red blood cells, even passively via diffusion (Rothen-Rutishauser et al. 2006, Wang et al. 2012). Specifically in the placenta, even though it is controversially discussed, NPs may additionally cross the syncytium via transtrophoblastic channels (Semmler-Behnke et al. 2014).

Endocytic uptake pathways

Endocytosis is a vesicular transport mechanism and comprises phagocytosis (‘cell eating’) and pinocytosis (‘cell drinking’). While phagocytosis is performed only by a few specialized immune cells (macrophages/monocytes, neutrophils and dendritic

cells), pinocytosis occurs in almost all eukaryotic cells. Pinocytosis can further be subdivided into macropinocytosis (non-specific), clathrin-mediated endocytosis (CME, receptor-mediated), caveolae-mediated endocytosis (CvME), and alternative pathways (clathrin-/caveolae independent (CIE/CvIE): e.g. flotilin-, Cdc42- and ARF6-mediated), which are distinguished by specific molecular regulators (Canton and Battaglia 2012, Kettler et al. 2014). Uptake via these pathways is restricted to a certain size range, which means that depending on the NP size, they are either phagocytized (> 500 nm), taken up via macropinocytosis (1-2 µm), CME (100-300 nm), CvME (50-80 nm) or CIE/CvIE (< 100 nm) (Canton and Battaglia 2012, Kettiger et al. 2013, Kettler et al. 2014). However, NP size is not the only parameter that has an impact on the cellular uptake mechanism. Other physico-chemical properties such as material, charge, shape, surface functionalization or the protein corona but also the composition of the surrounding media and the cell type are important factors that highly influence NP interactions with biological tissues (Figure 1.10) (Nel et al. 2009, Kunzmann et al. 2011, Zhu et al. 2013). For a detailed literature summary on NP translocation across the placental barrier, please see Chapter 1.1.

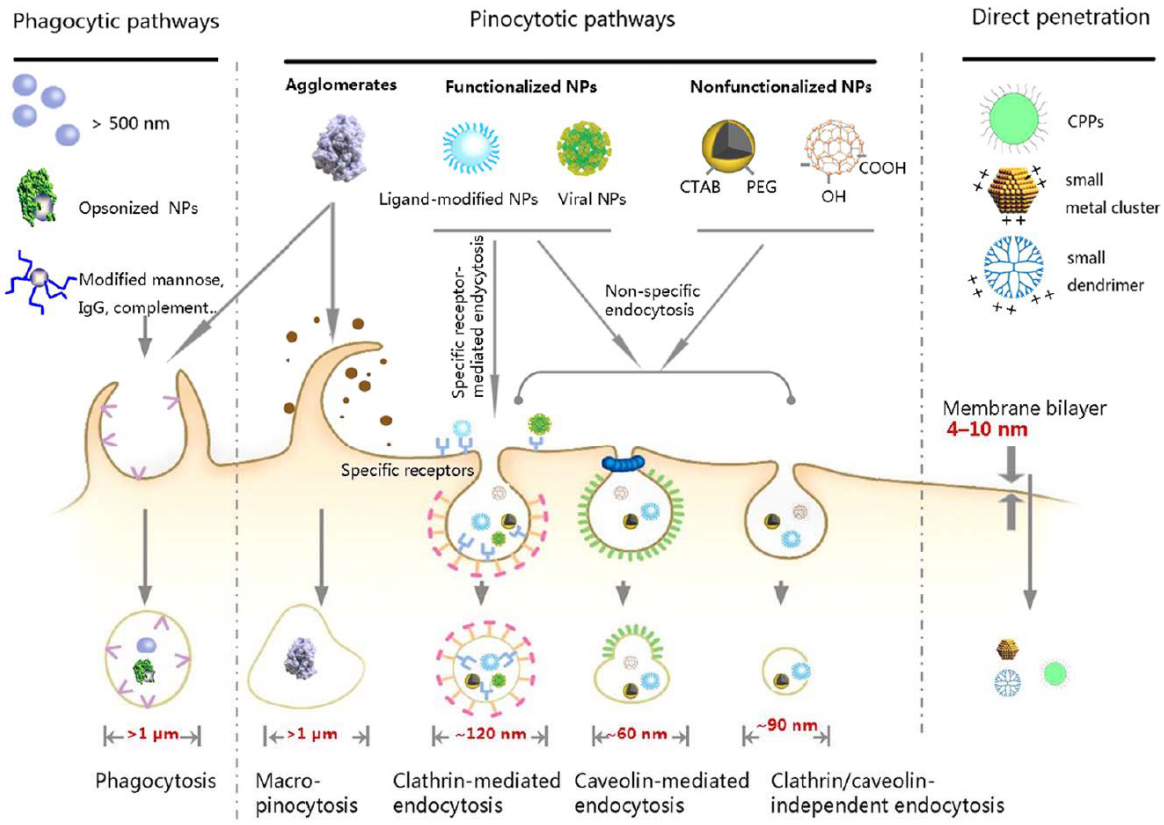

Figure 1.10. Different uptake mechanisms of NPs into cells in dependence of their physico-chemical properties. Figure taken from Zhu et al. (Zhu et al. 2013).

The possible role of actin in endocytosis

In endocytosis, dynamic polymerization of the actin cytoskeleton plays a crucial role. It is assumed that the actin network is involved in different processes such as the invagination of the plasma membrane to form primary endocytic vesicles, vesicle constriction, scission, and vesicle movement (Kaksonen et al. 2006, Galletta et al. 2010, Mooren et al. 2012). At endocytic sites, actin assembles into a network of branched actin filaments, the so-called actin patches. Initially, different proteins (N-WASP, cortactin) attach to the rim of the vesicle coat and activate the Arp2/3-complex, which leads to the nucleation of actin filaments. After the attachment of these filaments to the vesicle coat via actin-binding proteins (HIP1R, EPS15), nucleation continues until a cone of actin filaments is formed that pulls and invaginates the coated plasma membrane (Figure 1.11). Yet, there is no evidence of the exact role of motor proteins (type-I-myosins) in endocytic vesicle formation in mammalian cells (Kaksonen et al. 2006). After vesicle invagination is completed, the highly dynamic actin patches are disassembled by cofilin, actin-interacting protein 1 and coronin (Kueh et al. 2008) in order to remodel the actin cytoskeleton.

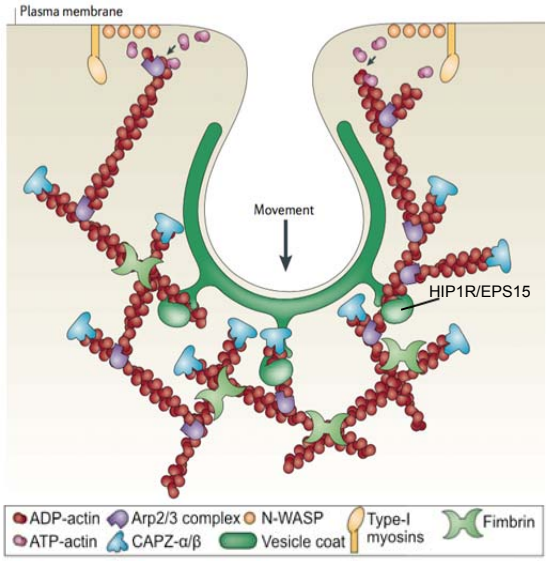

Figure 1.11. Actin-driven endocytosis. N-WASP and cortactin (Arp2/3-complex activating proteins) attach to the rim of the vesicle coat. Subsequent activation of the Arp2/3-complex leads to the crosslinking of actin filaments that grow via the addition of ATP-actin monomers. Fimbrin is responsible for further crosslinking. HIP1R and EPS15 (actin-binding proteins) link the branched actin network to the vesicle coat. CAPZ-α /-β cap older actin filaments at their barbed ends. Figure adapted from Kaksonen et al. (Kaksonen et al. 2006). Abbreviations: Arp, actin-related protein; CAPZ, capping protein muscle Z-line; EPS15, epidermal-growth-factor-receptor-pathway substrate-15; HIP1R, Huntingtin-interacting protein-1 related; N-WASP, neural wiskott aldrich syndrome protein.

Once the endocytic vesicles are internalized, dynamic actin filaments appear in form of “comet tails” on one side of the endosomes and seem to push the endosomes forward. The Brownian-ratchet model explains this mechanism by the addition of ATP-actin monomers to the actin filaments. If there is no space between the actin polymer and the endosome anymore, Brownian motion of the endosome will move it far enough from the actin polymer to enable the addition of a new actin monomer to the filament (Figure 1.12).

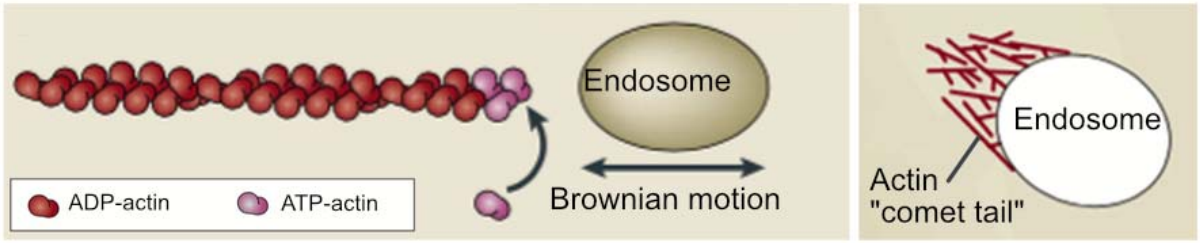

Figure 1.12. Brownian-ratchet model. Brownian motion of intracellular endosomes enables the addition of ATP-actin monomers to the polymerized actin filaments (“comet tails”) in order to push the cargo into the direction of the growing filament. Figure adapted from Kaksonen et al. (Kaksonen et al. 2006).

To conclude, there are several potential pathways for NPs to enter cells. On the other hand, there is the unique opportunity to steer NP uptake via their tunable physico-chemical properties and the possibility to specifically functionalize their surface. In the following review, current knowledge on transplacental translocation of NPs in dependence on their properties and surface functionalization is summarized and evaluated. In addition, the applicability of available placenta models for NP assessments was critically discussed and strategies were suggested on how they could be improved towards a higher *in vivo* predictability.

1.5 Introductory Review

Nanoparticle transport across the placental barrier: pushing the field forward!

Carina Muoth, Leonie Aengenheister, Melanie Kucki, Peter Wick,
Tina Buerki-Thurnherr

Author contribution

In this review, together with L. Aengenheister I summarized, evaluated and verified the literature on how NP physico-chemical properties and surface functionalization may influence their uptake and translocation through the placental barrier. I wrote the chapter *Influence of NP characteristics on placental transfer: is there a trend?*, finalized the tables and revised the manuscript.

Review

For reprint orders, please contact: reprints@futuremedicine.com

Nanomedicine

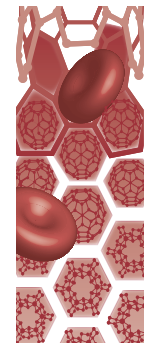

Nanoparticle transport across the placental barrier: pushing the field forward!

Carina Muoth[1], Leonie Aengenheister[1], Melanie Kucki[1], Peter Wick[1] & Tina Buerki-Thurnherr*[,1]

[1]Empa–Swiss Federal Laboratories for Materials Science & Technology, St. Gallen, Switzerland

*Author for correspondence: tina.buerki@empa.ch

The human placenta is a multifunctional organ constituting the barrier between maternal and fetal tissues. Nanoparticles can cross the placental barrier, and there is increasing evidence that the extent of transfer is dependent on particle characteristics and functionalization. While translocated particles may pose risks to the growing fetus particles may also be engineered to enable new particle-based therapies in pregnancy. In both cases, a comprehensive understanding of nanoparticle uptake, accumulation and translocation is indispensable and requires predictive placental transfer models. We examine and evaluate the current literature to draw first conclusions on the possibility to steer translocation of nanoparticles. In addition, we discuss if current placental models are suitable for nanoparticle transfer studies and suggest strategies to improve their predictability.

First draft submitted: 16 December 2015; Accepted for publication: 4 February 2016; Published online: 16 March 2016

Keywords: advanced *in vitro* models • nanoparticle translocation • placenta

Nanoparticle transport across the placental barrier: why should we care?

Selective transport of gases, essential nutrients, metabolic waste products and exclusion of harmful substances are among the key functions of the placental barrier. To fulfill the requirements of a highly effective barrier, a unique polarized epithelial cell layer, the so-called syncytiotrophoblast, is formed during the early days of pregnancy. It constitutes the primary barrier between maternal and fetal tissue and expresses a plethora of specific transporters, which function as either importers or exporters [1–3]. In addition, the chorionic connective tissue and the fetal endothelium supposedly also contribute toward placental barrier function. Nonetheless, the placental barrier does not provide perfect protection to the growing fetus although this was believed for a long time. Since the thalidomide scandal in the 1960's, if not earlier, the awareness of potential harm by drugs has raised and placental transfer has in the meantime been described for many environmental and pharmaceutical compounds [3,4]. Nanomaterials are no exception and recent research indicates that certain nanoparticles (NP) can reach the fetal circulation and accumulate in fetal organs [5–7]. For some NP types such as carbon nanotubes there is evidence of potential teratogenic effects but it is not yet clear if these are caused by translocated particles (direct effects) or due to a release of maternal or placental mediators (indirect effects) [7–9].

Maternal exposure to engineered nanomaterials is not just a fictive scenario anymore but becomes more common with the ever-increasing production and usage of these materials in various consumer products.

On the other hand, engineered nanomaterials are increasingly being used to develop novel medical therapies. Indeed, several examples show that NPs can successfully be applied as drug carriers, for molecular diagnostics or targeted therapy [10,11]. NP-based

Future Medicine part of fsg

medicine offers unique advantages, such as the targeting of specific cells or tissues. NP-based carriers with large surface-to-volume ratio can be decorated with different ligands and/or loaded with cargo in order to minimize dosing and side effects among others [12,13]. In pregnancy, no nanomedical therapies have yet been established; however, the clinical need for improved drug delivery systems with high selectivity and safety is tremendous [13]. Prescription drug use in pregnancy is widespread in many developed countries despite the fact that comprehensive safety and efficacy data for most drugs are essentially missing [13–15]. Alarmingly, the use of medicines with positive evidence of risk (US FDA category D) has been shown to range from 2% (Italy; 2004) to 59.3% (France; 1995–2001) [15]. With regard to unwanted side effects, NP-based drug carriers hold great promise to steer placental translocation, thereby enabling new ways to specifically treat the mother, the fetus or placental complications with reduced or absent off-target effects [13].

The development of novel NP-based therapies in pregnancy requires an in-depth understanding of the mechanisms of placental NP transfer and its dependency on distinct particle characteristics and functionalization, among others (Figure 1). To achieve such a detailed mechanistic insight, we need an efficient and predictive screening strategy, including advanced human *in vitro* and *ex vivo* placenta models. However, it remains to be investigated whether our current models are suitable for investigating the transport of particulate materials across the human placental barrier as these models have originally been established for and validated with small molecules. Additionally, we need to address how these placental models can be modified in order to make them more representative of the *in vivo* situation. An increasing number of studies briefly touch on issues with current models but a clear problem definition or more far-reaching suggestions for improvements are scarce.

This review aims to examine and evaluate whether the available studies already allow first conclusions to be drawn if placental NP translocation can be steered by specific NP properties or functionalization. Based on the outcome of our literature search, we identify major gaps and give recommendations on how to push the field forward. A prerequisite to achieve meaningful results is the use of predictive models and therefore, we will also briefly describe the existing placental transfer models focusing on their suitability for NP transfer studies and give advice on how to improve these models.

Influence of NP characteristics on placental transfer: is there a trend?

To gain a deeper understanding of the role of NP characteristics and functionalization in placental NP transfer, the available published data were collected and grouped according to the studied NP properties including size (Table 1), surface charge (Table 2) or shape. Studies which report the absence of placental transfer were also included (Table 3) as these particles may have potential for the treatment of maternal disorders. However, we did not consider any placental studies that focused on NP toxicity but did not report on their translocation. This grouping approach was applied to more efficiently identify trends, controversial results, gaps as well as needs for future studies.

Size-dependency

Most obviously, size seems to play a major role in placental translocation of different types of NPs including gold, polystyrene (PS) beads, silica, quantum dots and poly(lactic-co-glycolic acid) (PLGA) NPs (Table 1). Almost all studies have in common that the amount of transferred NPs was higher for smaller compared with larger NPs. To give one example, the size of PLGA NPs was shown to influence transfer by the BeWo b30 Transwell model with a 25% higher apparent permeability for 146 nm than for 232 nm PLGA NPs after 2 h of exposure [16]. Importantly, the general trend in size-dependent transfer of NPs was observed for all of the applied models independent of the species origin (rodent vs human) or the complexity (*in vivo* vs *ex vivo* vs *in vitro*).

The cut-off size where no or only very limited amounts of NPs were transferred through the placental barrier appears to be highly dependent on the material. In pregnant rats, gold NPs larger than 80 nm did not cross the placental barrier [17] whereas 519 nm silicon nanovectors were still measured in fetal organs [18]. For PS particles, the threshold size for maternal to fetal transfer was around 200–300 nm in the *ex vivo* human placenta perfusion model [19] and around 100 nm in the BeWo b30 Transwell model [20]. In contrast, transfer of up to 500 nm PS NPs without apparent size-dependency has been observed in pregnant mice by qualitative fluorescent microscopic analysis of fetal tissues [21]. This high variation in the cut-off sizes suggest that there might be differences in the tightness of the placental barrier for NP passage between the different models and it will be crucial to understand in how far these models are predictive of placental translocation in pregnant women. The qualitative analysis of SiO_2 NP transfer in mice revealed a similar cut-off size as for PS NPs. 70 nm but not 300 nm or 1000 nm particles were detected in fetal mouse tissues [22]. In contrast, 519 nm silicon nanovectors were still detected in fetal rat tissues [18]. But even if the same 25 nm SiO_2 NPs were used in the same BeWo b30 Transwell model [23,24], major differences were observed in the translocation

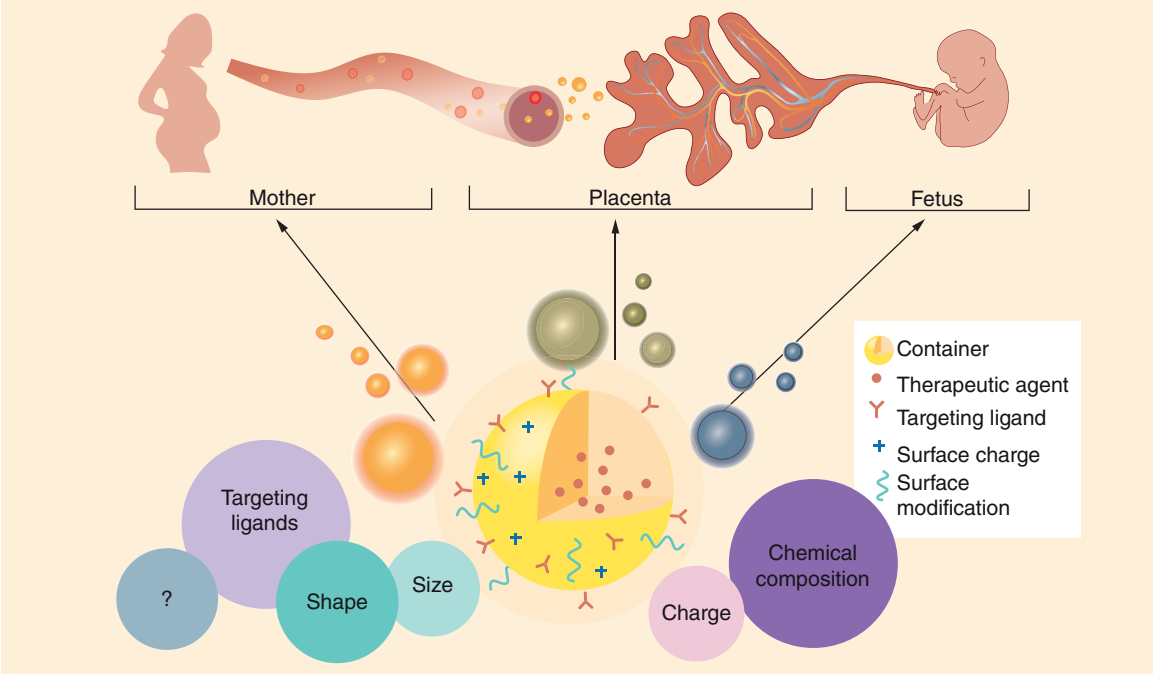

Figure 1. Toward novel nanomedical therapies in pregnancy. Achieving a comprehensive understanding on how NP characteristics such as size, shape, charge, chemical composition and targeting ligands impact on placental accumulation, translocation and biological effects is central to the development of new drug-delivery systems with the objective to preferentially treat the mother, the fetus or placental disorders. The identification of key parameters that allow steering of the particle transfer across the placental barrier is envisaged to greatly reduce off-target effects, which are of particular concern during pregnancy.

rates (P_e: 1.5 × 10^{-6} cm/s [24] versus 0.018 cm/s [23]). It should be noted that the cut-off size for placental translocation of NP might vary significantly between the applied models, especially due to species-specific differences (mice, rats, humans). This clearly shows the need for standardized procedures with regard to NP handling and standardization of the different models to obtain comparable results across different labs.

Interestingly, when looking at the lower size range minor changes in the primary particle size seem to have major effects on placental barrier crossing. For core/shell CdTe/CdS NPs, Chu et al. found a slightly increased transfer of 1.67 nm compared with 3.21 nm NPs [25]. However, the quantification of cadmium-based NPs is notoriously difficult since most analytical methods do not distinguish between free cadmium ions released from quantum dots and quantum dot NPs. This discrimination can probably only be achieved by a thorough characterization of the NP dissolution behavior in the appropriate biological medium combined with the use of advanced analytical methods that are capable of distinguishing ionic and particulate materials with high resolution, such as single-particle ICP-MS or asymmetrical flow field flow fractionation ICP-MS (AF4–ICP-MS) [26,27].

Finally, there were also a few publications confirming translocation of only one particular NP size such as 5.6 nm PAMAM dendrimers [28], <10 nm C^{14}-labeled fullerenes [29], 25–70 nm TiO_2 NPs [22,30], 20 nm ultrasmall superparamagnetic iron oxide particles (USPIO) [31] and 50 nm Ag NPs [32]. Although size-dependency was not explicitly addressed in these studies they were included here because they collectively provide further evidence that relatively small NPs (< 100 nm) of the majority of material classes can cross the placental barrier. Placental translocation was also observed for CNTs with length up to a few micrometers [33,34]. However, as CNTs are nonrigid structures and often are highly entangled, it is challenging to draw any conclusions on size-dependent transfer.

Surface charge-dependency

Besides size, different surface charges have been proposed to influence placental barrier crossing (Table 2). In general, it is often assumed that cellular uptake and translocation of negatively charged NPs is less likely to happen compared with neutral or positively charged NPs, as negatively charged particles may be electrostatically repelled from the negatively charged cell membrane [35]. For example, Grafmueller *et al.* showed in the *ex vivo* perfusion model that transfer of plain 50 nm PS particles was significantly higher than of 50 nm COOH-PS particles [36]. A similar but not significant trend was also observed for plain 220 and

Table 1. Summary of NP transfer studies across the placental barrier in dependence on different sizes.

Size (nm)	NP type	Coating/labeling	ζ-potential (mV)	Model (GD, admin)	Transfer (detection method)	Ref.
146 ± 2[5]	PLGA	Dexamethasone-loaded	-64.3 ± 1.3[1]	BeWo b30 Transwell	P_e: 6.0 × 10^{-5} ± 1.6 × 10^{-5} cm/s after 2 h	[16]
232 ± 1[5]	PLGA	Dexamethasone-loaded	-63.1 ± 1.1[1]	BeWo b30 Transwell	P_e: 4.8 × 10^{-5} ± 1.6 × 10^{-5} cm/s after 2 h	
145 ± 1[5]	PLGA	-/coumarin–6	-46.7 ± 1.7[1]	BeWo b30 Transwell	P_e: ~6 × 10^{-6} cm/s after 2 h	
196 ± 2[5]	PLGA	-/coumarin–6	-47.8 ± 1.1[1]	BeWo b30 Transwell	P_e: ~3 × 10^{-6} cm/s after 2 h	
1.4	Au	S-TPP/^{198}Au	-20 ± 2.4[1]	Rat (18, iv.)	30 ng (1.2 × 10^{11} NPs) after 24 h	[17]
18	Au	S-TPP/^{198}Au	-22.8 ± 3.1[1]	Rat (18, iv.)	0.12 ng (2.4 × 10^{6} NPs) after 24 h	
80	Au	S-TPP/^{198}Au	-27.1±1.3[1]	Rat (18, iv.)	<LOD after 24 h	
519	Si	-/fluorescein	-31.4 ± 0.8[2]	Rat (20, iv.)	5.93 ± 0.67 µg/g tissue after 4 h	[18]
834	Si	-/fluorescein	-41.5 ± 0.28[2]	Rat (20, iv.)	No transfer	
1000	Si	-/fluorescein	-53.2 ± 1.1[2]	Rat (20, iv.)	No transfer	
70	SiO_2	-/-	-52.7[1]	Mouse (16,17, iv.)	NPs in placenta and fetus after 48 h (qualitative)	[22]
300	SiO_2	-/-	-62.1[1]	Mouse (16,17, iv.)	NPs not detected in placenta and fetus after 48 h (qualitative)	
1000	SiO_2	-/-	-67.0[1]	Mouse (16,17, iv.)	NPs not detected in placenta and fetus after 48 h (qualitative)	
15–30	SiO_2	-/rhodamine	-20[1]	BeWo b30 Transwell	26.2 ± 0.8% of ID; P_e: 0.018 ± 0.007 cm/s after 6 h	[23]
25–50	SiO_2	-/rhodamine	-22[1]	BeWo b30 Transwell	29.0 ± 8.9% of ID; P_e: 0.017 ± 0.009 cm/s after 6 h	
25	SiO_2	-/rhodamine	ND	BeWo b30 Transwell	P_e: 1.54 × 10–^{6} ± 1.56 × 10–^{6} cm/s after 24h	[24]
25	SiO_2	-/rhodamine	ND	Human term placenta perfusion	4.2% ± 4.9% of ID after 6 h	
50	SiO_2	-/rhodamine	ND	Human term placenta perfusion	4.6% ± 2.4% of ID after 6 h	
50	PS	-/yellow	-58.7 ± 2.26[1]	Human term placenta perfusion	8.90 ± 1.80 µg/ml after 3 h	[19]
80	PS	-/Fluoresbrite®	-56.4 ± 2.12[1]	Human term placenta perfusion	7.47 ± 1.77 µg/ml after 3 h	
240	PS	-/yellow	-32.7 ± 0.78[1]	Human term placenta perfusion	2.03 ± 0.29 µg/ml after 3 h	
500	PS	-/Fluoresbrite®	-42.3 ± 0.49[1]	Human term placenta perfusion	0.31 ± 0.21 µg/ml after 3 h	
50	PS latex	-/Fluoresbrite®	ND	BeWo b30 Transwell	3.5% of ID after 24h; P_e: 3.8 ± 1.1 × 10^{-5} cm/s after 2 h	[20]
100	PS latex	-/Fluoresbrite®	ND	BeWo b30 Transwell	0.6% of ID after 24h; P_e: 1.8 ± 0.7 × 10^{-5} cm/s after 2 h	

NP size is given as the primary particle size unless in few cases where only the NP hydrodynamic diameter determined by DLS were reported (5). Zetapotential was either measured in H_2O (1), saline (2), maternal perfusate (3) or sodium citrate dihydrate (4).
GD: Gestational day; ID: Initial dose; iv.: Intravenous injection; MPA: 3-Mercaptopropionic acid; ND: Not determined; P_e: Permeability coefficient; PEG: Polyethylene glycol; PLGA: Poly(d, l-lactide-coglycolide); PS: Polystyrene; QDs: Quantum dots; S-TPP: Sulfonated triphenylphosphine.

Table 1. Summary of NP transfer studies across the placental barrier in dependence on different sizes (cont.).

Size (nm)	NP type	Coating/labeling	ζ-potential (mV)	Model (GD, admin)	Transfer (detection method)	Ref.
20	PS	COOH/yellow green	ND	Mouse (17, iv.)	NPs in placenta and fetus after 4h (qualitative)	[21]
40	PS	COOH/yellow green	ND	Mouse (17, iv.)	NPs in placenta and fetus after 4 h (qualitative)	
100	PS	COOH/yellow green	ND	Mouse (17, iv.)	NPs in placenta and fetus after 4 h (qualitative)	
200	PS	COOH/yellow green	ND	Mouse (17, iv.)	NPs in placenta and fetus after 4 h (qualitative)	
500	PS	COOH/yellow green	ND	Mouse (17, iv.)	NPs in placenta and fetus after 4 h (qualitative)	
1.67 ± 0.29	CdTe/CdS QDs	MPA/-	ND	Mouse (20–22, iv.)	20.69 ±7.23 ng Cd/g tissue	[25]
2.59 ± 0.43	CdTe/CdS QDs	MPA/-	ND	Mouse (20–22, iv.)	14.22 ±1.97 ng Cd/g tissue	
3.21 ± 0.32	CdTe/CdS QDs	MPA/-	ND	Mouse (20–22, iv.)	13.20 ± 3.24 ng Cd/g tissue	
0.5–2 µm × 1–2 nm	SWCNT	Amine/-	-1.3[5]	Mouse (10.5, 12.5,15.5, iv.)	20% of id/g in fetal liver 5% of id/g in placenta after 48 h	[33]
0.5–2 µm × <8 nm	MWCNT	Amine/-	-1[5]	Mouse (10.5, 12.5,15.5, iv.)	20% of id/g in fetal liver 5% of id/g in placenta after 48 h	
0.5–2 µm × 20–30 nm	MWCNT	Amine/-	-1.9[5]	Mouse (10.5, 12.5,15.5, iv.)	20% of id/g in fetal liver 5% of id/g in placenta after 48 h	
0.5–2 µm × 50 nm	MWCNT	Amine/-	-1.5[5]	Mouse (10.5, 12.5,15.5, iv.)	20% of id/g in fetal liver 5% of id/g in placenta after 48 h	
5.6	G4PAMAM	Neutral hydroxyl groups/Alexa 488	-8.23[3]	Human term placenta perfusion	2.26 ± 0.12 µg /ml after 5.5 h	[28]
<10	fullerenes	-/^{14}C radioactive	ND	Rat (15, iv.)	0.872 ± 0.213% of id after 24 h	[29]
25–70	TiO_2	-/-	ND	Mouse (3,7,10,14, subcutan)	NPs in fetal brain and testis (qualitative)	[30]
35	TiO_2	-/-	-22.5[1]	Mouse (16,17, iv.)	NPs in placenta and fetus after 48 h (qualitative)	[22]
20	USPIO	COOH, conjugated to anti-C3 Antibodies	ND	Mouse (15/ iv.)	NPs in placenta and fetal brain after 12–24 h (qualitative)	[31]
50	Ag	-/-	-29[4]	Mouse (7–9, i.v.)	0.008–0.009% of id	[32]
1–2 µm × 10–30 nm	oMWCNTs	-/^{99m}Tc	–	Mouse (17, i.v.)	0.5% of id/g after 2–24 h	[34]

NP size is given as the primary particle size unless in few cases where only the NP hydrodynamic diameter determined by DLS were reported (5). Zetapotential was either measured in H_20 (1), saline (2), maternal perfusate (3) or sodium citrate dihydrate (4).
GD: Gestational day; ID: Initial dose; iv.: Intravenous injection; MPA: 3-Mercaptopropionic acid; ND: Not determined; P_e: Permeability coefficient; PEG: Polyethylene glycol; PLGA: Poly(d, l-lactide-coglycolide); PS: Polystyrene; QDs: Quantum dots; S-TPP: Sulfonated triphenylphosphine.

290 nm COOH-PS beads [36]. And while no particle translocation was observable for negatively charged poly(acrylic acid)-coated iron oxide NPs, a substantial increase in iron content was detected in the fetal liver of newborn mice after exposure to positively charged iron oxide NPs coated with polyethyleneimine [37]. However, it remains unclear if this increase in total iron content was from transferred NPs (Fe_2O_3) or Fe^{3+}. In a study in pregnant mice, already slight differences in the surface charge of gold NPs obtained

by functionalization with ferritin, PEG or citrate led to a charge-dependent transfer of the particles with the lowest transfer observed for the most negatively charged particles [38]. Interestingly, there are also few examples that describe a higher transfer for particles with a more negative charge. Around 25% of the initial dose of iron oxide NPs with a sodium oleate micelle coating and a negative zeta potential was passing through the BeWo b30 Transwell model while plain iron oxide NPs were not identified in the basolateral compartment [23]. However, the latter particles apparently formed agglomerates, which presumably then blocked the pores of the membrane thus making it difficult to draw any conclusion on a charge-dependent transfer. In addition, sodium oleate functionalization renders the particles more hydrophobic hence potentially introducing a confounding factor. Another study using the BeWo b30 Transwell model observed that the apparent permeability of coumarin-6-loaded PLGA NPs was one order of magnitude lower as for dexamethasone-loaded PLGA NPs even though the zeta potential of coumarin–6-loaded NPs was higher [16]. Since the plain PLGA particles were not modified with functional groups, the different surface charges were probably due to the incorporated drugs. As long as it is not clear in how far these drugs may induce additional unexpected effects on NP translocation, it might be advisable to focus such mechanistic translocation studies on particles that are not loaded with any pharmaceutical compounds. Increased transfer of negatively charged particles was also observed in a study using positively and negatively charged PS particles [39]. However, there was an apparent conflict within the study as two PS NPs with a very similar negative charge showed completely different transfer behavior (high vs no transfer). The authors suggested that this difference was due to different chemical compositions of the coatings used by the two providers, indicating that the effect cannot solely be explained by surface charge. Finally, 70 nm plain, NH_2- and COOH-SiO_2 NPs were found to cross the placental barrier in mice as confirmed by TEM micrographs [22]. Since a quantitative analysis is lacking, this study does not provide further insight into surface charge-dependent placental NP transfer. Despite the general assumption that positively charged particles show higher translocation rates than negatively charged particles, we could not clearly identify this trend in the available literature. It should be noted that the induction of charges by functionalization of the particles is often connected with changes in other surface characteristics such as hydrophobicity/hydrophilicity, among others, which can further impact the particle translocation. To resolve the impact of charge-dependency on NP translocation more studies are required including a larger variety of NPs.

Shape-dependency

To date, shape-dependent NP translocation has not been directly evaluated for the placental barrier but may be of interest especially when considering recent studies showing a shape-dependent uptake of different NPs in conventional 2D cell cultures [40,41]. Especially antigen-sampling cells such as macrophages are able to recognize the shape of different NPs. Recently it has been shown that the uptake of different silica nanoparticle geometries [42], as well as of fiber-shaped particles and chain-forming bacteria by macrophages was dependent on the orientation of the particles to the cellular surface [43,44]. Therefore it is expected that shape might have a significant impact on the translocation behavior. Although maternal to fetal transfer has been observed for spherical as well as for fiber-shaped NPs [33,34], the influence of NP shape on placental translocation remains largely unknown and deserves further investigations. The emergence of 2D materials with sheet-like geometry such as graphene oxide and their potential biomedical application [43–45] further increases the diversity of nanomaterials, which can interact with biological barriers such as the placental barrier. A systematic approach using well-defined NP libraries with controlled sizes and shapes may be very effective to understand whether different shapes can provide an effective means to preferentially target the placenta, maternal or fetal circulation.

No placental transfer

A common problem for the quantification of NP transport is the low sensitivity of many analytical methods. Therefore, the proof of absence of NP transfer is challenging but as new analytical techniques such as AF4–ICP-MS have been developed, it is expected that detection limits will be significantly improved in the near future (see [5] for a recent overview on analytical techniques to quantify and characterize NP translocation).

So far, there are only few studies that suggested the absence of placental translocation (Table 3). No fetal uptake has been observed for 90 nm fluorescently capped single walled carbon nanotubes (SWCNTs) [8], 46 nm hydroxyl functionalized SWCNTs [46], 11 and 15 nm CdO NPs [47], 10, 15 and 30 nm PEG-Au NPs [48], 20 and 49 nm Au NPs [49] or 21 nm UV-Titan L181 [50]. Nevertheless, embryotoxicity was observed after both, exposure to CdO NPs [47] and SWCNTs [8,46]. However, it was difficult to identify a trend that would help to guide the design of novel

particles without placental transfer. The type of NP (i.e. CNT, CdO Au or TiO_2) or the size of the particles (< 100 nm) is probably not related to the lack of transfer as placental crossing has been detected for other Au, MWCNT or TiO_2 NPs of similar sizes (Table 1). Since no zeta potential values were provided in the studies summarized in Table 3, no correlation to surface charge was possible either.

We finally want to briefly reflect on some challenges we were facing while trying to allocate each study to an appropriate group and to identify underlying trends. The grouping was not always straightforward due to the fact that size, surface charge and shape were often partially interconnected [51,52]. Without systematic studies using more appropriate NPs varying in only one individual characteristic (NP libraries), it will not be possible to achieve a comprehensive understanding on the contribution of each factor toward placental transfer. Furthermore, we realized that many aspects with potential relevance for NP transfer such as the role of the protein corona or NP dosimetry remain largely untouched in this particular research field.

Future research on placental NP transfer: what are the urgent needs?

From our grouping approach where we tried to identify characteristics that may enable to control NP translocation at the placental barrier it was evident that a comparison of the available literature is very challenging. Reasons for that were insufficient NP characterization data, incomplete study description or different experimental conditions and models, among others. Moreover, many studies focused on potential embryotoxic effects of environmentally relevant NPs whereas translocation was not or only marginally addressed. Therefore, if we want to efficiently push our knowledge on how NP characteristics affect placental uptake, accumulation and transport we have to move on from rather descriptive investigations to more mechanistic transfer studies applying well-characterized NPs varying in either size, shape, surface chemistry or coating. The generation of NP libraries with a high degree of control over NP size or surface charge was already achieved [53,54] but whether such NP libraries can be obtained for each property is unclear.

Besides understanding how NP characteristics influence placental transport, it will be essential to achieve a comprehensive insight into the mechanisms underlying this transfer. Research in this direction is very limited and seemingly controversial results further complicate the picture. Since a variety of different placental transporter inhibitors did not result in any major influence on the translocation of positively or negatively charged 50 nm PS NPs in the BeWo transfer model, it was concluded that the translocation of these NPs preferentially occurs by passive diffusion [39]. In contrast, bidirectional *ex vivo* perfusion studies have shown an increased transfer of similar 50 nm PS particles in the fetal to maternal direction, which suggested the involvement of an active, energy-dependent pathway [36]. Active transport has also been proposed for gold NPs across the mouse placenta due to the increased amount of intracellular vesicles and an upregulation of clathrin- and caveolin-protein levels in the syncytiotrophoblast and fetal endothelial cells [49]. Predominant accumulation of particles in the syncytiotrophoblast layer has also been described for PS particles of different sizes and surface charge [36] raising the hypothesis that the syncytiotrophoblast may have a pivotal role in the regulation of NP translocation. Besides the use of inhibitors of different receptors, transporters and uptake pathways that can be problematic due to their low specificity or potential cytotoxicity, systems biology approaches such as transcriptomics or proteomics studies may help to identify novel candidates involved in NP translocation across the placental barrier [55]. Furthermore, newly emerging detection methods should be considered for future studies in order to achieve higher sensitivity in NP detection and to obtain accurate and quantitative transfer data (see [5] for an overview).

Another important aspect in NP passage across the human placenta is the role of the biocorona. In a biological environment, NPs will instantly acquire a corona of various biomolecules on their surface, which will have a major impact on their biological behavior [56]. The amount and type of biomolecules adsorbing to an NP surface has been shown to be dependent on the NP characteristics [57]. Therefore, it will be important to understand how the biocorona forms and evolves during the translocation across the placental barrier in particular when we aim to develop nanomedical treatments that target a specific placental or fetal tissue [58,59]. It was even proposed that the biocorona itself may be used to direct biological behavior and target diseases instead of chemical grafting [60]. Currently, there is only one *in vitro* placental transfer study that assessed the NP protein corona in cell culture medium [39]. Major differences were mainly found in the amount but not in the nature of the proteins in the corona of the differently charged PS NPs, which is in contrast to a previous work where surface properties had a significant impact on the composition of the protein corona [61]. To better approach the *in vivo* situation, future studies should try to use more complex, organotypic placental models and include human plasma pretreatment of the NPs to obtain a relevant protein corona.

Table 2. Summary of NP transfer studies across the placental barrier in dependence on different surface charges.

Size (nm)	NP type	Coating/ labelling	ζ-potential (mV)	Model (GD, admin)	Transfer (detection method)	Ref.
43.7 ± 8	PS	Neutral/yellow green	-19.8 ± 4.0[2]	Human term placenta perfusion	13.7 ± 8.4% of id after 6h	[36]
44.1 ± 7.1	PS	COOH/yellow green	-34.7 ± 7.1[2]	Human term placenta perfusion	1.4 ± 0.5% of id after 6h	
220.5 ± 5.1	PS	Neutral/yellow green	-20.5 ± 2.7[2]	Human term placenta perfusion	2.4 ± 0.7% of id after 6h	
289.4 ± 10.2	PS	COOH/yellow green	-55.6 ± 6.1[2]	Human term placenta perfusion	1.2 ± 0.7% of id after 6h	
56.5 ± 3.02[4]	PS (Magsphere)	NH_2/red	51.0[1]	BeWo b30 Transwell	P_{app}: 0.3 × 10^{-6} cm/s after 24 h	[39]
52.4 ± 0.1[4]	PS (Polyscience)	COOH/yellow green	-58.3[1]	BeWo b30 Transwell	P_{app}: 13 × 10^{-6} cm/s after 24 h	
50.4 ± 1.74[4]	PS (Magsphere)	COOH/red	-55.5[1]	BeWo b30 Transwell	No detection after 24 h	
28[4]	Fe_xO_y	PAA/-	-52[1]	Mouse (9–16, ip)	No accumulation of iron in fetus	[37]
30[4]	Fe_xO_y	PEI/-	51[1]	Mouse (9–16, ip)	Sign. accumulation of iron in fetal liver only after multiple doses (8 consec. days)	
10 × 7	Fe_3O_4	Neutral/-	-2.8[1]	BeWo b30 Transwell	No transport after 24 h	[23]
9 × 7	Fe_3O_4	Na-oleate micelle/-	-31.9[1]	BeWo b30 Transwell	24.1 ± 3.0% of id; P_e: 0.017 ± 0.002 cm/s after 6h	
~13	Au	Ferritin/-	-1.6[3]	Mouse (7.5 or 11.5, i.v.)	E7.5: ~0.8% of ID; E11.5: ~0.06% after 5h	[38]
~13	Au	PEG/-	-6.0[3]	Mouse (7.5 or 11.5, i.v.)	E7.5: ~0.6% of ID; E11.5: ~0.02% after 5h	
~13	Au	Citrate/-	-17.0[3]	Mouse (7.5 or 11.5, iv.)	E7.5: ~0.1% of id; E11.5: ~0.02% after 5 h	
145 ± 1[4]	PLGA	-/coumarin-6	-46.7 ± 1.7[1]	BeWo b30 Transwell	P_e: ~6 × 10^{-6} cm/s after 2 h	[16]
146 ± 2[4]	PLGA	Contains dexamethasone	-64.3 ± 1.3[1]	BeWo b30 Transwell	P_e: 6.0 × 10^{-5} ± 1.6 × 10^{-5} cm/s after 2 h	
70	SiO_2	-/-	-52.7[1]	Mouse (16,17, iv.)	NPs in placenta and fetus after 48 h (qualitative)	[22]
70	SiO_2	COOH/-	-76.3[1]	Mouse (16,17, iv.)	NPs in placenta and fetus after 48 h (qualitative)	
70	SiO_2	NH_2/-	-29.0[1]	Mouse (16,17, iv.)	NPs in placenta and fetus after 48 h (qualitative)	

NP size is given as the primary particle size unless in few cases where only the NP hydrodynamic diameter determined by DLS were reported (4). Zetapotential was either measured in H_20 (1), NaCl (2) or PBS (3).
GD: Gestational day; ID: Initial dose; ip: Intraperitoneal; iv.: Intravenous injection; MPA: 3-Mercaptopropionic acid; nd: Not determined; PAA: Poly(acrylicacid); P_e: Permeability coefficient; P_{app}: Apparent permeability (= P_e but no correction for blank); PEG: Polyethylene glycol; PEI: Polyethyleneimine; PLGA: Poly(D,L-lactide-coglycolide); PS: Polystyrene; QD: Quantum dot.

Finally, translocation of NPs is likely to be dependent on the different stages of pregnancy [62]. In the first trimester, the placental barrier is very thick in order to protect the developing embryo and becomes thin at term when substantial amounts of nutrients are required to sustain fetal growth [6]. The very sparse studies on NP translocation in early pregnancy use pregnant mice that have been exposed before the placenta has been completely matured (<gestational day 10) [38]. In general, placental transfer appears to be higher in early pregnancy [8,38]. However, to prevent uncertainties associated with species-specific differences, there is a need for the development of human models for NP transfer studies in early pregnancy. Although *ex vivo* perfusion of a first trimester placenta is technically feasible, it is not very attractive due to the

limited access to such placental tissues. Transwell systems may be a starting point to develop a first trimester model by changing to appropriate cell types representative of early pregnancy. In fact, the ideal placental transfer model would combine some of the following features: a reasonable throughput to test a large set of NPs, suitability for mechanistic NP transfer studies, possibility of extended NP exposure times and a high predictive value for human placental transfer at different stages of pregnancy.

Current placental transfer models: are they applicable to NP transfer studies?

Although a variety of placental models are currently available, only few are suited for translocation studies. These include *in vivo* transfer studies in rodents, *ex vivo* perfusion of human term placenta as well as *in vitro* transfer studies across a trophoblastic monolayer grown on a microporous membrane. Recent reviews comprehensively summarized the existing models and approaches to study the translocation and biological effects of xenobiotics at the human placenta [5,6,63–66]. Here, we focused on the suitability of these placental transfer models for NP translocation studies.

In vivo models

Exposure of pregnant rodents can provide important information on the biodistribution of NPs in a living organism including potential translocation to the fetus. However, the placenta is the most species-specific organ within the class of mammals [67,68]. Although the placenta fulfills the same functions across species, there are substantial differences in placental development, architecture, function and pathology between rodents and humans. Therefore the extrapolation from animal data to humans is challenging and needs an in-depth evaluation [63]. However, obtaining translocation data from pregnant women is difficult and probably only possible for certain therapeutic drugs where noninvasive clinical studies are available. In the case of NPs, an approximate estimation of the predictive value of animal models may be achieved by comparing the transfer of the same NPs during late-gestation in animals and in the *ex vivo* perfusion of human term placenta.

Ex vivo perfusion model

The most prominent placental model besides pregnant rodents is the dually perfused *ex vivo* human placenta model developed in 1967 [69]. This model was continuously improved over the last years [70,71] and has been shown to reliably predict placental transfer of therapeutic drugs at term when adjusting for extra parameters [64]. Since 2008, *ex vivo* placental perfusion studies have also been carried out with NPs, providing transfer data of high *in vivo* relevance at least for term pregnancy. It will be challenging but imperative to understand the predictive value of *ex vivo* perfusions for NP transfer studies as one cannot assume that NPs will exactly behave like small molecule compounds [72]: the uptake and biodistribution of NPs can differ significantly as compared with small molecules since the uptake mechanisms of NPs are not yet fully understood and depend on the NP properties, the particle surface can trigger chemical reactions such as the formation of a biocorona, the material properties (crystallinity, shape, allotropic form, etc.) can influence the biological response (for further reading see [51]), the high agglomeration propensity of NPs can have a significant influence on their placental transfer (for further reading see [73]).

In addition, it will be important to exclude any interferences of NPs with the *ex vivo* perfusion model. We have recently shown that NPs can cause artifacts which were related to particle agglomeration, functionalization and stability of the fluorescent labels (see [74] for a detailed description). To give one example, it has been observed that PS NPs lost a significant amount of their fluorescent marker only after contact with the placental tissue but not in conventional *in vitro* control experiments [74].

In vitro transfer models

To enable transfer studies across one or multiple cell layers, placental cells have been grown to confluence on the apical and/or basolateral side of commercial microporous membranes, vitrified collagen membranes [75,76] or the amniotic membrane [77]. While the latter two supports can be used to study the transfer of small molecules such as glucose or small molecule drugs, they will most likely constitute a considerable barrier to the transfer of NPs. Up to now, all *in vitro* transfer studies with NPs have been performed in the BeWo b30 Transwell model [16,20,23,24,39]. This model is capable of predicting similar relative placental transfer compared with the *ex vivo* placental perfusion model at least for small compounds [78,79]. However, the transfer rate was much slower in the BeWo b30 Transwell model compared with the *ex vivo* perfusion system, probably due to the lack of fluid flow [79]. Whether this *in vitro* model is also predictive for the transfer of NPs is not yet clear [80]. First comparative studies showed a limited transport of SiO_2 NPs [24] as well as a size-dependent transfer of PS NPs in both models [19,20]. But there are increasing concerns that the commercial microporous membranes may cause major problems for the study of NPs such as blocking of the pores, NP absorption to the membrane material or very slow transport across

Table 3. Summary of NP transfer studies that did not detect transfer of NPs across the placental barrier and accumulation in fetal tissue.

Size (nm)	NP type	Coating/ labeling	Model (GD, admin)	Transfer (detection method)	Ref.
90	SWCNTs	PEG/Seta750	Mouse (5.5 or 14.5, i.v.)	No transfer detected after 24h (qualitative)	[8]
5–30 µm × 1–2 nm	SWCNTs	Hydroxyl group/-	Mouse (9, gavage)	No transfer detected on GD 19 (TEM)	[46]
11.0 ± 0.1	CdO	-/-	Mouse (4.5–16.5, inhalation)	No transfer detected on GD 17.5 (ICP-MS, gAAS)	[47]
15.3 ± 0.1	CdO	-/-	Mouse (4.5–16.5, inhalation)	No transfer detected at GD 17.5 (ICP-MS, gAAS)	
10	Au	PEG/-	Human term placenta perfusion	No transfer detected after 6 h (ICP-MS, qualitative)	[48]
15	Au	PEG/-	Human term placenta perfusion	No transfer detected after 6 h (ICP-MS, qualitative)	
30	Au	PEG/-	Human term placenta perfusion	No transfer detected after 18 min (ICP-MS, qualitative)	
19.6	Au	-/-	Mouse (16/17, iv.)	No transfer detected after 48 h (ICP-MS)	[49]
49.3	Au	-/-	Mouse (16/17, iv.)	No transfer detected after 48 h (AMG)	
20.6 ± 0.3	UV-Titan L181	Polyalcohols/-	Mouse (8–18, inhalation)	<LOD after 5 or 26–27 days (ICP-MS)	[50]

AMG: Autometallography; gAAS: Graphite furnace atomic absorption spectroscopy; GD: Gestational day; iv.: Intravenous injection; LOD: Level of detection; PEG: Polyethylene glycol.

the empty membrane [24,81–83]. It is obvious that pore size is a critical parameter in particle transport that allows or restricts the passage of NPs or NP agglomerates of a certain size. For example, 0.4 µm pores extensively restricted the passage of 37 nm PS NPs [20] or 12 nm TiO_2 NPs [84] across the membrane. In addition, the distribution of pores in the membrane supports is rather random, which may prevent efficient NP transport across the membrane. Furthermore the surface properties of the membrane may attract or repel NPs, for example, based on their hydrophilicity/hydrophobicity or surface charge, leading to an inefficient transport and accumulation of the particles on the membrane surface [83]. Another shortcoming of the available commercial membranes is their rather large thickness of around 10–20 µm, which is in fact comparable to or higher than the thickness of a cell monolayer. Therefore, the ideal situation of short diffusion pathways is not given, and the pores should not be regarded as small holes but rather as relatively long tunnels, which NPs have to cross. Moreover, these tunnels are not strictly perpendicular to the membrane plane but in part follow slightly different angles (Figure 2). This in turn results in an increase in pore channel length and therefore leads to a nonhomogeneous travel distance for particles taking different routes through the membrane. In summary, *in vitro* transfer models will be important to prescreen the large variety of NPs and to allow mechanistic transfer studies but they need further improvements to increase their predictive value.

Next-generation placental transfer models: plenty of room for improvements?

Ex vivo perfusion model

To date, each laboratory is using its own customized placental perfusion setup and performs perfusions with its own modifications of the original protocol [85]. Although many parameters (e.g., glucose consumption, lactate production, pH, oxygen consumption) and control substances (e.g., antipyrine, FITC-dextran) are described to confirm tissue integrity and viability, there is no obligation to use a certain standard set of parameters and controls. Therefore, Mathiesen et al. have proposed a set of criteria to confirm successful perfusions [85]. But even better than detailed recommendations for the quality assessment of the individual placental perfusion protocols would be the implementation of standard operating procedures and a more standardized perfusion setup to improve interlaboratory comparisons and to increase the acceptance of the model by the broader research community and the regulatory bodies.

In vitro transfer models

Up to now, all *in vitro* NP translocation studies have been performed with cell lines, which may only have restricted capability to express all necessary functions and transporters or fail to form a functional syncytium. To overcome these limitations, cell lines should be replaced by human placental villous trophoblasts isolated from term placenta. In addition, there is evi-

dence from other barriers that the co-culture of different cell types has a major effect on NP uptake and translocation [84,86]. Therefore, inclusion of additional cell types (e.g., fetal endothelial cells, villous fibroblasts or Hofbauer macrophages) may allow mimicking of *in vivo* placental translocation more closely by enabling the interplay of relevant cell types and a more 3D tissue-like organization. For mechanistic studies on NP uptake pathways, development of 3D placental microtissues could be an interesting approach as cells would not be separated by a membrane support [87]. Another strategy to increase the predictability of *in vitro* transfer models is to move from static to dynamic culture conditions. Most recently it has been demonstrated that trophoblasts respond to fluid shear stress with induction of microvilli formation, changes in Ca^{2+} influx, *in vivo*-like localization of the GLUT1 membrane transporter as well as altered glucose uptake and transport [76].

Furthermore, there is a need for improved membranes that are readily permeable to NPs or NP agglomerates, which likely are formed within biological fluids or inside the cells. Parameters for potential modification include pore size, distribution and density as well as membrane thickness and composition. The pore size should be as large as possible to allow the fast passage of NPs or small agglomerates but small enough to prevent unwanted cell migration through the pores. A homogenous pore distribution and high pore density is also expected to improve NP transfer across microporous membranes. Reducing the membrane thickness is likely to improve NP crossing due to considerably lower diffusion times and reduced particle attachment to the channel walls, which in turn can lead to clogging of the membrane pores preventing further NP transport. However, the thickness of the membrane is directly linked to the mechanical properties of the membrane. As the membrane has to act as a support for the attachment and growth of cells, membranes for *in vitro* experiments have to comprise certain stability under the load of cells and liquid as well as during experimental handling. A first attempt to achieve improved membranes was the development of 500 nm thick silicon-nitride supports with ordered arrangements of pores that should allow easy and rapid NP transport [88]. The final

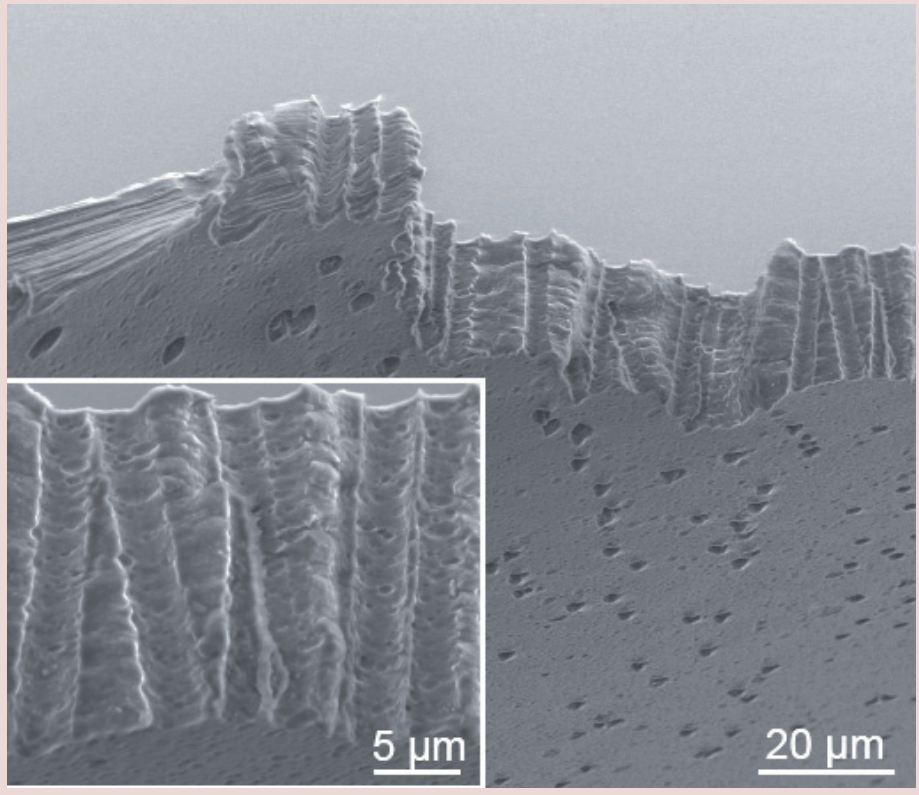

Figure 2. Example of a microporous membrane frequently applied for in vitro **translocation studies.** SEM images of a PET membrane of ThinCert™ Cell Culture Inserts (12 Well, Greiner Bio-One GmbH) with 3.0 µm pore size showing morphological features such as membrane thickness, course of pore channels and irregular pore distribution. Image courtesy of Dr. Marcus Koch, Head of Physical Analysis at the INM – Leibniz-Institute for New Materials gGmbH, Saarbruecken, Germany.

challenge will be to identify materials with optimal surface properties that support the attachment and growth of cells, while simultaneously preventing the adhesion of nanomaterials.

To summarize, there are several possibilities for the improvement of placental translocation models (Figure 3). Nevertheless, it needs to be shown which factors have the highest impact on particle translocation and which parameters are important to achieve predictive results.

Conclusion & future perspective

Studying translocation of NPs across the placental barrier is a relatively new research field as the initial focus was set on those biological barriers that would first get into contact with NPs such as the lung, GI tract or the skin. With the recognition of the large potential of NPs for medical applications, internal barriers become increasingly important. A comprehensive understanding of the uptake, accumulation, translocation and effects of NPs at the human placenta is compulsory for the development of novel nanomedical therapies to treat maternal, fetal or placental disorders with reduced off-target effects. The clinical need for new approaches to deliver drugs in pregnancy is substantial [13] and therefore research on the placental transfer of NPs is a relevant and timely endeavor. In the last decade, a considerable amount of work has been performed on the translocation of various NPs at the placental barrier. It is encouraging to see that it may indeed be possible to steer NP translocation across the placental barrier by the choice of NP properties and functionalization.

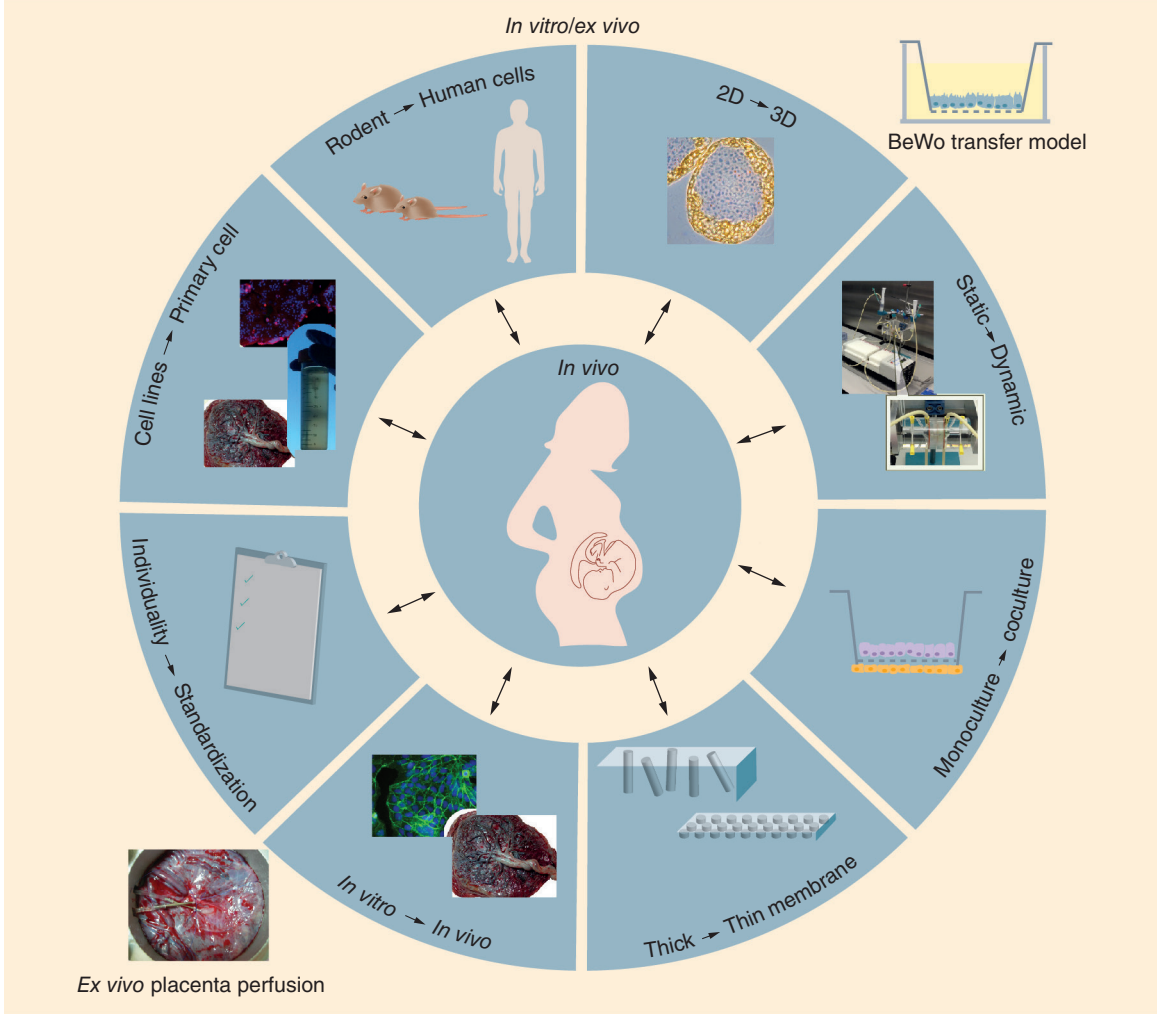

Figure 3. Strategies for the development of advanced placental models for more predictive NP transfer studies. To bridge the gap between *in vitro*/*ex vivo* transfer models and the pregnant women, improved models should be developed considering some of the following modifications: from cell lines to primary cells, from rodent to human cells, from 2D to 3D cultures, from static to dynamic cultures, from individual to standardized models and procedures, from *in vitro* to *ex vivo* models, from thick to thin membranes and from monocultures to co-cultures.

However, the current state of knowledge is too limited to support the design of such drug-delivery particles. To efficiently push this field of research forward, a systematic mechanism-based approach is a prerequisite and requires the development of predictive placental transfer models that are adapted to the use of NPs.

In vitro and *ex vivo* placental transfer models have been originally developed and used for the study of endogenous and pharmaceutical compounds. In this specific context, the models have been shown to exhibit a good predictive value for ranking the translocation of such small compounds. With the assumption that NPs will behave similar than small drugs, the models were directly applied to the study of NP transport. However, NPs have the potential to interfere with placental transfer models in unexpected ways. Therefore, a careful characterization of the NPs and the inclusion of appropriate controls will be crucial to obtain meaningful results. Furthermore, it will be essential that placental models do not only allow the ranking of placental NP transfer but also enable mechanistic studies on their uptake, accumulation, translocation and biological effects. This will require major improvements or the establishment of new *in vitro* placental models with high physiological relevance. For sure, the significant advances in various *in vitro* cell culture technologies such as microfluidics, 3D tissue cultures or 3D bioprinting should be exploited, and it will be interesting to see how different parameters such as a dynamic microenvironment, co-culturing or 3D structure will influence placental transfer. Nevertheless, only those parameters should be considered that substantially advance the predictive value of the models since they should remain relatively easy to handle, high-throughput compatible and cost effective. Another major challenge will be to carefully validate these models because access to human NP transfer data is not expected in the near future and comparison to animal studies is critical considering that the placenta is the most species-specific organ. Yet, validation of the models will be key to get them accepted and to identify their potentials and limits. This will in turn allow devising a strategy to efficiently screen a large variety of NPs as it was already previously proposed [65]. In essence, the development and identification of suitable placental model(s) predictive for human pregnancy will be decisive to push the limits of our understanding of placental transport of NPs.

On a long-term perspective, it will be exciting to see if advanced placental transfer models can be integrated into multi-organ chips to simulate systemic organ complexity. Combining relevant maternal organs (e.g., liver or spleen), the placental barrier and embryonic models (e.g., neurospheres or stem cell cultures) under dynamic conditions might enable the *in vitro* assessment of direct and indirect NP effects as well as potential teratogenic effects. Indeed such an approach might once be technically feasible as shown by the promising advances in multi-organ chip development for long-term substance testing [89]. To conclude, understanding of NP translocation at the placental barrier and how it can be steered

Executive summary

Influence of NP characteristics on placental transfer: is there a trend?

- NP size is a key characteristic that may allow controlling translocation across the placental barrier with higher transport for smaller particles.
- The threshold size for maternal to fetal transfer is dependent on the material type.
- Surface charge and shape are additional promising NP properties for steering placental transport that deserve increased attention.

Future research on placental NP transfer: what are the urgent needs?

- To more clearly understand how NP translocation is dependent on physical-chemical properties and functionalization, systematic studies using NP libraries, ideally varying in only one individual characteristic, are essential.
- Other relevant research topics related to NP transport are the identification of underlying transport mechanisms, the role of the protein corona and the impact of different stages of pregnancy.

Current placental transfer models: are they applicable to NP transfer studies?

- First prevalidation studies were performed comparing *in vitro* to *ex vivo* perfusion models but it is too early to draw conclusions on the predictive value of these models for NP transfer studies.
- There is increasing evidence that the current *in vitro* transfer models have limitations such as the lack of fluid flow resulting in unrealistic NP dosing or inadequate membranes that constitute a major barrier to the free transfer of NPs.

Next-generation placental transfer models: plenty of room for improvements?

- The *ex vivo* perfusion model is currently used with many small modifications and would benefit from the implementation of more standardized perfusion setups and protocols.
- Advanced *in vitro* transfer models with higher predictability are expected from the inclusion of a dynamic microenvironment, primary cells, co-cultures and optimization of the supporting membrane.

is an indispensable part in the whole development of novel NP-based drug delivery systems to specifically treat the mother, fetus or placental disorders. If efficient drug loading, targeting, release as well as particle safety can be ensured, the vision of new particle-based therapies in pregnancy may eventually become reality.

Acknowledgements

The authors thank Dr Marcus Koch, Head of Physical Analysis at the INM – Leibniz-Institute for New Materials gGmbH, Saarbruecken, Germany for the provision of SEM images of microporous membranes.

Financial & competing interests disclosure

This research is supported by funding from the BMBF-project NanoUmwelt (03X0150) and the 7th Framework Program of the European Commission (FP7-NANOSOLUTIONS, grant agreement number 309329 and Graphene Flagship, grant agreement number 604391). The authors have no other relevant affiliations or financial involvement with any organization or entity with a financial interest in or financial conflict with the subject matter or materials discussed in the manuscript apart from those disclosed.

No writing assistance was utilized in the production of this manuscript.

References

Papers of special note have been highlighted as: • of interest; •• of considerable interest

1 Evseenko D, Paxton JW, Keelan JA. Active transport across the human placenta: impact on drug efficacy and toxicity. *Expert Opin. Drug Metabol. Toxicol.* 2(1), 51–69 (2006).

2 Ganapathy V, Prasad PD, Ganapathy ME, Leibach FH. Placental transporters relevant to drug distribution across the maternal-fetal interface. *J. Pharmacol. Exp. Ther.* 294(2), 413–420 (2000).

3 Prouillac C, Lecoeur S. The role of the placenta in fetal exposure to xenobiotics: importance of membrane transporters and human models for transfer studies. *Drug Metab. Dispos.* 38(10), 1623–1635 (2010).

4 Vargesson N. Thalidomide-induced teratogenesis: History and mechanisms. *Birth Defects Res. C Embryo Today* 105(2), 140–156 (2015).

5 Braakhuis HM, Kloet SK, Kezic S *et al.* Progress and future of *in vitro* models to study translocation of nanoparticles. *Arch. Toxicol.* 89(9), 1469–1495 (2015).

• **Provides a detailed and critical overview on currently available *in vitro* models of the human lung, skin, intestinal and placental barrier, and highlights the need to validate these models.**

6 Buerki-Thurnherr T, Von Mandach U, Wick P. Knocking at the door of the unborn child: engineered nanoparticles at the human placental barrier. *Swiss Med. Wkly* 142, w13559 (2012).

7 Hougaard KS, Campagnolo L, Chavatte-Palmer P *et al.* A perspective on the developmental toxicity of inhaled nanoparticles. *Reprod. Toxicol.* 56, 118–140 (2015).

8 Campagnolo L, Massimiani M, Palmieri G *et al.* Biodistribution and toxicity of pegylated single wall carbon nanotubes in pregnant mice. *Part Fibre Toxicol.* 10, 21 (2013).

9 Pietroiusti A, Massimiani M, Fenoglio I *et al.* Low doses of pristine and oxidized single-wall carbon nanotubes affect mammalian embryonic development. *ACS Nano* 5(6), 4624–4633 (2011).

10 Weissig V, Guzman-Villanueva D. Nanopharmaceuticals (part 2): products in the pipeline. *Int. J. Nanomedicine* 10, 1245–1257 (2015).

11 Weissig V, Pettinger TK, Murdock N. Nanopharmaceuticals (part I): products on the market. *Int. J. Nanomedicine* 9, 4357–4373 (2014).

• **Extensive two-part review on nanoparmaceuticals currently on the market or in clinical trials.**

12 Juliano RL. The future of nanomedicine: promises and limitations. *Sci. Public Policy* 39(1), 99–104 (2012).

13 Keelan JA, Leong JW, Ho D, Iyer KS. Therapeutic and safety considerations of nanoparticle-mediated drug delivery in pregnancy. *Nanomedicine (Lond.)* 10(14), 2229–2247 (2015).

•• **Comprehensive review on the advantages and the potential use of nanomedical approaches including some examples of hypothetical NP–drug combinations for the treatment of maternal, placental or fetal diseases.**

14 Daw JR, Hanley GE, Greyson DL, Morgan SG. Prescription drug use during pregnancy in developed countries: a systematic review. *Pharmacoepidemiol. Drug Saf.* 20(9), 895–902 (2011).

• **Important review showing the widespread prescription drug use during pregnancy, including medicines recognized as having potential teratogenic risks.**

15 Thomas SHL, Yates LM. Prescribing without evidence - pregnancy. *Br. J. Clin. Pharmacol.* 74(4), 691–697 (2012).

16 Ali H, Kalashnikova I, White MA, Sherman M, Rytting E. Preparation, characterization, and transport of dexamethasone-loaded polymeric nanoparticles across a human placental *in vitro* model. *Int. J. Pharm.* 454(1), 149–157 (2013).

17 Semmler-Behnke M, Lipka J, Wenk A *et al.* Size dependent translocation and fetal accumulation of gold nanoparticles from maternal blood in the rat. *Particle Fibre Toxicol.* 11, 33 (2014).

18 Refuerzo JS, Godin B, Bishop K *et al.* Size of the nanovectors determines the transplacental passage in pregnancy: study in rats. *Am. J. Obstet. Gynecol.* 204(6), 546 e545–549 e545 (2011).

19 Wick P, Malek A, Manser P *et al.* Barrier capacity of human placenta for nanosized materials. *Environ. Health Perspect.* 118(3), 432–436 (2010).

20 Cartwright L, Poulsen MS, Nielsen HM *et al. In vitro* placental model optimization for nanoparticle transport studies. *Int. J. Nanomedicine* 7, 497–510 (2012).

21 Huang JP, Hsieh PC, Chen CY *et al.* Nanoparticles can cross mouse placenta and induce trophoblast apoptosis. *Placenta* 36(12), 1433–1441 (2015).

22 Yamashita K, Yoshioka Y, Higashisaka K *et al.* Silica and titanium dioxide nanoparticles cause pregnancy complications in mice. *Nat. Nanotechnol.* 6(5), 321–328 (2011).

23 Carreira SC, Walker L, Paul K, Saunders M. The toxicity, transport and uptake of nanoparticles in the *in vitro* BeWo b30 placental cell barrier model used within NanoTEST. *Nanotoxicology* 9, 66–78 (2015).

24 Poulsen MS, Mose T, Maroun LL, Mathiesen L, Knudsen LE, Rytting E. Kinetics of silica nanoparticles in the human placenta. *Nanotoxicology* 9, 79–86 (2015).

•• **This is the first study that compares the translocation of the same NPs in the *ex vivo* placenta perfusion model and the BeWo b30 Transwell system in order to identify the predictive value of this *in vitro* placenta model.**

25 Chu M, Wu Q, Yang H *et al.* Transfer of quantum dots from pregnant mice to pups across the placental barrier. *Small* 6(5), 670–678 (2010).

26 Lee S, Bi X, Reed RB, Ranville JF, Herckes P, Westerhoff P. Nanoparticle size detection limits by single particle ICP-MS for 40 elements. *Environ. Sci. Technol.* 48(17), 10291–10300 (2014).

27 Mitrano D, Renville J, Neubauer K, Thomas R. Field-flow fractionation coupled with ICP-MS for the analysis of engineered nanoparticles in environmental samples. *Lc Gc Europe* 25(12), 652–+ (2012).

•• **Exemplarily stands for the efforts to improve nanoparticle detection in different matrices, to lower detection limits and to enable the distinction between ionic and particulate materials.**

28 Menjoge AR, Rinderknecht AL, Navath RS *et al.* Transfer of PAMAM dendrimers across human placenta: prospects of its use as drug carrier during pregnancy. *J. Control. Release* 150(3), 326–338 (2011).

29 Sumner SC, Fennell TR, Snyder RW, Taylor GF, Lewin AH. Distribution of carbon–14 labeled C60 ([14C]C60) in the pregnant and in the lactating dam and the effect of C60 exposure on the biochemical profile of urine. *J. Appl. Toxicol.* 30(4), 354–360 (2010).

30 Takeda K, Suzuki K, Ishihara A *et al.* Nanoparticles tranferred from pregnant mice to their offspring can damage the genital and cranial nerve systems. *J. Health Sci.* 55, 95–102 (2009).

31 Girardi G, Fraser J, Lennen R, Vontell R, Jansen M, Hutchison G. Imaging of activated complement using ultrasmall superparamagnetic iron oxide particles (USPIO) – conjugated vectors: an *in vivo* in utero non-invasive method to predict placental insufficiency and abnormal fetal brain development. *Mol. Psychiatry* 20(8), 1017–1026 (2015).

32 Austin CA, Umbreit TH, Brown KM *et al.* Distribution of silver nanoparticles in pregnant mice and developing embryos. *Nanotoxicology* 6, 912–922 (2012).

33 Huang XL, Zhang F, Sun XL *et al.* The genotype-dependent influence of functionalized multiwalled carbon nanotubes on fetal development. *Biomaterials* 35(2), 856–865 (2014).

34 Qi W, Bi JJ, Zhang XY *et al.* Damaging effects of multi-walled carbon nanotubes on pregnant mice with different pregnancy times. *Sci. Rep.* 4, 4352 (2014).

35 Choi HS, Ashitate Y, Lee JH *et al.* Rapid translocation of nanoparticles from the lung airspaces to the body. *Nat. Biotechnol.* 28(12), U1300–U1113 (2010).

36 Grafmueller S, Manser P, Diener L *et al.* Bidirectional transfer study of polystyrene nanoparticles across the placental barrier in an human placental perfusion model. *Environ. Health Perspect.* doi:10.1289/ehp.1409271 (2015) (Epub ahead of print).

37 Di Bona KR, Xu YL, Ramirez PA *et al.* Surface charge and dosage dependent potential developmental toxicity and biodistribution of iron oxide nanoparticles in pregnant CD–1 mice. *Reprod. Toxicol.* 50, 36–42 (2014).

38 Yang H, Sun CJ, Fan ZL *et al.* Effects of gestational age and surface modification on materno-fetal transfer of nanoparticles in murine pregnancy. *Sci. Rep.* 2, 847 (2012).

39 Kloet SK, Walczak AP, Louisse J *et al.* Translocation of positively and negatively charged polystyrene nanoparticles in an *in vitro* placental model. *Toxicology* 29(7), 1701–1710 (2015).

40 Chithrani BD, Ghazani AA, Chan WCW. Determining the size and shape dependence of gold nanoparticle uptake into mammalian cells. *Nano Lett.* 6(4), 662–668 (2006).

41 Niikura K, Matsunaga T, Suzuki T *et al.* Gold nanoparticles as a vaccine platform: influence of size and shape on immunological responses *in vitro* and *in vivo*. *ACS Nano* 7(5), 3926–3938 (2013).

42 Herd H, Daum N, Jones AT, Huwer H, Ghandehari H, Lehr CM. Nanoparticle geometry and surface orientation influence mode of cellular uptake. *ACS Nano* 7(3), 1961–1973 (2013).

43 Bitounis D, Ali-Boucetta H, Hong BH, Min DH, Kostarelos K. Prospects and challenges of graphene in biomedical applications. *Adv. Mater.* 25(16), 2258–2268 (2013).

44 Kostarelos K, Novoselov KS. Exploring the interface of graphene and biology. *Science* 344(6181), 261–263 (2014).

45 Wick P, Louw-Gaume AE, Kucki M *et al.* Classification framework for graphene-based materials. *Angew. Chem. Int. Ed. Engl.* 53(30), 7714–7718 (2014).

46 Philbrook NA, Walker VK, Afrooz ARMN, Saleh NB, Winn LM. Investigating the effects of functionalized carbon nanotubes on reproduction and development in Drosophila melanogaster and CD–1 mice. *Reprod. Toxicol.* 32(4), 442–448 (2011).

47 Blum JL, Xiong JQ, Hoffman C, Zelikoff JT. Cadmium associated with inhaled cadmium oxide nanoparticles impacts fetal and neonatal development and growth. *Toxicol. Sci.* 126(2), 478–486 (2012).

48 Myllynen PK, Loughran MJ, Howard CV, Sormunen R, Walsh AA, Vahakangas KH. Kinetics of gold nanoparticles in the human placenta. *Reprod. Toxicol.* 26(2), 130–137 (2008).

49 Rattanapinyopituk K, Shimada A, Morita T *et al.* Demonstration of the clathrin- and caveolin-mediated endocytosis at the maternal-fetal barrier in mouse placenta

after intravenous administration of gold nanoparticles. *J. Vet. Med. Sci.* 76(3), 377–387 (2014).

50 Hougaard KS, Jackson P, Jensen KA *et al.* Effects of prenatal exposure to surface-coated nanosized titanium dioxide (UV-Titan). A study in mice. *Part Fibre Toxicol.* 7, 16 (2010).

51 Krug HF, Wick P. Nanotoxicology: an interdisciplinary challenge. *Angew. Chem. Int. Ed. Engl.* 50(6), 1260–1278 (2011).

52 Roesslein M, Richter V, Wick P, Krug HF. Nanomaterials and ceramic nanoparticles – use without side-effects? *J. Ceramic Sci. Technol.* 4(2), 123–129 (2013).

53 Jiang Y, Huo SD, Mizuhara T *et al.* The interplay of size and surface functionality on the cellular uptake of sub-10 nm gold nanoparticles. *ACS Nano* 9(10), 9986–9993 (2015).

54 Su G, Zhou G, Mu Q *et al.* Effective surface charge density determines the electrostatic attraction between nanoparticles and cells. *J. Phys. Chem. C* 116(8), 4993–4998 (2012).

55 Fadeel B. Systems biology in nanosafety research. *Nanomedicine* 10(7), 1039–1041 (2015).

56 Fadeel B, Feliu N, Vogt C, Abdelmonem AM, Parak WJ. Bridge over troubled waters: understanding the synthetic and biological identities of engineered nanomaterials. *Wiley Interdiscip. Rev. Nanomed. Nanobiotechnol.* 5(2), 111–129 (2013).

57 Mahmoudi M, Lynch I, Ejtehadi MR, Monopoli MP, Bombelli FB, Laurent S. Protein–nanoparticle interactions: opportunities and challenges. *Chem. Rev.* 111(9), 5610–5637 (2011).

58 Maiolo D, Del Pino P, Metrangolo P, Parak WJ, Baldelli Bombelli F. Nanomedicine delivery: does protein corona route to the target or off road? *Nanomedicine (Lond.)* 10(21), 3231–3247 (2015).

59 Pietroiusti A, Campagnolo L, Fadeel B. Interactions of engineered nanoparticles with organs protected by internal biological barriers. *Small* 9(9–10), 1557–1572 (2013).

60 Monopoli MP, Aberg C, Salvati A, Dawson KA. Biomolecular coronas provide the biological identity of nanosized materials. *Nat. Nanotechnol.* 7(12), 779–786 (2012).

61 Lundqvist M, Stigler J, Elia G, Lynch I, Cedervall T, Dawson KA. Nanoparticle size and surface properties determine the protein corona with possible implications for biological impacts. *Proc. Natl Acad. Sci. USA* 105(38), 14265–14270 (2008).

62 Juch H, Nikitina L, Debbage P, Dohr G, Gauster M. Nanomaterial interference with early human placenta: sophisticated matter meets sophisticated tissues. *Reprod. Toxicol.* 41, 73–79 (2013).

63 Dilworth MR, Sibley CP. Review: transport across the placenta of mice and women. *Placenta* 34(Suppl.), S34–S39 (2013).

64 Hutson JR, Garcia-Bournissen F, Davis A, Koren G. The human placental perfusion model: a systematic review and development of a model to predict *in vivo* transfer of therapeutic drugs. *Clin. Pharmacol. Ther.* 90(1), 67–76 (2011).

65 Mathiesen L, Morck TA, Zuri G *et al.* Modelling of human transplacental transport as performed in Copenhagen, Denmark. *Basic Clin. Pharmacol. Toxicol.* 115(1), 93–100 (2014).

66 Myllynen P, Vahakangas K. Placental transfer and metabolism: an overview of the experimental models utilizing human placental tissue. *Toxicol. in vitro* 27(1), 507–512 (2013).

67 Ala-Kokko TI, Myllynen P, Vähäkangas K. *Ex vivo* perfusion of the human placental cotyledon: implications for anesthetic pharmacology. *Int. J. Obstetr. Anesth.* 9(1), 26–38 (2000).

68 Enders AC, Blankenship TN. Comparative placental structure. *Adv. Drug Deliv. Rev.* 38(1), 3–15 (1999).

69 Panigel M, Pascaud M, Brun JL. [Radioangiographic study of circulation in the villi and intervillous space of isolated human placental cotyledon kept viable by perfusion]. *J. Physiol. (Paris)* 59(Suppl. 1), 277 (1967).

70 Grafmueller S, Manser P, Krug HF, Wick P, Von Mandach U. Determination of the transport rate of xenobiotics and nanomaterials across the placenta using the *ex vivo* human placental perfusion model. *J. Vis. Exp.* 76, e50401 (2013).

71 Malek A, Obrist C, Wenzinger S, Von Mandach U. The impact of cocaine and heroin on the placental transfer of methadone. *Reprod. Biol. Endocrinol.* 7, 61 (2009).

72 Stark WJ. Nanoparticles in biological systems. *Angew. Chem. Int. Ed. Engl.* 50(6), 1242–1258 (2011).

73 Bruinink A, Wang J, Wick P. Effect of particle agglomeration in nanotoxicology. *Arch. Toxicol.* 89(5), 659–675 (2015).

74 Grafmueller S, Manser P, Diener L *et al.* Transfer studies of polystyrene nanoparticles in the *ex vivo* human placenta perfusion model: key sources of artifacts. *Sci. Technol. Adv. Mater.* 16(4), 044602 (2015).

75 Lee JS, Romero R, Han YM *et al.* Placenta-on-a-chip: a novel platform to study the biology of the human placenta. *J. Matern. Fetal Neonatal Med.* 29(7), 1046–1054 (2015).

76 Miura S, Sato K, Kato-Negishi M, Teshima T, Takeuchi S. Fluid shear triggers microvilli formation via mechanosensitive activation of TRPV6. *Nat. Commun.* 6, 8871 (2015).

77 Levkovitz R, Zaretsky U, Gordon Z, Jaffa AJ, Elad D. *In vitro* simulation of placental transport: part I. Biological model of the placental barrier. *Placenta* 34(8), 699–707 (2013).

78 Li H, Van Ravenzwaay B, Rietjens IM, Louisse J. Assessment of an *in vitro* transport model using BeWo b30 cells to predict placental transfer of compounds. *Arch. Toxicol.* 87(9), 1661–1669 (2013).

79 Poulsen MS, Rytting E, Mose T, Knudsen LE. Modeling placental transport: correlation of *in vitro* BeWo cell permeability and *ex vivo* human placental perfusion. *Toxicol. In vitro* 23(7), 1380–1386 (2009).

80 Rytting E. Exploring the interactions of nanoparticles with multiple models of the maternal-fetal interface. *Nanotoxicology* 9(Suppl. 1), 137–138 (2015).

81 Dekali S, Gamez C, Kortulewski T, Blazy K, Rat P, Lacroix G. Assessment of an *in vitro* model of pulmonary barrier to study the translocation of nanoparticles. *Toxicol. Rep.* 1, 157–171 (2014).

82 George I, Vranic S, Boland S, Courtois A, Baeza-Squiban A. Development of an *in vitro* model of human bronchial epithelial barrier to study nanoparticle translocation. *Toxicol. In Vitro* 29(1), 51–58 (2015).

83 Ye D, Raghnaill MN, Bramini M *et al.* Nanoparticle accumulation and transcytosis in brain endothelial cell layers. *Nanoscale* 5(22), 11153–11165 (2013).

84 Brun E, Barreau F, Veronesi G *et al.* Titanium dioxide nanoparticle impact and translocation through *ex vivo*, *in vivo* and *in vitro* gut epithelia. *Particle Fibre Toxicol.* 11, 13 (2014).

85 Mathiesen L, Mose T, Morck TJ *et al.* Quality assessment of a placental perfusion protocol. *Reprod. Toxicol.* 30(1), 138–146 (2010).

86 Walczak AP, Kramer E, Hendriksen PJ *et al.* Translocation of differently sized and charged polystyrene nanoparticles in *in vitro* intestinal cell models of increasing complexity. *Nanotoxicology* 9(4), 453–461 (2015).

87 Kelm JM, Fussenegger M. Microscale tissue engineering using gravity-enforced cell assembly. *Trends Biotechnol.* 22(4), 195–202 (2004).

88 CSEM - Centre Suisse d'Electronique et de Microtechnique. www.csem.ch/site/card.asp?pId=19709

89 Maschmeyer I, Lorenz AK, Schimek K *et al.* A four-organ-chip for interconnected long-term co-culture of human intestine, liver, skin and kidney equivalents. *Lab Chip* 15(12), 2688–2699 (2015).

Chapter 2

Aim and Hypothesis of the Thesis

The development of targeted nanomedical therapies offers a highly promising approach to treat maternal, placental or fetal diseases with reduced side effects. However, fundamental knowledge on NP-placenta interactions is not yet established, and reproducible and predictive human placenta *in vitro* models that are required to assess these interactions are essentially lacking.

The aim of this thesis was to understand the mechanisms underlying NP uptake, translocation, distribution and toxicity at the human placental barrier and if these interactions can be steered by tailoring NP physico-chemical properties and surface functionalization.

To reach the aim, the following objectives were set to:

1. Establish micropatterned BeWo cells with highly distinct actin cytoskeletal organization but identical cell surface area using the microcontact printing technique
2. Assess the amount of internalized polystyrene NPs and their intracellular localization in micropatterned BeWo cells grown on different pattern geometries
3. Develop, characterize and verify an advanced 3D *in vitro* co-culture MT model resembling the human placental tissue
4. Study effects on MT viability and functionality after the exposure to quantum dots, titanium dioxide or copper oxide NPs
5. Qualitatively and quantitatively assess NP accumulation and penetration in co-culture MTs in dependence of two different sizes and surface functionalization (PEGylation, carboxylation)
6. Identify uptake pathways that are involved in NP internalization by the MTs

This work was carried out within the framework of the following hypotheses:

1. Actin-dependent endocytosis and the overall actin organization are involved in polystyrene NP uptake and distribution in BeWo cells
2. 3D placental co-culture MTs can provide predictive, tissue-relevant data on the impact of NPs on placental viability and functionality
3. 3D placental co-culture MTs enable reproducible mechanistic studies on NP uptake, accumulation and penetration across the human placental barrier
4. NP-placenta interactions can be steered by particle size and surface modification

Chapter 3

Results

Part I

A micropatterning approach to study the influence of actin cytoskeletal organization on polystyrene nanoparticle uptake by BeWo cells

Carina Muoth, Markus Rottmar, Angela Schipanski, Chasper Gmuender, Katharina Maniura-Weber, Peter Wick, Tina Buerki-Thurnherr

Author contribution

In this study, I adapted and optimized the µCP technique for BeWo cells, established the image analysis, performed all experiments with polystyrene NPs, analyzed the results and wrote the manuscript. I introduced Chasper Gmuender into the CLSM and image analysis.

RSC Advances

PAPER

View Article Online
View Journal | View Issue

Cite this: *RSC Adv.*, 2016, **6**, 72827

A micropatterning approach to study the influence of actin cytoskeletal organization on polystyrene nanoparticle uptake by BeWo cells†

C. Muoth,[a] M. Rottmar,[b] A. Schipanski,[b] C. Gmuender,[a] K. Maniura-Weber,[b] P. Wick[a] and T. Buerki-Thurnherr*[a]

Received 27th May 2016
Accepted 15th July 2016

DOI: 10.1039/c6ra13782b

www.rsc.org/advances

To ensure the safe design and effective application of nanomedical therapies, it is of major importance to understand nanoparticle (NP) uptake mechanisms. Actin-dependent endocytosis has been proposed as a major uptake mechanism for numerous NPs in different cells. However, it is not clear which aspect of the structure and dynamics of the actin cytoskeleton is of relevance in this process. Despite the fact that the cytoskeletal organization is very much dependent on the cellular microenvironment, most mechanistic uptake studies have been performed under classic 2D cell culture conditions, which fail to represent the morphological and mechanical constraints present in biological tissues. In this study, human choriocarcinoma BeWo cells were physically constrained on micropatterns of different geometries to study the uptake of 80 nm, 240 nm and carboxylate 300 nm polystyrene particles and the dependence on different actin structures. Interestingly, major differences in the actin cytoskeletal organization of BeWo cells did not affect the intracellular distribution and amount of internalized polystyrene NPs for all investigated particle sizes and modifications. Therefore, we suggest a more central role for actin dynamics in actin-dependent NP endocytosis, rather than the overall actin organization.

Introduction

The concept of nanomedicine is based on the unique physico-chemical properties of nanoparticles (NPs) that allow a broad range of applications in different medical fields such as imaging (*e.g.* semiconductor, metal or metal oxide NPs),[1] drug delivery (*e.g.* polymeric NPs),[2] organ repair (*e.g.* silica or iron oxide NPs)[3] or photodynamic therapies (*e.g.* inorganic NPs with tunable optical properties).[4] Many of these applications require NP uptake by the target tissue for optimal efficiency and to reduce side effects to a low level. However, despite the presence of many NP uptake studies, the current knowledge on NP internalization in complex biological tissues is still limited. It has emerged that the uptake and the intracellular fate of NPs are greatly dependent on the tissue type, with their respective delivery routes and the physico-chemical properties of the NPs (*i.e.* size, shape, material, surface charge and functionalization; for extensive reviews see ref. 1 and 5–10). In addition, many studies have reported the presence of NPs in membrane-bound vesicles and/or reduced uptake at low temperatures, both of which are indicative of an active endocytosis uptake mechanism (reviewed in ref. 11–14).

The actin cytoskeleton plays a fundamental role in different cellular processes, including many types of endocytosis, such as phagocytosis, macropinocytosis, circular dorsal ruffles or clathrin-mediated endocytosis (CME).[15,16] Actin assembly can create protrusions that engulf extracellular materials. Actin also supports the invagination of membrane segments into the cytoplasm, scission of new vesicles from the plasma membrane and intracellular movement of the vesicles. In CME in yeast, vesicle budding is completed by the formation of a tubular invagination that is driven by the attachment of filamentous actin (F-actin), which occurs concomitantly with nucleation of actin at the plasma membrane.[17,18] Similar events have been shown for mammalian cells, where a close association between F-actin accumulation and vesicle formation was observed at a late stage of CME.[19,20] In addition, there is also evidence that actin not only plays a mechanical role, but also a structural role in CME, where it guides the endocytic machinery to a specific site on the plasma membrane (reviewed in ref. 21). A central role for actin dynamics in NP uptake by different cell types has been proposed in several studies employing pharmacological inhibitors that affect actin reorganization and G/F-actin ratios, such as cytochalasin or latrunculin.[22–25] Although there is some indication that actin-dependent internalization may be

[a]*Particles-Biology Interactions, Empa, Swiss Federal Laboratories for Materials Science and Technology, Lerchenfeldstrasse 5, 9014 St. Gallen, Switzerland. E-mail: tina.buerki@empa.ch*

[b]*Biointerfaces, Empa, Swiss Federal Laboratories for Materials Science and Technology, Lerchenfeldstrasse 5, 9014 St. Gallen, Switzerland*

† Electronic supplementary information (ESI) available: Nanoparticle size distribution measurements, fluorescence intensity measurements, cell viability experiments. See DOI: 10.1039/c6ra13782b

dependent on particle size and aspect ratio/geometry,[26,27] the use of different cell types, pharmacological inhibitors or NP types makes it difficult to compare different studies and to obtain a clear mechanistic insight. As such, treatment of macrophages with cytochalasin B resulted in the reduced uptake of 1000 nm, but not that of 20 nm polystyrene (PS) NPs,[25] while cytochalasin D treatment significantly diminished the internalization of small 20 nm silica NPs in A549 lung epithelial cells.[24] In addition, the use of such pharmacological inhibitors has some drawbacks, including a low specificity and cytotoxicity at increased concentrations or prolonged exposure times. Furthermore, cytochalasin can also affect other biological processes unrelated to actin polymerization, such as protein synthesis[28] or glucose transport.[29] Besides actin dynamics, we hypothesize that the global organization of actin filaments, as well as their assembly into higher-order structures, such as contractile bundles or three-dimensional networks may be implicated in cellular NP uptake and subcellular localization.

The microcontact printing (μCP) technique presents an interesting approach to mechanically controlling the organization of the actin cytoskeleton and when creating defined patterns, a more tissue-like microenvironment can be mimicked.[30] On substrates produced by μCP, single cells can be cultivated on cell-adhesive islands of defined geometry and size to manipulate and control the cell spreading area, shape, cytoskeletal organization and cell contractility, among other factors.[31–34] It has been previously shown that geometric cues can guide the formation of actin stress fibers and lamellipodia.[35] While cell adhesive areas with concave edges promote the formation of actin stress fibers,[34] those with convex edges are strong cues for the formation of lamellipodia.[36] Both actin stress fibers and lamellipodia have been shown to influence cell polarity.[36,37] Micropatterns with increased substrate stiffness and shapes that promote high cytoskeletal tension enhanced the osteogenesis of mesenchymal stem cells,[35,38,39] whereas unspread, round cells tend to express elevated markers of adipogenesis.[35,39,40] Taken together, these reports demonstrate the potential of μCP to enable studies on basic cell responses to individual cues with shape-normalized single cells.

In this study, μCP was employed to investigate the influence of different actin cytoskeletal organizations on uptake and internalization of PS particles by BeWo cells. Therefore, BeWo cells were cultivated on four different pattern geometries, resulting in the same cell surface area but different shapes, which induced highly distinct organization of the actin cytoskeleton. Nontoxic, fluorescent and monodisperse PS particles were used as model particles for the uptake studies. BeWo cells were exposed to 80 nm, 240 nm and carboxylate 300 nm PS particles, followed by quantitative uptake analysis using confocal microscopy and a digital image analysis method. We achieved the successful normalization of BeWo cell shape and distinct actin filament arrangements, a prerequisite for subsequent studies on actin-dependent NP uptake. Intracellular distribution and the amount of internalized NPs by shape-normalized BeWo cells were independent of the cytoskeletal organization for all investigated sizes and modifications of PS particles. This model presents a novel approach to studying the role of actin structures in NP uptake, kinetics and intracellular fate over time, and its dependency on different NP properties and cell types. A detailed knowledge of these NP-cell interactions is crucial for the development of targeted drug delivery systems.

Results and discussion

Particle characterization and cytotoxicity assessment

Commercially available, fluorescence labelled PS particles were selected as model NPs because actin-dependent endocytosis has been observed for this type of NP.[22,25,41] PS particles with different physico-chemical properties were included to further investigate whether NP uptake by micropatterned cells is size – (plain 80 nm and 240 nm PS NPs) or charge-dependent (plain 240 nm particles and 300 nm COOH–PS NPs). This size range was chosen because 300 nm is considered to be the relevant cut-off size for nanomedical particles, where unique medical effects are often observed only for particles larger than 100 μm.[42] PS particles were characterized in terms of primary particle size, hydrodynamic particle size, zeta potential and stability of the fluorescent dye. Results for the selected particles from previous work,[43,44] as well as new characterization data from this study, are summarized in Table 1.

TEM analysis was performed in a previous study and showed a primary particle size of 78.1 ± 20.5 nm for the plain 80 nm PS particles,[44] 220.5 ± 5.1 nm for the plain 240 nm PS particles[43] and 289.4 ± 10.2 nm for the 300 nm COOH–PS particles.[43] In suspension, hydrodynamic diameters of 80 nm, 240 nm and 300 nm COOH–PS particles increased to 97 ± 0.8 nm, 230 ± 65.3 nm and 283 ± 85.2 nm in water and to 162 ± 5.3 nm, 207 ± 10.9 nm and 312 ± 9.4 nm in growth medium, respectively (ESI Fig. 1†). The zeta potential was negative for all PS particles suspended in 10 mM sodium chloride, but for 80 nm and 300 nm COOH–PS particles, it was significantly lower than for 240 nm PS particles. Since 240 nm and 300 nm PS particles were similar in size but with different zeta potential, they were included to investigate whether NP surface charges affect their internalization by micropatterned cells.

When working with fluorescent NPs, a common problem is the release of labile dye in a biological milieu, as free fluorophores may significantly alter the *in vitro* and *in vivo* outcomes.[45–48] Therefore, we assessed the stability of the fluorescent dye in growth medium at 37 °C over 72 h, and no decrease in fluorescence intensity or any leakage of free dye from the different PS particles used in this study were observed (ESI Fig. 2A and B†).

An important prerequisite to study the dependency of NP uptake on cytoskeletal organization is the absence of cytotoxic effects. Using the MTS assay, we confirmed that none of the PS particles decreased the viability of BeWo cells within 24 h of exposure (ESI Fig. 3A and B†).

Distinct cytoskeletal organization through micropatterning

In a μCP approach, we explored whether different cytoskeletal organization influenced NP uptake by single cells. The human epithelial choriocarcinoma cell line BeWo was chosen, as it

Table 1 Summary of PS particles characteristics[a]

	Plain		COOH
	80 nm	240 nm	300 nm
Diameter (nm)	87[b]	240	302.7[d]
Diameter TEM (nm)	78.1 ± 20.5[c]	220.5 ± 5.1[d]	289.4 ± 10.2[d]
Hydrodynamic diameter (nm) in DD water	97 ± 0.8[c]	230 ± 65.3[d]	283 ± 85.2[d]
Hydrodynamic diameter (nm) in growth medium[e]	162 ± 5.3	207 ± 10.9	312 ± 9.4
Initial no. of particles per mL in growth medium	2.18×10^{12}	1.70×10^{9}	7.50×10^{8}
Particle surface (nm^2) per mL in growth medium	1.31×10^{16}	2.59×10^{14}	1.97×10^{14}
Zeta potential in 10 mM NaCl (mV)	−50 ± 9.7[c]	−20.5 ± 2.7[d]	−55.6 ± 6.1[d]
Zeta potential in growth medium (mV)[e]	−10.9 ± 0.8	−10.9 ± 0.6	−9.3 ± 0.97
Fluorescent dye[b]	Yellow green	Yellow	Yellow green
Excitation/emission[b]	485/528	485/520	485/528
Manufacturer	Polyscience Inc	Spherotec Inc	Polyscience Inc

[a] Abbreviations: DD double distilled; TEM transmission electron microscopy. [b] According to manufacturer's information. [c] Grafmueller *et al.*[44] [d] Grafmueller *et al.*[43] [e] Experimentally determined (mean ± SD).

expresses a wide range of different transporters, including various exporters for the efflux of toxic xenobiotics.[49] Furthermore, uptake and translocation of different NPs have been shown by BeWo cells *in vitro*,[50–52] and the syncytiothrophoblast *ex vivo*.[43,53–55] The possibility to induce major differences in intracellular organization in a purely mechanical way, without the need for pharmacological inhibitors renders μCP a very interesting tool for mechanistic uptake studies. An additional advantage of the μCP technique in particular for NP uptake studies is that significantly prolonged exposure times (24 h or more, depending on the cell division rate) can be studied, as opposed to only few hours for the use of actin inhibitors.[56] Moreover, it has been shown for certain cell types such as endothelial cells, that the composition and stiffness of micropatterned substrates influence cell architecture, mechanics and the cytoskeletal organization in a similar way to that found for cells *in situ* within organs or tissues.[57–59]

In this study, BeWo cells were grown on adhesive micropatterns of different geometries (disc, H, crossbow (CB) and Y) (Fig. 1A) in order to achieve differences in cytoskeletal organization without changing the cell surface area. The optimal pattern size, which best supported the spreading of BeWo cells was 1600 μm^2. On smaller micropatterns (1100 and 700 μm^2), cells displayed a roundish morphology while on larger patterns (>2000 μm^2), they were not able to span over the entire adhesive area (data not shown). Major differences in the actin cytoskeleton occurred between Y patterns with three non-adhesive areas, CB and H patterns with two non-adhesive areas and disc patterns lacking non-adhesive areas. On Y patterns, filamentous actin (F-actin) stress fibers were concentrated along the whole outline of the cell, whereas on CB and H patterns, they only formed along two borders of the cell. In contrast, BeWo cells spread on the disc patterns displayed a strong actin network in the center of the cell where the cytoskeleton spanned over the nucleus (Fig. 1B). Furthermore, the formation of lamellipodial extensions and filopodial protrusions were detectable on adhesive areas in BeWo cells grown on disc, H and CB patterns (Fig. 2). To confirm that the cytoskeletal organization was reproducible, actin heatmaps of

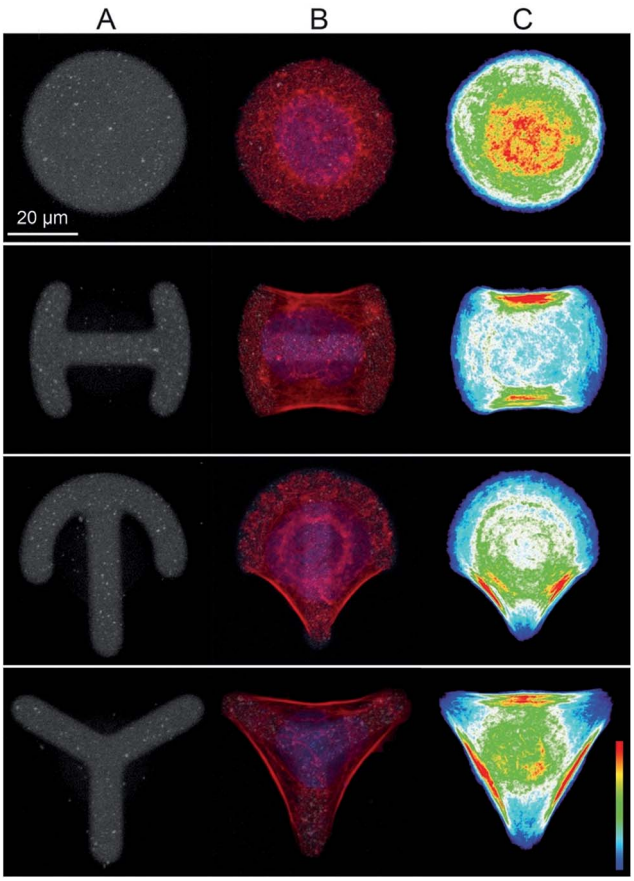

Fig. 1 Normalization of BeWo cells on disc, H, CB and Y micropatterns. The four different patterns on a chip without (A) and with BeWo cells (B). The actin cytoskeleton was visualized by phalloidin (red), cell nuclei by DAPI (blue) and the adhesive patterns by a fluorescent fibronectin coating (gray). Differential organization of the actin cytoskeleton on the different patterns was evident (63× magnification). Heat maps were calculated from 20 overlaid z-stack images per pattern geometry, showing the distribution of actin stress fibers (C). Red indicates a high pixel intensity of F-actin, whereas blue represents a low intensity.

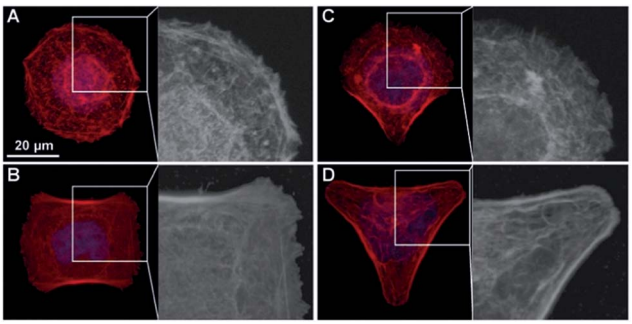

Fig. 2 Formation of actin protrusions in cell regions on adhesive areas. BeWo cells were spread on disc (A), H (B) and CB (C) patterns and stained for F-actin (red), showing filopodia-like protrusions and lamellipodia-like structures on the adhesive areas on the border of the cells. Actin protrusions of BeWo cells grown on Y patterns (D) were less prominent.

20 individual cells per pattern were made (Fig. 1C). Actin heatmaps showed a highly reproducible and distinct arrangement of the actin cytoskeleton within each pattern demonstrating the successful normalization of BeWo cells.

NP uptake by shape-normalized BeWo cells

BeWo cells that were completely spread on the different micropatterns were exposed to PS particles in order to specifically study the potential effects of differences in cytoskeletal organization on the amount and distribution of internalized NPs. Addition of NPs before or during cell spreading would prevent the achievement of the study aim, since unspread cells have a randomly organized actin cytoskeleton and NPs could interfere with cell adhesion and spreading.[60] Experiments using different NP concentrations were performed to identify a suitable NP concentration that resulted in a sufficient number of intracellular NPs in the majority of the cells to quantitatively analyze NP uptake by confocal microscopy (data not shown). While a low concentration of 10 μg mL^{-1} was sufficient for 240 nm (Fig. 3B) and 300 nm COOH–PS particles (Fig. 3C), a higher concentration of 100 μg mL^{-1} was required for 80 nm PS particles (Fig. 3A). An exposure time of 14 h was chosen because most BeWo cells had not yet entered mitosis, resulting in a high number of single cells that could be included in the analysis.

Heatmaps were made to show the average distribution of internalized PS particles. After an exposure time of 14 h, uptake was observed for all shape-normalized BeWo cells exposed either to 80 nm (Fig. 3D), 240 nm (Fig. 3E) or 300 nm COOH–PS particles (Fig. 3F). As expected, for single cell analysis,[61] the amount of internalized NPs was highly variable between different cells, even if cultivated on the same pattern. Independent of the different pattern geometries, all NPs were located predominantly in the perinuclear region, probably in the form of NP-filled vesicles. Although it may appear from several individual images in Fig. 3 that actin is also very much localized around the nuclei, heatmaps from 20 individual cells clearly showed that a consistent perinuclear localization of actin is only true for cells spread on the disc patterns (Fig. 2). Therefore, perinuclear actin structures are most likely not responsible for the observed nuclear localization of the NPs. Most importantly, NP heatmaps did not show any obvious differences in the amount or intracellular distribution of internalized NPs, despite the presence of highly distinct actin organization on the four pattern geometries.

In addition to the qualitative observations, the quantity of internalized NPs was analyzed by applying a macro specifically designed to reliably measure NP uptake by single cells ("Particle_in_Cell-3D"[61] for ImageJ). This macro requires the use of fluorescently labelled NPs, as well as a staining procedure to visualize the cell border or cell membrane. However, direct labelling of the cell membrane (*e.g.* with cell tracker dyes, DiI, DiO or DiD) led to the partial detachment of the cells from the patterns after fixation (data not shown). Therefore, labelling of the actin cytoskeleton was used as an indirect approach to identify the cell border. Integrated pixel intensities of internalized NPs were calculated for 20 cells per pattern geometry, using the same z-stack images as for the heatmaps (Fig. 4). Comparison of PS particle uptake by BeWo cells grown on disc, H, CB and Y patterns revealed no differences for either the 80 nm (Fig. 4A) or 240 nm PS particles (Fig. 4B). A slightly increased uptake was observed only for 300 nm COOH–PS particles by cells grown on Y patterns, compared to CB and H patterns (Fig. 4C), but this trend was not observed for 80 nm or 240 nm PS particles. As this increase was very modest and not consistent for all NP types, it is unlikely that cells with high levels of peripheral stress fibers incorporate more NPs than cells with a more central F-actin meshwork.

Our quantitative analysis indicates that actin cytoskeletal organization is not a key determinant of NP internalization. Specifically, PS NP uptake was independent of the presence of wide, peripheral stress fibers, filopodia or lamellipodial structures (Fig. 1C and 2). In addition, a more peripheral or central localization of most F-actin structures did not have any influence on the amount or intracellular distribution of PS NPs either (Fig. 1C). However, due to cell type-specific differences in NP uptake, it will be important to confirm these findings for other cell types. Moreover, it appears that cell contractility is not implicated in PS NP uptake, since previous work suggested that the level of contractile forces was altered in cells grown on different micropatterns.[34,36] According to these studies, cell contractility in micropatterned BeWo cells is expected to be highest on Y patterns forming three convex edges, intermediate on CB and H patterns forming two convex edges and lowest on disc patterns forming no such edges. However, to unambiguously prove that NP internalization is independent of cell contractility, contractile forces of cells on different micropatterns have to be accurately determined by appropriate force measurement methods. Finally, we suggest that the dynamic reorganization of the actin filaments, which was not significantly affected in our μCP study, is of key relevance for the active endocytic NP uptake as observed in previous studies.[22–25] This is supported by the fact that the presence of pharmacological inhibitors interfering with polymerization, depolymerization or rearrangement of the actin cytoskeleton resulted in the decreased uptake of several NPs.[22–25]

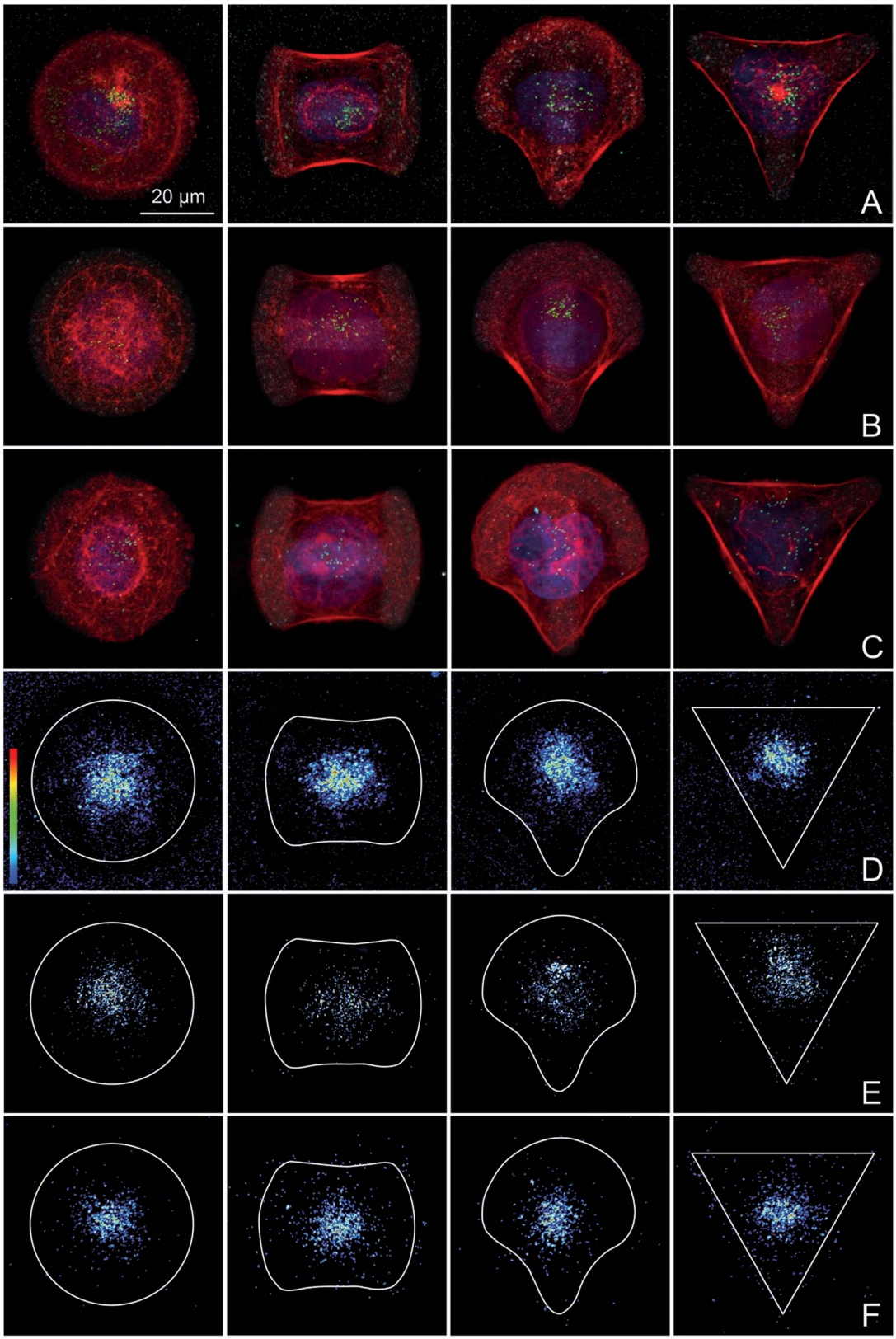

Fig. 3 NP uptake by shape-normalized single cells. BeWo cells cultivated on adhesive micropatterns (disc, H, CB and Y) were exposed to 100 μg mL^{-1} of 80 nm (A) and 10 μg mL^{-1} of 240 nm (B) and 300 nm green fluorescent COOH–PS particles (C) for 14 h. Cells were stained for F-actin (red) and DAPI (blue). Heatmaps were calculated from 20 overlaid z-stack images per pattern geometry, showing the distribution of internalized 80 nm (D), 240 nm (E) and 300 nm COOH–PS particles (F). Red indicates a high pixel intensity of F-actin, whereas blue represents a low intensity.

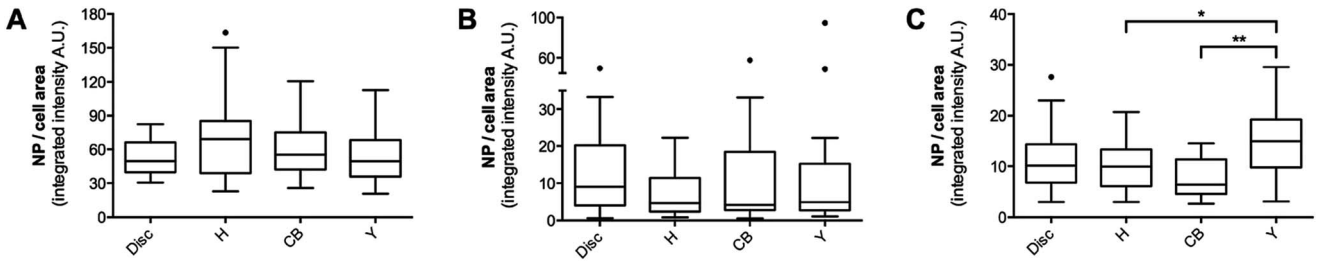

Fig. 4 Quantitative analysis of PS particle uptake by shape-normalized single cells grown on the different patterns. NP uptake of 20 individual cells per pattern was analyzed using the ImageJ macro "Particle_in_Cell-3D". Tukey box-and-whiskers plots show the integrated NP pixel intensity per cell surface area for all pattern geometries. Quantitative NP uptake by BeWo cells was calculated for (A) 80 nm, (B) 240 nm and (C) 300 nm COOH–PS particles.

The current knowledge on NP uptake mechanisms by different cell types ranges from actin-dependent endocytosis to non-endocytic pathways with no clear correlation to the physico-chemical properties of the particles. For example, dos Santos *et al.* described an energy dependent uptake process for 40 nm and 200 nm COOH–PS NPs in HeLa and glial astrocytoma 1321N1 cells.[22] In contrast, a nonendocytic uptake pathway was suggested for 78 nm and 200 nm PS NPs in pulmonary macrophages.[62] A more recent study in primary macrophages and a monocytic cell line has identified endocytosis, macropinocytosis or phagocytosis as the involved uptake mechanisms for 100 nm COOH– and NH_2–PS NPs.[41] These contradictory results clearly demonstrate the need for more detailed studies on NP uptake mechanisms, including, but not limited to the role of endocytosis and the actin cytoskeleton.

Conclusions

In this study, single BeWo cells with the same projected surface area, but highly distinct organization of the actin cytoskeleton were successfully obtained using commercial micropatterns with different geometries. Using μCP technology, we were able to exclude a major role of the global actin organization in the internalization of PS particles by BeWo cells. We propose that future work on actin-dependent NP uptake mechanisms should focus on the precise role of the dynamic reorganization of actin microfilaments. For such studies, the use of pharmacological inhibitors is inevitable, as major changes in actin dynamics or G/F-actin ratios cannot be easily achieved by a μCP approach. However, to obtain mechanistic insights that are predictive of the *in vivo* situation in biological tissues, such inhibitor studies should be performed on micropatterned cells or 3D microtissues, rather than highly artificial 2D cell cultures.

As nanotechnology is becoming a vital player in medicine, with various biomedical applications, such as drug delivery, therapeutics, diagnosis or imaging, it is necessary to understand the mechanisms by which NPs are internalized by cells. A comprehensive knowledge of NP internalization pathways in relation to distinct physico-chemical NP properties may enable the development of novel strategies to enhance or reduce NP uptake at specific sites.

Experimental section

Micropatterns

Micropatterns coated with fluorescent fibronectin with excitation at 650 nm were acquired from CYTOO Cell Architects (Grenoble, France). A CYTOOchip™ was 20 × 20 mm and contained four different geometries (disc, crossbow (CB), H and Y) (Fig. 1A) in three sizes (700, 1100 and 1600 μm^2 per pattern) and a control area uniformly covered with A650-labeled fibronectin.

Cell culture

BeWo (ATCC) cells, a human placental choriocarcinoma cell line with cytotrophoblastic characteristics, were cultured in growth medium (Ham's F-12K medium (Gibco, Luzern, Switzerland) supplemented with 10% fetal calf serum (Invitrogen, Basel, Switzerland), 2 mM L-glutamine (Gibco, Luzern, Switzerland) and 1% penicillin/streptomycin (Gibco, Luzern, Switzerland)). Cells were cultivated in a humidified incubator at 37 °C with 5% CO_2 atmosphere.

Polystyrene particles and characterization

Fluorescently yellow-green-labeled polystyrene (PS) particles of 80 nm (ex/em: 485/528 nm) and carboxylate-modified (COOH) 300 nm (ex/em: 485/528 nm) were purchased from Polyscience (Warrington, USA). Yellow-green-labeled 240 nm PS particles (ex/em: 485/520 nm) were purchased from Spherotech (Lake Forest, USA). Particles were vortexed for 2 min before preparation of experimental dilutions and exposure of cells.

The zeta potential of the particles in growth medium was determined with a Zetasizer NanoZS (Malvern Instruments, Malvern, UK).

Particle size distribution in growth medium and double distilled (DD) water was determined by nanoparticle tracking analysis (Nanosight LM 20 System, Amesbury, UK). Prior to analysis, growth medium and DD water were filtered using a 0.02 μm Anotop® 25 syringe filter (Whatman GmbH, Dassel, Germany). Results were normalized to the area under the NP concentration/size curve.

The stability of the fluorescence was assessed by analyzing the loss of fluorescence after incubation of 25 μg mL^{-1} PS

particles diluted in growth medium at 37 °C for 3, 6, 24, 48 and 72 h using a microplate reader (Biotek Synergy, Winooski, USA) with excitation and emission wavelengths of 485 nm and 528 nm. The loss of fluorescence was measured before and after filtration through a 0.1 μm syringe filter at the end of each incubation time.

In vitro cell viability assay

The MTS (3-(4,5-dimethylthiazol-2-yl)-5-(3-carboxymethoxyphenyl)-2-(4-sulfophenyl)-2*H*-tetrazolium) assay was used to test *in vitro* cytotoxicity of the different PS particles based on a colorimetric process to evaluate mitochondrial dehydrogenase activity of BeWo cells. In the presence of phenazine methosulfate, viable BeWo cells reduce MTS reagent to a colored formazan. 24 h prior to treatment, BeWo cells were seeded into a 96-well plate at 8000 cells per well. BeWo cells were exposed to 6.25, 12.5, 25, 50 and 100 μg mL^{-1} of plain 80 nm and 240 nm PS NPs and 300 nm COOH–PS particles for 3 h and 24 h at 37 °C and 5% CO_2. Exposure of cells to 1, 10, 100 and 1000 μM $CdSO_4$ served as positive control, whereas cells without treatment were used as the negative control. After incubation, an MTS assay (CellTiter96® AQueous One Solution Cell Proliferation Assay; Promega, Dübendorf, Switzerland) was performed according to the manufacturer's instructions. Results were presented as mean percentage of the untreated control from three independent experiments.

Uptake analysis on micropatterns

CYTOOchips™ were placed into P35 plastic culture dishes at 75 000 BeWo cells per chip. According to the manufacturer's protocol, dishes were not moved for 30 min after cell seeding to provide a uniform cell distribution and sedimentation, and were then transferred to the incubator. PS particles were added as soon as BeWo cells had spread onto the entire pattern area (after approximately 3 h) at a final concentration of 100 μg mL^{-1} for 80 nm and 10 μg mL^{-1} for 240 nm and 300 nm COOH–PS particles. After 14 h cells were fixed with 4% PFA (Sigma-Aldrich, Buchs, Switzerland)/0.2% TX100 (Sigma-Aldrich, Buchs, Switzerland) for 10 min, washed and incubated with Alexa Fluor 546 phalloidin (Invitrogen, Basel, Switzerland, 1 : 200) and DAPI (4′,6-diamidin-2-phenylindol) (Sigma-Aldrich, Buchs, Switzerland) for 1 h at room temperature. Prior to microscopic analysis CYTOOchips™ were mounted in Mowiol 4-88 (Sigma-Aldrich, Buchs, Switzerland).

Z-stack images were acquired with a 63× magnification oil immersion objective on a confocal laser scanning microscope (LSM 780, Zeiss, Feldbach, Switzerland) using the identical color intensity threshold for each type of NP. For each of the different experimental conditions 20 individual cells were imaged, which is a similar cell number to that used in other NP uptake studies.[63–65] After image processing (ZEN 2011, Zeiss, Feldbach, Switzerland; Photoshop CS6), heatmaps were determined from the 20 overlaid z-stacks/pattern for each pattern geometry, in order to visualize the average distribution of actin and internalized PS particles. Quantification of internalized 80 nm, 240 nm and 300 nm COOH–PS particles by single cells was performed from heatmap z-stack images using the ImageJ macro "Particle_in_Cell-3D".[61] Briefly, images of the actin cytoskeleton were used to recalculate the cell volume in which the particles were quantified. The total fluorescence of the internalized NPs was digitally assessed by the sum of all NP pixel intensities within each cell volume, which is assumed to be proportional to the amount of uptaken NPs.

Statistics

For statistical analysis of NP uptake, Tukey box-and-whiskers plots were created to compare median values of the integrated NP pixel intensities between the pattern geometries (Prism 6, GraphPad, California, USA). Values with a distance larger than 1.5 times the interquartile range from the 25th and 75th percentile were considered as outliers and shown individually. Results were analyzed by one-way ANOVA with Tukey's multiple comparison test and regarded as statistically significant at a *p*-value below 0.05.

Acknowledgements

We would like to thank Adriano A. Torrano for technical support in using the macro "Particles_in_Cell-3D". This project has received funding from the European Union's Seventh Framework Programme for research, technological development and demonstration under grant agreement no 309329 (NANOSOLUTIONS).

References

1 J. Nam, N. Won, J. Bang, H. Jin, J. Park, S. Jung, S. Jung, Y. Park and S. Kim, *Adv. Drug Delivery Rev.*, 2013, **65**, 622–648.
2 A. Z. Mirza and F. A. Siddiqui, *Int. Nano Lett.*, 2014, **4**, 1–7.
3 A. Meddahi-Pelle, A. Legrand, A. Marcellan, L. Louedec, D. Letourneur and L. Leibler, *Angew. Chem.*, 2014, **53**, 6369–6373.
4 T. L. Doane and C. Burda, *Chem. Soc. Rev.*, 2012, **41**, 2885–2911.
5 A. Albanese, P. S. Tang and W. C. Chan, *Annu. Rev. Biomed. Eng.*, 2012, **14**, 1–16.
6 H. Kettiger, A. Schipanski, P. Wick and J. Huwyler, *Int. J. Nanomed.*, 2013, **8**, 3255–3269.
7 A. E. Nel, L. Madler, D. Velegol, T. Xia, E. M. Hoek, P. Somasundaran, F. Klaessig, V. Castranova and M. Thompson, *Nat. Mater.*, 2009, **8**, 543–557.
8 L. Shang, K. Nienhaus and G. U. Nienhaus, *J. Nanobiotechnol.*, 2014, **12**, 1–11.
9 A. Verma and F. Stellacci, *Small*, 2010, **6**, 12–21.
10 F. Zhao, Y. Zhao, Y. Liu, X. Chang, C. Chen and Y. Zhao, *Small*, 2011, **7**, 1322–1337.
11 I. Canton and G. Battaglia, *Chem. Soc. Rev.*, 2012, **41**, 2718–2739.
12 T.-G. Iversen, T. Skotland and K. Sandvig, *Nano Today*, 2011, **6**, 176–185.
13 G. Sahay, D. Y. Alakhova and A. V. Kabanov, *J. Controlled Release*, 2010, **145**, 182–195.

14 L. Treuel, X. Jiang and G. U. Nienhaus, *J. R. Soc., Interface*, 2013, **10**, 1–14.
15 O. L. Mooren, B. J. Galletta and J. A. Cooper, *Annu. Rev. Biochem.*, 2012, **81**, 661–686.
16 M. Kaksonen, C. P. Toret and D. G. Drubin, *Nat. Rev. Mol. Cell Biol.*, 2006, **7**, 404–414.
17 F. Z. Idrissi, H. Grotsch, I. M. Fernandez-Golbano, C. Presciatto-Baschong, H. Riezman and M. I. Geli, *J. Cell Biol.*, 2008, **180**, 1219–1232.
18 M. Kaksonen, C. P. Toret and D. G. Drubin, *Cell*, 2005, **123**, 305–320.
19 C. J. Merrifield, D. Perrais and D. Zenisek, *Cell*, 2005, **121**, 593–606.
20 D. Yarar, C. M. Waterman-Storer and S. L. Schmid, *Mol. Biol. Cell*, 2005, **16**, 964–975.
21 A. E. Engqvist-Goldstein and D. G. Drubin, *Annu. Rev. Cell Dev. Biol.*, 2003, **19**, 287–332.
22 T. dos Santos, J. Varela, I. Lynch, A. Salvati and K. A. Dawson, *PLoS One*, 2011, **6**, e24438.
23 C. P. García, V. Sumbayev, D. Gilliland, I. M. Yasinska, B. F. Gibbs, D. Mehn, L. Calzolai and F. Rossi, *Sci. Rep.*, 2013, **1326**, 1–7.
24 J. S. Nowak, D. Mehn, P. Nativo, C. P. Garcia, S. Gioria, I. Ojea-Jimenez, D. Gilliland and F. Rossi, *Toxicol. Lett.*, 2014, **224**, 84–92.
25 B. Prietl, C. Meindl, E. Roblegg, T. R. Pieber, G. Lanzer and E. Frohlich, *Cell Biol. Toxicol.*, 2014, **30**, 1–16.
26 H. Herd, N. Daum, A. T. Jones, H. Huwer, H. Ghandehari and C. M. Lehr, *ACS Nano*, 2013, **7**, 1961–1973.
27 H. Meng, S. Yang, Z. X. Li, T. Xia, J. Chen, Z. X. Ji, H. Y. Zhang, X. Wang, S. J. Lin, C. Huang, Z. H. Zhou, J. I. Zink and A. E. Nel, *ACS Nano*, 2011, **5**, 4434–4447.
28 D. A. Ornelles, E. G. Fey and S. Penman, *Mol. Cell. Biol.*, 1986, **6**, 1650–1662.
29 A. L. Rampal, H. B. Pinkofsky and C. Y. Jung, *Biochemistry*, 1980, **19**, 679–683.
30 M. Thery, *J. Cell Sci.*, 2010, **123**, 4201–4213.
31 C. S. Chen, M. Mrksich, S. Huang, G. M. Whitesides and D. E. Ingber, *Biotechnol. Prog.*, 1998, **14**, 356–363.
32 K. K. Parker, A. L. Brock, C. Brangwynne, R. J. Mannix, N. Wang, E. Ostuni, N. A. Geisse, J. C. Adams, G. M. Whitesides and D. E. Ingber, *FASEB J.*, 2002, **16**, 1195–1204.
33 R. Singhvi, A. Kumar, G. P. Lopez, G. N. Stephanopoulos, D. I. C. Wang, G. M. Whitesides and D. E. Ingber, *Science*, 1994, **264**, 696–698.
34 M. Thery, A. Pepin, E. Dressaire, Y. Chen and M. Bornens, *Cell Motil. Cytoskeleton*, 2006, **63**, 341–355.
35 K. A. Kilian, B. Bugarija, B. T. Lahn and M. Mrksich, *Proc. Natl. Acad. Sci. U. S. A.*, 2010, **107**, 4872–4877.
36 J. James, E. D. Goluch, H. Hu, C. Liu and M. Mrksich, *Cell Motil. Cytoskeleton*, 2008, **65**, 841–852.
37 M. Thery, V. Racine, M. Piel, A. Pepin, A. Dimitrov, Y. Chen, J. B. Sibarita and M. Bornens, *Proc. Natl. Acad. Sci. U. S. A.*, 2006, **103**, 19771–19776.
38 J. Lee, A. A. Abdeen, T. H. Huang and K. A. Kilian, *J. Mech. Behav. Biomed. Mater.*, 2014, **38**, 209–218.
39 R. McBeath, D. Pirone, C. Nelson, K. Bhadriraju and C. Chen, *Dev. Cell*, 2004, **6**, 483–495.
40 J. Lee, A. A. Abdeen, D. Zhang and K. A. Kilian, *Biomaterials*, 2013, **34**, 8140–8148.
41 O. Lunov, T. Syrovets, C. Loos, J. Beil, M. Delecher, K. Tron, G. U. Nienhaus, A. Musyanovych, V. Mailander, K. Landfester and T. Simmet, *ACS Nano*, 2011, **5**, 1657–1669.
42 M. L. Etheridge, S. A. Campbell, A. G. Erdman, C. L. Haynes, S. M. Wolf and J. McCullough, *J. Nanomed. Nanotechnol.*, 2013, **9**, 1–14.
43 S. Grafmueller, P. Manser, L. Diener, P. A. Diener, X. Maeder-Althaus, L. Maurizi, W. Jochum, H. F. Krug, T. Buerki-Thurnherr, U. von Mandach and P. Wick, *Environ. Health Perspect.*, 2015, DOI: 10.1289/ehp.1409271.
44 S. Grafmueller, P. Manser, L. Diener, L. Maurizi, P. A. Diener, H. Hofmann, W. Jochum, H. F. Krug, T. Buerki-Thurnherr, U. von Mandach and P. Wick, *Sci. Technol. Adv. Mater.*, 2015, **16**(4), 044602, DOI: 10.1088/1468-6996/16/4/044602.
45 E. Mahon, D. R. Hristov and K. A. Dawson, *Chem. Commun.*, 2012, **48**, 7970–7972.
46 P. Pietzonka, B. Rothen-Rutishauser, P. Langguth, H. Wunderli-Allenspach, E. Walter and H. P. Merkle, *Pharm. Res.*, 2002, **19**, 595–601.
47 A. Salvati, C. Aberg, T. dos Santos, J. Varela, P. Pinto, I. Lynch and K. A. Dawson, *Nanomedicine*, 2011, **7**, 818–826.
48 T. Tenuta, M. P. Monopoli, J. Kim, A. Salvati, K. A. Dawson, P. Sandin and I. Lynch, *PLoS One*, 2011, **6**, e25556.
49 I. L. Aye and J. A. Keelan, *Chem.-Biol. Interact.*, 2013, **203**, 456–466.
50 H. Ali, I. Kalashnikova, M. A. White, M. Sherman and E. Rytting, *Int. J. Pharm.*, 2013, **454**, 149–157.
51 L. Cartwright, M. S. Poulsen, H. M. Nielsen, G. Pojana, L. E. Knudsen, M. Saunders and E. Rytting, *Int. J. Nanomed.*, 2012, **7**, 497–510.
52 S. Correia Carreira, L. Walker, K. Paul and M. Saunders, *Nanotoxicology*, 2013, **9**, 66–78.
53 A. R. Menjoge, A. L. Rinderknecht, R. S. Navath, M. Faridnia, C. J. Kim, R. Romero, R. K. Miller and R. M. Kannan, *J. Controlled Release*, 2011, **150**, 326–338.
54 M. S. Poulsen, T. Mose, L. L. Maroun, L. Mathiesen, L. E. Knudsen and E. Rytting, *Nanotoxicology*, 2013, **9**, 79–86.
55 P. Wick, A. Malek, P. Manser, D. Meili, X. Maeder-Althaus, L. Diener, P. A. Diener, A. Zisch, H. F. Krug and U. von Mandach, *Environ. Health Perspect.*, 2010, **118**, 432–436.
56 A. I. Ivanov, in *Exocytosis and Endocytosis*, ed. A. I. Ivanov, Humana Press, Totowa, NJ, 1st edn, 2008, pp. 15–33.
57 L. E. Dike, C. S. Chen, M. Mrksich, J. Tien, G. M. Whitesides and D. E. Ingber, *In Vitro Cell. Dev. Biol.: Anim.*, 1999, **35**, 441–448.
58 J. J. Moon, M. S. Hahn, I. Kim, B. A. Nsiah and J. L. West, *Tissue Eng., Part A*, 2009, **15**, 579–585.
59 S. Raghavan, C. M. Nelson, J. D. Baranski, E. Lim and C. S. Chen, *Tissue Eng., Part A*, 2010, **16**, 2255–2263.
60 J. P. Kaiser, T. Buerki-Thurnherr and P. Wick, *J. King Saud Univ., Sci.*, 2013, **25**, 15–27.

61 A. A. Torrano, J. Blechinger, C. Osseforth, C. Argyo, A. Reller, T. Bein, J. Michaelis and C. Brauchle, *Nanomedicine*, 2013, **8**, 1815–1828.
62 M. Geiser, B. Rothen-Rutishauser, N. Kapp, S. Schürch, W. Kreyling, H. Schulz, M. Semmler, V. I. Hof, J. Heyder and P. Gehr, *Environ. Health Perspect.*, 2005, **113**, 1555–1560.
63 F. G. Strobl, D. Breyer, P. Link, A. A. Torrano, C. Brauchle, M. F. Schneider and A. Wixforth, *Beilstein J. Nanotechnol.*, 2015, **6**, 414–419.
64 A. A. Torrano and C. Brauchle, *Beilstein J. Nanotechnol.*, 2014, **5**, 1616–1624.
65 J. Blechinger, A. T. Bauer, A. A. Torrano, C. Gorzelanny, C. Brauchle and S. W. Schneider, *Small*, 2013, **9**, 3970–3980.

Electronic Supplementary Information (ESI)

A micropatterning approach to study the influence of actin cytoskeletal organization on polystyrene nanoparticle uptake by BeWo cells

C. Muoth[a], M. Rottmar[b], A. Schipanski[b], C. Gmuender[a], K. Maniura-Weber[b], P. Wick[a] and T. Buerki-Thurnherr[a]

[a] Particles-Biology Interactions, Empa, Swiss Federal Laboratories for Materials Science and Technology, Lerchenfeldstrasse 5, 9014 St. Gallen, Switzerland

[b] Biointerfaces, Empa, Swiss Federal Laboratories for Materials Science and Technology, Lerchenfeldstrasse 5, 9014 St. Gallen, Switzerland

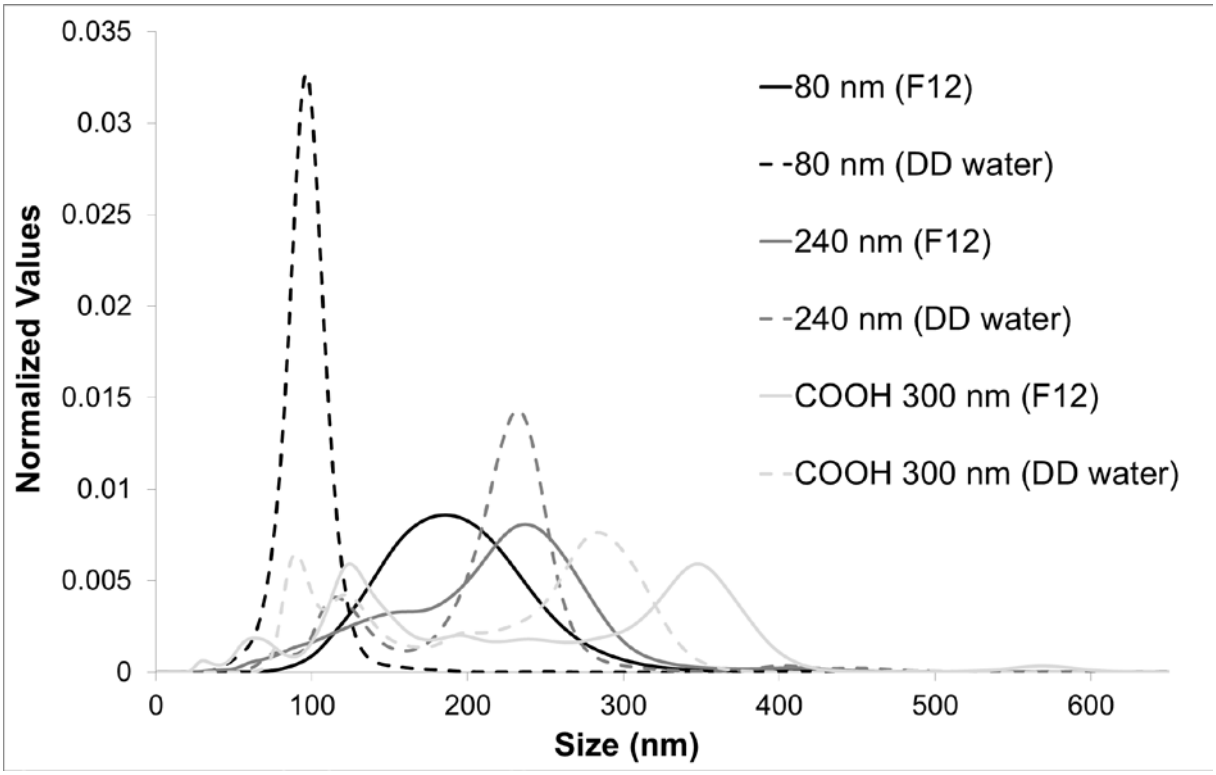

Figure 1. Size distribution of PS particles measured by nanoparticle tracking analysis. Size distributions were analyzed for 80 nm, 240 nm and COOH 300 nm PS particles diluted in either growth medium (F12) or DD water. For each particle, values were normalized to the area under the NP concentration/size curve.

A

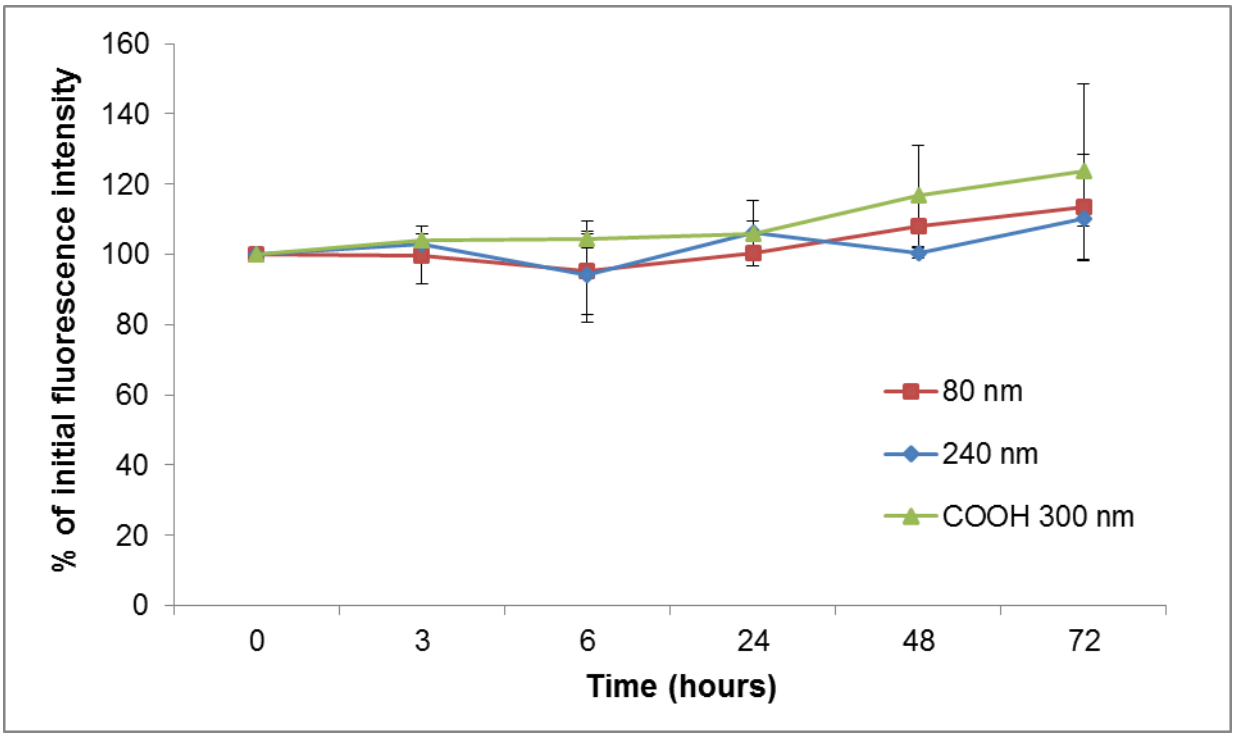

B

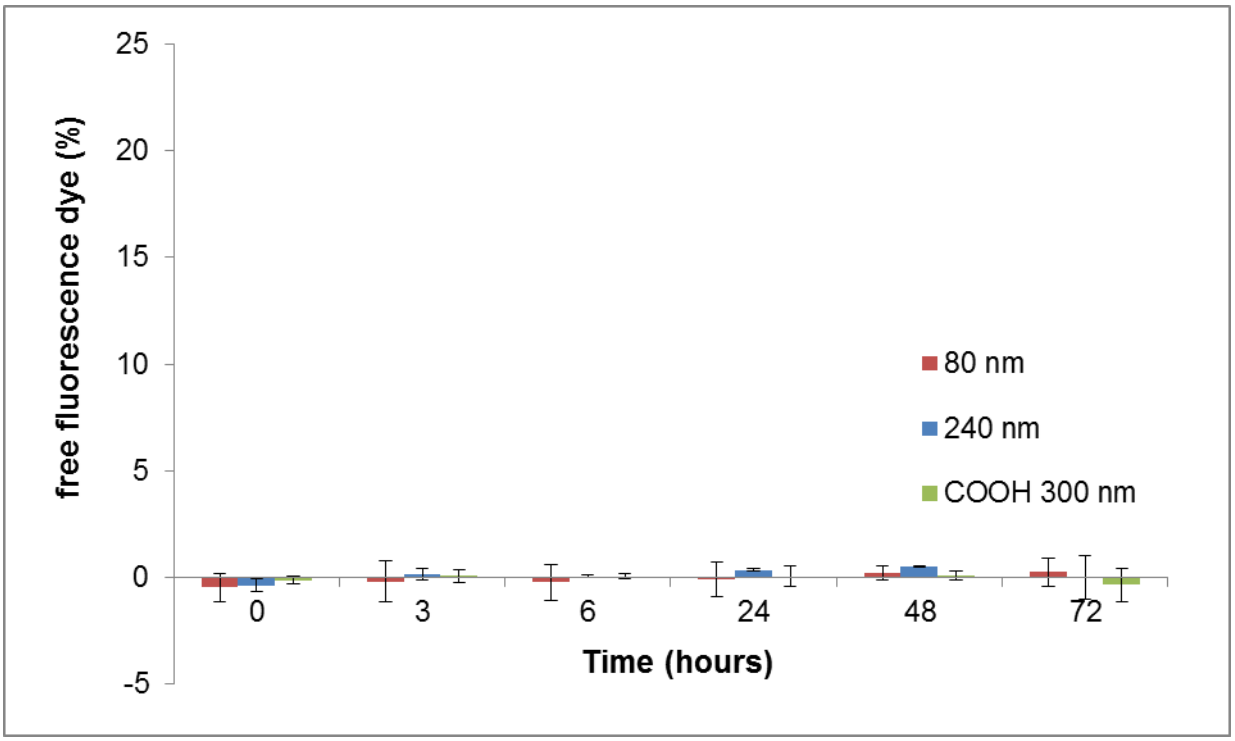

Figure 2. Fluorescence intensity measurements of PS particles. Fluorescence intensities of PS particles in growth medium at 37 °C were measured during 72 h. (A) Results are shown as the percentage of the initial fluorescence intensity at 0h. (B) Loss of the PS particle fluorescence in growth medium after filtration was determined over a time period of 72 h at 37 °C. Free fluorescence intensity is shown as percentage of total fluorescence intensity before filtration (mean ± SD, n=3).

A

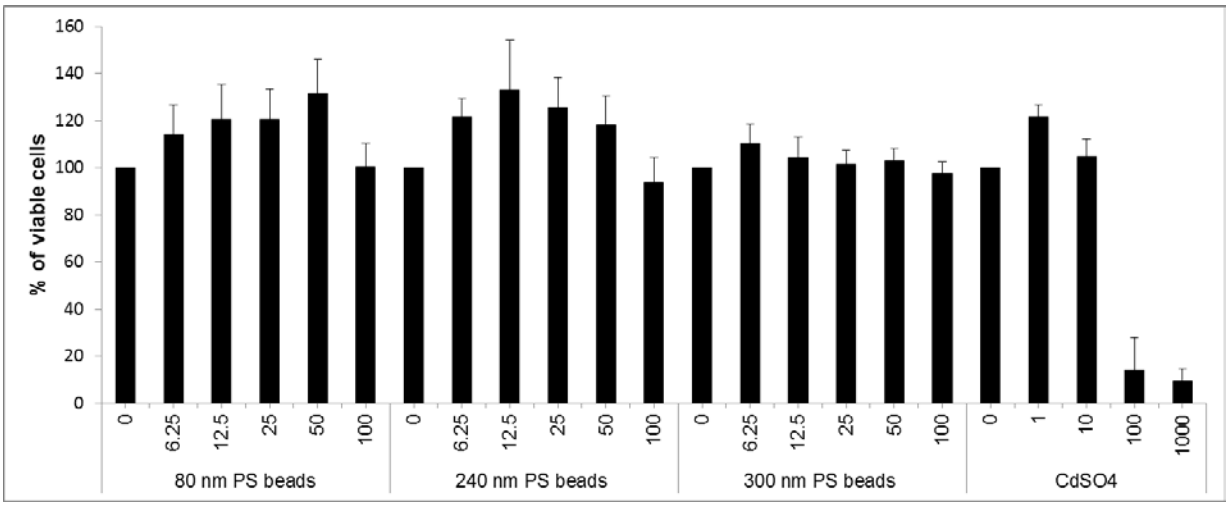

B

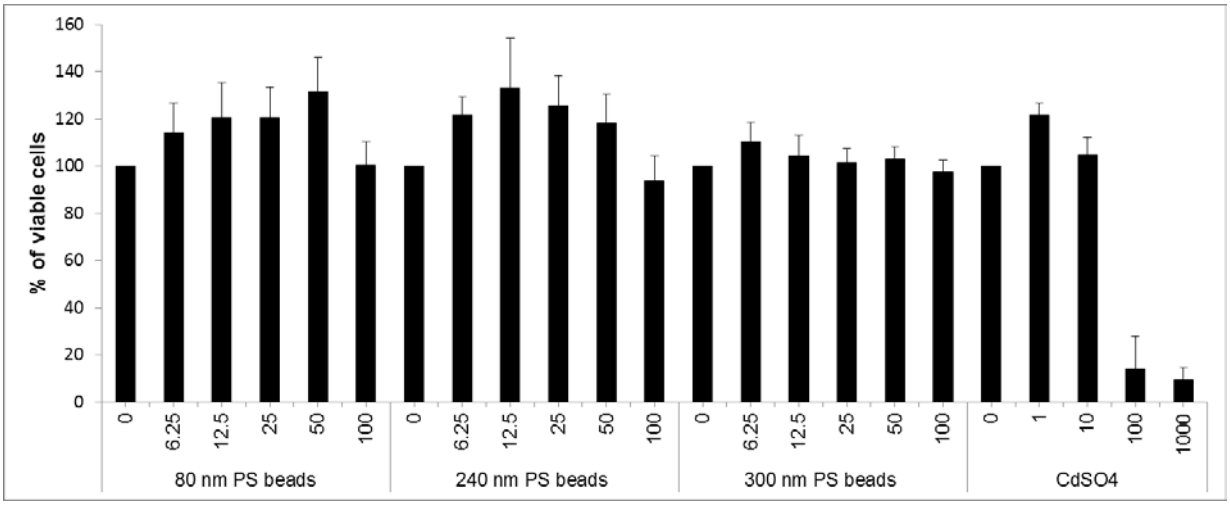

Figure 3. BeWo cell viability after exposure to PS particles. BeWo cell viability was assessed with a MTS assay after 3 h (A) and 24 h (B) of exposure to 80 nm, 240 nm and COOH 300 nm PS particles. $CdSO_4$ served as a positive control for cytotoxicity.

Data from 240 nm and COOH 300 nm PS particles have already been published by Grafmüller et al.[36] and were included in this figure to provide a complete overview on the cytotoxicity of all PS particles used in this study. Data represent the mean percentages of viable cells compared to the untreated control ± SD of 3 independent experiments.

Part II

A 3D microtissue co-culture model of the human placenta for nanotoxicity assessment

Carina Muoth, Adrian Wichser, Marco Monopoli, Manuel Correia, Nicky Ehrlich, Katrin Loeschner, Audrey Gallud, Melanie Kucki, Liliane Diener, Pius Manser, Wolfram Jochum, Peter Wick, Tina Buerki-Thurnherr

Author contribution

In this study, I developed, characterized and verified the co-culture MT model, established, adapted and performed all NP effect studies, analyzed and interpreted the results and wrote the manuscript.

This manuscript is under revision (Nanoscale).

Nanoscale

PAPER

View Article Online
View Journal | View Issue

Cite this: *Nanoscale*, 2016, **8**, 17322

A 3D co-culture microtissue model of the human placenta for nanotoxicity assessment†

Carina Muoth,[a] Adrian Wichser,[a] Marco Monopoli,‡[b] Manuel Correia,[c] Nicky Ehrlich,§[c] Katrin Loeschner,[c] Audrey Gallud,[d] Melanie Kucki,[a] Liliane Diener,[a] Pius Manser,[a] Wolfram Jochum,[e] Peter Wick[a] and Tina Buerki-Thurnherr*[a]

Received 25th August 2016,
Accepted 22nd September 2016

DOI: 10.1039/c6nr06749b

www.rsc.org/nanoscale

There is increasing evidence that certain nanoparticles (NPs) can overcome the placental barrier, raising concerns on potential adverse effects on the growing fetus. But even in the absence of placental transfer, NPs may pose a risk to proper fetal development if they interfere with the viability and functionality of the placental tissue. The effects of NPs on the human placenta are not well studied or understood, and predictive *in vitro* placenta models to achieve mechanistic insights on NP-placenta interactions are essentially lacking. Using the scaffold-free hanging drop technology, we developed a well-organized and highly reproducible 3D co-culture microtissue (MT) model consisting of a core of placental fibroblasts surrounded by a trophoblast cell layer, which resembles the structure of the *in vivo* placental tissue. We could show that secretion levels of human chorionic gonadotropin (hCG) were significantly higher in 3D than in 2D cell cultures, which indicates an enhanced differentiation of trophoblasts grown on 3D MTs. NP toxicity assessment revealed that cadmium telluride (CdTe) and copper oxide (CuO) NPs but not titanium dioxide (TiO_2) NPs decreased MT viability and reduced the release of hCG. NP acute toxicity was significantly reduced in 3D co-culture MTs compared to 2D monocultures. Taken together, 3D placental MTs provide a new and promising model for the fast generation of tissue-relevant acute NP toxicity data, which are indispensable for the safe development of NPs for industrial, commercial and medical applications.

Introduction

The developing fetus is highly vulnerable to toxic substances and adverse effects occur at doses that are usually not of any concern for adult individuals. To protect the growing fetus from potential harm, a key function of the placenta is to act as a tight barrier for the passage of pathogens and toxic compounds. However, there is increasing evidence that nanoparticles (NPs) can overcome this protective barrier and exert fetotoxic effects. Recent animal studies described placental uptake and/or translocation of gold (Au), silica (SiO_2), polystyrene (PS), cadmium oxide (CdO), titanium dioxide (TiO_2) NPs, quantum dots (Qdots) or carbon nanotubes (CNTs) among others (reviewed by ref. 1 and 2). Direct or indirect fetotoxic effects were observed after the exposure to multi-walled CNTs (MWCNTs),[3,4] single-walled CNTs (SWCNTs),[5,6] CdO,[7] cadmium telluride (CdTe)[8] or Cu NPs.[9] On the other hand, NPs hold great promises for the development of targeted therapies to treat patients more effectively and with reduced or absent off-target effects. In pregnancy, nanomedicine offers novel therapeutic approaches to specifically treat pregnant women, placental complications or fetal diseases by either preventing or enabling placental uptake or translocation of drug-loaded NPs.[2,10]

To ensure the safe development of NPs for various applications, a profound knowledge on NP effects and uptake mechanisms at the human placental barrier is crucial. Since the placenta is the most species-specific mammalian organ with unique anatomical and physiological properties,[11] it is difficult to extrapolate from animal data to humans. A well-established model with a high predictability of *in vivo*

[a]*Particles-Biology Interactions, Empa, Swiss Federal Laboratories for Materials Science and Technology, Lerchenfeldstrasse 5, 9014 St. Gallen, Switzerland. E-mail: tina.buerki@empa.ch*
[b]*Centre for BioNano Interactions, School of Chemistry and Chemical Biology, University College Dublin, Dublin 4, Ireland*
[c]*Research Group for Nano-Bio Science, Division for Food Technology, National Food Institute, Technical University of Denmark, Mørkhøj Bygade 19, DK-2860 Søborg, Denmark*
[d]*Division of Molecular Toxicology, Institute of Environmental Medicine, Karolinska Institutet, Nobels väg 13, 171 77 Stockholm, Sweden*
[e]*Institute of Pathology, Cantonal Hospital St. Gallen, Rorschacherstrasse 95, 9007 St. Gallen, Switzerland*

†Electronic supplementary information (ESI) available. See DOI: 10.1039/c6nr06749b

‡Current address: School of Pharmaceutical & Medicinal Chemistry, Royal College of Surgeons in Ireland, 123 Stephen's Green, Dublin 2, Ireland.
§Current address: CAPEC-PROCESS, DTU, Technical University of Denmark, Søltofts Plads, 2800 Kgs. Lyngby, Denmark.

placental transfer is the *ex vivo* perfusion of human full term placentas.[12,13,75] However, this model has certain drawbacks such as the restricted perfusion time of approximately 6–8 h, the low rate of successful perfusions as well as limited possibilities for mechanistic studies. In contrast, 2D *in vitro* cell culture models allow high-throughput studies but do not properly mimic the *in vivo* situation as they lack the complex organization and environment of the placental tissue such as the close interaction of different cell types or maternal and fetal blood flow. Hence, it is not surprising that 2D cultures often do not accurately predict *in vivo* toxicity and biological effects of NPs.[14] Moreover, key aspects of tissue distribution and penetration of NPs cannot be adequately addressed if cells are cultivated on artificial flat and rigid 2D surfaces.

Therefore, there is an urgent need for a predictive organotypic *in vitro* model of the human placenta that enables rapid nanotoxicity assessment of a large variety of different NPs as well as mechanistic studies on tissue uptake and penetration. A promising alternative to conventional 2D monocultures are co-culture microtissues (MTs). They provide extensive 3-dimensional cell–cell and cell–matrix interactions that promote the recovery of original tissue morphology and functionality.[15–17] Biological functions that were shown to be more similar to the *in vivo* situation in 3D MTs include cell proliferation, differentiation, morphogenesis, gene expression or drug response.[18–21] In the field of nanobiotechnology, MTs are increasingly used for toxicity and tissue penetration studies of different nanomaterials.[22] For instance, multiple exposure of liver MTs to silver (Ag) or zinc oxide (ZnO) NPs was associated with more significant adverse effects as compared to amine-modified TiO_2 NPs or MWCNTs.[23] Luo *et al.* investigated cytotoxic effects of bismuth (Bi) NPs with different surface modifications on 2D monolayer cultures and 3D MTs either consisting of epithelial cells (HeLa cells) or bone fibroblasts (MG-63 cells). Toxic effects on 3D MTs were significantly lower than on 2D monolayers.[24] This increased resistance to toxic substances in 3D MTs was confirmed by Lee *et al.* after the exposure of liver MTs to Qdots and Au NPs.[14] MT penetration studies showed a size-dependent penetration of carboxylate PS beads into tumor MTs, which could be significantly increased by collagenase treatment of MTs or immobilization of collagenase to the NP surface. Significant uptake was observed for 20 and 40 nm PS beads while less transport was detected for 100 and 200 nm PS beads.[25] Similarly, size-dependent penetration into breast cancer MTs (MCF-7 cells) was detected for 2 and 6 nm tiopronin-coated Au NPs whereas 15 nm NPs were localized in the outer rim of the MTs.[26] For 15 and 55 nm block copolymer micelles, Mikhail *et al.* found a size- and time-dependent penetration into cervical (HeLa) and colon (HT29) cancer MTs after 1 and 24 h but with much higher fluorescence signal intensity in HeLa MTs.[27] In summary, 3D MT models offer a promising approach to close the gap between 2D cell cultures and animal studies and to support the identification of safe nanomaterials for various applications.

In this study, we developed and characterized a high-throughput compatible *in vitro* co-culture MT model of the human placental barrier using the hanging drop technology.[28] MTs consisting of a core of human villous mesenchymal fibroblasts (HVMF) surrounded by a layer of human trophoblastic choriocarcinoma cells (BeWo cells) were generated and characterized with regard to MT morphology, growth, viability and expression of cell type-specific markers. Levels of human chorionic gonadotropin (hCG), an essential pregnancy-related hormone exclusively produced by trophoblasts, were compared between 3D MTs and BeWo cells grown on 2D plastic cell culture substrates. To evaluate the use of this model for nanosafety assessment, MT viability and functionality were investigated after the exposure to TiO_2, CdTe-COOH or CuO NPs for 24 h and viability data were compared to 2D monolayer cultures.

Experimental section

Cell culture

BeWo cells (b30 clone), a human placental choriocarcinoma cell line with cytotrophoblastic characteristics, were obtained from Prof. Dr Ursula Graf-Hausner (Zurich University of Applied Sciences, Wädenswil, Switzerland) with permission of Dr Alan L. Schwartz (Washington University School of Medicine, MO, USA) and cultured in Ham's F-12K medium (Gibco, Luzern, Switzerland) supplemented with 10% fetal calf serum (FCS, Invitrogen, Basel, Switzerland), 2 mM L-Glutamine (Gibco, Luzern, Switzerland) and 1% penicillin/streptomycin (Gibco, Luzern, Switzerland). BeWo cells between passages 18 to 38 were used for experiments. Primary human villous mesenchymal fibroblasts (HVMF, PromoCell) were cultured in fibroblast growth medium 2 (FGM, PromoCell) supplemented with 2 mM L-Glutamine (Gibco, Luzern, Switzerland), 1% penicillin/streptomycin (Gibco, Luzern, Switzerland) and one vial of Supplement Mix (PromoCell). Primary HVMFs were used for experiments between passages 4 and 10. HTR-8/SVneo cells originating from the extravillous cytotrophoblast were obtained from Dr Charles H. Graham (Queen University, Canada).[29] Cells were maintained in RPMI (Gibco, Luzern, Switzerland) supplemented with 5% FCS (Invitrogen, Basel, Switzerland), 2 mM L-Glutamine (Gibco, Luzern, Switzerland) and 1% penicillin/streptomycin (Gibco, Luzern, Switzerland)). All cell lines were cultivated in a humidified incubator at 37 °C with 5% CO_2 atmosphere and were sub-cultured twice a week.

Co-culture microtissue formation

The scaffold-free hanging drop system purchased from Insphero AG (Schlieren, Switzerland) was used to generate 3D co-culture MTs. HVMF were seeded into the GravityPLUS™ 96 well plates (©InSphero AG, Switzerland) at a density of 5000 cells per 40 µl (drop volume). MT formation was performed in FGM containing 20% FCS. At day 3, 300 BeWo or 500 HTR-8/SVneo cells in a volume of 20 µl were added to the fibroblastic core MTs. At day 5, MTs were transferred into GravityTRAP™ 96 well plates (©InSphero AG Switzerland) for subsequent NP exposure or analysis. Medium was replaced every second to

third day. The mean geometric diameter of spheroids was calculated according to the equation: $(a \times b)^{1/2}$, where a and b are the measured orthogonal diameters.[30]

Nanoparticle synthesis and dispersion

TiO_2, CdTe surface-functionalized with carboxylate moieties (CdTe-COOH) and CuO NPs were provided within the EU FP7 Nanosolutions project (http://www.nanosolutions.eu). Briefly, TiO_2 NPs were synthesized by forced hydrolysis of titanium tetrachloride solution followed by a washing step, stabilization with nitric acid and drying under vacuum at mild temperatures. CdTe-COOH NPs were manufactured by reacting Cd and Te precursors in aqueous solution in presence of mercaptocarboxylic acid as a stabilizing ligand. Upon reaching the desirable emission wavelength, quantum dots were precipitated by isopropanol. Several washing-centrifugations were followed by drying at 50 °C under vacuum to yield a dry powder. CuO NPs were fabricated in a two-step procedure including the synthesis of the freshly precipitated calcium hydroxycarbonate and its drying and calcination at the controlled heating rate.

Stock suspensions of 5 mg ml^{-1} of TiO_2 or CdTe-COOH NPs in ultra-pure water were obtained by bath sonication (1 min, 600 W, Sonorex RK156 BH, Bandelin). CuO NPs were dispersed in ultra-pure water to a stock suspension of 1 mg ml^{-1} using a probe sonicator operating at 230 V/50 Hz (Branson Sonifier 250, Branson Ultrasonic Co., Danbury, CT, USA, probe diameter of 6.5 mm, maximum peak-to-peak amplitude of 247 μm). The CuO NPs suspension was treated for 5 min at 30% of the maximum peak-to-peak amplitude, corresponding to a specific acoustic energy of 0.39 kJ dm^{-3} as determined by a calorimetric method for probe sonicator calibration.[31] Due to the potential dissolution of CdTe-COOH and CuO NPs, stock suspensions were prepared just prior to the experiments, diluted to the required final concentrations in supplemented FGM and immediately added to the placental co-culture MTs. NP powder and suspensions were characterized using different analytical methods (see ESI†) for a description of the NP characterization methods and Table S1† for a summary of the NP characteristics).

ATP assay

To determine the effects of different NPs on MT viability, MTs were exposed to 3, 6, 12, 25 and 50 μg ml^{-1} TiO_2, CdTe–COOH or CuO NPs for 24 h (final volume 70 μl). 0.1% Triton X-100 was used as the positive control and FGM as the medium control. Intracellular ATP levels were determined using a CellTiter-Glo® Luminescent Cell Viability Assay (Promega, USA), which is specifically adapted to 3D MTs. Samples were washed with PBS before addition of 40 μl per well of a 50 : 50 FGM/CellTiter-GLO® mixture and incubation for 30 min on a shaker at room temperature (RT). Cell lysates were transferred to a black 96-well plate (Microfluor™ 1, Thermoscientific, New York, USA) together with an ATP standard (Sigma, Buchs, Switzerland). Luminescent signals were measured with a microplate reader (Mithras^2 LB 943 Monochromator Multimode Reader, Berthold Technologies, Zug, Switzerland). Values were expressed in percentage of untreated control samples.

For viability assays with 2D BeWo and HVMF cultures, cells were seeded in 96-well plates at a density of 10 000 or 8000 cells per well in 200 μl FGM, respectively. After overnight incubation, cells were exposed to 3–50 μg ml^{-1} TiO_2, CdTe-COOH or CuO NPs for 24 h. The ATP assay was performed as described for 3D co-culture MTs but with the addition of 100 μl of the 50 : 50 FGM/CellTiter-GLO® mixture.

Immunohistochemical characterization of 3D MTs

For immunohistochemical (IHC) staining, 30–40 MTs were pooled, fixed with 4% formalin, embedded in paraffin and cut into 1.5–2 μm thick tissue sections. The IHC staining was performed using an automated staining system (BOND-MAX, Leica Microsystems). Hematoxylin and eosin (HE) staining was performed according to the standard protocol. For the antibody staining, sections were incubated with either MFN116 (1 : 400, 15 min, DAKO M0821), vimentin (1 : 1000, 15 min, DAKO M0725) or MIB-1 (1 : 60, 30 min, DAKO M7240) followed by visualization with 3,3′-Diaminobenzidine and counterstaining with hematoxylin (Bond Polymer Refine Detection Kit, Leica Microsystems). Prior to the antibody staining, antigen retrieval was performed using the Leica Bond Enzyme Pretreatment Kit for MNF116 or Leica Bond Epitope Retrieval Solution 2 for vimentin and MIB-1. The stained slices were captured with a Leica DM4000 B LED microscope (Leica Microsystems).

Live/dead staining

Cell viability of MTs was assessed using a Live/Dead Cell Imaging kit (R37601, Molecular Probes). MTs were exposed to 0.5, 1, 3 and 12 μg ml^{-1} CuO NPs for 24 h and immediately stained according to the manufacturer's protocol. *Z*-stack images were subsequently acquired with a 10x magnification objective on a confocal laser scanning microscope (LSM 780, Zeiss, Feldbach, Switzerland). Viable cells appeared green whereas dead cells appeared red.

hCG ELISA

The production of hCG was measured in 2D BeWo cell cultures and 3D co-culture MTs in the absence or presence of 20 μM forskolin (Sigma, Buchs, Switzerland). After transferring the MTs to trap plates, 70 μl of fresh FGM or FGM supplemented with 20 μM forskolin was added. Supernatants of four MTs per concentration were pooled and stored at −80 °C. For 2D BeWo cultures, cells were seeded in 96-well plates at a density of 3000 cells per well in 70 μl FGM and incubated for 48 h. Medium was thereafter replaced with fresh FGM or FGM supplemented with 20 μM forskolin. After 24 h, supernatants of four wells with the same treatment were pooled and stored at −80 °C. The effect of NPs on hCG production in 3D co-culture MTs was determined after treatment with 3–25 μg ml^{-1} CdTe-COOH, CuO or TiO_2 NPs for 24 h in FGM supplemented with 20 μM forskolin. To measure hCG production, the protocol from Malek *et al.* was adapted to MTs.[32] High protein binding

96 well plates (Corning, Root, Switzerland) were coated with polyclonal rabbit anti-human CG (Dako, A0231) in 50 mM $NaHCO_3$ (1 : 1000) over night at 4 °C. Blocking was performed with 0.5% bovine serum albumin (BSA) in PBS during 2 h at RT and plates were washed three times with 0.1% Tween 20 in PBS before standard or supernatants were added to the wells for 90 min at 37 °C. After three washing steps, the plates were incubated with mouse anti-human CG (BioSupply, UK) diluted in 1% BSA in PBS (1 : 5000) for 90 min at 37 °C followed by three washing steps. Goat anti-mouse-IgG-horse radish peroxidase conjugate (BioRad, Cressier, Switzerland) diluted in 1% BSA in PBS (1 : 5000) was added to the wells for 90 min at 37 °C followed by four washing steps. A *o*-phenylenediamine dihydrochloride I (OPD) tablet of 20 mg (Sigma, Buchs, Switzerland) was dissolved in 21 ml 0.05 M phosphate-citrate buffer with 0.03% sodium perborate (pH 5.0, Sigma, Buchs, Switzerland) and 100 µl of the solution were added to each well for 18 min at RT before the reaction was stopped with 2 N H_2SO_4. Absorbance was measured at 492 nm with a microplate reader (Mithras^2 LB 943 Monochromator Multimode Reader, Berthold Technologies, Zug, Switzerland). Concentration linearity for the standard was given between 0 and 30 mU ml^{-1}. Values were blank-corrected.

Scanning electron microscopy (SEM)

SEM was used to evaluate the surface morphology of the co-culture MTs. Briefly, MTs were fixed with modified Karnovsky solution (containing 4% paraformaldehyde, 2.5% glutaraldehyde and 50 : 50 mix of ddH_2O and PBS) at RT for 1 h. Samples were washed twice with PBS, followed by a dehydration series in ethanol (50–100%). MTs were placed on glass cover slips and exposed to hexamethyldisilazane (HMDS) for 30 min before drying at RT. Samples were stored in a vacuum-assisted desiccator until sputter-coating with a 10 nm thick layer of gold–palladium (Au/Pd: 80/20) alloy. Analysis was performed with a scanning electron microscope (Hitachi S-4800, Japan).

Transmission electron microscopy (TEM)

MTs were fixed in 3% glutaraldehyde in 0.1 M sodium cacodylate buffer and washed in 0.2 M sodium cacodylate buffer. After a post-fixation step in 2% osmium tetroxide in 0.1 M sodium cacodylate buffer, samples were dehydrated through a graded ethanol series followed by acetone and finally embedded in Epon resin (Sigma, Buchs Switzerland). Ultrathin sections were contrasted with 2% uranyl acetate and lead citrate (Reynolds 1963) before imaged in a Zeiss EM 900 (Carl Zeiss Microscopy, GmbH, Germany) at 80 kV.

Statistical analysis

Data are represented as the mean ± standard error of the mean (SEM) from at least three independent experiments. Statistical significance was determined using a two-tailed Student's *t*-test. A *p*-value below 0.05 was considered to be statistically significant. The web application WebAPP MDRA (available at http://biostatistics.dkfz.de/mdra/, access date: 30th of May 2016) was used to calculate EC_{50} values.

Results and discussion

Establishment and characterization of a human placental co-culture MT model

To develop a reproducible 3D *in vitro* co-culture MT model of the human placenta we employed the scaffold-free hanging drop technology (GravityPLUS™ plates). Compared to other methods used to generate 3D MTs (*e.g.* natural or synthetic hydrogels, solid scaffolds, rotary cultures or liquid overlay) the hanging drop technology allows for the precise and reproducible control of MT size and composition *via* the cell seeding number. Moreover, co-culturing is feasible and direct contact between different cell types enables their natural intercellular organization, polarization and development of an extracellular matrix. The 96-well format makes this technique compatible with high-throughput assay systems and thus offers an interesting method to screen various drugs or NPs on different tissue models.[33,34] In the human term placenta, fetal capillaries are embedded in villous trees that are in direct contact with maternal blood (Fig. 1). In order to enter the fetal blood stream, NPs have to cross the trophoblast cell layer that confines the villous trees, the villous stroma containing fibroblasts as well as the fetal capillary endothelium.[35,36] Trophoblasts are among the most important cells of the placental barrier and express highly specialized importers and exporters to regulate the transfer of gases, nutrients, waste products and different toxic substances. Moreover, they secrete a variety of hormones

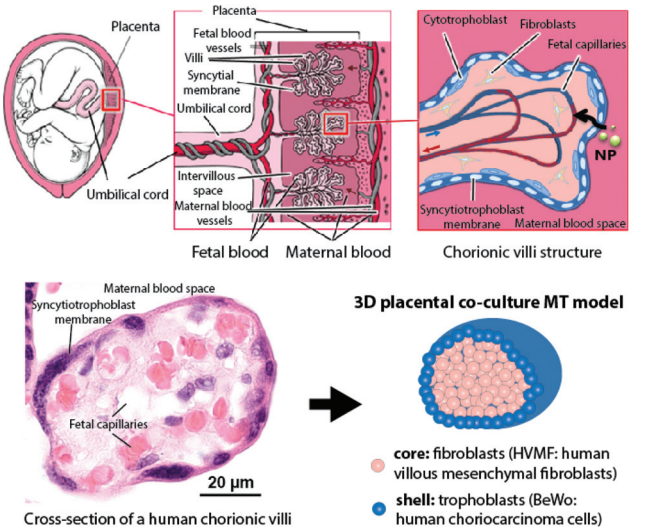

Fig. 1 Scheme of the human placenta and MT model. In the intervillous space, chorionic villi are surrounded by maternal blood that provides gases and nutrients for the fetus. In order to enter the fetal blood stream, NPs first have to cross the syncytiotrophoblast layer that confine the villi, penetrate through the villous stroma containing fibroblasts and finally cross the fetal capillary endothelium. Our newly developed 3D co-culture MT model is composed of an inner core of fibroblasts that derive from the villous stroma (rose) surrounded by trophoblasts (blue), which contribute most to the specific barrier function of the placenta. Figure was reproduced and adapted with permission from Nanomedicine as agreed by Future Medicine Ltd.[2]

that are essential to fetal life and placental development. To mimic the human placental tissue in a 3D co-culture MT model, we established fibroblastic core MTs from HVMFs that were surrounded by an outer layer of trophoblasts (Fig. 1). For the latter, the well-characterized and widely used choriocarcinoma cell line BeWo was chosen since these cells reveal many of the morphological and functional characteristics of villouos trophoblasts, including partial syncytial fusion, syncytin 1 and 2 regulation, expression of transporters as well as secretion of hormones such as hCG, human placental lactogen, progesterone and estradiol.[37–39] Furthermore, BeWo cells are of human origin, which is important to circumvent species-specific differences in *in vitro* placenta models. The optimal medium that best sustained the viability of HVMFs and BeWo cells was FGM (data not shown). To obtain well-structured co-culture MTs, we first established the formation of a stable fibroblastic core MT. Cell seeding number and incubation time for HVMFs were optimized in order to obtain tightly packed core MTs that resisted major invasion by BeWo cells. Spheroid sizes should not exceed 500 μm in order to avoid necrotic cores due to diffusion limitations for oxygen and nutrients.[20] Stable core MTs with a highly reproducible size of 223 ± 8.3 μm were obtained 3 days after seeding of 5000 HVMFs per well of a 96-well hanging drop plate. To obtain a continuous BeWo cell coat around the core MTs, 300 BeWo cells were added to the fibroblastic core MTs and further cultivated in the hanging drop for 2 days. After 5 days, MTs were transferred into non-adhesive GravityTRAP™ plates, fixed and subjected to morphological analysis. Highly spherical and compact spheroids were formed as evidenced by SEM analysis of the MT surface (Fig. 2A). TEM micrographs further revealed that BeWo cells exhibited a polarized morphology with numerous microvilli on their apical cell surface (Fig. 2B). Moreover, they developed tight junctional complexes and desmosomes between neighboring cells (Fig. 2B). Immunohistochemical staining of paraffin sections for vimentin (marker of fibroblasts) and cytokeratin (marker of trophoblasts) confirmed the formation of highly organized co-culture MTs with a distinct core–shell structure (Fig. 3A and B). HVMFs built a stable core spheroid surrounded by one to three layers of BeWo cells, which did not invade the fibroblastic core. Only in rare cases, BeWo cells did not cover the entire surface of the fibroblastic MTs. Interruptions of the syncytiotrophoblast barrier are also a regular finding, which occur in every placenta and throughout pregnancy.[21] It has been described that approximately 7% of the villous surface contains such gaps filled with fibrin as a result of blood clotting after degeneration or mechanical forces.[40] The established 3D co-culture MTs were highly viable as no necrotic core formation was evident on HE stained paraffin sections (Fig. 3C). Furthermore, a live/dead staining confirmed the absence of dead cells (Fig. S5†). Upon staining for the proliferation marker MIB-1, co-culture MTs showed positive cells exclusively in the outer shell, indicating that BeWo cells continued to divide (Fig. 3D). To see if a stable MT size can be obtained as previously observed for some cell lines[24] we performed a growth profile of the co-culture MTs over 14 days starting on day 5 after MT formation was completed (Fig. 4 and ESI Fig. S3†). While HVMF core MTs gradually compacted and obtained a stable size of 164 ± 6.9 μm, BeWo/HVMF MTs steadily increased in size and exceeded a critical diameter of 500 μm at day 10. Since BeWo cells lack cell contact inhibition when cultivated in 2D, we explored if the use of HTR-8/SVneo trophoblast cells, which grow to a confluent monolayer could be used to obtain stable co-culture MTs. However, HTR-8/SVneo cells continued to proliferate in 3D co-culture MTs, albeit at a lower growth rate as compared to BeWo cells (Fig. 4). In future studies, the replacement of BeWo cells by post-mitotic primary trophoblasts may provide a solution to obtain stable co-culture MTs for long-term exposure studies.

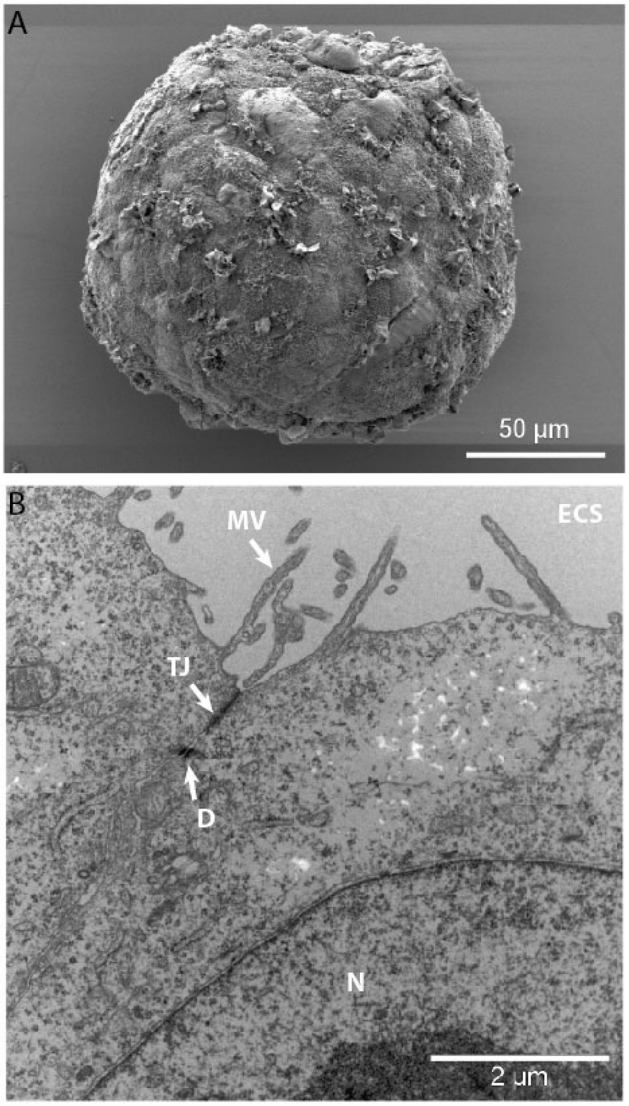

Fig. 2 Electron microscopy of human placental co-culture MTs. After 5 days of cultivation, MTs were processed for SEM or TEM analysis. (A) Representative SEM image of a 3D co-culture MT. (B) TEM micrograph of BeWo cells on the edge of a 3D co-culture MT. Abbreviations: ECS, extra cellular space; D, desmosome; N, nucleus; MV, microvilli; TJ, tight junction.

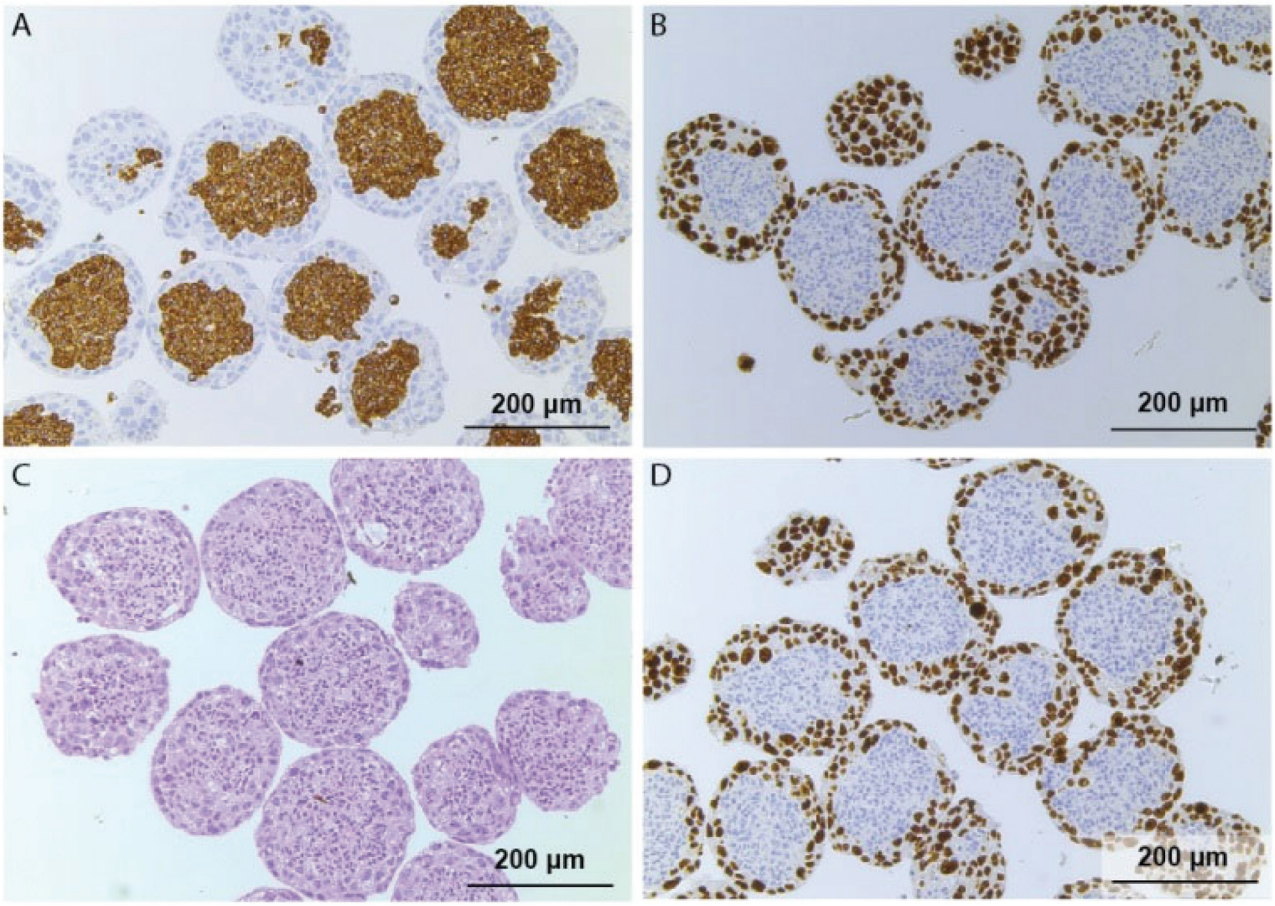

Fig. 3 Immunohistochemical characterization of human placental co-culture MTs. After 5 days of cultivation, MTs were processed for immunohistochemical analysis. Paraffin sections were stained with either the mesenchymal cell marker vimentin to visualize HVMF (A), the epithelial cell marker MNF116 to label cytokeratins specifically expressed by BeWo cells (B), hematoxylin/eosin (C) or MIB-1 to show proliferating cells (D).

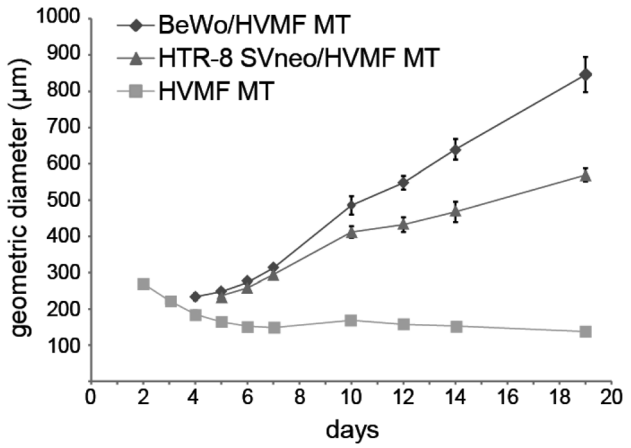

Fig. 4 Growth profiles of fibroblastic core MTs and co-culture MTs over 19 days. The geometric diameter was calculated for HVMF, BeWo/HVMF and HTR-8/SVneo/HVMF co-culture MTs.

One of the major functions of the human placenta is the production of different hormones in order to support pregnancy and fetal growth. Among these, human chorionic gonadotropin (hCG) is a key hormone, which is produced by the syncytiotrophoblast of the chorionic villi and is secreted into the intervillous space. hCG fulfills many essential functions in pregnancy, including the promotion of progesterone production, implantation and decidualization, angiogenesis, cytotrophoblast differentiation, and immune cell regulation.[41] Potential hCG dysregulation could therefore lead to adverse pregnancy outcomes.[42] In this study, hCG levels were measured as an indicator for the functionality of BeWo cells and later on to study if NPs may interfere with endocrine functions of the placenta. When cultured in 3D co-culture MTs, BeWo cells released significantly more hCG as compared to 2D monocultures (Fig. 5). Moreover, hCG production could be stimulated by forskolin, a known inducer of trophoblast differentiation. These results confirm that BeWo cells cultivated in 3D are highly functional. In addition, the significantly increased hCG levels suggest that BeWo cells may be in a more differentiated state towards the formation of a syncytium when grown under 3D culture conditions.[43] In order to visualize potential syncytium formation of BeWo cells on the MTs, tight junctions were immunofluorescently stained with an anti-ZO-1 antibody (ESI Fig. S4†). Small multinucleated areas with

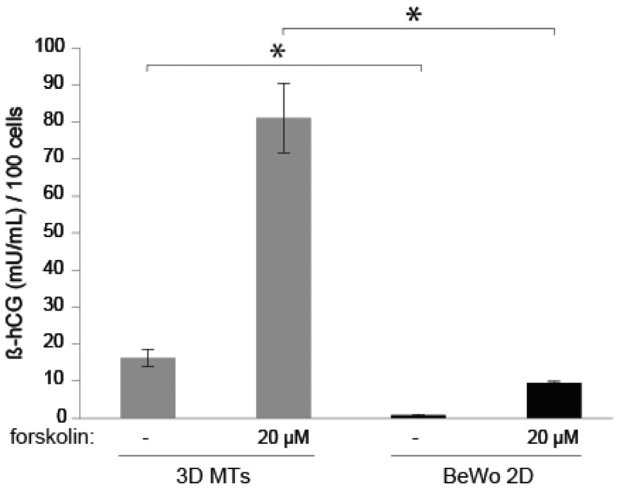

Fig. 5 Functional characterization of 3D MTs for the production of β-hCG and comparison to 2D BeWo monocultures. The release of the placental hormone β-hCG from BeWo cells grown in 3D co-culture MTs or as 2D monocultures was determined after 24 h of cultivation with and without stimulation of BeWo cell differentiation with 20 µM forskolin.

syncytia characteristics were observed in untreated control MTs and forskolin addition did not further increase the extent of syncytialization. However, the visualization of tight junctions in 3D MTs is challenging and further studies should be performed to unambiguously confirm syncytium formation on 3D MTs.

Single cell type spheroids of human choriocarcinoma cells have been established previously and are mostly used to study various aspects of implantation and placental physiology.[44,45] Introduction of a fibroblast core as in the here presented model was performed to better mimic the placental barrier structure, which is particularly relevant for NP uptake/penetration studies. Moreover, inclusion of fibroblasts is expected to provide more tissue-relevant responses since uptake and biological effects of NPs can be highly dependent on the cell type as well as cell type to cell type interactions.[46,47] Finally, hCG production in co-culture MTs is limited to the outer layers formed by BeWo cells similar to the syncytiotrophoblast layer covering the maternal surface of the placental tissue barrier. In mono-BeWo spheroids, cells in the core will be partially protected from NP exposure and may continue to produce hCG, thereby potentially masking subtle effects of NPs on hormone secretion.

Nanoparticle selection and characterization

Different NPs of industrial relevance were provided within the EU FP7 Nanosolutions project. We have selected non-toxic TiO_2 NPs[48] as well as generally toxic CuO and CdTe-COOH NPs[49,50] in order to evaluate the potential of the 3D MT model for nanotoxicity assessment. Different methods were applied to assess the physico-chemical characteristics of these NPs (for a summary on NP characteristics see Table S1 in the ESI†). The average primary particle size determined by TEM was around 4 nm for TiO_2 NPs and 10–20 nm for CuO NPs (ESI Fig. S1†). BET analysis revealed a specific surface area of 98 ± 10 $m^2\ g^{-1}$ for TiO_2 NPs and of 42 ± 2 $m^2\ g^{-1}$ for CuO NPs. The average particle size according to BET was 14 nm for TiO_2 NPs and 20 nm for CuO NPs. Dynamic light scattering (DLS) analysis showed a hydrodynamic size of the dispersed particles of 17 ± 0.3 nm for TiO_2 and 1165 ± 71 nm for CuO NPs in water and of 8284 ± 900 nm for TiO_2 and 1851 ± 159 nm for CuO NPs in medium, indicating a strong agglomeration of particles in medium. UV-Vis absorption and fluorescence spectroscopy was applied to characterize CdTe-COOH NP suspensions. Absorption spectra displayed a maximum located at 549 nm wavelength (ESI Fig. S2†), while the fluorescence emission spectra were characterized by a peak at 580 nm wavelength (data not shown). The diameter of CdTe-COOH NPs as calculated from the position of the exciton band was around 3.2 nm.[42] These values are typical for CdTe NPs, and together with the high fluorescence quantum yield, indicate that the CdTe-COOH NPs were well dispersed in the aqueous suspension. All NPs have been tested for endotoxin contamination and were endotoxin free (<0.5 EU ml^{-1} in Chromogenic LAL assay).

Impact of the selected NPs on placental co-culture MT viability

The effects of TiO_2, CuO or CdTe-COOH NPs on co-culture MT viability were quantified using a luminescent cell viability assay, which measures the intracellular ATP content. In this assay, MTs are lysed before ATP is determined, which results in a higher sensitivity as compared to *e.g.* the MTS assay where the diffusion of the substrate is limited by the 3D structure. While TiO_2 NPs did not affect MT viability, CdTe-COOH and CuO NPs induced a dose-dependent decrease in ATP levels (Fig. 6). CdTe-COOH NPs were slightly more toxic to co-culture MTs than CuO NPs. The cytotoxic effects of CuO and CdTe-COOH NPs were also observed when performing the same ATP assay in 2D HVMF or BeWo monocultures (ESI Fig. S5†). The reduction in ATP levels was highly similar for both cell types, suggesting that HVMF and BeWo cells are equally sensitive to CuO and CdTe-NPs. However, EC_{50} values for CuO and CdTe-COOH NPs were significantly higher for 3D MTs (9.34 µg ml^{-1} and 27.3 µg ml^{-1}) than for 2D monocultures (6.41 µg ml^{-1} and 8.62 µg ml^{-1} for HVMFs or 2.9 µg ml^{-1} and 6.51 µg ml^{-1} for BeWo cells). These results suggest that 3D placental MTs are

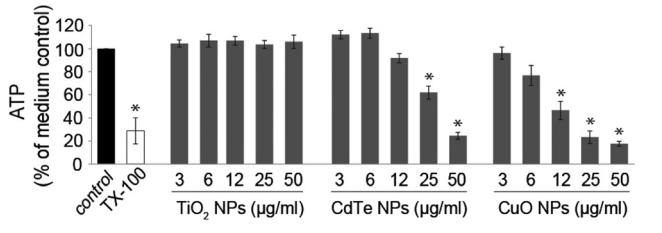

Fig. 6 Effects of different NPs on the 3D MT viability. Co-culture MTs were exposed to TiO_2, CdTe-COOH or CuO NPs for 24 h. Cell viability was assessed using the ATP assay. As a positive control cells were treated with 0.1% TX-100. Data represent the mean percentages triplicates compared to the untreated medium control ± SEM of 3–4 independent experiments. *p < 0.05 compared to untreated medium controls.

more resistant to toxic NPs than 2D cell cultures. Yet, a direct comparison is challenging due to differences in cell numbers or the use of mono- *versus* co-cultures, among others. Nevertheless, an increased resistance of 3D MTs to toxic NPs has been previously observed such as for liver MTs exposed to CdTe NPs,[14] colon MTs exposed to Zn NPs[51] or MTs from human adipose-derived mesenchymal stem cells exposed to carboxyl-functionalized CdTe/CdS/ZnS Qdots.[52] The differences are likely due to the fact that close cell–cell and cell–matrix interactions as well as the tissue-like structure provided by 3D MTs limit the penetration of particles. Consequently, cells in the core of the MTs will be partially protected from the exposure to toxic NPs by the cells of the outer layers.[24,52] In the case of the placental co-culture MTs, BeWo cells will be preferentially affected by the NPs due to the core–shell structure with BeWo cells on the outer edge of the spheroid. Indeed, live/dead staining confirmed that mostly the outer cells were dying after exposure to increasing concentrations of CuO NPs whereas cells in the core remained viable (ESI Fig. S6†). Therefore, even if the viability of 3D MTs is only slightly reduced by a few percentages, placental barrier integrity may already be severely compromised. As CuO and CdTe-COOH induced major cytotoxicity on HVMF and BeWo cells both in 2D monocultures as well as in 3D co-cultures the exposure to such NPs during pregnancy should be avoided. Adverse effects were also observed in many other *in vitro* and *in vivo* studies after exposure to CuO NPs[53–56] or semiconducting NPs (*e.g.* CdTe[57–59] or CdSe/ZnS[60,61]).

It appears that the mechanisms underlying the toxicity of these NPs include particle dissolution and/or the generation of reactive oxygen species (ROS).[55,56,58,60,62,63] Leaching of toxic ions from NPs can occur outside of cells or intracellularly, in particular in lysosomes where a low pH favors dissolution (Trojan horse mechanism).[64] Free cadmium and copper ions act as catalysts in the formation of ROS, which may result in oxidative tissue damage.[65,66] Dissolution studies of TiO_2 and CuO NPs were performed in cell culture medium and ions were separated from NPs by centrifugation. CdTe-COOH NPs were not included as they were too small to remove particles by centrifugation or ultrafiltration. We measured only a minor release of Ti ions from TiO_2 NPs (1.5% Ti after 24 h) whereas the percentage of Cu ions was 13% after 10 min and 59% after 24 h of incubation (ESI Table S1†). Since centrifugation might not remove all NPs from the supernatant, ultrafiltration was used as an alternative method. The amount of released Cu ions was 7% after 10 min and 50% after 24 h of incubation, which was highly similar to the results obtained by centrifugation. Although solubility studies in the absence of cells do not fully reflect the experimental conditions, the high dissolution of CuO NPs in medium suggests that toxic Cu ions are at least partially involved in CuO NP-mediated toxicity to placental cells. To understand if the absence of cytotoxic effects upon exposure to TiO_2 NPs was due to the lack of particle uptake we performed TEM analysis. TiO_2 NPs were internalized by BeWo cells and large agglomerates were present either freely in the cytoplasm or in membrane-bound vesicles (ESI Fig. S7†). However, no TiO_2 NPs were observed in the fibroblastic core. We do not exclude that single TiO_2 NPs or small agglomerates may have penetrated into the fibroblastic core but as this area is highly compact and electron dense (ESI Fig. S8†), it is much more difficult to detect internalized particles in the MT core.

Validation of the obtained results in order to understand the predictive value of the co-culture MTs is challenging as only few *in vivo* data are available from animal studies, which may not be representative for human pregnancy due to major species-specific differences. In mice, 1–3 nm CdTe/CdS Qdots and 35 nm TiO_2 NPs appeared to cross the placental barrier, although in very low amounts.[8,67] While no histological defects to the placental tissue were observed after Qdot exposure,[8] TiO_2 NPs affected tissue viability and structure.[67] However, to circumvent uncertainties due to the use of different NPs or rodent models, we performed additional *ex vivo* human placenta perfusion studies with TiO_2 NPs used for co-culture MTs exposure (ESI Fig. S9†). Ti concentrations determined in the fetal circuit were only 1% of the initial dose applied to the maternal circuit. However, similar Ti concentrations were also measured in control perfusions where no TiO_2 NPs were applied (data not shown), indicating that TiO_2 NP translocation was very low or even absent. The measured Ti background signal of approximately 0.2 $\mu g\ g^{-1}$ was still above the detection limit (0.004 $\mu g\ g^{-1}$). In the maternal circulation, Ti levels decreased to 20% of the initial amount suggesting that particles agglomerated in the placental tissue. The absence of vascular leakage and NP transfer indicates that TiO_2 NPs did not elicit major damage to placental barrier integrity. Similar conclusions have been obtained from our co-culture MT studies where TiO_2 NPs did accumulate in the trophoblast layer (ESI Fig. S7†) but did not affect BeWo cell viability (Fig. 6). From these comparisons it appears that co-culture placenta MTs may indeed be a valuable model to assess NP-placenta interactions, which could then be further validated in *ex vivo* perfusion or animal studies. However, to fully understand the predictive value and limitations of placental co-culture MTs further characterization and validation studies will be required.

Impact of the selected NPs on the secretion of hCG from placental co-culture MTs

Even if NPs do not elicit direct cytotoxic effects on the placental tissue they might affect fetal health if they interfere with proper placental function. A hugely important function of the human placenta is the production of many hormones, which affect the status of pregnancy and maternal physiology. A malfunction may result in fetal complications or even a miscarriage.[42] To understand if TiO_2, CdTe-COOH or CuO NPs may act as endocrine disruptors at the placental barrier, we assessed their effects on the release of hCG in 3D co-culture MTs. These studies were performed in the presence of 20 μM forskolin in order to upregulate the differentiation of BeWo cells and to allow a decreases in hCG levels to be easily detected. TiO_2 NPs did not affect hCG levels whereas already

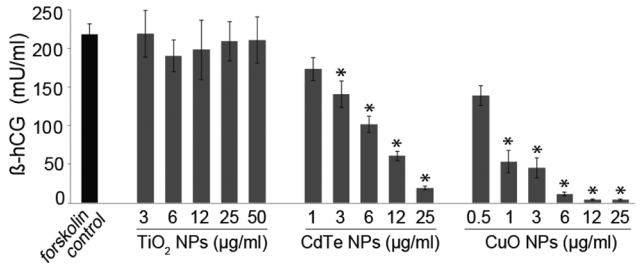

Fig. 7 β-hCG levels of co-culture MTs after exposure to different NPs. MTs were exposed to TiO_2, CdTe-COOH or CuO NPs diluted in medium containing 20 μM forskolin for 24 h. Data represent the mean ± SEM (NPs n = 3–4, forskolin control n = 14). *p < 0.05 *vs.* 20 μM forskolin control.

low concentrations of CuO or CdTe-COOH NPs significantly reduced hCG production (Fig. 7). However, it was difficult to identify subtoxic NP doses, which was required to exclude that the observed reduction was a secondary effect due to cell death. Since hCG in co-culture MTs is only produced by BeWo cells, dose–response curves for the individual cell types in the co-culture MTs would be required. Attempts to obtain such toxicity data using FACS analysis of dissociated MTs stained with PI and pre-labeled HVMFs (Cell Tracker™ green CMFDA) failed due to non-specific staining of BeWo cells with dye released from dead HVMFs. Nevertheless, live/dead staining and microscopic images of the co-culture MTs after exposure to CuO NPs showed that 0.5 μg ml^{-1} was likely to reflect a non-toxic concentration since only few dead cells were present on the MT surface and the edge of the MTs was still compact (ESI Fig. S6A and B†). No live/dead images were possible for CdTe-COOH NPs due to their fluorescent properties but bright-field images revealed MTs with a compact surface for concentrations up to 3 μg ml^{-1} (ESI Fig. S6C†). In addition, ATP assay of 2D BeWo monocultures showed that after treatment with 0.5 μg ml^{-1} CuO NPs or 3 μg ml^{-1} CdTe-COOH NPs, cell viability was around 80% or higher, indicating that these are likely to reflect subtoxic concentrations.

At 3 μg ml^{-1} CdTe-COOH NPs, hCG levels were significantly decreased whereas only a slight (non-significant) reduction was observed for 0.5 μg ml^{-1} CuO NPs (Fig. 7). Collectively, these findings suggest that CdTe-COOH NPs may have the potential to interfere with the endocrine function of the placenta but further studies including additional placenta-relevant hormones as well as *in vivo* studies would be required to corroborate this hypothesis. Interestingly, there is supporting evidence from studies on smoking women showing that exposure to Cd and other toxic metals interferes with placental hormone production (*e.g.* Cd affects placental leptin and progesterone production[68]).

Conclusions

During the last years, a large variety of highly sophisticated 3D models have been developed for different biological tissues and barrier such as the lung,[69–71] the liver[72] or the brain.[73] These models achieved major improvements in regard to toxicity assessment of drugs or NPs as compared to 2D models. However, 3D models of the placental barrier are scarce despite the urgent need for reliable nanosafety data in human pregnancy.[1,2,74] With the development of the first human 3D placental co-culture microtissue model using the high-throughput compatible hanging drop technology we enable a more realistic mechanistic toxicity assessment at tissue level. Cell morphology, hormone secretion by trophoblasts and structural organization of the co-culture MTs were shown to better recapitulate the *in vivo* situation as compared to 2D cell cultures. We confirmed that this model is suitable for the rapid evaluation of acute toxicity and hormone secretion levels after the exposure to different NPs. Importantly, our results on CdTe-COOH NPs showed that for core/shell-type co-culture MTs it is critical to not only study cell type-independent endpoints such as ATP levels as these may underestimate NP toxicity at the placental barrier. To obtain a fundamental understanding of NP-placenta interactions, it will be critical to relate adverse effects to the individual cell types and/or to include cell type-specific measurements such as hormone production. In addition to acute toxicity assessment, the co-culture MT model holds great potential for the assessment of NP penetration and uptake mechanisms because a more tissue-like transport of NPs can be expected due to the 3D structure. Finally, we anticipate that the inclusion of additional cell types such as immune cells or endothelial cells as well as the replacement of BeWo cells with primary trophoblasts will further improve the predictive value of this promising new 3D placental microtissue model.

Acknowledgements

We thank Dr Matthias Roesslein, Empa, for support in statistical analysis and Prof. Bengt Fadeel, Karolinska Institutet, for helpful comments on the manuscript. This project has received funding from the European Union's Seventh Framework Programme for research, technological development and demonstration under grant agreement no 309329 (NANOSOLUTIONS) and no. 263215 (MARINA).

References

1 C. Muoth, L. Aengenheister, M. Kucki, P. Wick and T. Buerki-Thurnherr, *Nanomedicine*, 2016, **11**, 941–957.
2 J. A. Keelan, J. W. Leong, D. Ho and K. S. Iyer, *Nanomedicine*, 2015, **10**, 2229–2247.
3 W. Qi, J. Bi, X. Zhang, J. Wang, J. Wang, P. Liu, Z. Li and W. Wu, *Sci. Rep.*, 2014, **4**, 4352.
4 X. L. Huang, F. Zhang, X. L. Sun, K. Y. Choi, G. Niu, G. F. Zhang, J. X. Guo, S. Lee and X. Y. Chen, *Biomaterials*, 2014, **35**, 856–865.
5 L. Campagnolo, M. Massimiani, G. Palmieri, R. Bernardini, C. Sacchetti, A. Bergamaschi, L. Vecchione, A. Magrini, M. Bottini and A. Pietroiusti, *Part. Fibre Toxicol.*, 2013, **10**, 21.

6 A. Pietroiusti, M. Massimiani, I. Fenoglio, M. Colonna, F. Valentini, G. Palleschi, A. Camaioni, A. Magrini, G. Siracusa, A. Bergamaschi, A. Sgambato and L. Campagnolo, *ACS Nano*, 2011, **5**, 4624–4633.
7 J. L. Blum, J. Q. Xiong, C. Hoffman and J. T. Zelikoff, *Toxicol. Sci.*, 2012, **126**, 478–486.
8 M. Chu, Q. Wu, H. Yang, R. Yuan, S. Hou, Y. Yang, Y. Zou, S. Xu, K. Xu, A. Ji and L. Sheng, *Small*, 2010, **6**, 670–678.
9 A. Adamcakova-Dodd, M. M. Monick, L. S. Powers, K. N. Gibson-Corley and P. S. Thorne, *Part. Fibre Toxicol.*, 2015, **12**, 30.
10 T. Buerki-Thurnherr, U. von Mandach and P. Wick, *Swiss Med. Wkly.*, 2012, **142**, w13559.
11 A. Malassine, J. L. Frendo and D. Evain-Brion, *Hum. Reprod. Update*, 2003, **9**, 531–539.
12 S. Grafmüller, P. Manser, H. F. Krug, P. Wick and U. von Mandach, *J. Visualized Exp.*, 2013, **76**, e50401.
13 J. R. Hutson, F. Garcia-Bournissen, A. Davis and G. Koren, *Clin. Pharmacol. Ther. Ser.*, 2011, **90**, 67–76.
14 J. Lee, G. D. Lilly, R. C. Doty, P. Podsiadlo and N. A. Kotov, *Small*, 2009, **5**, 1213–1221.
15 K. M. Yamada and E. Cukierman, *Cell*, 2007, **130**, 601–610.
16 E. R. Shamir and A. J. Ewald, *Nat. Rev. Mol. Cell Biol.*, 2014, **15**, 647–664.
17 K. S. Smalley, M. Lioni and M. Herlyn, *In Vitro Cell. Dev. Biol.: Anim.*, 2006, **42**, 242–247.
18 F. Pampaloni, E. G. Reynaud and E. H. Stelzer, *Nat. Rev. Mol. Cell Biol.*, 2007, **8**, 839–845.
19 A. I. Minchinton and I. F. Tannock, *Nat. Rev. Cancer*, 2006, **6**, 583–592.
20 F. Hirschhaeuser, H. Menne, C. Dittfeld, J. West, W. Mueller-Klieser and L. A. Kunz-Schughart, *J. Biotechnol.*, 2010, **148**, 3–15.
21 P. Kaufmann, B. Huppertz and H.-G. Frank, *Ann. Anat.*, 1996, **178**, 485–501.
22 D. T. Leong and K. W. Ng, *Adv. Drug Delivery Rev.*, 2014, **79–80**, 95–106.
23 A. Kermanizadeh, M. Lohr, M. Roursgaard, S. Messner, P. Gunness, J. M. Kelm, P. Moller, V. Stone and S. Loft, *Part. Fibre Toxicol.*, 2014, **11**, 56.
24 Y. Luo, C. Wang, M. Hossain, Y. Qiao, L. Ma, J. An and M. Su, *Anal. Chem.*, 2012, **84**, 6731–6738.
25 T. T. Goodman, P. L. Olive and S. H. Pun, *Int. J. Nanomed.*, 2007, **2**, 265–274.
26 K. Huang, H. Ma, J. Liu, S. Huo, A. Kumar, T. Wei, X. Zhang, S. Jin, Y. Gan, P. C. Wang, S. He, X. Zhang and X. J. Liang, *ACS Nano*, 2012, **6**, 4483–4493.
27 A. S. Mikhail, S. Eetezadi, S. N. Ekdawi, J. Stewart and C. Allen, *Int. J. Pharm.*, 2014, **464**, 168–177.
28 J. M. Kelm and M. Fussenegger, *Trends Biotechnol.*, 2004, **22**, 195–202.
29 C. H. Graham, T. S. Hawley, R. G. Hawley, J. R. MacDougall, R. S. Kerbel, N. Khoo and P. K. Lala, *Exp. Cell Res.*, 1993, **206**, 204–211.
30 J. M. Kelm, N. E. Timmins, C. J. Brown, M. Fussenegger and L. K. Nielsen, *Biotechnol. Bioeng.*, 2003, **83**, 173–180.
31 J. S. Taurozzi, V. A. Hackley and M. R. Wiesner, *Nanotoxicology*, 2011, **5**, 711–729.
32 A. Malek, R. Sager, A. B. Lang and H. Schneider, *Am. J. Reprod. Immunol.*, 1997, **38**, 263–271.
33 M. Rimann and U. Graf-Hausner, *Curr. Opin. Biotechnol*, 2012, **23**, 803–809.
34 J. M. Kelm and M. Fussenegger, *Trends Biotechnol.*, 2004, **22**, 195–202.
35 P. Kaufmann, J. Stark and H. E. Stegner, *Cell Tissue Res.*, 1977, **177**, 105–121.
36 M. Castellucci and P. Kaufmann, in *Pathology of the Human Placenta*, 5 edn, 2006, pp. 50–120.
37 D. A. Evseenko, J. W. Paxton and J. A. Keelan, *Am. J. Physiol. Regul. Integr. Comp. Physiol.*, 2006, **290**, R1357–R1365.
38 K. Orendi, V. Kivity, M. Sammar, Y. Grimpel, R. Gonen, H. Meiri, E. Lubzens and B. Huppertz, *Placenta*, 2011, **32**(Suppl.), S49–S54.
39 K. Orendi, M. Gauster, G. Moser, H. Meiri and B. Huppertz, *Reproduction*, 2010, **140**, 759–766.
40 D. M. Nelson, *Placenta*, 1996, **17**, 387–391.
41 L. A. Cole, *Reprod. Biol. Endocrinol.*, 2010, **8**, 102.
42 W. Norris, T. Nevers, S. Sharma and S. Kalkunte, *Placenta*, 2011, **32**(Suppl. 2), S182–S185.
43 T. M. Butler, P. A. Elustondo, G. E. Hannigan and D. J. MacPhee, *Reprod. Biol. Endocrinol.*, 2009, **7**, 51.
44 R. Grümmer, H. P. Hohn, M. M. Mareel and H. W. Denker, *Placenta*, 1994, **15**, 411–429.
45 R. Grümmer, H.-P. Hohn and H.-W. Denker, in *Trophoblast Invasion and Endometrial Receptivity: Novel Aspects of the Cell Biology of Embryo Implantation*, ed. H.-W. Denker and J. D. Aplin, Springer US, Boston, MA, 1990, pp. 97–111, DOI: 10.1007/978-1-4613-0615-3_5.
46 I. Y. Kim, E. Joachim, H. Choi and K. Kim, *Nanomedicine*, 2015, **11**, 1407–1416.
47 M. J. Clift, C. Endes, D. Vanhecke, P. Wick, P. Gehr, R. P. Schins, A. Petri-Fink and B. Rothen-Rutishauser, *Toxicol. Sci.*, 2014, **137**, 55–64.
48 L. Farcal, F. Torres Andon, L. Di Cristo, B. M. Rotoli, O. Bussolati, E. Bergamaschi, A. Mech, N. B. Hartmann, K. Rasmussen, J. Riego-Sintes, J. Ponti, A. Kinsner-Ovaskainen, F. Rossi, A. Oomen, P. Bos, R. Chen, R. Bai, C. Chen, L. Rocks, N. Fulton, B. Ross, G. Hutchison, L. Tran, S. Mues, R. Ossig, J. Schnekenburger, L. Campagnolo, L. Vecchione, A. Pietroiusti and B. Fadeel, *PLoS One*, 2015, **10**, e0127174.
49 R. Hardman, *Environ. Health Perspect.*, 2006, **114**, 165–172.
50 A. Ivask, K. Juganson, O. Bondarenko, M. Mortimer, V. Aruoja, K. Kasemets, I. Blinova, M. Heinlaan, V. Slaveykova and A. Kahru, *Nanotoxicology*, 2014, **8**(Suppl. 1), 57–71.
51 S. L. Chia, C. Y. Tay, M. I. Setyawati and D. T. Leong, *Small*, 2015, **11**, 702–712.
52 M. Ulusoy, A. Lavrentieva, J.-G. Walter, F. Sambale, M. Green, F. Stahl and T. Scheper, *Toxicol. Res.*, 2016, **5**, 126–135.

53 M. Ahamed, M. J. Akhtar, H. A. Alhadlaq and S. A. Alrokayan, *Nanomedicine*, 2015, **10**, 2365–2377.
54 M. Caicedo, J. J. Jacobs, A. Reddy and N. J. Hallab, *J. Biomed. Mater. Res., Part A*, 2008, **86**, 905–913.
55 B. Fahmy and S. A. Cormier, *Toxicol. in Vitro*, 2009, **23**, 1365–1371.
56 K. Midander, P. Cronholm, H. L. Karlsson, K. Elihn, L. Moller, C. Leygraf and I. O. Wallinder, *Small*, 2009, **5**, 389–399.
57 X. Li, X. Yang, L. Yuwen, W. Yang, L. Weng, Z. Teng and L. Wang, *Biomaterials*, 2016, **96**, 24–32.
58 J. Lovric, S. J. Cho, F. M. Winnik and D. Maysinger, *Chem. Biol.*, 2005, **12**, 1227–1234.
59 T. Zhang, Y. Hu, M. Tang, L. Kong, J. Ying, T. Wu, Y. Xue and Y. Pu, *Int. J. Mol. Sci.*, 2015, **16**, 23279–23299.
60 Y. Lu, S. Xu, H. Chen, M. He, Y. Deng, Z. Cao, H. Pi, C. Chen, M. Li, Q. Ma, P. Gao, Y. Ji, L. Zhang, Z. Yu and Z. Zhou, *Biomaterials*, 2016, **90**, 27–39.
61 X. Wang, J. Tian, K. T. Yong, X. Zhu, M. C. Lin, W. Jiang, J. Li, Q. Huang and G. Lin, *J. Nanobiotechnol.*, 2016, **14**, 10.
62 A. M. Derfus, W. C. W. Chan and S. N. Bhatia, *Nano Lett.*, 2004, **4**, 11–18.
63 C. Kirchner, A. M. Javier, A. S. Susha, A. L. Rogach, O. Kreft, G. B. Sukhorukov and W. J. Parak, *Talanta*, 2005, **67**, 486–491.
64 L. K. Limbach, Y. Li, R. N. Grass, T. J. Brunner, M. A. Hintermann, M. Muller, D. Gunther and W. J. Stark, *Environ. Sci. Technol.*, 2005, **39**, 9370–9376.
65 E. Birben, U. M. Sahiner, C. Sackesen, S. Erzurum and O. Kalayci, *World Allergy Organ. J.*, 2012, **5**, 9–19.
66 S. J. Stohs and D. Bagchi, *Free Radical Biol. Med.*, 1995, **18**, 321–336.
67 K. Yamashita, Y. Yoshioka, K. Higashisaka, K. Mimura, Y. Morishita, M. Nozaki, T. Yoshida, T. Ogura, H. Nabeshi, K. Nagano, Y. Abe, H. Kamada, Y. Monobe, T. Imazawa, H. Aoshima, K. Shishido, Y. Kawai, T. Mayumi, S. Tsunoda, N. Itoh, T. Yoshikawa, I. Yanagihara, S. Saito and Y. Tsutsumi, *Nat. Nanotechnol.*, 2011, **6**, 321–328.
68 S. Stasenko, E. M. Bradford, M. Piasek, M. C. Henson, V. M. Varnai, J. Jurasović and V. Kušec, *J. Appl. Toxicol.*, 2010, **30**, 242–253.
69 C. Jud, S. Ahmed, L. Müller, C. Kinnear, D. Vanhecke, Y. Umehara, S. Frey, M. Liley, S. Angeloni, A. Petri-Fink and B. Rothen-Rutishauser, *BioRes. Open Access*, 2015, **4**, 457–468.
70 D. Huh, B. D. Matthews, A. Mammoto, M. Montoya-Zavala, H. Y. Hsin and D. E. Ingber, *Science*, 2010, **328**, 1662–1668.
71 S. G. Klein, T. Serchi, L. Hoffmann, B. Blomeke and A. C. Gutleb, *Part. Fibre Toxicol.*, 2013, **10**, 31.
72 S. Messner, I. Agarkova, W. Moritz and J. M. Kelm, *Arch. Toxicol.*, 2013, **87**, 209–213.
73 E. Urich, C. Patsch, S. Aigner, M. Graf, R. Iacone and P. O. Freskgard, *Sci. Rep.*, 2013, **3**, 1500.
74 K. S. Hougaard, L. Campagnolo, P. Chavatte-Palmer, A. Tarrade, D. Rousseau-Ralliard, S. Valentino, M. V. Park, W. H. de Jong, G. Wolterink, A. H. Piersma, B. L. Ross, G. R. Hutchison, J. S. Hansen, U. Vogel, P. Jackson, R. Slama, A. Pietroiusti and F. R. Cassee, *Reprod. Toxicol.*, 2015, **56**, 118–140.
75 S. Grafmueller, P. Manser, L. Diener, P. A. Diener, X. Maeder-Althaus, L. Maurizi, W. Jochum, H. F. Krug, T. Buerki-Thurnherr, U. von Mandach and P. Wick, *Environ. Health Perspect.*, 2015, **123**, 1280–1286.

Electronic supplementary information (ESI)

A 3D co-culture microtissue model of the human placenta for nanotoxicity assessment

Carina Muoth[a], Adrian Wichser[a], Marco Monopoli[b,#], Manuel Correia[c], Nicky Ehrlich[c,§], Katrin Loeschner[c], Audrey Gallud[d], Melanie Kucki[a], Liliane Diener[a], Pius Manser[a], Wolfram Jochum[e], Peter Wick[a] and Tina Buerki-Thurnherr[a]

[a] Particles-Biology Interactions, Empa, Swiss Federal Laboratories for Materials Science and Technology, Lerchenfeldstrasse 5, 9014 St. Gallen, Switzerland.

[b] Centre for BioNano Interactions, School of Chemistry and Chemical Biology, University College Dublin, Dublin 4, Ireland.

[c] Research Group for Nano-Bio Science, Division for Food Technology, National Food Institute, Technical University of Denmark, Mørkhøj Bygade 19, DK-2860 Søborg, Denmark.

[d] Division of Molecular Toxicology, Institute of Environmental Medicine, Karolinska Institutet, Nobels väg 13, 171 77 Stockholm, Sweden.

[e] Institute of Pathology, Cantonal Hospital St.Gallen, Rorschacherstrasse 95, 9007 St. Gallen, Switzerland.

[§] current address: CAPEC-PROCESS, DTU, Technical University of Denmark, Søltofts Plads, 2800 Kgs. Lyngby, Denmark.

[#] current address: School of Pharmaceutical & Medicinal Chemistry, Royal College of Surgeons in Ireland, 123 Stephen's Green, Dublin 2, Ireland.

1. Experimental section

1.1. *Nanoparticle characterization*

The CuO NPs were characterized by transmission electron microscopy (TEM) by applying 10 µl of diluted CuO NP suspensions (10 µg/ml) in deionized water to a 200 mesh Formvar/carbon-coated copper grid (FCF-200-Cu, FORMVAR CARBON FILM, Electron Microscopy Science, USA). TEM micrographs were obtained using a Tecnai G2 T20 instrument (FEI, Eindhoven, The Netherlands) operated at 200 kV accelerating voltage. Surface area was determined by nitrogen adsorption/desorption on a Belsorp Mini II instrument (BEL, Japan), after pre-treating the samples under vacuum at 140°C for 0.5 h. The specific surface area of TiO_2 and CuO NPs was obtained from nitrogen adsorption isotherms, according to the Brunauer−Emmett−Teller (BET) equation. UV-Vis spectra of CdTe-COOH NP stock suspensions diluted in ultra-pure water or supplemented FGM to a final concentration of 100 or 250 µg/ml were recorded in the range of 400 - 800 nm using a Genesis 10S UV-Vis spectrophotometer (Thermo Scientific, Reinach, Switzerland). Hydrodynamic diameters of the NP suspensions were determined using a Zetasizer Nano ZS (Malvern Instruments, UK). Stock suspensions (1 mg/ml) were prepared as described in Materials & Methods and were further diluted to 100 µg/ml in H_2O or FGM. Measurements (three consecutive measurements with a minimum of 15 runs of 10 s each) were performed at 25 °C at a detection angle of 90° using a He-Ne laser operating at a wavelength of 633 nm. The release of ions from CuO or TiO_2 NPs was determined by ICP-MS. Therefore, suspensions of 50 µg/ml CuO or TiO_2 NPs in FGM were prepared as described in Materials and Methods part and incubated at 37 °C/ 5 % CO_2 for 10 min or 24 h. Ions were separated from NPs either by ultrafiltration (only CuO NPs; Amicon Ultra-4 Centrifugal Filter Unit, 3kDa, Milipore, USA) or by centrifugation at 10,000xg for 10 min (Heraeus Multifuge 3S-R, Thermo Fisher Scientific, Reinach, Switzerland). Supernatants were transferred into a test tube containing concentrated nitric acid. The solution was allowed to stand for 24 h and then subjected to ICP-MS analysis (sector field inductively coupled plasma mass spectrometer (SF-ICP-MS); Element 2, Thermo Finnigan, Bremen, Germany) with external calibration. Values were corrected for the background levels of Ti (0.7 %) or Cu (0.03 %) in the medium and expressed as percentage of total mass. Endotoxin content was evaluated using the QCL-1000™ Endpoint Chromogenic LAL Assay (Lonza) protocol. The enzymatic reaction was per-

formed on NPs alone, or NPs in presence of lipopolysaccharide (LPS). Briefly, the stock suspensions of NPs were diluted at 100 µg/ml in endotoxin-free culture medium and 50 µL of each suspension were dispensed into a 96-well plate. LPS was added at 1 EU/ml, followed by 1 h incubation at RT. The reaction was initiated by adding first the proenzyme and then the substrate. After 16 min, a stop solution of acetic acid 25 % v/v in dH_2O was added and the absorbance was read at 405 nm, using an Infinite 200 Tecan microplate reader operating with Magellan v7.2 software.

1.2. *ZO-1 staining*

MTs were incubated with FGM either in the presence or absence of 20 µM forskolin for 24 h. Prior to the whole mount tissue staining, MTs were washed with PBS, fixed using 4 % PFA for 60 min and treated with 0.2 % Triton X-100 for 30 min. Subsequently, MTs were washed with PBS, blocked in 5 % goat serum for 60 min and incubated with the primary antibody mouse anti-ZO-1 (1:100, 339100, Invitrogen, Basel, Switzerland) over night at 4 ºC. After washing in PBS, MTs were exposed to the secondary antibody Alexa Fluor 488 goat anti-mouse IgG (1:400, A11029, Molecular Probes, USA) and to Dapi (4′,6-Diamidin-2-phenylindol) (Sigma-Aldrich, Buchs, Switzerland) for 5 h at room temperature. Following another washing step with PBS, MTs were analyzed by confocal microscopy.

1.3. *Ex vivo human placenta perfusion*

The placentas were obtained from uncomplicated term pregnancies after caesarean section at the Kantonsspital and the Klinik Stephanshorn in St. Gallen. Written informed consent was obtained prior to delivery. The project was approved by the local ethics committee and performed in accordance with the principles of the Declaration of Helsinki. A dually perfused, closed placenta perfusion system was used as described previously [12, 75]. The perfusions were performed with M199 tissue culture medium (Sigma-Aldrich, Buchs, Switzerland) diluted with Earl's buffer (dilution 1: 2), 1 g/l glucose (Sigma-Aldrich, Buchs, Switzerland), 10 g/l bovine serum albumin (Sigma-Aldrich, Buchs, Switzerland), 10 g/l dextran 40 (Sigma-Aldrich, Buchs, Switzerland), 2500 IU/l sodium heparin (Sigma-Aldrich, Buchs, Switzerland), 250 mg/l amoxicillin (Sigma-Aldrich, Buchs, Switzerland) and 2.2 g/l sodium bicarbonate (Sigma-Aldrich, Buchs, Switzerland). 25 µg/ml TiO_2 NPs were added to the maternal and particle concentration in the fetal and maternal circuit was determined after 0, 15, 30, 60,

120, 180, 240, 300 and 360 min by ICP-MS analysis (SF-ICP-MS; Element 2, Thermo Finnigan, Bremen, Germany) with external calibration. Particle concentrations were corrected for the perfusion medium volume in the tubes and volume loss due to sampling before placental transfer was calculated as percentage of transferred PS beads compared to the initially added particle amount.

2. Results

2.1. *Nanoparticle characterization*

Table S1: NP characterization

	TiO_2	CuO	CdTe-COOH
Primary Particle Size (nm)	4[1]	20[1]	3.2[2]
Hydrodynamic diameter (nm) in DD water/PDI	17/0.375	1165/0.335	N/A
Hydrodynamic diameter (nm) in medium/ PDI	8284/0.541	1852/0.442	N/A
Specific surface Area (BET) (m^2/g)	98 ± 10	42 ± 2	N/A
UV-vis peak (nm)	N/A	N/A	549
Dissolution in medium (%) after 10 min/ 24 h[3]	0.5/1.5	13/59	N/A

Abbreviations: DD, double distilled; PDI, polydispersity index; TEM, transmission electron microscopy; N/A, not applicable
[1] calculated from TEM micrographs; [2] calculated from the position of the exciton band; [3] Separation of ions from NPs by centrifugation

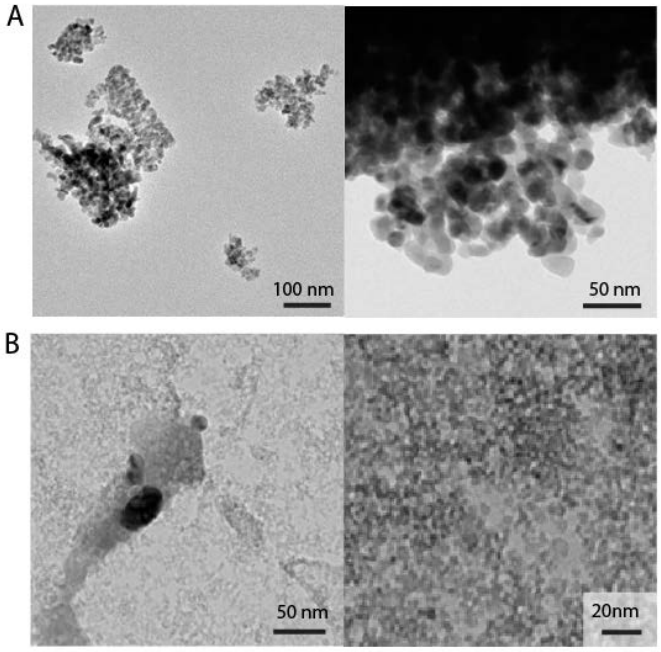

Figure S1. TEM of CuO and TiO_2 NPs. Representative micrographs of CuO NPs (A) and TiO_2 NPs (B).

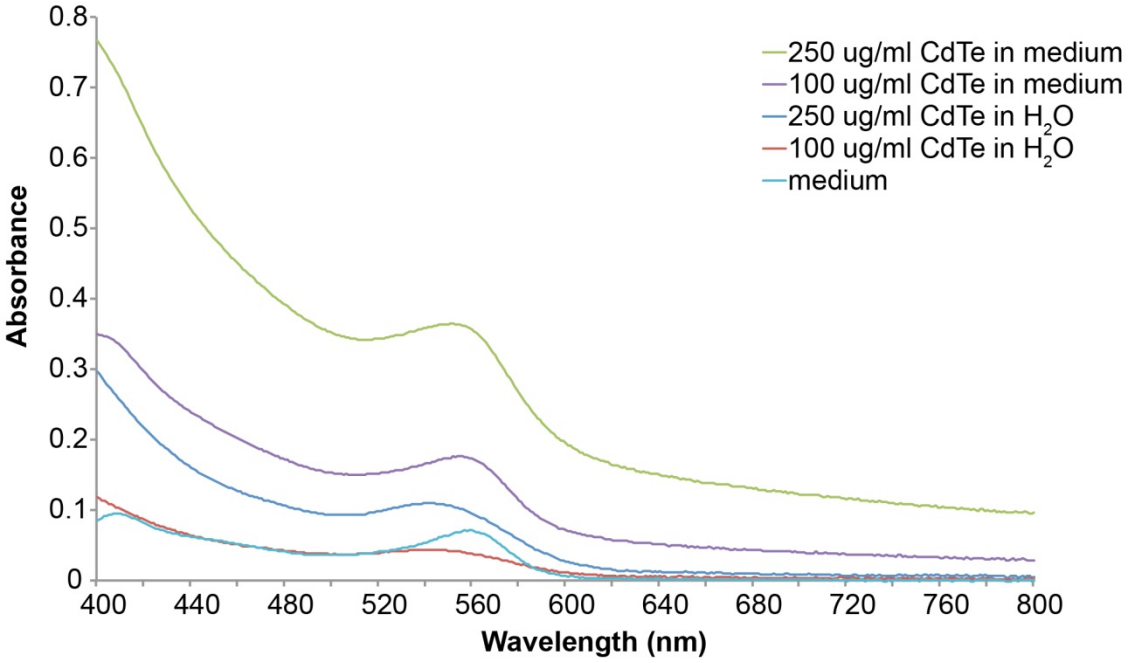

Figure S2. UV-Vis measurements of CdTe-COOH NPs in FGM and water. Absorbance was measured for 100 and 250 µg/ml CdTe-COOH NPs either in cell culture medium or in water.

2.2. *Characterization of placental co-culture MTs*

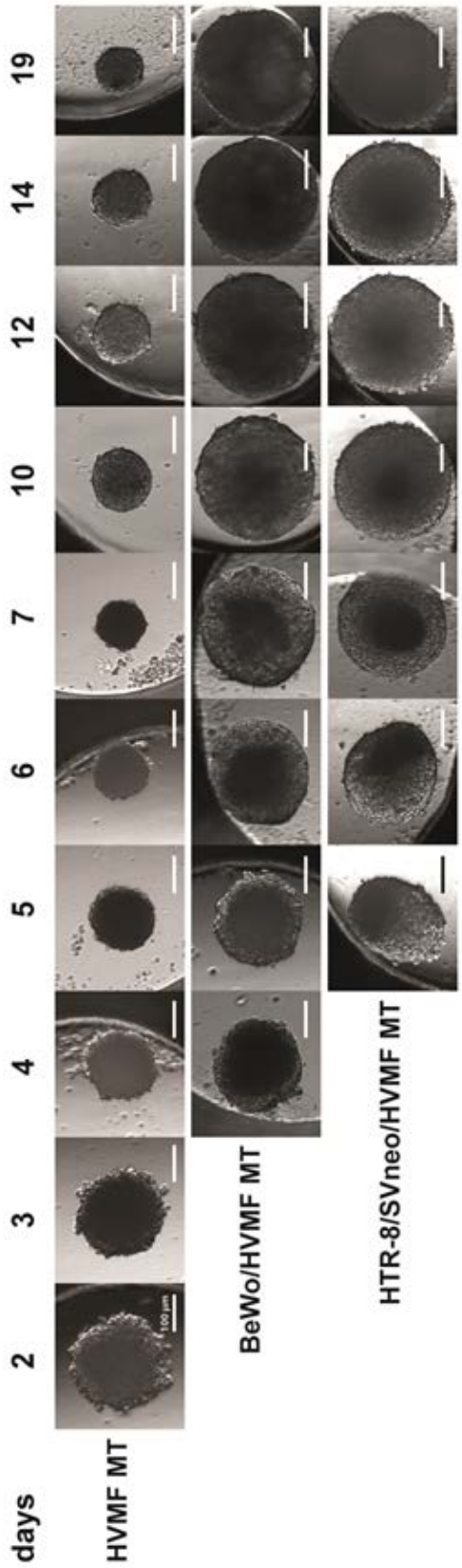

Figure S3. Bright-field microscopic analysis of core and co-culture MTs. Representative images of HVMF MTs (upper row), BeWo/HVMF MTs (middle row) and HTR-8/SVneo/HVMF MTs (lower row) at different days of cultivation. Scale bar is 100 µm.

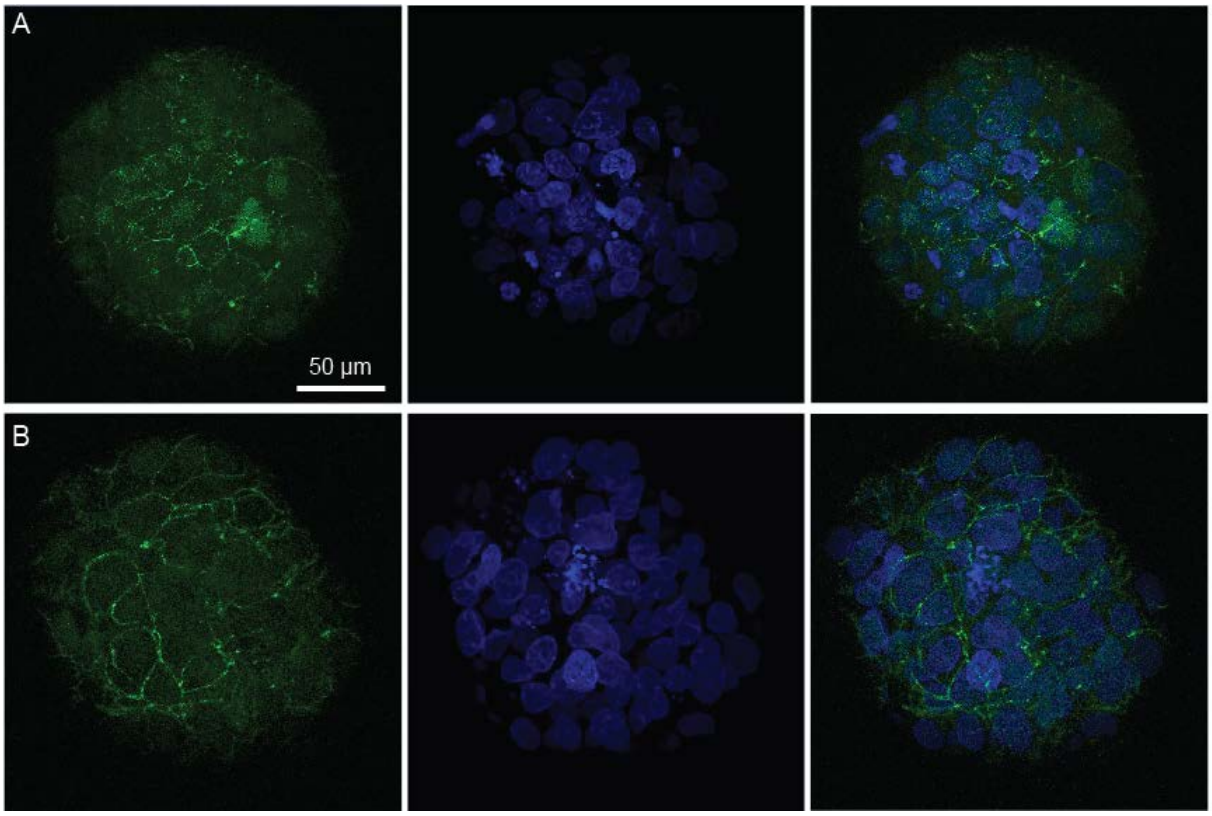

Figure S4. Confocal microscopic analysis of tight junctions in co-culture MTs. MTs were cultivated in the absence (A) or presence of 20 µM forskolin for 24 h (B) followed by a fluorescent staining using anti-ZO-1 antibody (green) to visualize tight junctions and Dapi (blue) to visualize nuclei.

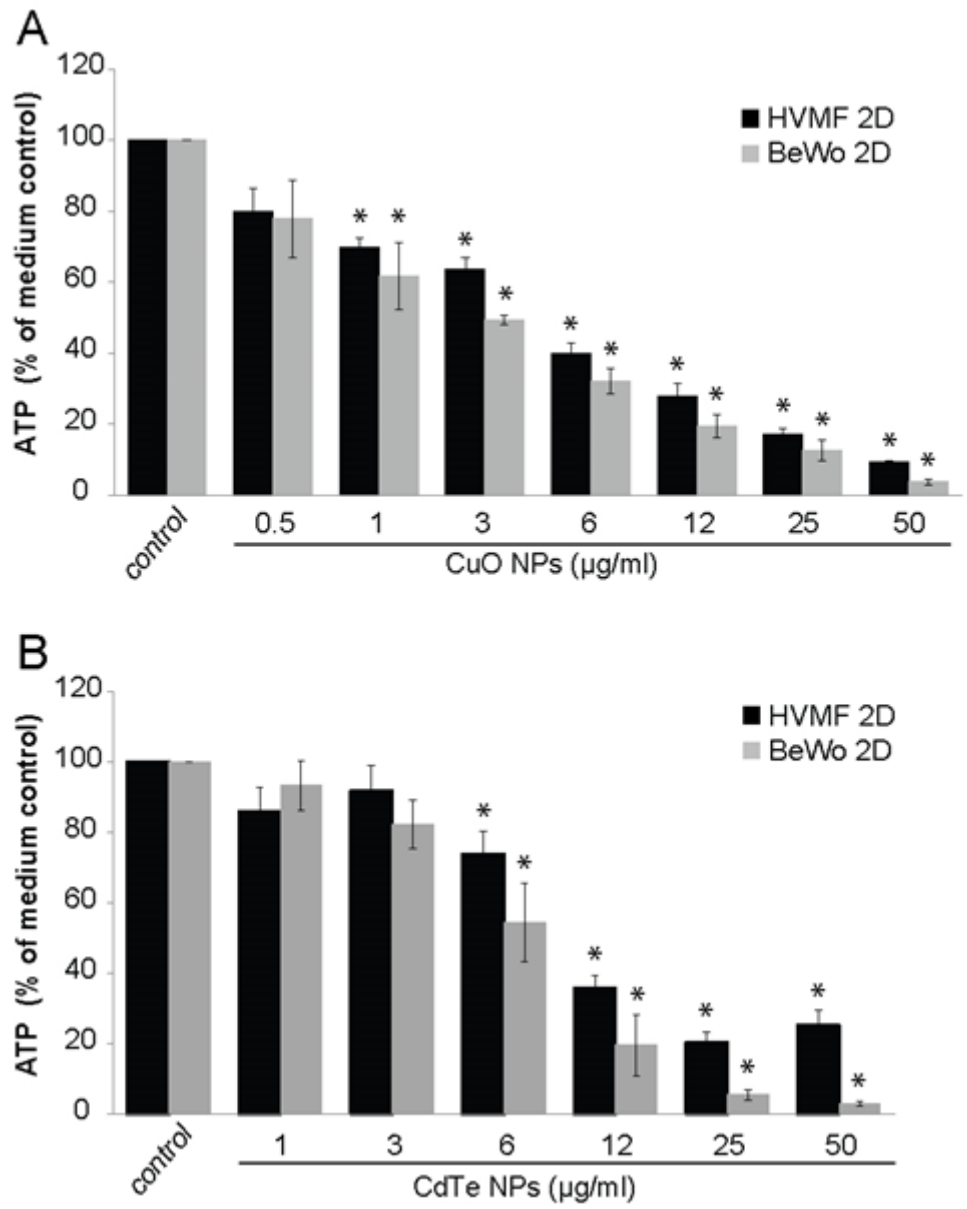

Figure S5. Effects of CuO NPs and CdTe-COOH NPs on 2D BeWo and HVMF cell viability. 2D BeWo or 2D HVMF monocultures were exposed to CuO (A) or CdTe-COOH NPs (B) at concentrations ranging from 0.5 to 50 µg/ml for 24 h in order to evaluate NP cytotoxicity using the ATP assay. Data represent the mean percentages of duplicates compared to the untreated medium control ± SEM of 3 - 5 independent experiments. Note that the data for 2D BeWo were reproduced from Figure 6 to highlight differences to 2D HVMFs.

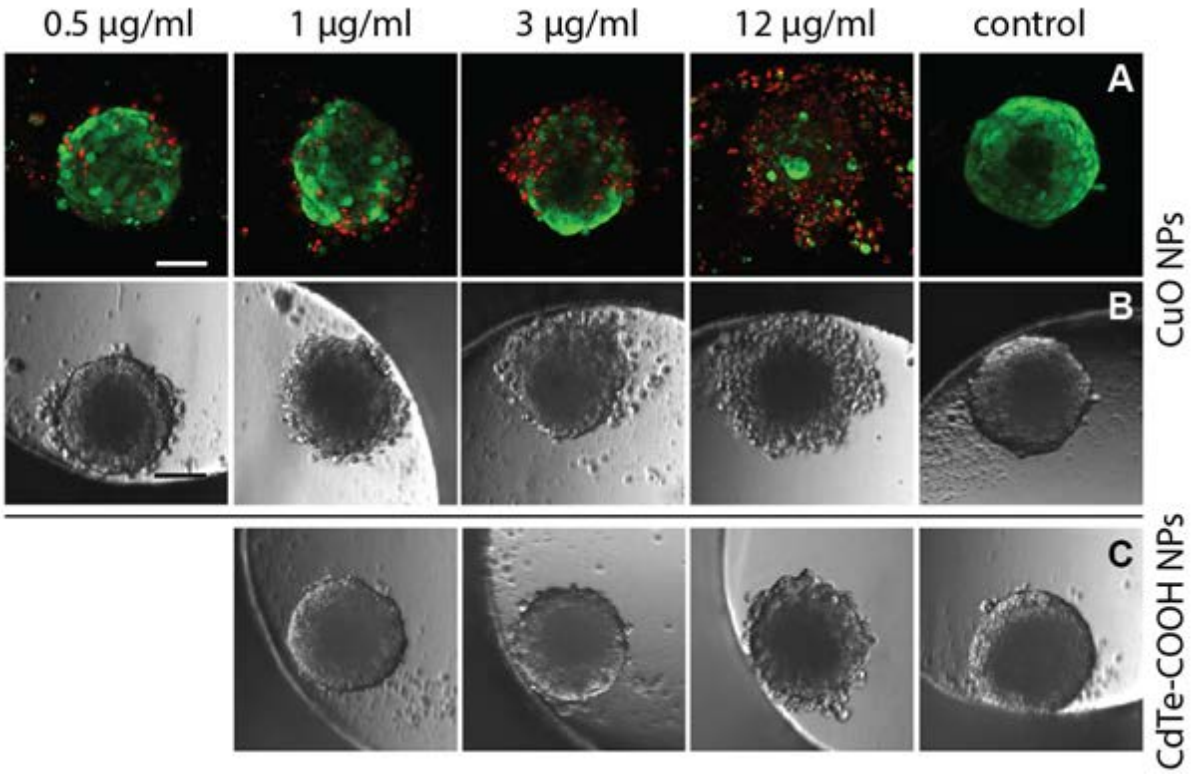

Figure S6. Live/dead staining and bright-field microscopy of co-culture MTs after the exposure to CuO NPs or CdTe-COOH NPs. BeWo/HVMF MTs were exposed to 0.5, 1, 3 or 12 µg/ml of CuO (A and B) or to 1, 3 or 12 µg/ml of CdTe-COOH NPs (C) for 24 h. Representative images show viable cells in green and dead cells in red as well as tissue morphology. Note that live/dead staining was not performed for CdTe-COOH NPs as they are highly fluorescent. Scale bar is 100 µm.

2.4. *TiO_2 NP uptake in co-culture MTs and translocation in the ex vivo human placenta perfusion model*

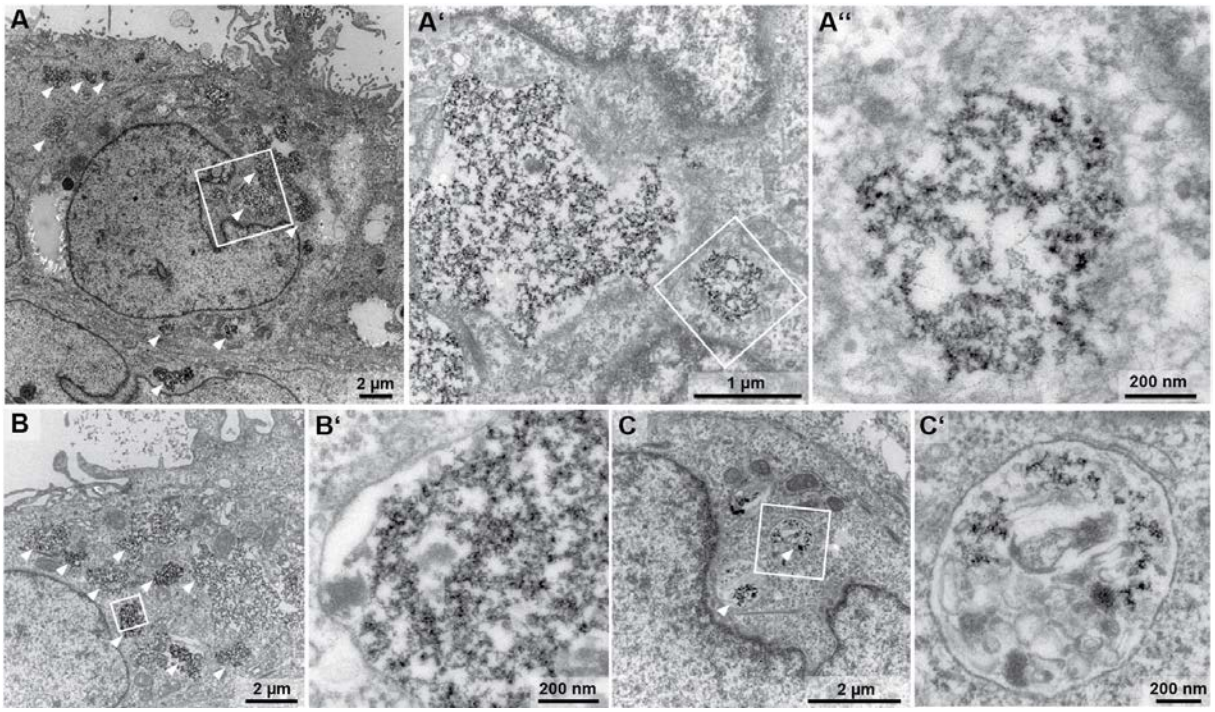

Figure S7. TEM micrographs of a co-culture MT exposed to TiO_2 NPs. After co-culture MT formation was complete, MTs were exposed to 100 µg/ml TiO_2 NPs for 24 h and subsequently processed for TEM analysis. TiO_2 NP agglomerates (arrowheads) were found freely in the cytoplasm (A-A'') or in membrane-bound vesicles (B,B'; putative endosome; C,C' putative lysosome). X' and X'' represent enlargements of the quadrants in X or X', respectively.

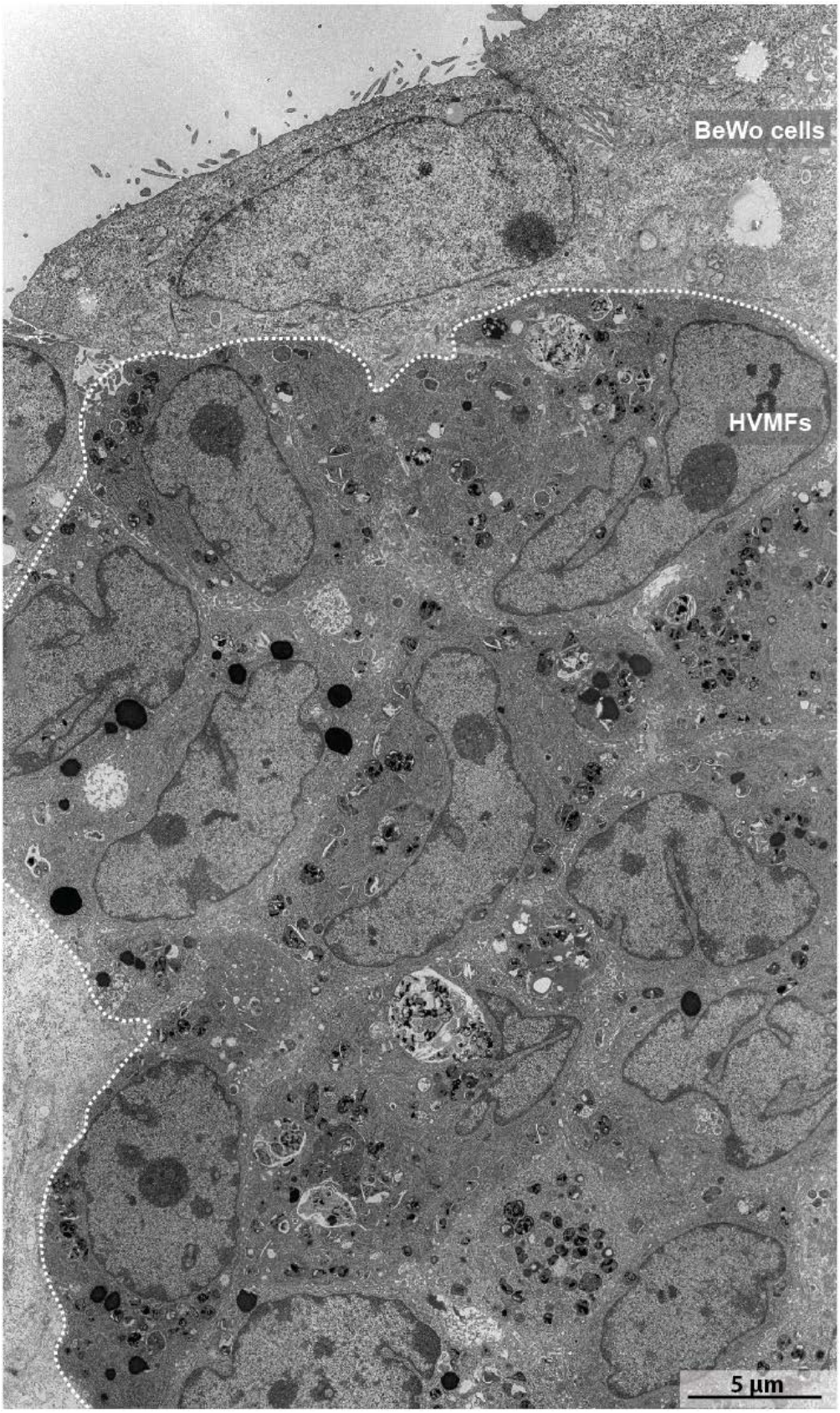

Figure S8. TEM micrograph of a representative control co-culture MT. After co-culture MT formation was complete, MTs were cultivated in medium for 24 h and subsequently processed for TEM analysis.

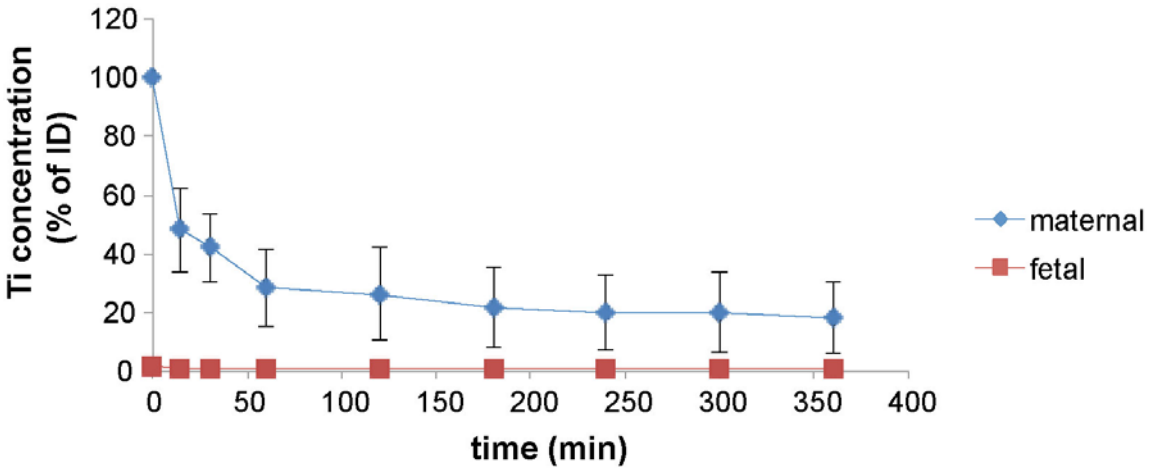

Figure S9. *Ex vivo* placenta perfusion studies with TiO_2 NPs. The initial dose (ID) of TiO_2 NPs added to the maternal circuit was 25 µg/ml. The amount of particles was measured in the maternal and fetal circuits after the indicated time points by ICP-MS.

Part III

Impact of particle size and surface modification on the localization and penetration of gold nanoparticles in human placental co-culture microtissues

Carina Muoth, Mandy Großgarten, Uwe Karst, Jaime Ruiz Aranzaes, Didier Astruc, Sergio Moya, Liliane Diener, Kathrin Grieder, Adrian Wichser, Wolfram Jochum, Peter Wick, Tina Buerki-Thunherr

Author contribution

In this study, I optimized and performed all AuNP exposure experiments with the co-culture MTs, analyzed and interpreted the results and wrote the manuscript.

This manuscript is in preparation to be submitted to Nanomedicine (Future Medicine).

Impact of particle size and surface modification on the localization and penetration of gold nanoparticles in human placental co-culture microtissues

Carina Muoth[1], Mandy Großgarten[2], Uwe Karst[2], Jaime Ruiz Aranzaes[3], Didier Astruc[3], Sergio Moya[4], Liliane Diener[1], Kathrin Grieder[1], Adrian Wichser[1], Wolfram Jochum[5], Peter Wick[1], Tina Buerki-Thunherr[1,*]

[1] Particles-Biology Interactions, Empa, Swiss Federal Laboratories for Materials Science and Technology, Lerchenfeldstrasse 5, 9014 St. Gallen, Switzerland.
[2] Institute of Inorganic and Analytical Chemistry, Westfälische Wilhelms-Universität Münster, Corrensstraße 28/30, 48149 Münster, Germany
[3] ISM, Université de Bordeaux, 351 Cours de la Libération, 33405 Talence Cedex, France
[4] bCIC biomaGUNE, Unidad Biosuperficies, Paseo Miramon No. 182, Edif “C” 20009 Donostia-San Sebastian, Spain
[5] Institute of Pathology, Cantonal Hospital St.Gallen, Rorschacherstrasse 95, 9007 St. Gallen, Switzerland.

Abstract

Aim: Nanoparticle-based drug carriers hold great promises for the development of targeted therapies in pregnancy with reduced off-target effects. Here, we performed a mechanistic study on the placental localization and penetration of gold nanoparticles (AuNPs) in dependence of particle size and surface modification. **Materials & methods:** AuNP uptake and penetration in human placental co-culture microtissues was assessed by ICP-MS, TEM and laser ablation-ICP-MS. **Results:** Higher uptake and deeper penetration was observed for smaller (3-4 nm) or carboxylate-modified AuNPs compared to larger (13-14 nm) or PEGylate AuNPs, which barely passed the trophoblast barrier layer. **Conclusion:** It is possible to steer placental uptake and penetration of AuNPs by tailoring their physico-chemical properties, which is a prerequisite for the development of targeted therapies in pregnancy.

Introduction

In contrast to conventional drugs, nanoparticle (NP)-based drug delivery (DD) systems offer several advantages. In detail, most medical NPs are engineered in a size range between a few to approximately 300 nm (Etheridge et al. 2013), which facilitates their intracellular uptake and results in a high surface-area-to-volume ratio that increases their chemical reactivity and drug loading capacity. NP surface functionalization with different targeting ligands further offers the possibility to develop nanomedical therapeutics with a high specificity for different cells/tissues. Several types of NPs (e.g. liposomes, mesoporous silica NPs) are able to encapsulate various drugs and to release them in a controlled manner. Moreover, surface coatings (e.g. polyethylene glycol (PEG)) are used to protect NPs from clearance by the immune system in order to increase their half-life in the blood circulation (Dobrovolskaia et al. 2008, Pelaz et al. 2015). All of these aspects may effectively contribute to minimize dosing and reduce off-target effects, which are associated with the systemic administration of conventional drugs. So far, most DD systems that obtained FDA approval belong to anti-cancer treatments. Yet, numerous clinical trials for NP-based treatments of other diseases are currently running (examples are listed on www.clinicaltrials.gov) (Ryan and Brayden 2014, Tinkle et al. 2014). As mentioned by Keelan et al., the advantages offered by NP-based DD systems are also of particular interest in the case of pregnant women (Keelan et al. 2015). Different scenarios are conceivable such as individually treating the mother, placental disorders or the fetus from which both, the mother and the fetus would benefit. For example, several observational cohort studies on maternal diabetes or epilepsy during pregnancy confirmed an increased rate of fetal malformations (Tomson et al. 2011, Veiby et al. 2014, Ornoy et al. 2015). An elevated risk of having a child with autism was shown after multiple or bacterial infections (Zerbo et al. 2015) and a higher prevalence of preterm birth was observed after the treatment of maternal cancer (Van Calsteren et al. 2010). For placental disorders (e.g. pre-eclampsia, intrauterine growth restriction), current treatment is limited and preterm delivery is often induced in order to avoid further growth restriction (Cindrova-Davies 2014). Regarding fetal therapies, administration of drugs via maternal injection is ineffective and goes along with maternal side effects while direct fetal injection bears the risk of infections or fetal death (Rytting et al. 2013).

These hurdles of administration to the fetus could be substantially improved through the encapsulation of drugs into placenta-penetrating NPs (Kliment et al. 1970, Keelan et al. 2015). Nevertheless, there are major challenges in developing fetal nanomedicine such as to ensure the site-specific accumulation of NPs at a concentration that is sufficient for an effective treatment or, among other considerations, to confirm the absence of side-effects (Burd et al. 2014).

Despite the urgent need for safe and effective treatments during pregnancy, only few studies are currently available that investigated possible NP-based treatments during pregnancy. Recently, a mouse model carrying healthy and growth-restricted pups was used to assess whether liposomes decorated with tumor-homing peptides were able to deliver insulin-like growth factor 2 to the placenta. Indeed, placental function was significantly improved resulting in increased fetal weight of the smallest pups while the weight of the wild-type pups remained unaffected (King et al. 2016).

In a different approach, neuro inflammation in newborns has been addressed. A prerequisite to treat such an inflammation is the co-localization of NPs with astrocytes, microglia and oligodendrocytes. This was confirmed for dendrimers following intraperitoneal injection into neonatal mice. In addition, dendrimers with anti-inflammatory and anti-oxidant properties were found to suppress the pro-inflammatory response of microglia/macrophages and in turn improved myelination in newborns (Nance et al. 2015). On the other hand, transplacental translocation of drug-conjugated Polyamidoamine (PAMAM) dendrimers across the human *ex vivo* placenta was shown to be very low and thus may be a promising candidate to treat the pregnant mother without significantly affecting the fetus (Menjoge et al. 2011). Another study revealed the successful delivery of Doxorubicin loaded nanospheres into trophoblasts of human *ex vivo* placentas, which was enhanced via NP targeting against endothelial growth factor receptors. Placental uptake of these nanospheres resulted in decreased cell proliferation and increased apoptosis, which is a promising approach to treat disorders of trophoblast overgrowth (e.g. ectopic pregnancy, choriocarcinoma) (Kaitu'u-Lino et al. 2013).

However, many studies are conducted in rodents and since the placenta is the most species-specific mammalian organ, it is uncertain in how far these results can be correlated to humans (Malassine et al. 2003). On the other hand, NP translocation studies in human *ex vivo* placentas are time-consuming, limited to approximately 6-8 h and do not allow to assess NP uptake mechanisms. To overcome these limitations,

several studies on NP translocation have been conducted with the human *in vitro* placenta Transwell® model (Cartwright et al. 2012, Carreira et al. 2015, Lopalco et al. 2015). For example, Ali et al. investigated the translocation of dexamethasone-loaded Poly(lactic-co-glycolic acid) (PLGA) NPs for the potential prenatal treatment of congenital adrenal hyperplasia, an inherited metabolic disease. Results confirmed a size-dependent translocation and a significantly higher apparent permeability of dexamethasone when encapsulated into the PLGA NPs as compared to free dexamethasone (Ali et al. 2013). Fetal cardiac arrhythmia is generally treated with Digoxin but it often causes severe maternal side effects due to its low transplacental passage, which requires high and more frequent dosing. Significantly increased transplacental passage was obtained after encapsulation of Digoxin within PEGylated PLGA NPs as compared to free Digoxin. It was shown that such NP encapsulation protects Digoxin from P-glycoprotein-mediated efflux from the placental trophoblast layer (Albekairi et al. 2015). Nevertheless, it should be mentioned that the porous membrane of such Transwell® models prevents direct contact between different cell types, substantially restricts passage of various NPs and lacks a tissue-like environment that is required to investigate NP penetration (Muoth et al. 2016). Therefore, we previously demonstrated the development of a novel scaffold-free 3D co-culture microtissue (MT) model resembling the human placental tissue structure and its suitability for the fast generation of acute toxicity data of different NPs. Briefly, highly-reproducible MTs were generated consisting of a core of human villous mesenchymal fibroblasts (HVMFs) surrounded by a layer of human trophoblastic choriocarcinoma cells (BeWo cells) with the hanging drop technology (©InSphero). Exposure to CdTe-COOH or CuO NPs resulted in a concentration-dependent decrease of tissue-viability and placental hormone production whereas TiO_2 NP treatment did not lead to any adverse effects (see Part II, paper under revision).

Steering NP uptake, accumulation or translocation through the human placental barrier via the particle physico-chemical properties is a prerequisite for the development of site-specific nanomedical therapies or diagnostics in pregnancy. Therefore, we qualitatively and quantitatively analyzed if uptake, accumulation and penetration of gold (Au)NPs into the 3D placental co-culture MTs were size (3-4 versus 13-14 nm) or surface modification dependent (COOH versus PEGylation).

Materials & Methods

Cell culture

The human placental choriocarcinoma cell line BeWo b30 was obtained from Prof. Dr. Ursula Graf-Hausner (Zurich University of Applied Sciences, Wädenswil, Switzerland) with permission from Dr. Alan Schwartz (Washington University School of Medicine, MO, USA). Cells were cultured in Ham´s F-12K medium (Gibco, Luzern, Switzerland) supplemented with 10 % fetal calf serum (FCS, Invitrogen, Basel, Switzerland), 2 mM L-Glutamine (Gibco, Luzern, Switzerland) and 1 % penicillin/streptomycin (Gibco, Luzern, Switzerland). Human villous mesenchymal fibroblasts (HVMF, PromoCell) were cultured in supplemented fibroblast growth medium 2 (FGM, PromoCell) as described elsewhere (see Part II).

Both cell types were cultivated at 37°C with 5 % CO_2 in a humidified atmosphere and sub-cultured twice a week using trypsin-EDTA solution. All NP exposure experiments were conducted in FGM containing 10 % FCS.

Formation of co-culture microtissues

Microtissues (MTs) were generated as described in our previous work (see Part II, paper under revision). Briefly, 5000 human villous mesenchymal fibroblasts (HVMFs) were seeded per well of a GravityPLUS^{TM} 96 well plate (©InSphero AG). After 3 days, 300 BeWo cells were added to the fibroblastic core MT. The total drop volume of the MTs was 40 µl of FGM containing 20 % FCS. After 5 days, co-culture MT formation was complete and MTs were transferred into a GravityTRAP^{TM} 96 well plate (©InSphero AG Switzerland) for subsequent NP exposure and analysis.

Synthesis and dispersion of gold NPs

Gold NPs (Au-3-PEG, Au-13-PEG, Au-4-COOH and Au-14-COOH) were provided within the EU FP7 Nanosolutions project (http://www.nanosolutions.eu).

Au-3-PEG (Zheng et al. 2004). 60 ml of methanol and 10 ml of acetic acid were mixed in a 200 ml Erlenmeyer flask by stirring for 5 min. Then 0.158 g (0.4 mmol) of Tetrachloroauric acid trihydrate ($HAuCl_4$ x $3H_2O$, Sigma Aldrich, France) and 0.117 g (0.2 mmol) of SH-$PEG_{(550)}CH_3$ were added to the above mixed solvents and dissolved by stirring for 5 min. Next, 0.150 g (4 mmol) of sodium borohydride was dissolved in 10 ml of water. The $NaBH_4$ solution was added drop wise into the above

solution under rapid stirring. With the first drop of $NaBH_4$ added, the $HAuCl_4$ solution immediately turned from yellow to dark brown. Rapid stirring was continued for 2 h. The reaction was let to stir overnight. The solvents were removed under reduced pressure. CH_2Cl_2 (100 ml) was added to the waxy AuNPs. The dark brown organic solution was washed twice with brine and subsequently dried over Na_2SO_4. After filtration the solvent was removed under reduced pressure and the solid was dissolved in 100 ml water. The NPs were further purified by dialysis. Dialysis was conducted from aqueous NP solutions in segments of cellulose ester dialysis membrane (MWCO = 14 000) in stirred 4-L beakers containing 18 MΩ cm water, changed daily.

Au-4-COOH (Shi et al. 2004). 0.087 g (0.4 mmol) of 11-mercaptoundecanoic acid dissolved in 10 ml of methanol was added to a solution of $HAuCl_4 \times 3H_2O$ (0.079 mg; 0.2 mmol) (Chen et al. 2006) in 20 ml of methanol with vigorous stirring. After 10 min, 10 ml of a freshly prepared aqueous solution of sodium borohydride (113 mg; 3 mmol) was added to the mixture under vigorous stirring. The reaction mixture turned brown indicating the formation of AuNPs. Stirring was continued for one hour. The AuNPs were further purified by dialysis.

Au-13-PEG and Au-14-COOH were obtained from citrate gold NPs by exchange of citrate ligands by the thiolate ligand upon addition of the thiol. Concentrated citrate stabilized AuNPs (~1 mM) were synthesized using a modified Frens method (Ghann et al. 2012). In a 500 ml two-neck round-bottom flask equipped with a condenser and a stir bar, 250 ml of 1.056 mM aqueous solution of $HAuCl_4$ was brought to boil while stirring vigorously. 11 ml of 5 % aqueous solution of trisodium citrate ($C_6H_5Na_3O_7$, Sigma Aldrich, France) ($n_{citrate}/n_{Au}$ = 7) was quickly added to the gold chloride solution, resulting in a series of color changes from pale yellow to colorless, then dark gray, purple, red, and finally dark wine red. The color change occurred within a period of 5 min, and the solution was subsequently refluxed for an additional 15 min, the oil bath was removed and the flask was allowed to cool to room temperature.

Au-13-PEG. 0.437 g (0.75 mmol) of $SH\text{-}PEG_{(550)}CH_3$ (Zheng et al. 2004) was then added quickly to a 500 ml Erlenmeyer flask containing 250 ml of citrate-stabilized AuNP solution previously prepared and kept stirring overnight at room temperature**.** Au-13-PEG was purified by dialysis from aqueous AuNP solutions in pure water over a 7-day period during which the water was changed daily.

Au-14-COOH. 0.328 g (0.75 mmol) of $HS(CH_2)_{10}CH_2O(C_2H_4O)_3C_2H_4OCH_2CO_2H$ (Chen et al. 2006) was added quickly to a 500 ml Erlenmeyer flask containing 250 ml of citrate-stabilized AuNP solution previously prepared and kept stirring overnight at room temperature. Au-14-COOH was purified by dialysis from aqueous AuNP solutions in pure water over a 7-day period during which the water was changed daily.

Prior to NP experiments, AuNP stock suspensions were vortexed and sonicated using an ultrasonic bath (Bandelin Sonorex SUPER RK 156 BH) for 1 min each, diluted to the required concentrations in supplemented FGM containing 10 % FCS and immediately added to the co-culture MTs.

Characterization of gold NPs

FTIR spectrometry. A Perkin Elmer 100 FTIR spectrometer was used to acquire IR spectra of NPs. Spectra were taken from KBr pellets made by sintering mixtures of small amounts of the NPs and KBr. Approximately 5 mg of the NPs were mixed with approximately 500 mg of potassium bromide, and the resulting suspension was ground via mortar and pestle into a fine powder. A portion of this material was pressed into a transparent disk at a pressure of 10 ton cm^{-2}. No smoothing was applied to the spectra, but a baseline correction was always made before determination of the peak frequencies.

TEM. For TEM observation, the working suspension (0.1 mg/ml) was first vortex-mixed for 30 seconds. 5 µl of the working suspension was added onto a copper grid (Ultrathin carbon film (< 3 nm thick) supported by a lacey carbon film on a 400 mesh copper grid (Ted Pella). TEM (JEOL JEM-1400PLUS-HC, operated at 120 kV, equipped with a GATAN US1000 CCD camera (2k x 2k)) was performed to characterize the average core size from 100 particles per AuNP type.

UV-vis. absorption spectroscopy. For UV-vis. measurements, the working suspension (0.1 mg/ml) was vortex-mixed for 0.5 min. Measurements were performed using UV-vis. equipment (UV-VIS-NIR spectrometer Cary5000 (Varian)).

XPS. XPS experiments were performed on a SPECS Sage HR 100 spectrometer with a non-monochromatic X ray source (Magnesium Kα line of 1253.6 eV energy and an applied power of 250 W). XPS spectra were calibrated using the 3d5/2 line of Ag with a full width at half maximum (FWHM) of 1.1 eV. An electron flood gun was used to compensate for charging during XPS data acquisition. The selected

resolution for the spectra was 30 eV Pass Energy and 0.5 eV/step for the general survey spectra and 15 eV Pass Energy and 0.15 eV/step for high resolution atomic environment spectra. All measurements were accomplished in an ultra-high vacuum (UHV) chamber at a pressure of around 5 x 10^{-8} mbar. NP samples were dispersed in water and casted on pre-cleaned Si wafers, followed by drying in a vacuum oven.

ATP assay

The CellTiter-Glo® Luminescent Cell Viability Assay (Promega, USA) was used to assess effects of different AuNPs on MT viability. MTs were exposed to 3, 6, 12, 25 and 50 µg/ml of Au-3-PEG, Au-13-PEG or Au-14-COOH in a final volume of 70 µl FGM containing 10 % FCS/MT for 24 h. 0.1 % Triton X-100 and FGM were used as the positive or medium control, respectively. In order to remove NPs in the MT supernatants, samples were washed with PBS prior to the addition of 40 µl/well of a 50:50 FGM/CellTiter-Glo® mixture. After an incubation of 30 min on a shaker at room temperature, cell lysates were transferred to a black 96-well plate (Microfluore™ 1, Thermoscientific, New York, USA) together with an ATP standard (Sigma Aldrich, Switzerland) and luminescent signals were immediately measured with a microplate reader (Mitras[1] LB 943 Monochromator Multimode Reader, Berthold Technologies, Zug, Switzerland).

Histology

For LA-ICP-MS analysis, immunohistochemical (IHC) stainings of 30-40 MTs per condition were performed. After MT exposure to 50 µg/ml of Au-3-PEG, Au-13-PEG, and Au-14-COOH for 24 h, MTs were pooled, fixed with 4 % formalin, embedded in paraffin and cut into 1.5 µm thick tissue sections.

Hematoxylin and eosin (HE) staining was performed according to the standard protocol and for trophoblast staining, sections were incubated with MNF116 (1:400, 15 min, DAKO M0821) for 15 min, visualized with 3,3'-Diaminobenzidine and counterstained with hematoxylin (Bond Polymer Refine Detection Kit, Leica Microsystems, Heerbrugg, Schweiz). Prior to the cytokeratin staining, antigen retrieval was performed with the Leica Bond Enzyme Pretreatment Kit. Both stainings were performed using an automated staining system (BOND-MAX, Leica Microsystems, Heerbrugg, Schweiz).

Laser ablation inductively coupled mass spectrometry (LA-ICP-MS)

In order to qualitatively analyze the distribution of gold NPs in the co-culture MTs and quantify the gold concentrations, LA-ICP-MS was conducted on paraffin sections of MTs stained with HE. For this purpose, a commercial laser ablation system LSX 213 (Cetac Technologies, Omaha, NE, USA) operating at a wavelength of 213 nm was provided with an in house-built ablation chamber and coupled to a quadrupole-based inductively coupled plasma-mass spectrometer (iCapQc, Thermo Fisher Scientific, Bremen, Germany). Laser parameters were optimized to reveal best compromise between lateral resolution, scan speed and sensitivity of MS detection. Spot sizes of 10 and 5 µm, with two-fold scan speed (20 or 10 µm/s, respectively), were selected, while the laser was operated in line-by-line ablation mode (0 µm space between lines) at a shot frequency of 20 Hz. Laser energy was adjusted to 0.4 mJ to realize quantitative ablation of the thin sections. As carrier gas, 800 ml/min helium was applied to achieve a washout time of the ablated sample aerosol from the laser ablation cell in less than 500 ms. Furthermore, argon (400 ml/min) was added prior to the ICP-MS to improve plasma stability, which was monitored during all measurements by introducing an internal liquid standard (300 ng/ml Rh solution, diluted from 998 µg/ml, 20 % HCl, Single element Aqueous CRM, Spetel, Erding, Germany, in 2 % HNO_3) by the use of a PFA nebulizer combined with a cyclonic spray chamber. All experiments were performed in kinetic energy discrimination mode of the ICP-MS instrument using approx. 4 ml/min helium as collision cell gas. Sampler and skimmer made of nickel as well as quartz injector pipe with an inner diameter of 3.5 mm were used during all measurements. The ICP-MS (RF power of 1550 W) was tuned for maximum intensity (sequenced tuning of torch horizontal and vertical position, nebulizer gas flow (0.5 l/min), second extraction lens potential, and cell focus lens potential) while on-line coupled to laser ablation and liquid introduction of an multi-element standard solution. Besides gold (^{197}Au, dwell time: 0.35 s) and rhodium (^{103}Rh, dwell time: 0.05 s), bromine (^{79}Br, dwell time: 0.1 s) resulting from eosin staining was monitored to visualize the MTs for the purpose of orientation. To convert the transient signals of all line scans in color coded elemental distribution maps, data processing was carried out using ImageJ (ImageJ 1.47n, National Institute of Health, Bethesda, MD, USA) software. Quantification was performed by external calibration with matrix-matched standards based on the embedment of gold stock solution (1000 mg/l gold ICP standard, 7 % HCl, Merck KGaA, Darmstadt,

Germany) into gelatin (pure gelatin powdered, Grüssing GmbH Analytica, Filsum, Germany) as described elsewhere (Niehaus et al. 2015). 10 µm thick standard sections were prepared at concentrations between 0 to 50 µg/g. Signal intensities were subsequently adjusted to sample thickness of 1.5 µm, revealing a standard concentration range of 0 to 333.3 µg/g.

Inductively coupled mass spectrometry (ICP-MS)

Conventional ICP-MS analysis was performed in order to quantify AuNP uptake into co-culture MTs. Therefore, 40 MTs were either exposed to 50 µg/ml of Au-3-PEG, Au-5-COOH, Au-13-PEG or Au-14-COOH NPs for 24 h, pooled and thoroughly washed. Digestion of MTs was performed in open vials using 0.4 ml 67 % HNO_3 and 0.2 ml 30 % HCl for approximately 4 hours at room temperature. Total amount of Au in the MTs was determined by SF-ICP-MS using a Sectorfield ICP mass spectrometer (Series 2, Thermo Fisher Scientific GmbH, Germany). For the Au detection, the ^{197}Au isotope was selected. As an internal standard 40Ar40Ar and 187Re were used. Prior to analysis, digested samples were filled up with ultrapure water to 10 ml with 10 ppb of 187Re as internal standard. Calibrations were performed using an ionic Au standard in a matrix matched solution (2 ml of 67 % HNO_3 and 1 ml of 30 % HCl per 50 ml) ranging from 0 to 50 µg/l Au.

Transmission Electron Microscopy (TEM)

For TEM analysis, MTs were exposed to 50 µg/ml of Au-13-PEG or Au-14-COOH for 24 h and fixed in 3 % glutaraldehyde in 0.1 M sodium cacodylate buffer. After a washing step in 0.2 M sodium cacodylate buffer, MTs were post-fixated in 2 % osmium tetroxide in 0.1 M sodium cacodylate buffer. After dehydration through a graded ethanol series followed by acetone, samples were embedded in Epon resin (Sigma Aldrich, Switzerland). Ultrathin sections were contrasted with 2 % uranyl acetate and lead citrate (Reynolds 1963). Images were taken with a Zeiss EM 900 (Carl Zeiss Microscopy, GmbH, Germany) at 80 kV.

Mechanistic uptake studies

Initially, control experiments were performed using transferrin conjugated to Alexa Fluor 488 (Tf_{488}). MTs were exposed to 25 µg/ml Tf_{488} diluted in non-supplemented FGM containing 10 mM HEPES (Sigma Aldrich, Switzerland) and incubated for 30 min either at 4 or 37ºC. Subsequently, MTs were pooled, washed and fixed with 4 %

paraformaldehyde (PFA) for 60 min followed by 0.2 % Triton X-100 treatment for 30 min. After one washing step, MTs were blocked in 5 % goat serum for 60 min and incubated with the primary antibody monoclonal mouse anti-human cytokeratin 7 (1:200, M7018, DAKO, Denmark) over night at 4ºC. MTs were washed three times prior to the addition of the secondary antibody Alexa Fluor 488 goat anti-mouse IgG (1:400, A11029, Molecular Probes, USA) for 5 h at room temperature. After another three washing steps, MTs were analyzed by confocal microscopy. For quantitative uptake analysis of AuNPs, 40 MTs were exposed to 100 µg/ml of Au-14-COOH diluted in non-supplemented FGM containing 10 mM HEPES and incubated for 30 min either at 4 or 37ºC. Afterwards, MTs were pooled, washed and subsequently analyzed by ICP-MS as described above.

Statistical analysis

Data are represented as mean ± standard deviation (SD) of at least three independent experiments. Statistical analysis was performed using a two-tailed Student's t-test. P-value < 0.05 was considered significant.

Results

Nanoparticle synthesis and characterization

AuNPs with core size < 5 nm have been prepared by reduction of $HAu(III)Cl_4$ to Au^0 with $NaBH_4$ in the presence of bifunctional thiols of the type XRSH (X = COOH, and CH_3) that provide thiolate ligands XRS bonded as one-electron ligands to Au(I) atoms of the AuNP surface. Reduction of $HAu(III)Cl_4$ to Au^0 atoms forming AuNPs with Na_3 citrate yields AuNPs of core size > 10 nm in the presence of these bifunctional thiols that bind AuNPs as indicated above as thiolate ligands. The syntheses of these bifunctional AuNPs have already been previously reported in the literature (Shi et al. 2004, Zheng et al. 2004, Chen et al. 2006, Ghann et al. 2012). AuNP were carefully characterized and a summary of their properties is presented in Table 1.

Table 1: Summary of AuNP characteristics

	Au-3-PEG	Au-13-PEG	Au-4-COOH	Au-14-COOH
TEM: Primary Particle Size (nm)	3.5 ± 1.2[1]	13.5 ± 3[1]	4.5 ± 1.5[1]	14 ± 3.5[1]
Zeta Potential (mV)	-16.5 ± 3	-37 ± 3	-28.8 ± 0.4	-26 ± 3
UV-vis. peak (nm)	520	524	528	529
FTIR (cm^{-1})	2917, 2879, 1099	2909, 2874, 1103	1738	1731
Surface functionalization	$SH\text{-}PEG_{(550)}CH_3$	$SH\text{-}PEG_{(550)}CH_3$	$SH\text{-}(CH_2)_{10}\text{-}COOH$	$HS(CH_2)_{10}CH_2O(C_2H_4O)_3C_2H_4OCH_2CO_2H$
ICP-OES: Au content (%)	76.98	45.17	38.38	47.28

Data represent mean ± SD.
Abbreviations: FTIR, Fourier transform infrared spectroscopy; TEM, transmission electron microscopy; XPS, X-ray photoelectron spectroscopy

The formation of AuNPs was verified by UV-vis. absorption spectroscopy (Figure 1B), including the characteristic plasmon band of the AuNPs. The TEM images showed that the sizes of these AuNP cores were approximately 3 and 4 nm for the small PEGylate and carboxylate AuNPs and approximately 13 and 14 nm for the large PEGylate and carboxylate AuNPs, respectively (Figure 1A). AuNPs coated with ligands bearing -COOH at the periphery of the AuNPs showed a peak at 1730 cm^{-1} in their FTIR spectrum that was assigned to the carbonyl group of carboxylic acids. On the other hand the AuNPs coated with the PEG ligand showed strong and sharp peaks at 2916 and 2845 cm^{-1} in the spectra corresponding to the asymmetric and symmetric stretching of methylene groups, and in the fingerprint region a strong band

due to the C–O–C stretching mode that was centered at approximately 1100 cm^{-1}. The zeta potential was -16.5 ± 3 mV for Au-3-PEG, -28.8 ± 0.4 for Au-4-COOH, -28.8 ± 0.4 mV for Au-13-PEG and -26 ± 3 mV for Au-14-COOH NPs. Au contents of AuNPs were determined by ICP-OES analysis and were 76.98 % for Au-3-PEG, 45.17 % for Au-13-PEG, 38.38 % for Au-4-COOH and 47.28 % for Au-14-COOH NPs. AuNPs have been tested for endotoxin contamination and were endotoxin free (data not shown).

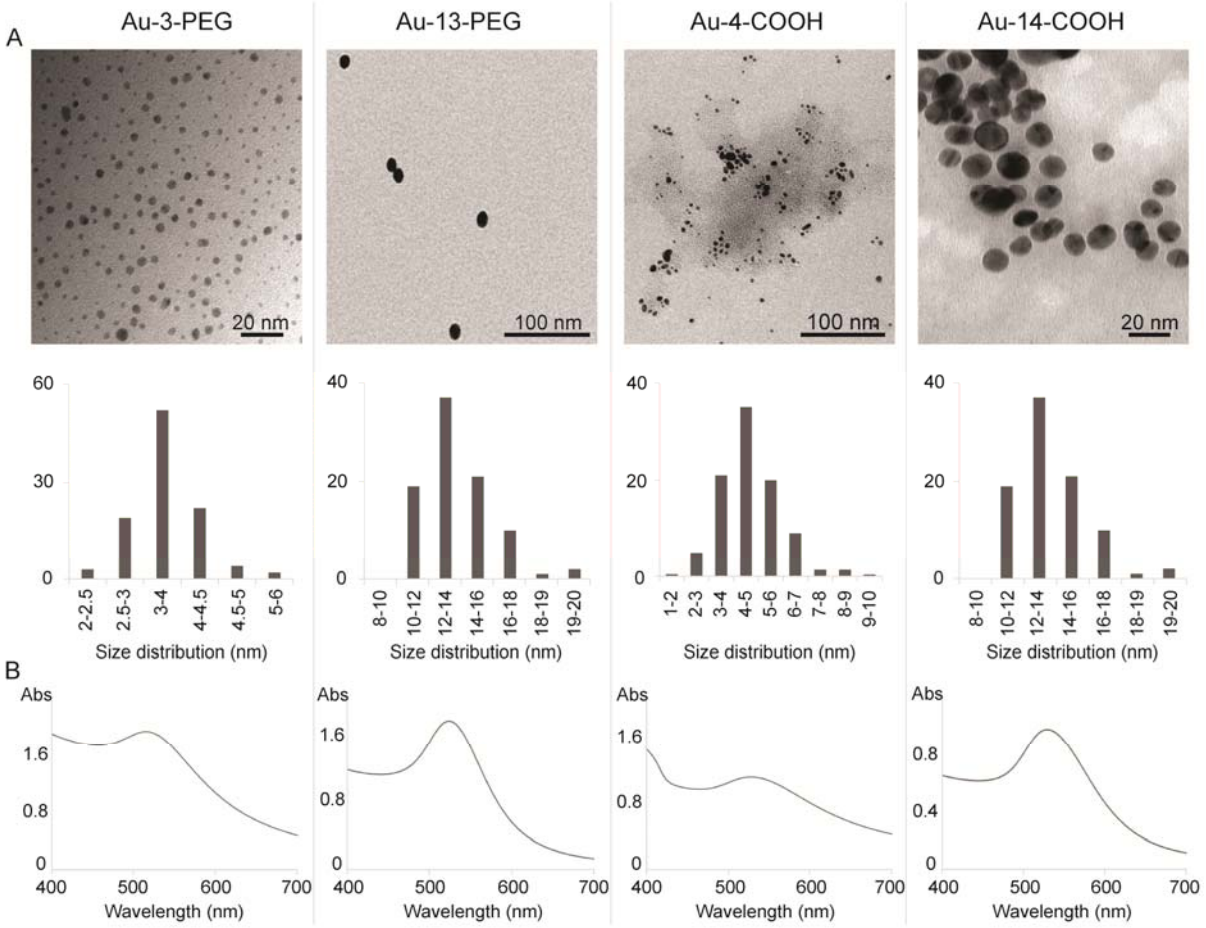

Figure 1. Characterization of Au-3-PEG, Au-13-PEG, Au-4-COOH and Au-14-COOH NPs. TEM images with corresponding size distributions **(A)** and UV-vis. absorption spectra measured at wavelengths between 400 and 700 nm **(B)**.

Penetration, localization and quantitative uptake of AuNPs in co-culture MTs

Distribution and uptake of AuNPs in dependence of different sizes (3-4 or 13-14 nm in diameter) and surface modifications (carboxylate or PEGylate) were assessed using human placental *in vitro* co-culture MTs. Prior to AuNP experiments, the absence of cytotoxic effects on the co-culture MTs was confirmed for all AuNPs using

an ATP assay (Figure S1). LA-ICP-MS was applied in order to determine the distribution and quantitative amount of internalized Au on paraffin sections of co-culture MTs. For each NP type used in this study, the fraction of Au was different and Au concentrations were adjusted to a constant level of 50 µg/ml Au for all NPs (Au-3-PEG, Au-13-PEG, Au-4-COOH and Au-14-COOH NPs) in order to allow direct comparison between different particle types. A Bromine (^{79}Br) distribution map (Figure 2c) was used to distinguish between Au signals (Figure 2d) in- or outside the MT area (overlay of elemental distribution images of ^{79}Br and ^{197}Au signals are shown in Figure 2e. To evaluate Au penetration into the co-culture MTs, paraffin sections were stained with the epithelial cell marker MNF116 to label cytokeratin, which is specifically expressed by BeWo cells (Figure 2b) and thus enables to assign Au signals to the BeWo cell or HVMF area. Penetration of Au from MTs exposed to Au-3-PEG (Figure 2A) was deeper than for Au-13-PEG (Figure 2B) or Au-14-COOH NPs (Figure 2C), respectively. Regarding different surface modifications, Au uptake of Au-14-COOH NPs into the BeWo cell layer (Figure 2C) was higher compared to Au-13-PEG NPs, which appeared to mainly stick to the MT surface (Figure 2B). LA-ICP-MS analysis of Au-4-COOH NP uptake into co-culture MTs is currently being performed.

In detail, Au distribution maps of co-culture MTs exposed to Au-3-PEG NPs revealed an Au penetration into the fibroblastic core with a homogenous distribution therein (Figure 2A). Average Au concentrations were highest in the fibroblastic area and reached approximately 20-60 µg/g Au with a maximum of > 100 µg/g Au whereas Au concentrations in the BeWo cell area were considerably lower (~15 µg/g Au). Occasionally, signals from accumulated Au were detected outside the MTs (Figure 2A (a,d)). In contrast, Au from MTs treated with Au-13-PEG NPs predominantly accumulated at the surface of the MTs (> 200 µg/g Au) and only low concentrations were measured in the BeWo cell layer as well as in the fibroblastic core (~10 µg/g) (Figure 2B).

The highest accumulation of Au in BeWo cells was measured after the exposure to Au-14-COOH NPs with average concentrations of 100-150 µg/g Au and local maxima of > 250 µg/g Au (Figure 2C). Regarding Au penetration of Au-14-COOH NPs into the core of the MTs, only minor fractions of approximately 10 µg/g Au reached the fibroblasts.

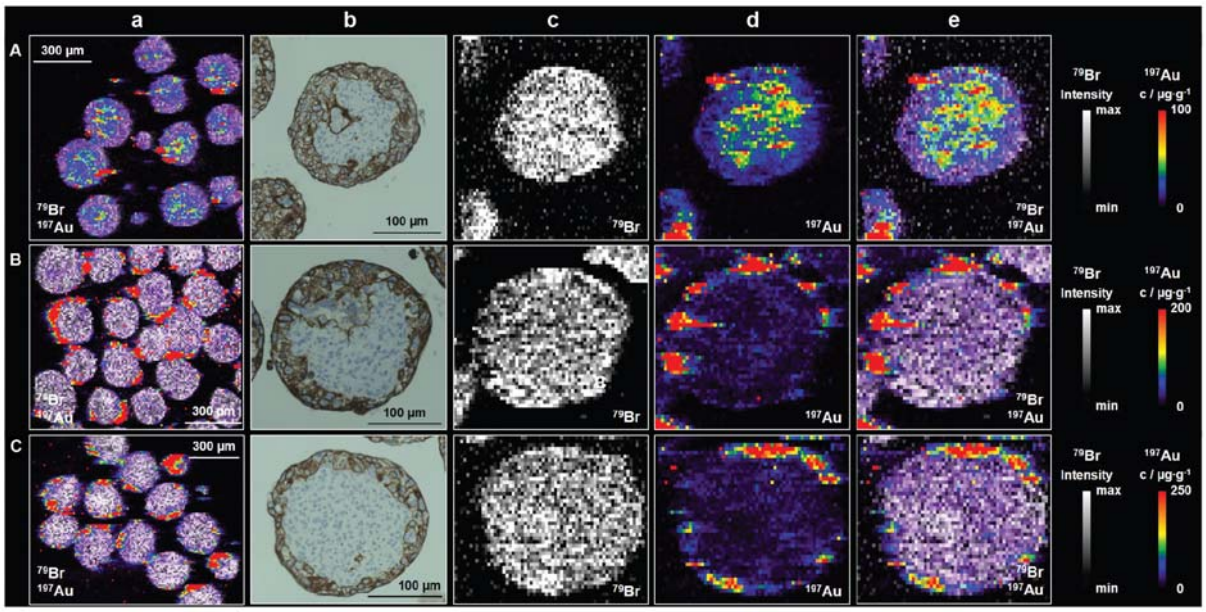

Figure 2. Penetration and quantification of Au by LA-ICP-MS. Co-culture MTs were exposed to 50 µg/ml of Au-3-PEG **(A)**, Au-13-PEG **(B)**, and Au-14-COOH NPs **(C)** for 24 h. From left to right: Overlay of elemental distribution maps (laser spot size: 10 µm) of ^{79}Br, resulting from eosin staining to visualize MTs, and ^{197}Au, resulting from AuNPs; cytokeratin staining of MT enables allocation of Au signals to fibroblasts (blueish stain) and trophoblasts (brownish stain); elemental distribution maps of distinct MT (laser spot size: 5 µm): ^{79}Br to visualize MT structure, ^{197}Au to localize distribution of AuNPs, overlay of ^{79}Br and ^{197}Au to co-localize Au signals to cell types occurring in MTs. Dashed lines (based on bromine distribution map) indicate MT borders. Elemental distribution map of ^{79}Br is depicted in grey scale, representing signal intensities (black: minimum, white: maximum). Elemental distribution map of ^{197}Au is depicted as heatmap color code, representing Au concentrations from 0 (minimum, shown in black color) to > 100, 200 or 250 µg/g (maximum, shown in red color), respectively.

In addition to LA-ICP-MS, the total amount of Au in the co-culture MTs was quantified using conventional ICP-MS analysis (Figure 3). Specifically, Au quantities per MT were similar after exposure to both, Au-3-PEG and Au-13-PEG NPs with average values of 1.28 ± 0.93 and 1.66 ± 1.0 ng Au per MT, respectively, and were not significantly higher than those of untreated controls (0.05 ± 0.05 ng/ml Au). After exposure to Au-14-COOH NPs, an average quantity of 3.93 ± 1.26 ng Au per MT was measured, which was slightly increased as compared to Au-13-PEG NPs but significantly higher than for Au-3-PEG and control samples. However, the highest amount of Au was observed after the exposure to Au-4-COOH NPs with 47.5 ± 9.3 ng Au per MT. When expressed in percentages of the initial dose (% ID) added to the MTs, uptake was 0.043 % for Au-3-PEG, 0.073 % for Au-13-PEG, 2.13 % for Au-4-COOH and 0.17 % for Au-14-COOH NPs (Table 2).

A

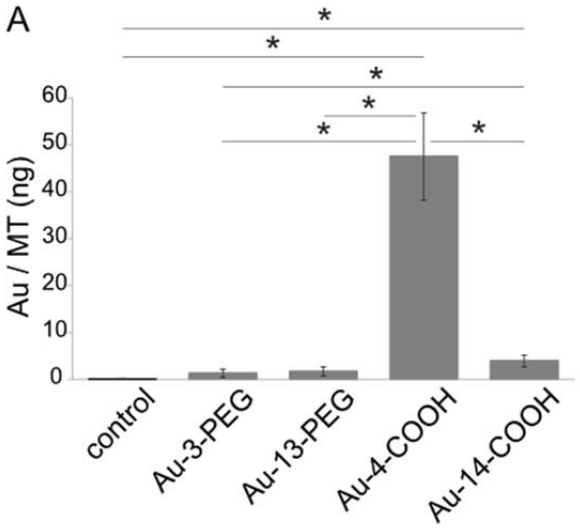

B

NP Type	mean (% ID)	SD
Au-3-PEG	0.043	0.032
Au-13-PEG	0.073	0.043
Au-4-COOH	2.133	0.068
Au-14-COOH	0.172	0.051

Figure 3. Quantification of AuNP uptake into co-culture MTs by ICP-MS determination of Au. Co-culture MTs were exposed to 50 µg/ml of Au-3-PEG, Au-13-PEG, Au-4-COOH and Au-14-COOH NPs for 24 h. Au uptake into co-culture MTs is shown as absolute quantities **(A)** and as percentages of the initial dose (% ID) **(B)**. Data represent the mean ± SD of 3-4 independent experiments. *$p < 0.05$ vs. medium control.

In addition, TEM analysis was performed for the larger AuNPs in order to confirm cellular uptake of AuNPs and to reveal their subcellular localization. TEM micrographs of untreated control MTs showed that BeWo cells and HVMFs were in a viable state (Figure S2). TEM micrographs of MTs exposed to Au-13-PEG (Figure 4A) or Au-14-COOH NPs (Figure 4D) confirmed their intracellular uptake into the BeWo cell layer where they were present as single particles localized predominantly in membrane-bound vesicles. Despite the low amount of internalized AuNPs for both NP types, cellular uptake seemed to be slightly higher for Au-14-COOH than for Au-13-PEG NPs. Regarding penetration of AuNPs into the fibroblastic core, it was difficult to unambiguously identify these NPs due to the electron-dense interior of the fibroblasts that could be easily misinterpreted as small agglomerates of NPs.

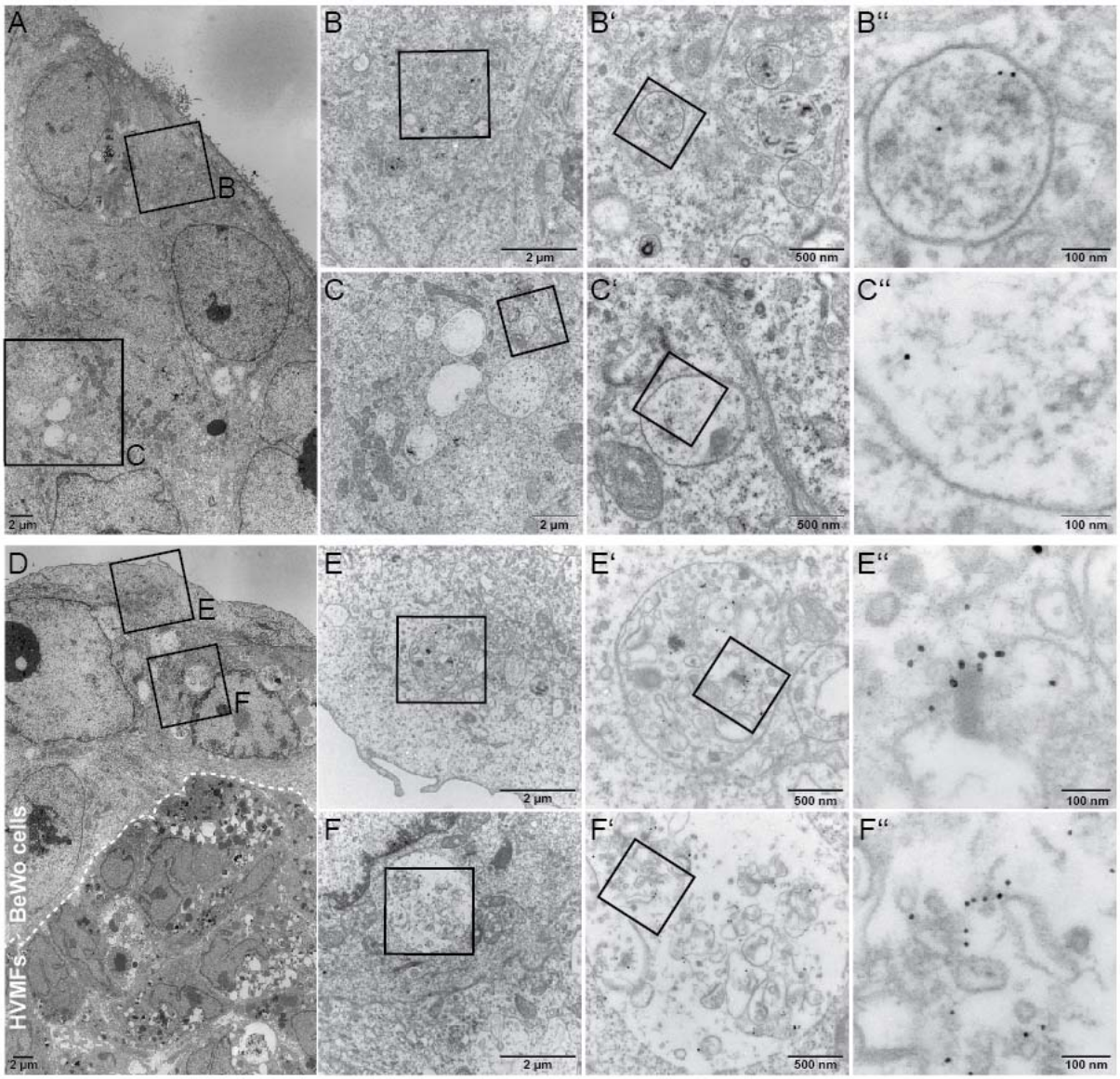

Figure 4. Intracellular uptake of Au-13-PEG and Au-14-COOH NPs into BeWo cells of co-culture MTs. TEM micrographs of co-culture MTs exposed to 50 µg/ml of Au-13-PEG **(A)** or Au-14-COOH NPs **(D)** for 24 h. X' and X'' represent enlargements of the quadrants in X or X', respectively.

Uptake mechanisms of AuNPs into co-culture MTs

In order to elucidate whether passive or active uptake mechanisms were involved in the internalization of Au-14-COOH NPs into the MTs, AuNP exposure studies were conducted at 4 or 37ºC. To confirm the successful inhibition of energy-dependent uptake pathways at 4ºC in 3D MTs, control experiments were performed using Tf_{488} (i.e. transferrin conjugated to Alexa Fluor 488), which is taken up by mammalian cells via receptor-mediated endocytosis (Harding et al. 1983). Incubation at 37ºC resulted in a considerable amount of internalized Tf_{488} (Figure S3B) while active uptake of Tf_{488} into the MTs was effectively inhibited at 4ºC (Figure S3C). Finally, uptake of Au-

14-COOH NPs into the MTs was quantified by ICP-MS and revealed similar Au amounts after the incubation at 4 or 37ºC with values of 5.4 ± 0.73 or 7.12 ± 3.2 ng, respectively (Figure 5).

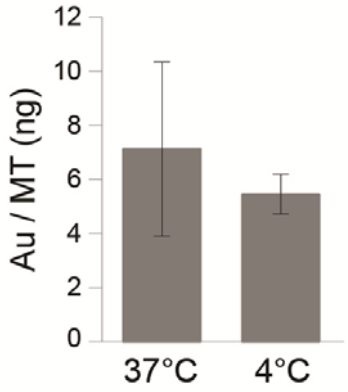

Figure 5. Quantitative uptake analysis of Au-14-COOH NPs into co-culture MTs at 4 or 37ºC. Co-culture MTs were exposed to 100 µg/ml of Au-14-COOH NPs for 30 min and incubated either at 37 or 4ºC. Uptake into the MTs was quantified by means of ICP-MS.

Discussion

In this study, we used the co-culture MT model to investigate uptake and penetration of nontoxic AuNPs in dependence of different sizes and surface modifications. AuNPs were excellent candidates due to their tunable physico-chemical properties, high stability in aqueous solutions, low agglomeration, narrow size distribution, good optical properties and their wide use in the development of novel nanomedical therapies (Dreaden et al. 2012). Moreover, from AuNPs functionalized with carboxyl groups we expected a higher placental uptake and penetration compared to PEGylate AuNPs. PEGylation is being used as an efficient strategy to reduce protein absorption resulting in lower cellular uptake (Pozzi et al. 2014, Pelaz et al. 2015). Even though amine-modified AuNPs may be potential/valid candidates for increased placental uptake and penetration, these NPs were excluded due to their potential cytotoxic effects (Goodman et al. 2004). In order to allow for a direct comparison of the different AuNPs, the amount of Au to which the co-culture MTs were exposed to was kept constant at 50 µg/ml Au from Au-4-COOH, Au-3-PEG, Au-14-COOH and Au-13-PEG NPs. This concentration was required to obtain sufficient amounts of internalized Au for the uptake analysis in co-culture MTs. Furthermore such an exposure scenario mirrors *in vivo* medical applications. The combination of qualitative and quantitative methods enabled the comprehensive analysis of AuNP uptake into the co-culture MTs in dependence of their size and surface modification. LA-ICP-MS was used as a powerful tool to determine the elemental distribution in biological tissue samples (Becker et al. 2014). Among microanalytical element imaging techniques (e.g. X-ray spectroscopy, secondary ion mass spectrometry) LA-ICP-MS offers a very low limit of detection, a wide dynamic range and a high spatial resolution down to the subcellular level. In addition, we demonstrated the potential of this technique to quantify the amount of Au within paraffin sections of co-culture MTs. The elemental fractionation during ablation processes as well as plasma conditions and thus, ionization of the analytes of interest are highly matrix-dependent. Therefore, a robust and reliable quantification requires the use of matrix-matched standards that are either commercially available as certificated reference materials (CRM) or prepared in-house (Hare et al. 2012). Since the availability of CRMs for biological tissues is very limited, gelatin-based standards were produced in our laboratory, spiked with defined amounts of Au stock solution and used for the external calibration of Au signals in the MT samples. A spot size of 5 µm was applied

to obtain an optimal lateral resolution for the localization of Au signals in the tissue sections (MT diameter approximately 250 µm). In order to allocate these Au signals to the MT area, paraffin sections were stained with HE. As eosin contains four bromine atoms in its molecular structure, visualization of the whole MTs was realized with the elemental distribution image of ^{79}Br (Reifschneider et al. 2013) to determine the MT border. Furthermore, signals were allocated to different cell types of the MTs by comparing Au images with microphotographs of MTs stained for cytokeratin. During the last two decades, LA-ICP-MS was extensively employed for generating spatially resolved information on the distribution of different elements in biological tissues from humans, animals or plants (Becker et al. 2014, Pozebon et al. 2014). Only recently, this approach was utilized to assess subcellular distribution and quantitative amount of internalized NPs into single cells (Drescher et al. 2012, Bohme et al. 2014, Buchner et al. 2014, Wang et al. 2014). The proof of concept was shown by several studies that assessed uptake of silver or AuNPs into single fibroblasts (Drescher et al. 2012), aluminium oxide NPs into human skin keratinocytes or lung epithelial cells (Bohme et al. 2014) and AuNPs into human fibroblasts (Buchner et al. 2014) or mouse monocyte macrophages (Wang et al. 2014). In contrast to LA-ICP-MS of single cells, it is important for the analysis of MTs to focus on cross sections through the center of the MTs. In the case of a peripheral cut through the BeWo cell layer, results may not adequately represent the elemental distribution throughout the MT.

In addition to LA-ICP-MS, where the content of Au was quantified within single paraffin sections of 1.5 µm in thickness, quantitative uptake of Au into the whole MTs was measured by ICP-MS analysis. Both, LA-ICP-MS and ICP-MS analysis confirmed a size- and surface modification-dependent uptake of Au after the exposure to Au-4-COOH, Au-3-PEG, Au-14-COOH and Au-13-PEG NPs. Since ICP-MS analysis did not differentiate between ionic Au and AuNPs or between their presence in the cytoplasm or in paracellular spaces, this complementary information was revealed by TEM analysis. Indeed, Au from Au-14-COOH and Au-13-PEG NPs was present in the form of particles and predominantly located in vesicles of BeWo cells. However, their existence in the fibroblastic core could not be confirmed due to the highly dense cell interior/cytoplasm of the HVMFs. Au-4-COOH and Au-3-PEG NPs were excluded from TEM analysis because of their small sizes.

Currently, there are only a few studies available that investigated translocation of different AuNPs through the placental barrier. For example, a size dependent translocation was observed after intravenous injection of sulfonated triphenylphosphine coated AuNPs in pregnant rats. Au quantities of 30 ng and 0.12 ng were measured after exposure to 1.4 or 18 nm AuNPs, respectively, while 80 nm AuNPs did not cross the placental barrier (Semmler-Behnke et al. 2014). Similarly, intravenous injection of 20 nm AuNPs into mice resulted in significant amounts of Au in the placenta but not in fetal organs while Au levels after exposure to 50 nm AuNPs remained lower (Rattanapinyopituk et al. 2014). In a mouse study, translocation of 13 nm AuNPs was dependent on their surface coating with 0.02 % ID for PEGylate or citrate AuNPs and 0.06 % ID for ferritin coated AuNPs (Yang et al. 2012). Values observed in our study were slightly higher with 0.07 % and 0.17 % ID for Au-13-PEG and Au-14-COOH NPs, respectively. Moreover, we observed a surface coating dependent uptake with higher amounts for carboxylate than for PEGylate AuNPs, which was not confirmed in the study of Yang et al. Possible reasons for this discrepancy in the results certainly include the species-specific differences in the placental structure and function (Malassine et al. 2003). Regarding different transplacental transfer rates, levels of fetal IgG in the second half of gestation remained low in mice and rats while pre-natal transfer in human was considerably higher (Pentsuk and van der Laan 2009). From a material's perspective, significantly different zeta potentials of the AuNPs used for these studies may also contribute to dissimilar results. In contrast, no translocation (below level of detection) was observed for 10, 15 or 30 nm PEGylate AuNPs using the human *ex vivo* placenta perfusion model (Myllynen et al. 2008). TEM and silver enhancement confirmed the presence of AuNPs in the syncytiotrophoblast and cytotrophoblasts of the human placental tissue. This is in good agreement with the results obtained in our study where we showed a high accumulation of Au-13-PEG NPs outside the MTs and only low levels in the BeWo cell layer or the fibroblastic core (Figure 2B). These findings provide further evidence that PEGylation of NPs may significantly reduce placental uptake and thus, are promising candidates as drug carriers to specifically treat maternal disorders.

Regarding studies on NP uptake pathways only limited knowledge is currently available and most conclusions are based on assumptions. For example, Semmler-Behnke et al. suggested that diffusion, transtrophoblastic channels and/or receptor-

mediated endocytosis are the mechanisms involved in the translocation of 1.4 and 18 nm AuNPs (Semmler-Behnke et al. 2014). In the study of Rattanapinyopituk et al., exposure to 20 or 50 nm AuNPs led to an upregulation in the formation of endocytic vesicles in the syncytiotrophoblasts and the fetal endothelial cells. Furthermore, immunohistochemical analysis revealed a higher clathrin intensity indicating that endocytosis was upregulated after the administration of AuNPs (Rattanapinyopituk et al. 2014). In this study, we were interested in investigating whether active or passive pathways were involved in the intracellular uptake of AuNPs into co-culture MTs. Since the intracellular presence of Au-14-COOH NPs was confirmed by TEM analysis and quantitative amounts were significantly higher than for Au-13-PEG NPs, they were included in further mechanistic uptake studies. Co-culture MT exposure to Au-14-COOH NPs either at 4 or 37ºC resulted in similar amounts of Au, which was indicative for a passive uptake of these NPs into the MTs. Even though intracellular uptake of these NPs was confirmed, it cannot be completely excluded that a fraction of AuNPs may be surface-bound or taken up via paracellular routes. However, in future studies uptake of different types of NPs into the MTs should be investigated and to more precisely reveal the underlying uptake mechanisms, chemical inhibitors need to be established and optimized for 3D co-culture MTs.

Conclusion

Developing safe, effective and site-specific nanomedical therapies during pregnancy requires reliable and high-throughput compatible model systems. In this study, we demonstrated the potential of 3D MTs to evaluate uptake and penetration of AuNPs in dependence of different physico-chemical properties and surface functionalization. The distinct core/shell-structure of MTs enabled NP penetration studies in a more tissue-like microenvironment as conventional 2D cell cultures. The possibility to create elemental distribution maps of MTs by LA-ICP-MS allowed assessing to which extent AuNPs were able to cross the BeWo cell layer and reach the fibroblastic core. In addition, our results on uptake and penetration of Au-13-PEG NPs indicate a good correlation with the results obtained from human *ex vivo* placenta perfusion model. This further supports that the MT model is a valid tool to study mechanistic aspects of NP uptake and penetration at the human placental barrier. Finally, we confirmed that this model allow studying uptake mechanisms of AuNP into co-culture MTs, which provides crucial information on the intracellular fate of these NPs and may further support the identification of suitable NPs for the development of site-specific nanomedical applications.

Electronic Supplementary Information (ESI)

Impact of particle size and surface modification on the localization and penetration of gold nanoparticles in human placental co-culture microtissues

Carina Muoth[1], Mandy Großgarten[2], Uwe Karst[2], Jaime Ruiz Aranzaes[3], Didier Astruc[3], Sergio Moya[4], Liliane Diener[1], Kathrin Grieder[1], Adrian Wichser[1], Wolfram Jochum[5], Peter Wick[1] and Tina Buerki-Thunherr[1]

[1] Particles-Biology Interactions, Empa, Swiss Federal Laboratories for Materials Science and Technology, Lerchenfeldstrasse 5, 9014 St. Gallen, Switzerland.

[2] Institute of Inorganic and Analytical Chemistry, Westfälische Wilhelms-Universität Münster, Corrensstraße 28/30, 48149 Münster, Germany

[3] ISM, Université de Bordeaux, 351 Cours de la Libération, 33405 Talence Cedex, France

[4] bCIC biomaGUNE, Unidad Biosuperficies, Paseo Miramon No. 182, Edif “C” 20009 Donostia-San Sebastian, Spain

[5] Institute of Pathology, Cantonal Hospital St.Gallen, Rorschacherstrasse 95, 9007 St. Gallen, Switzerland.

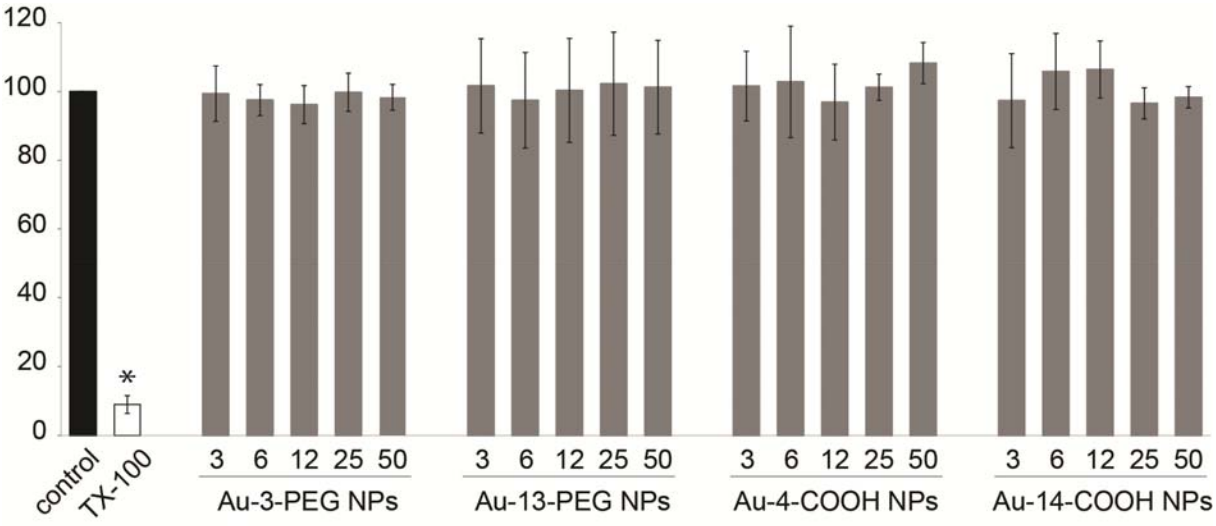

Figure S1. Effects of AuNPs on 3D MT viability. ATP assay was used to assess cell viability of co-culture MTs after exposure to 3-50 µg/ml of Au-3-PEG, Au-13-PEG, Au-3-COOH and Au-14-COOH NPs for 24 h. Treatment of MTs with 0.1 % TX-100 was used as a positive control. Data represented as mean percentages of triplicates compared to untreated medium control (FGM) ± SD of 3 independent experiments. *$p < 0.05$ compared to untreated medium controls.

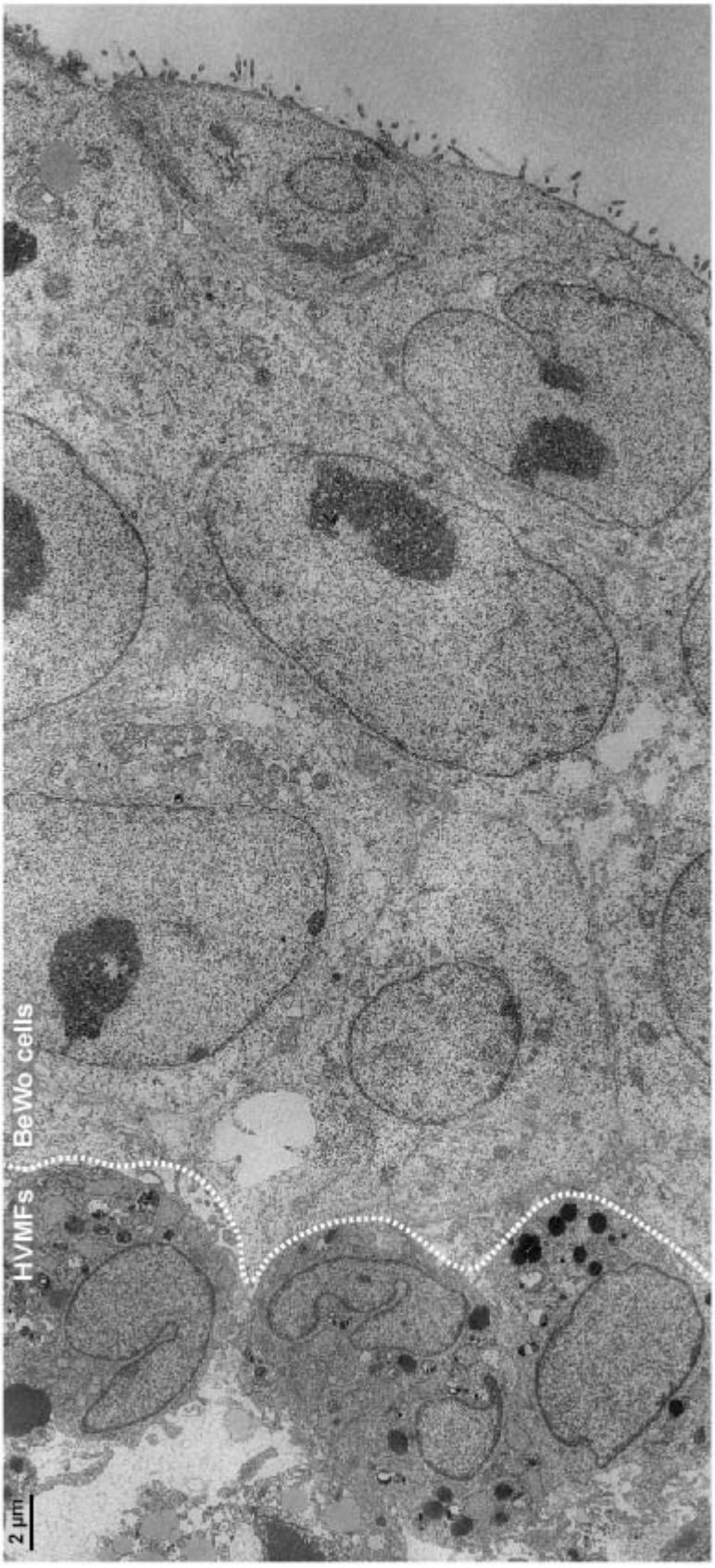

Figure S2. Electron micrograph of an untreated co-culture MT with an outer layer of BeWo cells and an inner core of HVMFs.

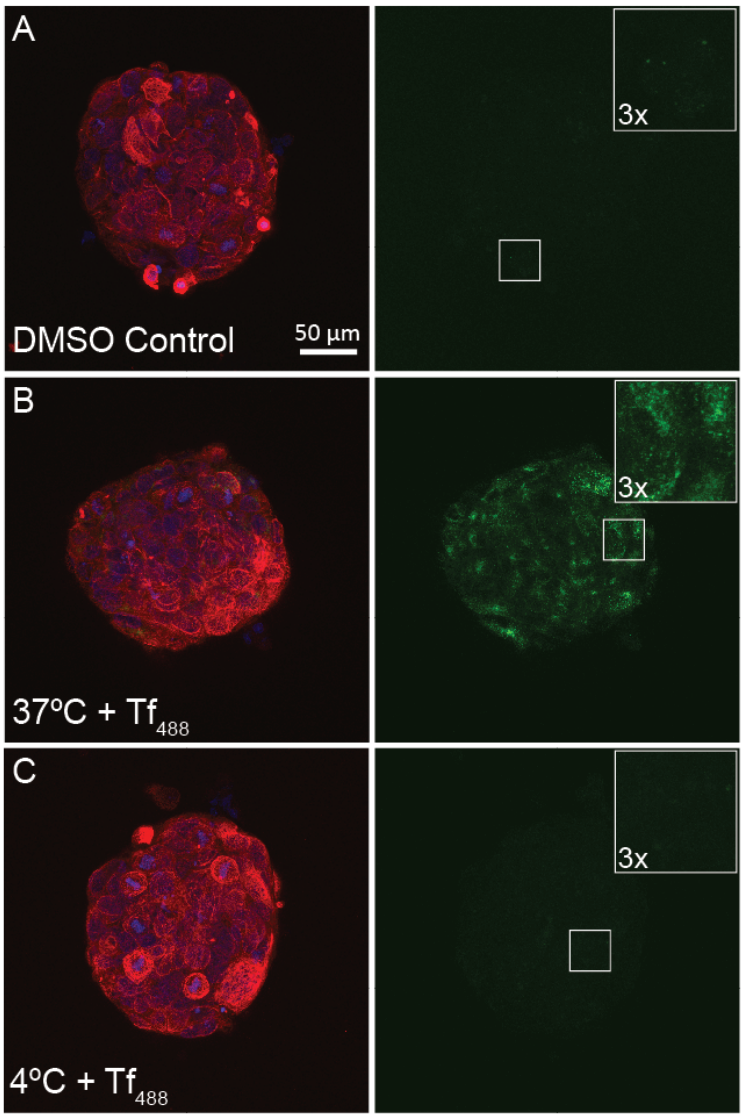

Figure S3. Uptake of Tf_{488} into co-culture MTs. Confocal microscopy of co-culture MTs exposed to 25 µg/ml Tf_{488} for 30 min incubated either at 37°C (**B**) or 4°C (**C**). The DMSO control (**A**) was not exposed to Tf_{488} and used as the negative control. Whole-mount staining of co-culture MTs was performed using cytokeratin 7 to specifically label BeWo cells (red) and Dapi (blue) to visualize nuclei

.

Chapter 4

Discussion and Outlook

4.1 Discussion

A thorough understanding of NP uptake, accumulation, penetration and safety at the human placental barrier, based on their physical, chemical and biological properties, is crucial for the design of safe, effective and site-specific nanomedical therapies in pregnancy. Such NP-based approaches offer the unique advantage to individually treat the mother, the placenta or the fetus with reduced off-target effects.

In the current work, we exploited different cutting edge technologies to develop novel human placenta *in vitro* models for the assessment of NP uptake mechanisms, distribution, penetration, and toxicity.

Micropatterned BeWo cells to study NP uptake in dependence of distinct actin structures

Although the number of descriptive studies on the translocation of NPs across the placenta is increasing, the underlying transport mechanisms are largely unknown. The complexity of the placental tissue organization makes it challenging to extensively examine NP uptake pathways in human *ex vivo* placenta perfusion or in *in vivo* animal models. The use of 2D cell cultures may help to reduce this complexity. On the other hand, such models only provide an oversimplified and highly artificial environment and further research is needed to address these challenges and mimic the *in vivo* situation. In a first step, and to recreate a more tissue-like microenvironment, we employed a micropatterning approach where cells are morphologically and physically constraint on adhesive fibronectin-coated micropatterns similar to biological tissues (Thery 2010). Moreover, and from an experimental point of view, micropatterned cells exhibit a highly reproducible shape and intracellular organization, thereby facilitating quantitative NP uptake studies.

In a recent study of our lab, we have demonstrated that placental translocation of PS NPs is not based on passive diffusion but involves energy-dependent uptake pathways (Grafmueller et al. 2015). Moreover, several uptake studies with various cell types have proposed actin-dependent endocytosis for different NPs including PS NPs (Dausend et al. 2008, dos Santos et al. 2011, Lunov et al. 2011). Therefore, we hypothesized that an active, actin-dependent uptake mechanism may be involved in the internalization and translocation of PS NPs across the placental barrier.

To reveal the role of the actin cytoskeleton in PS NP uptake, BeWo cells were cultivated on micropatterns of four different geometries, which induced highly distinct

actin structures. Compared to conventional 2D approaches, the microcontact printing technique added additional complexity such as cell-ECM interactions on micropatterns of a defined area that were shown to exhibit improved physiological behavior. However, we did not observe a correlation between intracellular uptake and distribution of 80, 240 and carboxylate 300 nm PS NPs in BeWo cells in dependence of their global actin cytoskeletal organization. To a certain extent, this result was unexpected since numerous studies confirmed a strong impact of cytochalasin treatment, a chemical inhibitor widely used to prevent actin polymerization, on for example carboxylate PS NP uptake by HeLa cells (Dausend et al. 2008, dos Santos et al. 2011) and macrophages (Lunov et al. 2011), silica NP uptake by lung epithelial cells (Nowak et al. 2014) or polymeric NP uptake by glioblastoma cells (Gao et al. 2013). Nevertheless, other studies did not confirm this inhibitory effect on cellular uptake of NPs upon cytochalasin treatment. For instance, there was no decrease on PS NP uptake by pulmonary macrophages (Geiser et al. 2005) and THP-1 cells (Lunov et al. 2011) or on PLGA NP uptake by A549 cells (Tahara et al. 2009). The reason for these discrepancies in the results may lie in the use of different cell types, experimental setups or NPs, which make it difficult to directly compare these studies and to draw a general conclusion on the underlying uptake mechanism. These findings further indicate that a thorough analysis of the interaction between NP-based therapies and human tissue is of paramount importance. One may even consider patient-specific responses to such therapies due to the genetic variability between different individuals. It further implies the importance of human models, rather than extrapolating data from *in vivo* animal studies. Regarding our approach, it is important to note that the impact of global actin cytoskeleton organization rather than actin dynamics or the G/F-actin ratios was addressed, which were expected to be similar for the differently micropatterned cells. Therefore, additional experiments using such inhibitors will be required to cover all aspects of actin-dependent endocytosis and to draw a final conclusion whether this particular uptake mechanism is implicated in placental uptake and translocation of PS NPs. Moreover, studies with other types of NPs are needed for a comprehensive understanding on the role of actin in the endocytic uptake of NPs by BeWo cells.

To conclude, using micropatterned single cells, we were able to exclude a major role of the actin cytoskeleton structure on NP uptake and distribution. However, this model essentially lacks a 3D structure comprising cell-cell interactions, which is

critical for proper cell functionality as well as for uptake and penetration studies. We therefore proceeded with the development of a 3D co-culture MT model in order to more closely mimic the human placental barrier tissue *in vivo*.

A 3D human placental in vitro co-culture microtissue model to study effects, uptake and penetration of different nanoparticles

Since structure and function of the placenta are considerably different among mammalian species (see Chapter 1.1.3), *in vivo* experiments in rodents severely lack relevance for clinical translation, and the use of human placenta models is inevitable to obtain human-relevant data. For NP translocation studies, the human *ex vivo* placenta perfusion is a well characterized and widely used model with a high *in vivo* predictability (Hutson et al. 2011, Grafmueller et al. 2013). Though, it lacks the possibility to study NP uptake mechanisms and toxic effects. In principle, a first estimate of NP impact on placental cell viability could be obtained from simplified 2D cell cultures but to achieve fundamental insights into complex NP-placenta interactions at tissue level a more sophisticated approach is indispensable. With the 3D human *in vitro* co-culture MT model resembling the structure of the *in vivo* placental tissue, we developed a promising tool to qualitatively and quantitatively assess NP toxicity, uptake mechanisms and penetration. When developing an *in vitro* model, the full *in vivo* complexity of an organ cannot be recapitulated (Shamir and Ewald 2014) and the focus needs to be set on the important parameters necessary to achieve the model's purpose. The design of this model was chosen to enable studying different aspects of NP uptake in dependence of particle physico-chemical properties. Specifically, co-culture MTs were generated consisting of a fibroblastic core providing structural support, surrounded by a layer of BeWo cells that are responsible for the specific barrier function of the human placenta. In Part II of this thesis, we demonstrated the generation of highly reproducible co-culture MTs and their applicability to reliably study acute toxicity and adverse effects on placental functionality using different NPs. Yet, effect studies of NPs on the MTs over several weeks would be highly valuable for commercialization of the model or its incorporation into body-on-a-chip devices, among others. To achieve MTs with a stable size, differentiation of BeWo cells into a syncytium may help to overcome the limitations of the current model. In addition to enabling long-term studies, the formation of a syncytium would also reduce the chance that NPs are taken up via

paracellular routes, a pathway that is only rarely present in the *in vivo* placental barrier. Forskolin is widely used to induce syncytium formation in BeWo cells (Wice et al. 1990). However, this process is often very inefficient (10-30 % syncytialization) and only in few cases, syncytialization of around 80 % was achieved (Lin et al. 1999, Das et al. 2004). Moreover, several studies provide evidence that forskolin stimulation did not only induce syncytium formation but also provoked undesirable off-target effects such as extensive externalization of the membrane phospholipid phosphatidylserine (PSe) (reviewed by (Gauster and Huppertz 2008, Riddell et al. 2013). Modulating effects of forskolin on the activity of plasma membrane transporters (i.e. K^+ channels, GLUT1 and MDR1 transporters) may be responsible for the significant externalization of PSe (Riddell et al. 2013). To conclude, as long as the exact effects of forskolin on these transporters are unknown, we cannot exclude that forskolin may interfere with NP uptake pathways and confound the outcome of NP uptake studies. Therefore, the replacement of BeWo cells with human primary CTBs may be of advantage because they spontaneously form a syncytium without the need for forskolin treatment. Moreover, CTBs are promising candidates to improve the *in vivo* predictability of the MT model in terms of NP uptake and penetration as they better reflect the physiological properties of the trophoblast barrier *in vivo*. On the other hand, the isolation of highly pure CTBs is challenging, and they do not proliferate in culture. Secondly, fusion of CTBs into a syncytium does not necessarily result in a continuous monolayer but may rather form islands of fused trophoblasts with large cell-free gaps in between (Hemmings et al. 2001) (Chapter 5.1.2). However, under appropriate culture conditions, it has been shown that a tight CTB barrier can be achieved (Huang et al. 2016). In addition, CTBs are genetically heterogeneous, which better reflects the variability within the population but may introduce difficulties in the generation of consistent results. Therefore, primary CTBs have a lot of potential to improve the MT model and thus it will be important to push the optimization of the seeding and culture conditions for these cells on co-culture MTs and to reveal their impact on the predictive value of the model (see Chapter 5.1.2).

Regarding the MT model from a material's perspective, the detection of NPs within the MTs is currently established for fluorescently labeled or metallic NPs that were visualized or quantified for example by confocal microscopy or ICP-MS, respectively (see Part III and Chapter 5.2.2). In addition, TEM analysis was applied to assess the

subcellular localization of internalized NPs at high resolution but only at a qualitative level due to the large volume of the MTs. To unambiguously identify NPs in the fibroblastic core, TEM should be further combined with Energy-dispersive X-ray Spectroscopy (EDX) analysis. The interior of fibroblasts is very electron-dense with structures that could be easily misinterpreted as small clusters of NPs. In addition to the analytics used in this thesis, several other technologies such as Ion Beam Microscopy (IBM), Enhanced Darkfield Hyperspectral Microscopy (CytoViva, Inc.) or Raman Spectroscopy could alternatively be applied for the assessment of NP uptake into the MTs. In case of drugs or drug-loaded nanocarriers (e.g. micelles, liposomes), detection methods based on High Pressure Liquid Chromatography-Mass Spectrometry (HPLC-MS) could be established to obtain a quantitative readout of particle and/or drug uptake. Finally, with the rapid development of novel, highly sensitive analytics, we anticipate that new possibilities may arise for the detection of different types of NPs within biological tissues. Further promising analytical techniques that could be established to increase the throughput and thus the attractiveness of the placental MTs for industrial applications may include fully automated, multiparametric cell assays (high-content screening) or correlative imaging techniques (e.g. correlative Raman imaging and SEM).

Every model needs to be validated in order to estimate the model's accuracy in making *in vivo* relevant predictions (Eddy et al. 2012). With the placenta, we have the unique opportunity to obtain human placental tissue in sufficient amounts and in a healthy state, which is not the case for most other tissues obtained from small biopsies from or next to a diseased area. For the co-culture MT model, a good correlation of the results obtained from NP uptake and penetration studies with results from other model systems such as the human *ex vivo* placenta perfusion is crucial for its validation. Yet, research on NP-placenta interactions is still in its infancy and only a few studies are available for such comparisons. We selected AuNPs (see Part III) based on available data from *in vivo*, *ex vivo* and *in vitro* placenta studies. Indeed, using the MT model we were able to reproduce the size- and surface-modification dependent interaction of AuNPs that was previously identified in these studies. This first comparison is promising for the establishment of the MT model as a reliable tool to assess the behavior of NPs at the human placental barrier. Nevertheless, additional validation of the MT model is required by studying and comparing the behavior of other NPs or molecules with known bioresponses at the

human placental barrier tissue to fully comprehend the predictive value and limitations of this model for NP uptake, penetration and effect studies.

A detailed knowledge on NP uptake mechanisms is essential for the development of site-specific nanomedical therapies because they determine the intracellular fate of the NPs. There is ample evidence that cellular uptake and distribution within cells or tissues are influenced by the NP physico-chemical properties (Albanese et al. 2012, Zhu et al. 2013), which was also observed in studies on transplacental translocation of different NPs (reviewed by (Muoth et al. 2016)). In Part III, we showed that placental uptake and penetration was successfully reduced for PEGylate AuNPs compared to carboxylate AuNPs with higher uptake and deeper penetration into the placental barrier. This implies that steering NP accumulation and translocation through the placental barrier via their physico-chemical properties and surface functionalization is indeed a valid approach to specifically treat maternal, placental or fetal disorders. Moreover, we demonstrated the applicability of the MT model to investigate mechanistic aspects of AuNP uptake. While AuNP uptake experiments at 4 or 37ºC indicated that predominantly passive mechanisms were involved in their uptake, Pst2 did not sufficiently inhibit clathrin-mediated endocytosis (see Chapter 5.2.1). Therefore, additional chemical inhibitors should be explored in order to reveal the underlying uptake pathways for different types of NPs into the co-culture MTs, which is a prerequisite to identify suitable NPs for DD systems.

In summary, we successfully developed a reproducible and high-throughput compatible 3D *in vitro* co-culture MT model, which delivers predictive results on placental toxicity, uptake mechanism and penetration of NPs. Importantly, subsequent NP exposure studies provided first insights how NP-placenta interactions can be controlled by tailoring particle properties and modifications. With our work, we considerably contributed to reduce the existing knowledge gap and to pave the way for the development of effective and site-specific particle-based therapies in pregnancy.

This challenging and highly interdisciplinary project provides a good example of how the combination of extensive nanomaterial and biology knowhow, cutting edge *in vitro* technologies and sophisticated analytics can contribute to solve clinical needs. With respect to the ethical 3R principles for animal experiments (Replacement, Reduction and Refinement) (Russell et al. 1959), our newly developed placental MT model may help to reduce animal testing and as such save life, time and costs.

These aspects are highly attractive for pharmaceutical companies regarding the implementation of such models into industry.

4.2 Outlook

For obvious ethical reasons, NP-placenta interactions cannot be directly studied in pregnant women. Similarly, ethical concerns for *in vivo* animal studies, especially with non-human primates, are considerably high (Carter 2007). Therefore, the development and use of advanced human placenta *in vitro/ex vivo* models is inevitable for NP toxicity assessments and to progress in the development of safe and effective nanomedical applications during pregnancy. Every model can only represent a specific part of the reality and is designed to answer a certain question. Thus, different models need to be combined in order to obtain a holistic understanding on all aspects of NP-placenta interactions including effects on placental physiology, cytotoxicity, barrier integrity, translocation or uptake mechanisms. Several human placenta models were established which vary in their *in vivo* relevance, throughput capacity and possible readouts (Figure 4.1).

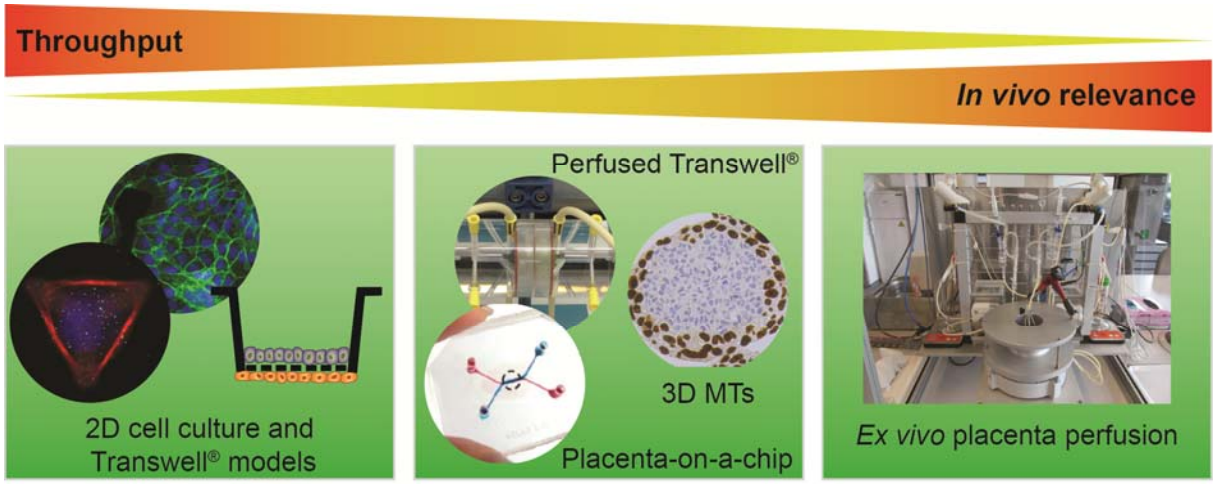

Figure 4.1 Human placenta *in vitro* and *ex vivo* models. 2D cell cultures, the static Transwell® model and the *ex vivo* placenta perfusion are widely used models to study NP toxicity and translocation. To fill the gap between low throughput *ex vivo* and simplified *in vitro* models we are developing novel advanced human placenta *in vitro* models such as the 3D co-culture MTs presented in this work, the perfused co-culture Transwell® or microfluidic placenta-on-a-chip models to study NP-placenta interactions with an improved *in vivo* relevance as compared to conventional 2D cell cultures. Placenta-on-a-chip figure taken from Lee et al. (Lee et al. 2015).

The gold standard *ex vivo* placenta perfusion model has a high *in vivo* predictability and is extensively used for translocation studies (up to 6 h). The 3D MT model is most suitable for NP toxicity assessments and mechanistic uptake/penetration

studies at tissue level, while the Transwell® model enables prolonged and more mechanistic translocation studies (up to 24 h) of various substances including chemicals or NPs (Li et al. 2013, Carreira et al. 2015). For a fast pre-screening on the toxicity of a large variety of NPs, 2D trophoblast cultures may help to identify the most relevant NPs that should be further validated in more complex *in vitro/ex vivo* placenta models. Collectively, these models can provide answers to a wide range of different questions regarding NP-placenta interactions. However, we still see ample opportunities to further increase the physiological relevance of the newly developed 3D MTs and to expand their applicability to assess NP interactions with healthy and diseased placental tissue (Figure 4.3).

As shown in Chapter 5.1.2, we successfully isolated and purified primary CTBs and started to optimize seeding and culture conditions to establish a CTB coating on the MTs with the aim to replace the BeWo cells. So far, CTBs were only isolated from healthy donors but generating MTs with CTBs from diseased placentas (e.g. preeclampsia) may offer the opportunity to study the effectiveness of nanomedical therapies for specific placental diseases (Keelan et al. 2015). Besides CTBs, additional cell types such as macrophages (Hofbauer cells) or endothelial cells could be added to the fibroblastic core in order to better recapitulate the composition and function of the fetal stroma *in vivo*. To simulate the highly dynamic microenvironment of the human placenta (maternal and fetal circulation) multiple MTs could be connected through microfluidic channels on tilting plates (Figure 4.2) (Kim et al. 2015) or incorporated into an organ-on-a-chip device (Skardal et al. 2016). A perfused microenvironment may help to more accurately mimic the NP exposure scenario *in vivo*. Under static conditions, there is no fluid flow and due to gravitational forces, NPs start to sediment on top of the cells resulting in an increased particle number delivered per cell (Cho et al. 2011). Inclusion of a dynamic flow, however, may reduce NP sedimentation resulting in a lower NP internalization rate and NP fraction associated with the cell or MT surface as compared to a static system (Breitner et al. 2015). In addition to a dynamic system, a more realistic exposure scenario could further be achieved by mimicking a physiologically relevant NP bio-corona, for example by pre-incubation of NPs with human blood serum. Previously, it was reported that the formation and composition of such a corona highly influences NP-cell interactions (Nel et al. 2009). Understanding if and how the bio-corona of

NPs affect uptake, accumulation, penetration and biological effects will be essential to obtain *in vivo* relevant data.

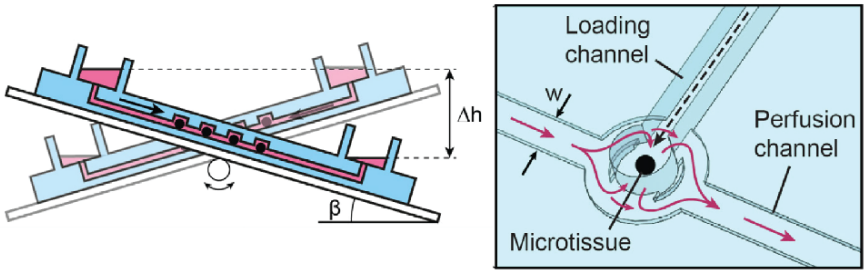

Figure 4.2. Scheme of interconnected MTs on a tilting plate. Figure taken from Kim et al. (Kim et al. 2015).

Moreover, MTs representing different organs could be linked via flow channels in a multi-organ-chip in order to better simulate whole body responses. A possibility would be, for example, to connect a human lung Transwell® model (Tenenbaum-Katan et al. 2015) with placental MTs in order to assess placental effects that arise directly from NPs that crossed the lung barrier or indirectly from signaling molecules released by the exposed lung cells. Such indirect effects have already been described for cobalt-chromium NPs, which induced DNA damage in fibroblasts across an intact BeWo cell barrier via the release of ATP (Bhabra et al. 2009).

In order to better understand NP effects on MT viability and functionality, the establishment of further assays should be considered for future studies. One of the most frequently reported toxicities associated with NPs is the generation of reactive oxygen species (ROS) (Manke et al. 2013). This so called oxidative stress paradigm suggests that NP uptake causes an imbalance of oxidants to antioxidants resulting in the production of ROS and subsequent oxidative stress. As a consequence, cytosolic calcium (Ca^{2+}) is increased, which was shown to induce the production of proinflammatory cytokines associated with the activation of specific transcription pathways (Clift and Rothen-Rutishauser 2013). To study oxidative stress in 3D MTs following NP exposure, the use of a high-throughput compatible ROS assay (e.g. ROS-Glo™ H_2O_2 Assay, Promega) is recommended. Regarding the visual detection of apoptotic cells in the MTs, immunohistochemical analysis using for example a caspase-3/-7 or TUNEL staining could be established. However, it is controversially discussed whether the TUNEL assay reliably discriminates between different forms

of cell death (Kraupp et al. 1995, Kyrylkova et al. 2012) and it is thus recommended to use a combination of different antibodies to avoid misleading results (Bressenot et al. 2009). Since indirect and direct effects of NPs may further lead to DNA damage, a fluorescent staining of tissue sections with anti-γH2AX may be established as a potential readout for the detection of DNA damage in 3D MTs (Igaz et al. 2016). Finally, another promising approach is the use of omics technologies to assess changes in proteins, genome or metabolites, which may help to identify novel biomarkers or adverse outcome pathways (AOPs).

In the field of nanomedicine, placental co-culture MTs offer a promising model to develop novel targeting strategies at the placental barrier. For example, MTs could be applied to investigate penetration of NP formulations that were designed to treat maternal diseases. Since for such treatments, only low NP uptake is expected by the MTs, highly sensitive analytics are required for their detection (examples of analytical methods are listed in Chapter 4.1). Additional approaches to treat pregnant women may also include NPs carrying antibiotics to target specific bacteria or NPs conjugated with anti-depressant/anti-epileptic agents that cross the blood-brain barrier while avoiding the placenta. In particular for the latter, advanced *in vitro* Transwell® models could be considered to investigate translocation of these NP formulations through both, the placental and the maternal blood-brain barrier. Moreover, MTs could be used to identify NP formulations for the treatment of placental diseases. For this purpose, it is important to elucidate NP uptake routes because they determine the intracellular fate and thus the ability of NPs to target intracellular structures in trophoblast cells (e.g. nuclei). Identification of the underlying uptake mechanisms could be achieved using different uptake inhibitors (for an extensive review on uptake inhibitors see (von Kleist et al. 2011)) and performing co-localization studies of NPs with different intracellular compartments (e.g. vesicles, cytoplasm, endoplasmic reticulum). Regarding the development of NP formulations that are intended to cross the placental barrier, MTs could be used to assess NP penetration through the trophoblast layer into the fibroblastic core. For example, drug-loaded NPs (e.g. liposomes, mesoporous silica NPs) could be conjugated to amino acids, from which it is known that they are transferred through the placenta via specific amino acid transporters (see Chapter 1.1.2). Specifically, NPs could be functionalized with peptides that are able to cross epithelial barriers and avoid

macrophage recognition resulting in a high transplacental translocation rate (Figure 4.3) (Komin et al. 2016).

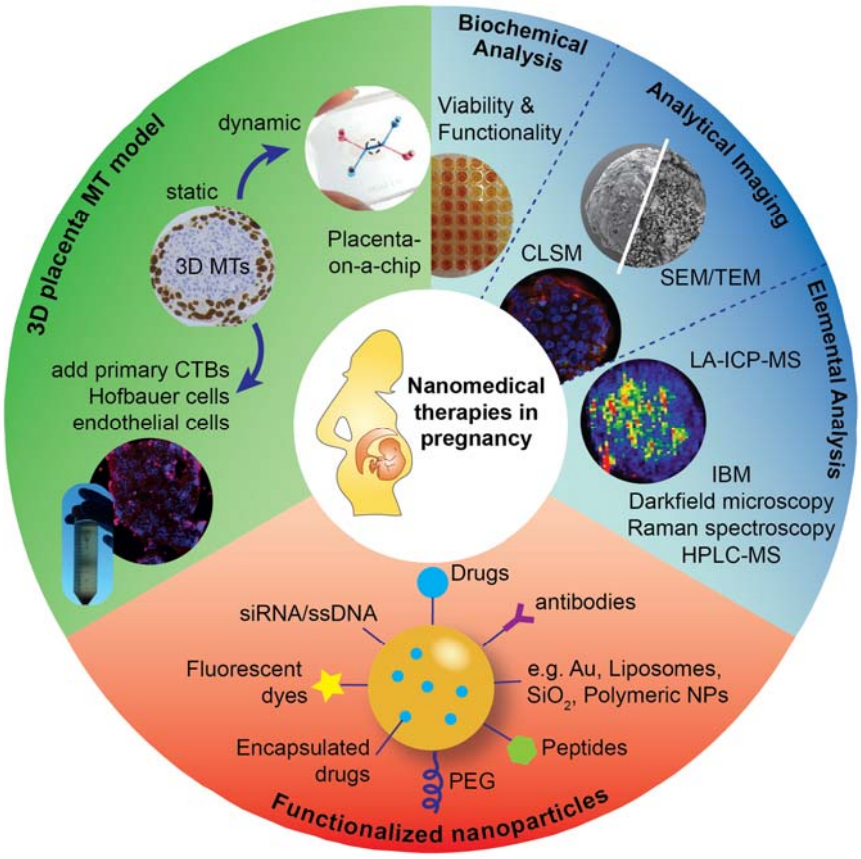

Figure 4.3. Placental MTs, sophisticated analytics and customizable NP designs significantly contribute to the development of nanomedical therapies in pregnancy. Abbreviations: Au, gold; CLSM, confocal laser scanning microscopy; CTB, cytotrophoblast; HPLC-MS, high pressure liquid chromatography-mass spectrometry; IBM, ion beam microscopy, LA-ICP-MS, laser ablation inductively coupled plasma mass spectrometry; MT, microtissue; PEG, polyethylene glycol; SEM, scanning electron microscope; siRNA, small interfering ribonucleic acid; ssDNA, single-stranded deoxyribonucleic acid; TEM, transmission electron microscope. Placenta-on-a-chip figure taken from Lee at al. (Lee et al. 2015).

Appendix

Attachment to Results
Acknowledgement
Curriculum Vitae
Bibliography

5.1 Attachment to Results Part II

5.1.1 FACS analysis of co-culture MTs after exposure to CuO NPs

To assess the impact of NPs on placental functionality, subtoxic concentrations should be assessed in order to avoid that observed effects are secondary due to cell death. In particular for functionality assays that only consider one cell type (e.g. hCG ELISA where only BeWo cells secrete hCG), subtoxic doses for this cell type are needed. To determine subtoxic concentrations of CuO NPs on each individual cell type of the co-culture MTs, flow cytometry was established to quantify the amount of viable and dead HVMFs and BeWo cells. This was required since the ATP assay only addresses the overall cell viability from the whole MT. As there are no specific surface markers available for BeWo cells or HVMF that could be used to distinguish the two cell types, fluorescent dyes were used to pre-label live cells.

In a first approach, co-culture MTs were generated using unstained HVMFs and BeWo cells that were pre-labeled with the lipophilic membrane dye DiI (Molecular Probes, Switzerland). However, this strategy was not effective since the dye was partially transferred to unstained HVMFs resulting in a weak DiI staining of HVMFs probably due to close cell-cell contacts in the co-culture MTs (data not shown).

As an alternative approach, CellTracker™ green (Life Technologies, Switzerland) was chosen to stain HVMFs because this dye transforms into a cell-impermeant fluorescent product once it is inside the cells, leaving BeWo cells unstained. Dissociation of control MTs was achieved by collagenase treatment with > 90 % viable cells (data not shown). The gates for CellTracker™ green were set with the stained and unstained HVMF control from 2D cell cultures (Figure 5.1A). FACS analysis of co-culture MTs showed a dominating peak for CellTracker™ green positive cells (Figure 5.1B) and a total amount of approximately 20 % unstained cells, which is a realistic number of BeWo cells due to their proliferative capacity (see Results Part II). In Figure 5.2C, CellTracker™ green analysis of dissociated co-culture MTs after the exposure to 6 µg/ml CuO NPs for 24 h revealed three distinct peaks. It was assumed that the first and the third peak account for cells that were negative or positive for CellTracker™ green, respectively. The middle peak may be explained by HVMFs with an impaired plasma membrane that partially lost CellTracker™ green dye. However, it was difficult to estimate in how far BeWo cells received this dye and also became positive for CellTracker™ green. In addition, there

was an increased fraction of unstained cells as compared to the control, which may be due to HVMFs that were not labelled, where the dye leached out. To conclude, the artifacts that are introduced when performing FACS analysis of unspecific dye-labeled cells in the presence of toxic NPs do not allow to unambiguously determining the percentage of dead cells for the individual cell types.

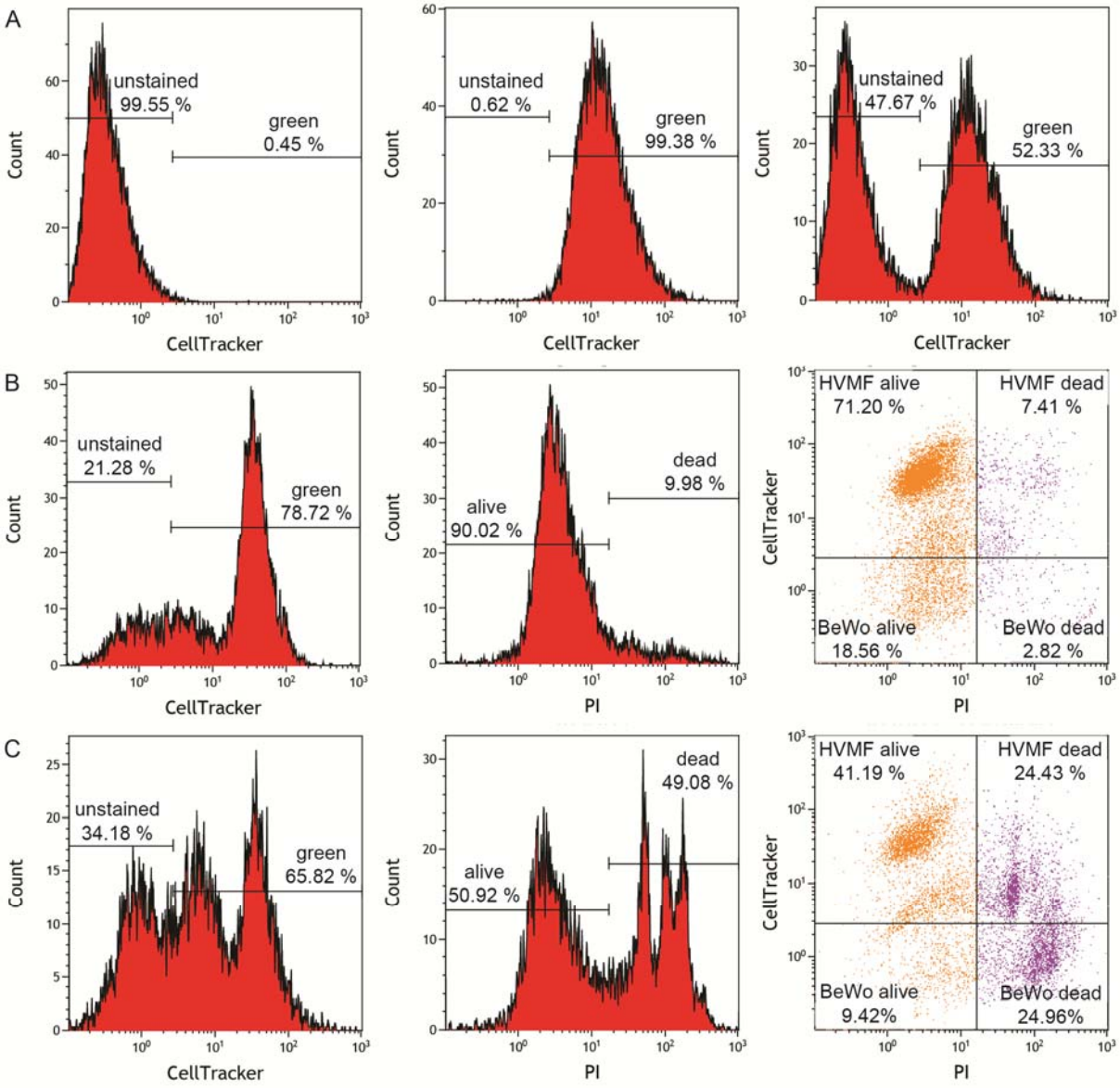

Figure 5.1. FACS analysis of co-culture MTs. Unstained and CellTracker™ green labeled HVMFs from 2D cell cultures were used to set the gates for CellTracker™ green analysis **(A)**. Prior to co-culture MT formation, HVMFs were labeled with CellTracker™ green and BeWo cells remained unstained. MTs were either maintained in FGM **(B)** or exposed to 6 µg/ml CuO NPs **(C)** for 24 h. Approximately 20 MTs were dissociated with 0.25 mg/ml collagenase, stained with PI and immediately analyzed by flow cytometry.

5.1.2 Isolation of primary trophoblasts and their use for co-culture MTs

In order to improve the *in vivo* relevance and predictability of 3D co-culture MTs for NP effects, uptake and penetration, primary villous cytotrophoblasts (CTBs) were obtained from fresh human term placentas to replace the BeWo cell line. Briefly, CTBs were successfully isolated by triple enzymatic digestion of several cotyledons followed by Percoll-gradient separation and immunomagnetic bead purification (Figure 5.2) (modified protocol according to Petroff et al. (Petroff et al. 2006).

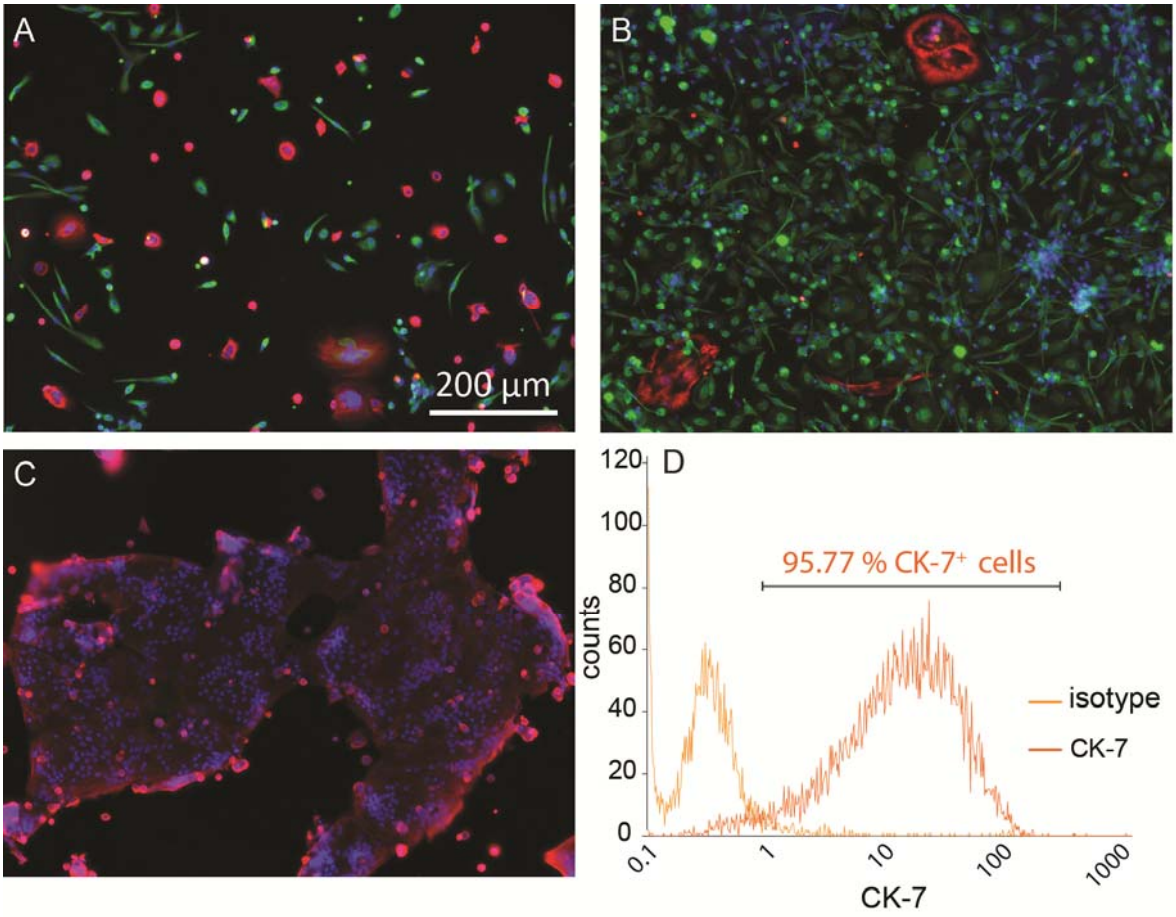

Figure 5.2. Epifluorescence images of isolated CTBs before **(A)** and after **(C)** immunomagnetic beads **(B)** (negative selection for HLA class I antigen). CTBs were stained for the trophoblast marker cytokeratin-7 (CK-7, red), fibroblast marker vimentin (green) and Dapi (blue) to visualize nuclei. FACS analysis of CTBs after immunomagnetic bead purification was 95.77 % positive for CK-7 cells **(D)**.

To obtain a tight and continuous monolayer of CTBs around the fibroblastic core MTs, we tried to optimize seeding and culture conditions of co-culture MT formation. Prior to every experiment, CTBs were thawed and cell seeding numbers (600, 2000 or 4000 CTBs), medium compositions (FGM, DMEM), cultivation times (2-10 days), addition of endothelial growth factor (EGF) fetal calf serum (FCS) concentration (0, 1,

5, 10 or 20 %) were varied. As shown in the examples of Figure 5.3A-D, only few CTBs remained viable and they did not properly attach and spread on the surface of the fibroblastic core MTs. Therefore, different techniques were applied after thawing in order to increase the amount of viable CTBs before they were added to the MTs. As such, CTBs were pre-seeded on rat collagen coated tissue culture dishes overnight. Only few remaining single CTBs were able to attach to the MTs while most cells were already differentiated into a syncytium (Figure 5.3E). Therefore, pre-seeding was performed on human collagen coated thermoresponsive plates, on which cells sufficiently adhered within 4 h and no enzymatic treatment was required for cell detachment. With this approach, we succeeded in obtaining improved cultures with a high number of viable cells. However, attachment and spreading of CTBs on the co-culture MTs was still weak and they did not form a tight monolayer around the MTs (Figure 5.3F). In order to improve cell-cell interactions of CTBs with the fibroblastic core, CTBs were alternately coated with type IV-collagen and laminin (protocol according to (Curtis et al. 2014)) but most CTBs were lost during the washing steps that were required for this coating (data not shown).

To conclude, we were not yet successful in generating stable co-culture MTs using CTBs instead of BeWo cells, and seeding and culture conditions still require further optimization in order to achieve the formation of a tight CTB monolayer around the fibroblastic core MTs.

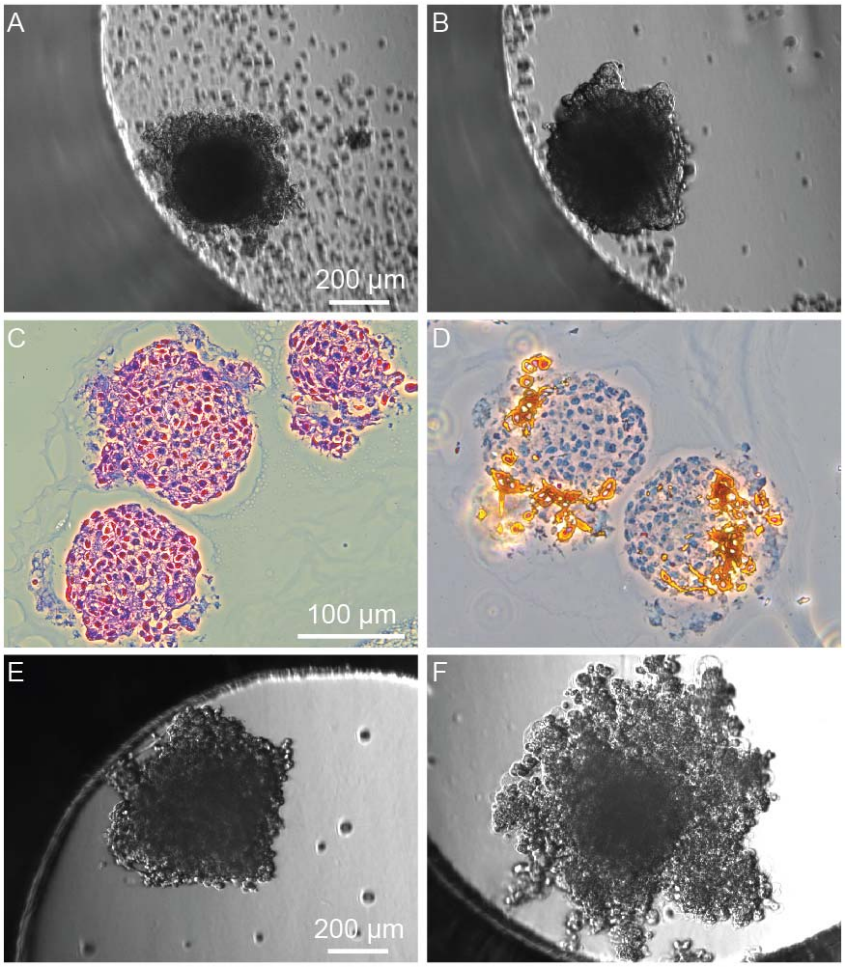

Figure 5.3. Examples of CTBs cultured on fibroblastic core MTs. 2000 CTBs were added to the MTs and cultivated in FGM containing 20 % FCS either in the absence **(A)** or presence of 10 ng/ml EGF **(B)**. Corresponding paraffin sections of **B** are shown in **C** (HE) and **D** (cytokeratin stained MTs). Furthermore, CTBs were pre-seeded on rat collagen coated tissue culture plastic overnight, detached and added to the fibroblastic MTs (4000 CTBs/MT) in FGM containing 20 % FCS and 10 ng/ml EGF **(E)**. In **F**, CTBs were seeded onto thermoresponsive plates for 4.5 h, detached and added to the fibroblastic MTs (600 CTBs/MT) in FGM containing 1 % FCS and 10 ng/ml EGF.

5.2 Attachment to Results Part III

5.2.1 Pitstop 2: an inhibitor of clathrin-mediated endocytosis

In addition to uptake experiments shown in Results Part III, Pitstop 2 (Pst2; Abcam) was chosen as a highly selective chemical inhibitor of clathrin-mediated endocytosis (CME) (von Kleist et al. 2011) in order to elucidate the role of CME in the internalization of AuNPs by the co-culture MTs. First, Pst2 was established on 2D BeWo cell cultures using transferrin conjugated to Alexa Fluor 488 (Tf_{488}; Molecular Probes) as a reference molecule, which is internalized via receptor-mediated endocytosis by mammalian cells (Harding et al. 1983). Inhibition of CME was

qualitatively assessed using confocal microscopy. Uptake of Tf_{488} by BeWo cells was assumed to be maximal in the absence of Pst2 (Figure 5.4B). Uptake of Tf_{488} by BeWo cells was successfully inhibited with increasing concentrations of Pst2. While only small inhibition was observed for 10 µM Pst2 (Figure 5.4C), 20 µM Pst2 blocked more than 80 % of the uptake (Figure 5.4D), and 30 µM Pst2 completely inhibited Tf_{488} uptake by BeWo cells (Figure 5.4E). Nevertheless, it should be noted that even in the absence of cytotoxic effects of Pst2 (von Kleist et al. 2011), incubation with 30 µM Pst2 slightly changed BeWo cell morphology (Figure 5.4E).

Based on the Pst2 results obtained from 2D BeWo cell culture experiments described above, 3D co-culture MTs were pre-incubated with 20 µM Pst2 for 10 min followed by the addition of Tf_{488}. However, no inhibition of Tf_{488} uptake was observed by CLSM analysis (Figure 5.5C). Consequently, pre-incubation time and Pst2 concentrations were increased to 30 min and to 30 µM (Figure 5.5D) and to 50 µM Pst2 (Figure 5.5E), respectively. Since neither of these concentrations resulted in a significant decrease of Tf_{488} uptake into the co-culture MTs as compared to the positive control (Figure 5.5B), this inhibitor was not used for further experiments. Nevertheless, there are other CME inhibitors such as chlorpromazine (von Kleist and Haucke 2012), or Dynasore that could be used to inhibit dynamin-dependent uptake pathways (Macia et al. 2006).

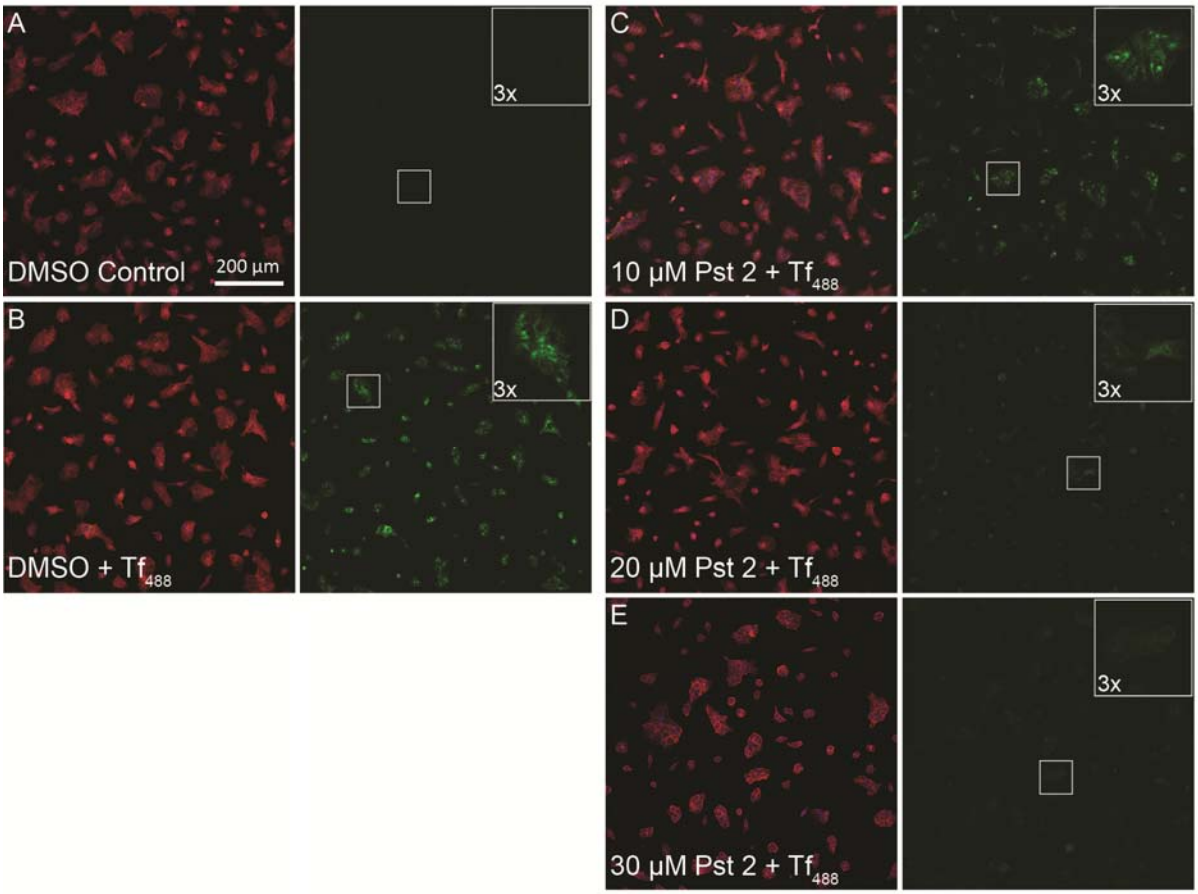

Figure 5.4. Establishment of Pst2 in 2D BeWo cell cultures. Prior to the addition of 25 µg/ml Tf_{488} (green) for 30 min, BeWo cells were pre-incubated with FGM containing 10 mM HEPES and 0.5 % DMSO **(B)** or supplemented with 10 **(C)**, 20 **(D)** or 30 µM Pst2 **(E)** for 10 min at 37°C. The 0.5 % DMSO control **(A)** was not exposed to Tf_{488} and used as the negative control. After exposure experiments, samples were fixed, stained with Alexa Fluor Phalloidin 546 (red) and Dapi (blue), and images were acquired with a CLSM.

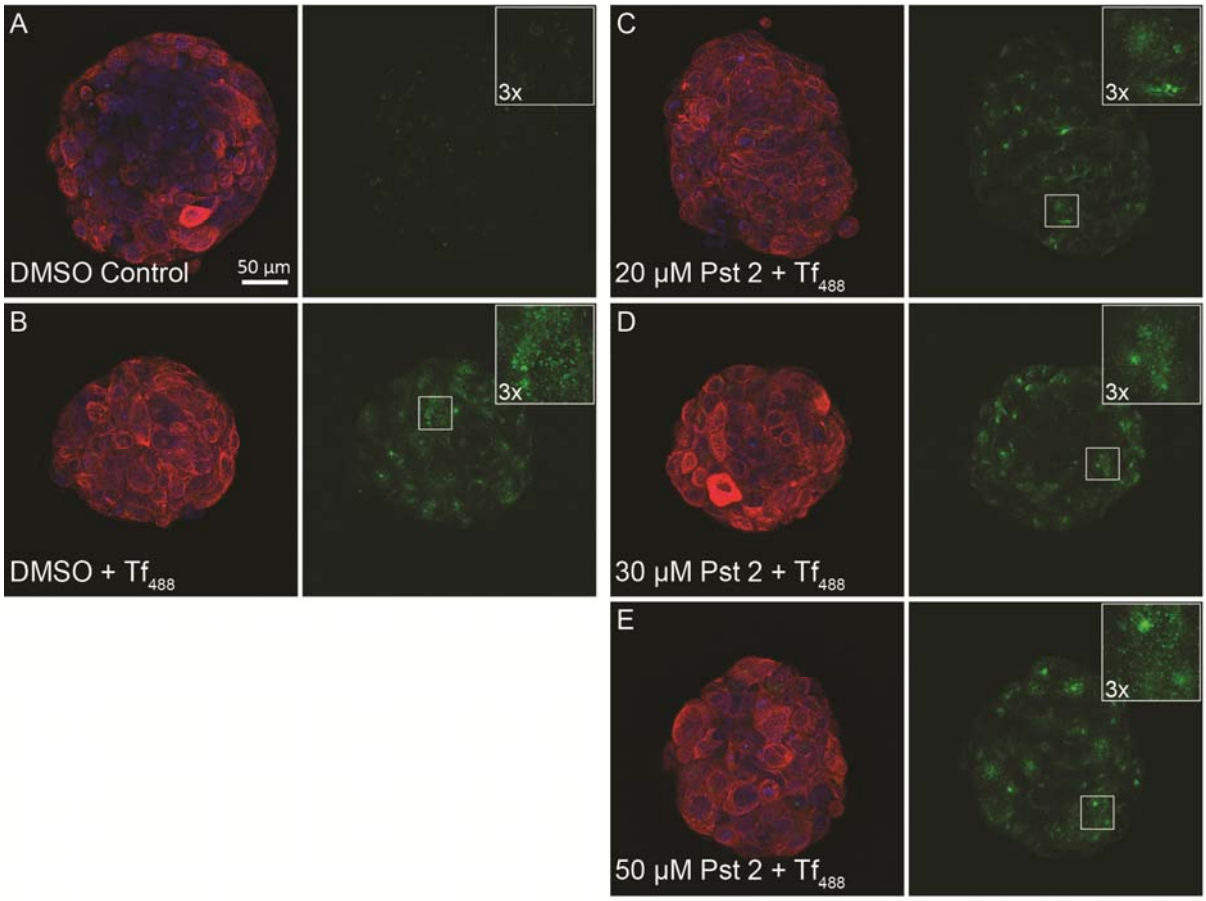

Figure 5.5. Establishment of Pst2 in 3D co-culture MTs. Prior to the addition of 25 µg/ml Tf_{488} (green) for 30 min, co-culture MTs were pre-incubated with FGM containing 10 mM HEPES and 0.5 % DMSO **(B)** or supplemented with 20 **(C)**, 30 (**D**) or 50 µM Pst2 **(E)** for 30 min (10 min for 20 µM Pst2) at 37°C. The 0.5 % DMSO control **(A)** was not exposed to Tf_{488} and used as the negative control. After exposure experiments, samples were fixed and stained with cytokeratin to specifically stain BeWo cells (red) and Dapi (blue) to visualized nuclei. 40 stacks per MT were acquired with a CLSM at 40 x magnification.

5.2.2 Uptake analysis of fluorescent PS NPs into co-culture MTs

Additional uptake studies with co-culture MTs were performed for fluorescently labeled polystyrene (PS) NPs and internalization was analyzed by confocal microscopy. PS NPs of different sizes were chosen in order to compare our results with the study of Wick et al. where they investigated PS NP translocation using the human *ex vivo* placenta perfusion model (Wick et al. 2010).

Uptake and distribution of fluorescent 87 nm or 240 nm PS NPs into co-culture MTs were either assessed on whole mount MT stainings (data not shown) or on paraffin sections. Confocal micrographs confirmed uptake into co-culture MTs for both, 87 nm and 240 nm PS NPs (Figure 5.6A and B). Furthermore, quantitative uptake analysis

using “Particle_in_Cell-3D” for ImageJ (see Part I) indicated a size dependent uptake into the MTs with a higher internalized amount of 87 nm than of 240 nm PS NPs (Figure 5.6C). These preliminary results are in good agreement with the study of Wick et al. where transplacental translocation was significantly higher for 87 nm PS NPs than for 240 nm PS beads (Wick et al. 2010). However, in order to confirm the reproducibility of our findings, PS NP uptake studies need to be repeated.

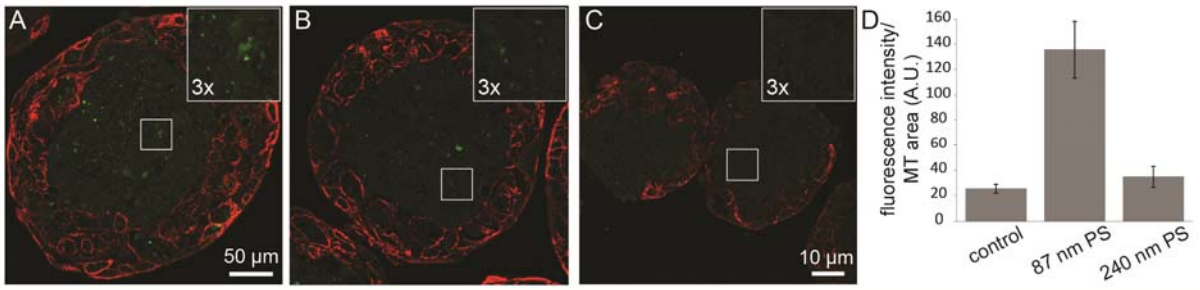

Figure 5.6. Uptake analysis of PS NPs into co-culture MTs. Representative paraffin sections of MTs stained for cytokeratin (red) and exposed to 50 µg/ml of 87 nm PS NPs (green) **(A)** or 240 nm PS NPs **(B)** for 24 h. MTs that were not exposed to PS NPs were used as the negative control **(C)**. Uptake was quantitatively assessed based on paraffin sections using the macro “Particle_in_Cell-3D” for ImageJ (control: n = 3 MTs, 87 nm PS NPs: n = 8 MTs, 240 nm PS NPs: n = 6 MTs).

5.3 Acknowledgement

First of all, I would like to express my gratitude to my mentor and group leader Dr. Tina Buerki for introducing me into the exciting field of nanoparticle-biology interactions and especially for her open mind and patience during the last years. Without her encouraging words, continuous guidance and support, this work would not have been accomplished.

I am grateful to Dr. Peter Wick for giving me the opportunity to join his lab, for his support and for his great trust in me and my work. He was always challenging me with critical questions and discussions from which I have learned a lot.
I would like to thank to all professors of my thesis committee: Prof. Dr. Hanspeter Nägeli, Prof. Dr. Michael Arand and Prof. Dr. Jörg Huwyler for their help and valuable advices during my work.

I am very thankful to Margreth Hell and her team from the Kantonsspital St. Gallen. I was always very impressed about their excellent work that substantially contributed to the quality of my thesis.

Many thanks go to all current and former members of the Particles-Biology Interactions Laboratory for their scientific, technical and in particular for their personal support – anytime and everywhere. They made my time at Empa to a great pleasure. Special thanks go to my friends and colleagues

… Stefanie, Vera, Brigitte, Magda and Annabé, for always listening to me, cheering me up, helping me with scientific and writing problems and for all the nice moments we spent besides work.

… Arie and Sarah, my wonderful office mates and friends, I will miss our nice time we had together in the office, our creative discussions, sharing hard times but mostly, I enjoyed laughing together.

… Leonie, Cordu, Nils, Melanie and Alexandra, for giving valuable scientific inputs, for proofreading but most of all, for having fun times in the lab, during our coffee breaks, with skiing in Arosa, drinking prosecco or with dancing in the deepest mud of the Open Air St. Gallen.

… Géraldine, for critically proofreading my thesis, for being my flat mate, building awesome castles in the air and for sharing a beer on the balcony after climbing.

… Liliane, Pius, Yvonne and Ursina for their endless support with technical questions, valuable help in the lab but also for their encouragement and open ear during the last years.

… Adrian, for his tremendous effort in analyzing all my samples with ICP-MS during the last few months.

… Markus for introducing me into the microcontact printing technique and for sharing his expertise in confocal microscopy with me.

…Matthias, for his statistical support and his help with all computer problems.

Finally, I would like to thank my parents and Thomas. Without their support and love, I would not be where I am today.

5.4 Curriculum Vitae

Name	Carina Muoth
Address	Riedgasse 3 CH-7205 Zizers
Phone	+41 79 685 38 89
E-mail	c.muoth@gmail.com

Personal Data

Date of birth:	17.07.1988
Place of birth:	Grabs SG, Switzerland
Marital status:	Single
Citizenship:	Swiss

Education

2013 – (Aug 2016)	Swiss Federal Laboratories for Materials Science and Technology (Empa) St. Gallen Life Science Zurich Graduate School **PhD thesis** *Steering Nanoparticle-Placenta Interactions: Impact of Particle Properties and Functionalization on Placental Uptake, Penetration and Biological Effects*
2010 - 2012	Swiss Federal Institute of Technology (ETH), Zurich Department of Health Sciences and Technology **Master** in Human Movement Sciences and Sport Major in Biomechanics Master thesis at Empa St.Gallen *Uptake of nanoparticles by shape-normalized adherent cells*
2007 - 2010	Swiss Federal Institute of Technology (ETH), Zurich Department of Biology **Bachelor** in Human Movement Sciences and Sport
2003 - 2007	**Matura** on Biology and Chemistry Kantonsschule Sargans

Practical Experience

Sept 10 - Feb 11	Master internship at Schulthess Klinik Zurich Research and development of the upper extremities Measurement, analysis and documentation of the finger strength and quality of life of patients with different hand disorders

Publications

C. Muoth, M. Großgarten, U. Karst, J. Ruiz Aranzaes, D. Astruc, S. Moya, L. Diener, K. Grieder, A. Wichser, W. Jochum, P. Wick and T. Buerki-Thurnherr (2016). *Impact of particle size and surface modification on the localization and penetration of gold nanoparticles in human placental co-culture microtissues.* In preparation to be submitted to Nanomedicine (Future Medicine).

C. Muoth, A. Wichser, M. Monopoli, M. Correia, N. Ehrlich, K. Loeschner, A. Gallud, M. Kucki, L. Diener, W. Jochum, P. Wick and T. Buerki-Thurnherr (2016). *A 3D co-culture microtissue model of the human placenta for nanotoxicity assessment.* Nanoscale, 8(39): 17322-17332.

C. Muoth, M. Rottmar, A. Schipanski, C. Gmuender, K. Maniura-Weber, P. Wick and T. Buerki-Thurnherr (2016). *A micropatterning approach to study the influence of actin cytoskeletal organization on polystyrene nanoparticle uptake by BeWo cells.* RSC Advances, 6(76): 72827-72835.

C. Muoth, L. Aengenheister, M. Kucki, P. Wick and T. Buerki-Thurnherr (2016). *Nanoparticle transport across the placental barrier: pushing the field forward!* Nanomedicine (Lond), 11(8): 941-957.

M. Marks, C. Muoth, J. Goldhahn, A. Liebmann, I. Schreib, S. F. Schindele, B. R. Simmen and T. P. Vliet Vlieland (2012). *Packaging-a problem for patients with hand disorders? A cross-sectional study on the forces applied to packaging tear tabs.* J Hand Ther, 25(4): 387-395; quiz 396.

Scientific Conferences

2016	3D Cell Culture (DECHEMA), Germany Talk *A 3D human co-culture microtissue model for nanoparticle effect and uptake studies at the placental barrier* Carina Muoth, Liliane Diener, Jochum Wolfram, Peter Wick, Tina Buerki-Thurnherr
2015	PhD Symposium Empa, Switzerland Postersession *A 3D human co-culture microtissue model for nanoparticle effect and uptake studies at the placental barrier* Carina Muoth, Wolfram Jochum, Melanie Kucki, Liliane Diener, Peter Wick, Tina Buerki-Thurnherr
2015	5th Zing Bionanomaterials Conference, Portugal Postersession *Development and use of a 3D placental co-culture microtissue model for nanoparticle effects and uptake studies* Carina Muoth, Tina Buerki-Thurnherr, Liliane Diener, Peter Wick

2014 Swiss Aerosol Meeting, Switzerland
Talk
Advanced 3D in vitro tissue model to study nanoparticle effects and uptake mechanisms at the placental barrier
Carina Muoth, Tina Buerki-Thurnherr, Liliane Diener, Peter Wick

2014 PhD Symposium Empa, Switzerland
Postersession
Studying nanoparticle behavior and uptake at the human placental barrier in a newly developed 3d in vitro co-culture model
Carina Muoth, Tina Buerki-Thurnherr, Liliane Diener, Peter Wick

2014 Nanosafety Forum for Young Scientists, Sicily
Talk
Studying nanoparticle behavior and uptake at the human placental barrier in a newly developed 3D placental in vitro co-culture model
Carina Muoth, Tina Buerki-Thurnherr, Liliane Diener, Peter Wick

2014 Nanotox 2014 ACS Nano, Turkey
Talk
Does the cell architecture influence engineered nanomaterial uptake? – an experimental approach
Carina Muoth, Angela Schipanski, Tina Buerki-Thurnherr, Markus Rottmar, Peter Wick, Katharina Maniura

Postersession
Advanced placental in vitro co-culture models to study nanoparticle uptake mechanisms, translocation and placental effects
Carina Muoth, Tina Buerki-Thurnherr, Liliane Diener, Peter Wick

2013 PhD Symposium Empa, Switzerland
Talk
Advanced in vitro placental models to study nanoparticle effects and uptake mechanism
Carina Muoth, Helene Annaheim, Tina Bürki, Katharina Maniura, Peter Wick

Awards

2014 Nanosafety Forum for Young Scientists, Sicily
Best Talk Award
Studying nanoparticle behavior and uptake at the human placental barrier in a newly developed 3D placental in vitro co-culture model
Carina Muoth, Tina Buerki-Thurnherr, Liliane Diener, Peter Wick

2014	Nanotox 2014 ACS Nano, Turkey 2nd Best Talk Award *Does the cell architecture influence engineered nanomaterial uptake? – an experimental approach* Carina Muoth, Angela Schipanski, Tina Buerki-Thurnherr, Markus Rottmar, Peter Wick, Katharina Maniura

5.5 Bibliography

Abu-Absi, S. F., J. R. Friend, L. K. Hansen and W. S. Hu (2002). *Structural polarity and functional bile canaliculi in rat hepatocyte spheroids.* Exp Cell Res, 274(1): 56-67.

Adamcakova-Dodd, A., M. M. Monick, L. S. Powers, K. N. Gibson-Corley and P. S. Thorne (2015). *Effects of prenatal inhalation exposure to copper nanoparticles on murine dams and offspring.* Particle and Fibre Toxicology, 12(1).

Al-Nasiry, S., B. Spitz, M. Hanssens, C. Luyten and R. Pijnenborg (2006). *Differential effects of inducers of syncytialization and apoptosis on BeWo and JEG-3 choriocarcinoma cells.* Hum Reprod, 21(1): 193-201.

Albanese, A., P. S. Tang and W. C. Chan (2012). *The effect of nanoparticle size, shape, and surface chemistry on biological systems.* Annu Rev Biomed Eng, 14: 1-16.

Albekairi, N. A., S. Al-Enazy, S. Ali and E. Rytting (2015). *Transport of digoxin-loaded polymeric nanoparticles across BeWo cells, an in vitro model of human placental trophoblast.* Ther Deliv, 6(12): 1325-1334.

Ali, H., I. Kalashnikova, M. A. White, M. Sherman and E. Rytting (2013). *Preparation, characterization, and transport of dexamethasone-loaded polymeric nanoparticles across a human placental in vitro model.* Int J Pharm, 454(1): 149-157.

Aplin, J. D. and S. J. Kimber (2004). *Trophoblast-uterine interactions at implantation.* Reprod Biol Endocrinol, 2(48): 48.

Baker, B. M. and C. S. Chen (2012). *Deconstructing the third dimension: how 3D culture microenvironments alter cellular cues.* J Cell Sci, 125(Pt 13): 3015-3024.

Beauchamp, P., W. Moritz, J. M. Kelm, N. D. Ullrich, I. Agarkova, et al. (2015). *Development and Characterization of a Scaffold-Free 3D Spheroid Model of Induced Pluripotent Stem Cell-Derived Human Cardiomyocytes.* Tissue Eng Part C Methods, 21(8): 852-861.

Becker, J. S., A. Matusch and B. Wu (2014). *Bioimaging mass spectrometry of trace elements - recent advance and applications of LA-ICP-MS: A review.* Analytica Chimica Acta, 835: 1-18.

Benirschke, K. and S. G. Driscoll (1967). *The pathology of the human placenta*, Springer.

Benya, P. D. and J. D. Shaffer (1982). *Dedifferentiated chondrocytes reexpress the differentiated collagen phenotype when cultured in agarose gels.* Cell, 30(1): 215-224.

Bhabra, G., A. Sood, B. Fisher, L. Cartwright, M. Saunders, et al. (2009). *Nanoparticles can cause DNA damage across a cellular barrier.* Nature nanotechnology, 4(12): 876-883.

Bissonnette, J. M. (1982). *Review article: membrane vesicles from trophoblast cells as models for placental exchange studies.* Placenta, 3(1): 99-106.

Blum, J. L., J. Q. Xiong, C. Hoffman and J. T. Zelikoff (2012). *Cadmium Associated With Inhaled Cadmium Oxide Nanoparticles Impacts Fetal and Neonatal Development and Growth.* Toxicological Sciences, 126(2): 478-486.

Bode, C. J., H. Jin, E. Rytting, P. S. Silverstein, A. M. Young, et al. (2006). *In vitro models for studying trophoblast transcellular transport.* Methods Mol Med, 122: 225-239.

Bohme, S., H. J. Stark, T. Meissner, A. Springer, T. Reemtsma, et al. (2014). *Quantification of Al2O3 nanoparticles in human cell lines applying inductively coupled plasma mass spectrometry (neb-ICP-MS, LA-ICP-MS) and flow cytometry-based methods.* Journal of Nanoparticle Research, 16(9): 1-15.

Breitner, E. K., S. M. Hussain and K. K. Comfort (2015). *The role of biological fluid and dynamic flow in the behavior and cellular interactions of gold nanoparticles.* J Nanobiotechnology, 13: 56.

Breslin, S. and L. O'Driscoll (2013). *Three-dimensional cell culture: the missing link in drug discovery.* Drug Discov Today, 18(5-6): 240-249.

Bressenot, A., S. Marchal, L. Bezdetnaya, J. Garrier, F. Guillemin, et al. (2009). *Assessment of apoptosis by immunohistochemistry to active caspase-3, active caspase-7, or cleaved PARP in monolayer cells and spheroid and subcutaneous xenografts of human carcinoma.* J Histochem Cytochem, 57(4): 289-300.

Buchner, T., D. Drescher, H. Traub, P. Schrade, S. Bachmann, et al. (2014). *Relating surface-enhanced Raman scattering signals of cells to gold nanoparticle aggregation as determined by LA-ICP-MS micromapping.* Analytical and Bioanalytical Chemistry, 406(27): 7003-7014.

Burd, I., F. Zhang, T. Dada, M. K. Mishra, T. Borbiev, et al. (2014). *Fetal uptake of intra-amniotically delivered dendrimers in a mouse model of intrauterine inflammation and preterm birth.* Nanomedicine-Nanotechnology Biology and Medicine, 10(6): 1343-1351.

Burton, G. J. and A. L. Fowden (2015). *The placenta: a multifaceted, transient organ.* Philos Trans R Soc Lond B Biol Sci, 370(1663): 20140066.

Burton, G. J., A. L. Watson, J. Hempstock, J. N. Skepper and E. Jauniaux (2002). *Uterine glands provide histiotrophic nutrition for the human fetus during the first trimester of pregnancy.* J Clin Endocrinol Metab, 87(6): 2954-2959.

Campagnolo, L., M. Massimiani, G. Palmieri, R. Bernardini, C. Sacchetti, et al. (2013). *Biodistribution and toxicity of pegylated single wall carbon nanotubes in pregnant mice.* Part Fibre Toxicol, 10: 21.

Canton, I. and G. Battaglia (2012). *Endocytosis at the nanoscale.* Chem Soc Rev, 41(7): 2718-2739.

Carreira, S. C., L. Walker, K. Paul and M. Saunders (2015). *The toxicity, transport and uptake of nanoparticles in the in vitro BeWo b30 placental cell barrier model used within NanoTEST.* Nanotoxicology, 9: 66-78.

Carter, A. M. (2007). *Animal models of human placentation--a review.* Placenta, 28 Suppl A: S41-47.

Cartwright, L., M. S. Poulsen, H. M. Nielsen, G. Pojana, L. E. Knudsen, et al. (2012). *In vitro placental model optimization for nanoparticle transport studies.* Int J Nanomedicine, 7: 497-510.

Chen, C., M. C. Daniel, Z. T. Quinkert, M. De, B. Stein, et al. (2006). *Nanoparticle-templated assembly of viral protein cages.* Nano Lett, 6(4): 611-615.

Cho, E. C., Q. Zhang and Y. Xia (2011). *The effect of sedimentation and diffusion on cellular uptake of gold nanoparticles.* Nat Nanotechnol, 6(6): 385-391.

Chou, J. Y. (1982). *Effects of retinoic acid on differentiation of choriocarcinoma cells in vitro.* J Clin Endocrinol Metab, 54(6): 1174-1180.

Chu, M., Q. Wu, H. Yang, R. Yuan, S. Hou, et al. (2010). *Transfer of quantum dots from pregnant mice to pups across the placental barrier.* Small, 6(5): 670-678.

Cindrova-Davies, T. (2014). *The therapeutic potential of antioxidants, ER chaperones, NO and H2S donors, and statins for treatment of preeclampsia.* Front Pharmacol, 5: 119.

Clift, M. J. and B. Rothen-Rutishauser (2013). *Studying the oxidative stress paradigm in vitro: a theoretical and practical perspective.* Methods Mol Biol, 1028: 115-133.

Cole, L. A. (2010). *Biological functions of hCG and hCG-related molecules.* Reproductive Biology and Endocrinology, 8(1).

Curtis, D. J., A. Sood, T. J. Phillips, V. H. Leinster, A. Nishiguchi, et al. (2014). *Secretions from placenta, after hypoxia/reoxygenation, can damage developing neurones of brain under experimental conditions.* Exp Neurol, 261: 386-395.

Das, M., B. Xu, L. Lin, S. Chakrabarti, V. Shivaswamy, et al. (2004). *Phosphatidylserine efflux and intercellular fusion in a BeWo model of human villous cytotrophoblast.* Placenta, 25(5): 396-407.

Dausend, J., A. Musyanovych, M. Dass, P. Walther, H. Schrezenmeier, et al. (2008). *Uptake mechanism of oppositely charged fluorescent nanoparticles in HeLa cells.* Macromol Biosci, 8(12): 1135-1143.

Di Bona, K. R., Y. L. Xu, P. A. Ramirez, J. DeLaine, C. Parker, et al. (2014). *Surface charge and dosage dependent potential developmental toxicity and biodistribution of iron oxide nanoparticles in pregnant CD-1 mice.* Reproductive Toxicology, 50: 36-42.

Dobrovolskaia, M. A., P. Aggarwal, J. B. Hall and S. E. McNeil (2008). *Preclinical studies to understand nanoparticle interaction with the immune system and its potential effects on nanoparticle biodistribution.* Mol Pharm, 5(4): 487-495.

dos Santos, T., J. Varela, I. Lynch, A. Salvati and K. A. Dawson (2011). *Effects of transport inhibitors on the cellular uptake of carboxylated polystyrene nanoparticles in different cell lines.* PLoS One, 6(9): e24438.

Dreaden, E. C., A. M. Alkilany, X. Huang, C. J. Murphy and M. A. El-Sayed (2012). *The golden age: gold nanoparticles for biomedicine.* Chem Soc Rev, 41(7): 2740-2779.

Drescher, D., C. Giesen, H. Traub, U. Panne, J. Kneipp, et al. (2012). *Quantitative Imaging of Gold and Silver Nanoparticles in Single Eukaryotic Cells by Laser Ablation ICP-MS.* Analytical Chemistry, 84(22): 9684-9688.

Eddy, D. M., W. Hollingworth, J. J. Caro, J. Tsevat, K. M. McDonald, et al. (2012). *Model transparency and validation: a report of the ISPOR-SMDM Modeling Good Research Practices Task Force-7.* Med Decis Making, 32(5): 733-743.

Edmondson, R., J. J. Broglie, A. F. Adcock and L. Yang (2014). *Three-dimensional cell culture systems and their applications in drug discovery and cell-based biosensors.* Assay Drug Dev Technol, 12(4): 207-218.

Elbialy, N. S., M. M. Fathy and W. M. Khalil (2015). *Doxorubicin loaded magnetic gold nanoparticles for in vivo targeted drug delivery.* Int J Pharm, 490(1-2): 190-199.

Enders, A. C. and T. N. Blankenship (1999). *Comparative placental structure.* Adv Drug Deliv Rev, 38(1): 3-15.

Erlebacher, A., D. Vencato, K. A. Price, D. Zhang and L. H. Glimcher (2007). *Constraints in antigen presentation severely restrict T cell recognition of the allogeneic fetus.* Journal of Clinical Investigation, 117(5): 1399-1411.

Etheridge, M. L., S. A. Campbell, A. G. Erdman, C. L. Haynes, S. M. Wolf, et al. (2013). *The big picture on nanomedicine: the state of investigational and approved nanomedicine products.* Nanomedicine, 9(1): 1-14.

Evseenko, D. A., J. W. Paxton and J. A. Keelan (2006). *ABC drug transporter expression and functional activity in trophoblast-like cell lines and differentiating primary trophoblast.* American Journal of Physiology-Regulatory Integrative and Comparative Physiology, 290(5): R1357-R1365.

Falkenberg, N., I. Hofig, M. Rosemann, J. Szumielewski, S. Richter, et al. (2016). *Three-dimensional microtissues essentially contribute to preclinical validations of therapeutic targets in breast cancer.* Cancer Med, 5(4): 703-710.

Freyer, C. and M. B. Renfree (2009). *The Mammalian Yolk Sac Placenta.* Journal of Experimental Zoology Part B-Molecular and Developmental Evolution, 312b(6): 545-554.

Fujitani, T., K. Ohyama, A. Hirose, T. Nishimura, D. Nakae, et al. (2012). *Teratogenicity of multi-wall carbon nanotube (MWCNT) in ICR mice.* Journal of Toxicological Sciences, 37(1): 81-89.

Furukawa, S., S. Hayashi, K. Usuda, M. Abe, S. Hagio, et al. (2011). *Toxicological Pathology in the Rat Placenta.* Journal of Toxicologic Pathology, 24(2): 95-111.

Galan, H. L., A. M. Marconi, C. L. Paolini, A. Cheung and F. C. Battaglia (2009). *The transplacental transport of essential amino acids in uncomplicated human pregnancies.* American Journal of Obstetrics and Gynecology, 200(1).

Galletta, B. J., O. L. Mooren and J. A. Cooper (2010). *Actin dynamics and endocytosis in yeast and mammals.* Curr Opin Biotechnol, 21(5): 604-610.

Gao, H., Z. Yang, S. Zhang, S. Cao, S. Shen, et al. (2013). *Ligand modified nanoparticles increases cell uptake, alters endocytosis and elevates glioma distribution and internalization.* Sci Rep, 3: 2534.

Gauster, M. and B. Huppertz (2008). *Fusion of cytothrophoblast with syncytiotrophoblast in the human placenta: Factors involved in syncytialization.* Journal für Reproduktionsmedizin und Endokrinologie-Journal of Reproductive Medicine and Endocrinology, 5(2): 76-82.

Geiser, M., B. Rothen-Rutishauser, N. Kapp, S. Schürch, W. Kreyling, et al. (2005). *Ultrafine Particles Cross Cellular Membranes by Nonphagocytic Mechanisms in Lungs and in Cultured Cells.* Environmental Health Perspectives, 113(11): 1555-1560.

Georgiades, P., A. C. Ferguson-Smith and G. J. Burton (2002). *Comparative developmental anatomy of the murine and human definitive placentae.* Placenta, 23(1): 3-19.

Ghann, W. E., O. Aras, T. Fleiter and M.-C. Daniel (2012). *Syntheses and characterization of lisinopril-coated gold nanoparticles as highly stable targeted CT contrast agents in cardiovascular diseases.* Langmuir, 28(28): 10398-10408.

Glazier, J. D. and C. P. Sibley (2006). *In vitro methods for studying human placental amino acid transport: placental plasma membrane vesicles.* Methods Mol Med, 122: 241-252.

Goesmann, H. and C. Feldmann (2010). *Nanoparticulate functional materials.* Angew Chem Int Ed Engl, 49(8): 1362-1395.

Goodman, C. M., C. D. McCusker, T. Yilmaz and V. M. Rotello (2004). *Toxicity of gold nanoparticles functionalized with cationic and anionic side chains.* Bioconjug Chem, 15(4): 897-900.

Grafmueller, S., P. Manser, L. Diener, P. A. Diener, X. Maeder-Althaus, et al. (2015). *Bidirectional Transfer Study of Polystyrene Nanoparticles across the Placental Barrier in an ex Vivo Human Placental Perfusion Model.* Environ Health Perspect, 123(12): 1280-1286.

Grafmueller, S., P. Manser, H. F. Krug, P. Wick and U. von Mandach (2013). *Determination of the Transport Rate of Xenobiotics and Nanomaterials Across the Placenta using the ex vivo Human Placental Perfusion Model.* (76): e50401.

Graham, C. H., T. S. Hawley, R. G. Hawley, J. R. MacDougall, R. S. Kerbel, et al. (1993). *Establishment and characterization of first trimester human trophoblast cells with extended lifespan.* Exp Cell Res, 206(2): 204-211.

Gude, N. M., C. T. Roberts, B. Kalionis and R. G. King (2004). *Growth and function of the normal human placenta.* Thromb Res, 114(5-6): 397-407.

Handwerger, S. and M. Freemark (2000). *The roles of placental growth hormone and placental lactogen in the regulation of human fetal growth and development.* Journal of Pediatric Endocrinology & Metabolism, 13(4): 343-356.

Harding, C., J. Heuser and P. Stahl (1983). *Receptor-mediated endocytosis of transferrin and recycling of the transferrin receptor in rat reticulocytes.* J Cell Biol, 97(2): 329-339.

Hare, D., C. Austin and P. Doble (2012). *Quantification strategies for elemental imaging of biological samples using laser ablation-inductively coupled plasma-mass spectrometry.* Analyst, 137(7): 1527-1537.

Hemmings, D. G., B. Lowen, R. Sherburne, G. Sawicki and L. J. Guilbert (2001). *Villous trophoblasts cultured on semi-permeable membranes form an effective barrier to the passage of high and low molecular weight particles.* Placenta, 22(1): 70-79.

Hertz, R. (1959). *Choriocarcinoma of Women Maintained in Serial Passage in Hamster and Rat.* Proceedings of the Society for Experimental Biology and Medicine, 102(1): 77-81.

Hirano, T., S. Yasuda, Y. Osaka, M. Asari, M. Kobayashi, et al. (2008). *The inhibitory effects of fluoroquinolones on L-carnitine transport in placental cell line BeWo.* International Journal of Pharmaceutics, 351(1-2): 113-118.

Huang, X., M. Luthi, E. C. Ontsouka, S. Kallol, M. U. Baumann, et al. (2016). *Establishment of a confluent monolayer model with human primary trophoblast cells: novel insights into placental glucose transport.* Mol Hum Reprod, 22(6): 442-456.

Huang, X. L., F. Zhang, X. L. Sun, K. Y. Choi, G. Niu, et al. (2014). *The genotype-dependent influence of functionalized multiwalled carbon nanotubes on fetal development.* Biomaterials, 35(2): 856-865.

Hughes, C. S., L. M. Postovit and G. A. Lajoie (2010). *Matrigel: a complex protein mixture required for optimal growth of cell culture.* Proteomics, 10(9): 1886-1890.

Hutson, J. R., F. Garcia-Bournissen, A. Davis and G. Koren (2011). *The human placental perfusion model: a systematic review and development of a model to predict in vivo transfer of therapeutic drugs.* Clin Pharmacol Ther, 90(1): 67-76.

Igaz, N., D. Kovacs, Z. Razga, Z. Konya, I. M. Boros, et al. (2016). *Modulating chromatin structure and DNA accessibility by deacetylase inhibition enhances the anti-cancer activity of silver nanoparticles.* Colloids Surf B Biointerfaces, 146: 670-677.

Illsley, N. P. (2000). *Glucose transporters in the human placenta.* Placenta, 21(1): 14-22.

Jauniaux, E., B. Gulbis and G. J. Burton (2003). *IFPA award in Placentaology Lecture 2002 - The human first trimester gestational sac limits rather than facilitates oxygen transfer to the foetus - A review.* Placenta, 24: S86-S93.

Jauniaux, E., A. L. Watson, J. Hempstock, Y. P. Bao, J. N. Skepper, et al. (2000). *Onset of maternal arterial blood flow and placental oxidative stress - A possible factor in human early pregnancy failure.* American Journal of Pathology, 157(6): 2111-2122.

Jollie, W. P. (1990). *Development, Morphology, and Function of the Yolk-Sac Placenta of Laboratory Rodents.* Teratology, 41(4): 361-381.

Kaitu'u-Lino, T. J., S. Pattison, L. Ye, L. Tuohey, P. Sluka, et al. (2013). *Targeted nanoparticle delivery of doxorubicin into placental tissues to treat ectopic pregnancies.* Endocrinology, 154(2): 911-919.

Kaksonen, M., C. P. Toret and D. G. Drubin (2006). *Harnessing actin dynamics for clathrin-mediated endocytosis.* Nat Rev Mol Cell Biol, 7(6): 404-414.

Kamila, S., C. McEwan, D. Costley, J. Atchison, Y. Sheng, et al. (2016). *Diagnostic and Therapeutic Applications of Quantum Dots in Nanomedicine.* Top Curr Chem, 370: 203-224.

Kato, Y. and G. D. Braunstein (1991). *Retinoic acid stimulates placental hormone secretion by choriocarcinoma cell lines in vitro.* Endocrinology, 128(1): 401-407.

Kaufmann, P., J. Stark and H. E. Stegner (1977). *Villous Stroma of Human Placenta .1. Ultrastructure of Fixed Connective-Tissue Cells.* Cell and Tissue Research, 177(1): 105-121.

Keelan, J. A., J. W. Leong, D. Ho and K. S. Iyer (2015). *Therapeutic and safety considerations of nanoparticle-mediated drug delivery in pregnancy.* Nanomedicine (Lond), 10(14): 2229-2247.

Kelm, J. M. and M. Fussenegger (2004). *Microscale tissue engineering using gravity-enforced cell assembly.* Trends in Biotechnology, 22(4): 195-202.

Kettiger, H., A. Schipanski, P. Wick and J. Huwyler (2013). *Engineered nanomaterial uptake and tissue distribution: from cell to organism.* Int J Nanomedicine, 8: 3255-3269.

Kettler, K., K. Veltman, D. van de Meent, A. van Wezel and A. J. Hendriks (2014). *Cellular uptake of nanoparticles as determined by particle properties, experimental conditions, and cell type.* Environ Toxicol Chem, 33(3): 481-492.

Kim, J. Y., D. A. Fluri, J. M. Kelm, A. Hierlemann and O. Frey (2015). *96-well format-based microfluidic platform for parallel interconnection of multiple multicellular spheroids.* J Lab Autom, 20(3): 274-282.

King, A., C. Ndifon, S. Lui, K. Widdows, V. R. Kotamraju, et al. (2016). *Tumor-homing peptides as tools for targeted delivery of payloads to the placenta.* Sci Adv, 2(5): e1600349.

Kliman, H. J., J. E. Nestler, E. Sermasi, J. M. Sanger and J. F. Strauss, 3rd (1986). *Purification, characterization, and in vitro differentiation of cytotrophoblasts from human term placentae.* Endocrinology, 118(4): 1567-1582.

Kliment, K., V. Majkus, Z. Ott, M. Stol, V. Stoy, et al. (1970). Carriers for biologically active substances, Google Patents.

Knerr, I., S. W. Schubert, C. Wich, K. Amann, T. Aigner, et al. (2005). *Stimulation of GCMa and syncytin via cAMP mediated PKA signaling in human trophoblastic cells under normoxic and hypoxic conditions.* Febs Letters, 579(18): 3991-3998.

Knofler, M. (2010). *Critical growth factors and signalling pathways controlling human trophoblast invasion.* Int J Dev Biol, 54(2-3): 269-280.

Komin, A., L. M. Russell, K. A. Hristova and P. C. Searson (2016). *Peptide-based strategies for enhanced cell uptake, transcellular transport, and circulation: Mechanisms and challenges.* Adv Drug Deliv Rev.

Kratschmar, D. V., S. Messner, W. Moritz and A. Odermatt (2013). *Characterization of a rat multi-cell type 3D-liver microtissue system.* Journal of Tissue Science & Engineering, 2013.

Kraupp, B. G., B. Ruttkay‐Nedecky, H. Koudelka, K. Bukowska, W. Bursch, et al. (1995). *In situ detection of fragmented DNA (TUNEL assay) fails to discriminate among apoptosis, necrosis, and autolytic cell death: a cautionary note.* Hepatology, 21(5): 1465-1468.

Kueh, H. Y., G. T. Charras, T. J. Mitchison and W. M. Brieher (2008). *Actin disassembly by cofilin, coronin, and Aip1 occurs in bursts and is inhibited by barbed-end cappers.* J Cell Biol, 182(2): 341-353.

Kunzmann, A., B. Andersson, C. Vogt, N. Feliu, F. Ye, et al. (2011). *Efficient internalization of silica-coated iron oxide nanoparticles of different sizes by primary human macrophages and dendritic cells.* Toxicol Appl Pharmacol, 253(2): 81-93.

Kyrylkova, K., S. Kyryachenko, M. Leid and C. Kioussi (2012). *Detection of apoptosis by TUNEL assay.* Methods Mol Biol, 887: 41-47.

La Rocca, C., F. Carbone, S. Longobardi and G. Matarese (2014). *The immunology of pregnancy: regulatory T cells control maternal immune tolerance toward the fetus.* Immunol Lett, 162(1 Pt A): 41-48.

Larsen, L. G., H. V. Clausen and L. Jonsson (2002). *Stereologic examination of placentas from mothers who smoke during pregnancy.* Am J Obstet Gynecol, 186(3): 531-537.

Lee, J. S., R. Romero, Y. M. Han, H. C. Kim, C. J. Kim, et al. (2015). *Placenta-on-a-chip: a novel platform to study the biology of the human placenta.* J Matern Fetal Neonatal Med: 1-9.

Li, H., B. van Ravenzwaay, I. M. Rietjens and J. Louisse (2013). *Assessment of an in vitro transport model using BeWo b30 cells to predict placental transfer of compounds.* Arch Toxicol, 87(9): 1661-1669.

Lin, L., B. Xu and N. S. Rote (1999). *Expression of endogenous retrovirus ERV-3 induces differentiation in BeWo, a choriocarcinoma model of human placental trophoblast.* Placenta, 20(1): 109-118.

Lin, R. Z. and H. Y. Chang (2008). *Recent advances in three-dimensional multicellular spheroid culture for biomedical research.* Biotechnol J, 3(9-10): 1172-1184.

Liu, F., M. J. Soares and K. L. Audus (1997). *Permeability properties of monolayers of the human trophoblast cell line BeWo.* American Journal of Physiology-Cell Physiology, 273(5): C1596-C1604.

Longati, P., X. Jia, J. Eimer, A. Wagman, M. R. Witt, et al. (2013). *3D pancreatic carcinoma spheroids induce a matrix-rich, chemoresistant phenotype offering a better model for drug testing.* BMC Cancer, 13: 95.

Lopalco, A., H. Ali, N. Denora and E. Rytting (2015). *Oxcarbazepine-loaded polymeric nanoparticles: development and permeability studies across in vitro models of the blood-brain barrier and human placental trophoblast.* Int J Nanomedicine, 10: 1985-1996.

Lunov, O., T. Syrovets, C. Loos, J. Beil, M. Delecher, et al. (2011). *Differential Uptake of Functionalized Polystyrene Nanoparticles by Human Macrophages and a Monocytic Cell Line.* Acs Nano, 5(3): 1657-1669.

Macia, E., M. Ehrlich, R. Massol, E. Boucrot, C. Brunner, et al. (2006). *Dynasore, a cell-permeable inhibitor of dynamin.* Dev Cell, 10(6): 839-850.

Malassine, A., J. L. Frendo and D. Evain-Brion (2003). *A comparison of placental development and endocrine functions between the human and mouse model.* Hum Reprod Update, 9(6): 531-539.

Manke, A., L. Wang and Y. Rojanasakul (2013). *Mechanisms of nanoparticle-induced oxidative stress and toxicity.* Biomed Res Int, 2013: 942916.

Marin, J. J. G., R. I. R. Macias and M. A. Serrano (2003). *The hepatobiliary-like excretory function of the placenta. A review.* Placenta, 24(5): 431-438.

Markovitz-Bishitz, Y., Y. Tauber, E. Afrimzon, N. Zurgil, M. Sobolev, et al. (2010). *A polymer microstructure array for the formation, culturing, and high throughput drug screening of breast cancer spheroids.* Biomaterials, 31(32): 8436-8444.

Maroun, L. L., L. Mathiesen, M. Hedegaard, L. E. Knudsen and L. G. Larsen (2014). *Pathologic evaluation of normal and perfused term placental tissue.* Pediatr Dev Pathol, 17(5): 330-338.

Mathur, A., P. Loskill, K. Shao, N. Huebsch, S. Hong, et al. (2015). *Human iPSC-based cardiac microphysiological system for drug screening applications.* Sci Rep, 5: 8883.

Menjoge, A. R., A. L. Rinderknecht, R. S. Navath, M. Faridnia, C. J. Kim, et al. (2011). *Transfer of PAMAM dendrimers across human placenta: prospects of its use as drug carrier during pregnancy.* J Control Release, 150(3): 326-338.

Messner, S., I. Agarkova, W. Moritz and J. M. Kelm (2013). *Multi-cell type human liver microtissues for hepatotoxicity testing.* Arch Toxicol, 87(1): 209-213.

Mi, S., X. Lee, X. P. Li, G. M. Veldman, H. Finnerty, et al. (2000). *Syncytin is a captive retroviral envelope protein involved in human placental morphogenesis.* Nature, 403(6771): 785-789.

Miele, E., G. P. Spinelli, E. Miele, F. Tomao and S. Tomao (2009). *Albumin-bound formulation of paclitaxel (Abraxane ABI-007) in the treatment of breast cancer.* Int J Nanomedicine, 4: 99-105.

Miller, R. K., O. Genbacev, M. A. Turner, J. D. Aplin, I. Caniggia, et al. (2005). *Human placental explants in culture: Approaches and assessments.* Placenta, 26(6): 439-448.

Mooren, O. L., B. J. Galletta and J. A. Cooper (2012). *Roles for actin assembly in endocytosis.* Annu Rev Biochem, 81: 661-686.

Mueller, D., L. Kramer, E. Hoffmann, S. Klein and F. Noor (2014). *3D organotypic HepaRG cultures as in vitro model for acute and repeated dose toxicity studies.* Toxicol In Vitro, 28(1): 104-112.

Muoth, C., L. Aengenheister, M. Kucki, P. Wick and T. Buerki-Thurnherr (2016). *Nanoparticle transport across the placental barrier: pushing the field forward!* Nanomedicine (Lond), 11(8): 941-957.

Mura, S., J. Nicolas and P. Couvreur (2013). *Stimuli-responsive nanocarriers for drug delivery.* Nat Mater, 12(11): 991-1003.

Myllynen, P. K., M. J. Loughran, C. V. Howard, R. Sormunen, A. A. Walsh, et al. (2008). *Kinetics of gold nanoparticles in the human placenta.* Reprod Toxicol, 26(2): 130-137.

Nance, E., M. Porambo, F. Zhang, M. K. Mishra, M. Buelow, et al. (2015). *Systemic dendrimer-drug treatment of ischemia-induced neonatal white matter injury.* J Control Release, 214: 112-120.

Nel, A. E., L. Madler, D. Velegol, T. Xia, E. M. Hoek, et al. (2009). *Understanding biophysicochemical interactions at the nano-bio interface.* Nat Mater, 8(7): 543-557.

Niehaus, R., M. Sperling and U. Karst (2015). *Study on aerosol characteristics and fractionation effects of organic standard materials for bioimaging by means of LA-ICP-MS.* Journal of Analytical Atomic Spectrometry, 30(10): 2056-2065.

Nowak, J. S., D. Mehn, P. Nativo, C. P. Garcia, S. Gioria, et al. (2014). *Silica nanoparticle uptake induces survival mechanism in A549 cells by the activation of autophagy but not apoptosis.* Toxicol Lett, 224(1): 84-92.

Ong, S. M., Z. Zhao, T. Arooz, D. Zhao, S. Zhang, et al. (2010). *Engineering a scaffold-free 3D tumor model for in vitro drug penetration studies.* Biomaterials, 31(6): 1180-1190.

Orendi, K., M. Gauster, G. Moser, H. Meiri and B. Huppertz (2010). *The choriocarcinoma cell line BeWo: syncytial fusion and expression of syncytium-specific proteins.* Reproduction, 140(5): 759-766.

Orendi, K., V. Kivity, M. Sammar, Y. Grimpel, R. Gonen, et al. (2011). *Placental and trophoblastic in vitro models to study preventive and therapeutic agents for preeclampsia.* Placenta, 32 Suppl: S49-54.

Ornoy, A., E. A. Reece, G. Pavlinkova, C. Kappen and R. K. Miller (2015). *Effect of maternal diabetes on the embryo, fetus, and children: congenital anomalies, genetic and epigenetic changes and developmental outcomes.* Birth Defects Res C Embryo Today, 105(1): 53-72.

Page, K. (1993). *The Physiology of the Human Placenta*, CRC Press.

Pampaloni, F., E. G. Reynaud and E. H. Stelzer (2007). *The third dimension bridges the gap between cell culture and live tissue.* Nat Rev Mol Cell Biol, 8(10): 839-845.

Panigel, M., M. Pascaud and J. L. Brun (1967). *Radioangiographic study of circulation in the villi and intervillous space of isolated human placental cotyledon kept viable by perfusion.* J Physiol (Paris), 59(1 Suppl): 277.

Patra, C. R., R. Bhattacharya, E. Wang, A. Katarya, J. S. Lau, et al. (2008). *Targeted delivery of gemcitabine to pancreatic adenocarcinoma using cetuximab as a targeting agent.* Cancer Res, 68(6): 1970-1978.

Pattillo, R. A. and G. O. Gey (1968). *Establishment of a Cell Line of Human Hormone-Synthesizing Trophoblastic Cells in Vitro.* Cancer Research, 28(7): 1231-6.

Pattillo, R. A., G. O. Gey, E. Delfs, W. Y. Huang, L. Hause, et al. (1971). *Hormone-Synthesizing Trophoblastic Cell in-Vitro - Model for Cancer Research and Placental Hormone Synthesis.* Annals of the New York Academy of Sciences, 172(10): 288-98.

Pelaz, B., P. del Pino, P. Maffre, R. Hartmann, M. Gallego, et al. (2015). *Surface Functionalization of Nanoparticles with Polyethylene Glycol: Effects on Protein Adsorption and Cellular Uptake.* ACS Nano, 9(7): 6996-7008.

Pentsuk, N. and J. W. van der Laan (2009). *An Interspecies Comparison of Placental Antibody Transfer: New Insights Into Developmental Toxicity Testing of Monoclonal Antibodies.* Birth Defects Research Part B-Developmental and Reproductive Toxicology, 86(4): 328-344.

Petroff, M. G., T. A. Phillips, H. Ka, J. L. Pace and J. S. Hunt (2006). *Isolation and culture of term human trophoblast cells.* Methods Mol Med, 121: 203-217.

Petros, R. A. and J. M. DeSimone (2010). *Strategies in the design of nanoparticles for therapeutic applications.* Nat Rev Drug Discov, 9(8): 615-627.

Philbrook, N. A., V. K. Walker, A. R. M. N. Afrooz, N. B. Saleh and L. M. Winn (2011). *Investigating the effects of functionalized carbon nanotubes on reproduction and development in Drosophila melanogaster and CD-1 mice.* Reproductive Toxicology, 32(4): 442-448.

Pietroiusti, A., M. Massimiani, I. Fenoglio, M. Colonna, F. Valentini, et al. (2011). *Low doses of pristine and oxidized single-wall carbon nanotubes affect mammalian embryonic development.* ACS Nano, 5(6): 4624-4633.

Pozebon, D., G. L. Scheffler, V. L. Dressler and M. A. G. Nunes (2014). *Review of the applications of laser ablation inductively coupled plasma mass spectrometry (LA-ICP-MS) to the analysis of biological samples.* Journal of Analytical Atomic Spectrometry, 29(12): 2204-2228.

Pozzi, D., V. Colapicchioni, G. Caracciolo, S. Piovesana, A. L. Capriotti, et al. (2014). *Effect of polyethyleneglycol (PEG) chain length on the bio-nano-interactions between PEGylated lipid nanoparticles and biological fluids: from nanostructure to uptake in cancer cells.* Nanoscale, 6(5): 2782-2792.

Prouillac, C. and S. Lecoeur (2010). *The role of the placenta in fetal exposure to xenobiotics: importance of membrane transporters and human models for transfer studies.* Drug Metab Dispos, 38(10): 1623-1635.

Qi, W., J. J. Bi, X. Y. Zhang, J. Wang, J. J. Wang, et al. (2014). *Damaging Effects of Multi-walled Carbon Nanotubes on Pregnant Mice with Different Pregnancy Times.* Scientific Reports, 4.

Ramaiahgari, S. C., M. W. den Braver, B. Herpers, V. Terpstra, J. N. Commandeur, et al. (2014). *A 3D in vitro model of differentiated HepG2 cell spheroids with improved liver-like properties for repeated dose high-throughput toxicity studies.* Arch Toxicol, 88(5): 1083-1095.

Rattanapinyopituk, K., A. Shimada, T. Morita, M. Sakurai, A. Asano, et al. (2014). *Demonstration of the Clathrin- and Caveolin-Mediated Endocytosis at the Maternal-Fetal Barrier in Mouse Placenta after Intravenous Administration of Gold Nanoparticles.* Journal of Veterinary Medical Science, 76(3): 377-387.

Reifschneider, O., C. A. Wehe, K. Diebold, C. Becker, M. Sperling, et al. (2013). *Elemental bioimaging of haematoxylin and eosin-stained tissues by laser ablation ICP-MS.* Journal of Analytical Atomic Spectrometry, 28(7): 989-993.

Ren, G., D. Hu, E. W. Cheng, M. A. Vargas-Reus, P. Reip, et al. (2009). *Characterisation of copper oxide nanoparticles for antimicrobial applications.* Int J Antimicrob Agents, 33(6): 587-590.

Riddell, M. R., B. Winkler-Lowen, Y. Jiang, S. T. Davidge and L. J. Guilbert (2013). *Pleiotropic actions of forskolin result in phosphatidylserine exposure in primary trophoblasts.* PLoS One, 8(12): e81273.

Rimann, M. and U. Graf-Hausner (2012). *Synthetic 3D multicellular systems for drug development.* Curr Opin Biotechnol, 23(5): 803-809.

Rossant, J. and J. C. Cross (2001). *Placental development: Lessons from mouse mutants.* Nature Reviews Genetics, 2(7): 538-548.

Rothen-Rutishauser, B. M., S. Schurch, B. Haenni, N. Kapp and P. Gehr (2006). *Interaction of fine particles and nanoparticles with red blood cells visualized with advanced microscopic techniques.* Environ Sci Technol, 40(14): 4353-4359.

Rouas-Freiss, N., R. M. B. Goncalves, C. Menier, J. Dausset and E. D. Carosella (1997). *Direct evidence to support the role of HLA-G in protecting the fetus from maternal uterine natural killer cytolysis.* Proceedings of the National Academy of Sciences of the United States of America, 94(21): 11520-11525.

Russell, W. M. S., R. L. Burch and C. W. Hume (1959). *The principles of humane experimental technique.*

Ryan, S. M. and D. J. Brayden (2014). *Progress in the delivery of nanoparticle constructs: towards clinical translation.* Curr Opin Pharmacol, 18: 120-128.

Rytting, E., M. S. Ahmed and D. Mattison (2013). *Fetal drug therapy.* Clinical pharmacology during pregnancy: 55.

Rytting, E. and K. L. Audus (2008). *Contributions of phosphorylation to regulation of OCTN2 uptake of carnitine are minimal in BeWo cells.* Biochemical Pharmacology, 75(3): 745-751.

Saha, K., S. S. Agasti, C. Kim, X. Li and V. M. Rotello (2012). *Gold nanoparticles in chemical and biological sensing.* Chem Rev, 112(5): 2739-2779.

Saunders, M. (2009). *Transplacental transport of nanomaterials.* Wiley Interdiscip Rev Nanomed Nanobiotechnol, 1(6): 671-684.

Schneider, H., M. Panigel and J. Dancis (1972). *Transfer across the perfused human placenta of antipyrine, sodium and leucine.* Am J Obstet Gynecol, 114(6): 822-828.

Schumacher, H., D. A. Blake, J. M. Gurian and J. R. Gillette (1968). *A comparison of the teratogenic activity of thalidomide in rabbits and rats.* Journal of Pharmacology and Experimental Therapeutics, 160(1): 189-200.

Semmler-Behnke, M., J. Lipka, A. Wenk, S. Hirn, M. Schaffler, et al. (2014). *Size dependent translocation and fetal accumulation of gold nanoparticles from maternal blood in the rat.* Particle and Fibre Toxicology, 11(1).

Seval, Y., E. T. Korgun and R. Demir (2007). *Hofbauer cells in early human placenta: Possible implications in vasculogenesis and angiogenesis.* Placenta, 28(8-9): 841-845.

Shamir, E. R. and A. J. Ewald (2014). *Three-dimensional organotypic culture: experimental models of mammalian biology and disease.* Nat Rev Mol Cell Biol, 15(10): 647-664.

Shi, W., Y. Sahoo and M. T. Swihart (2004). *Gold nanoparticles surface-terminated with bifunctional ligands.* Colloids and Surfaces A: Physicochemical and Engineering Aspects, 246(1): 109-113.

Sibley, C. P. (2009). *Understanding placental nutrient transfer--why bother? New biomarkers of fetal growth.* J Physiol, 587(Pt 14): 3431-3440.

Simpson, J. K., R. F. Miller and M. F. Spittle (1993). *Liposomal doxorubicin for treatment of AIDS-related Kaposi's sarcoma.* Clin Oncol (R Coll Radiol), 5(6): 372-374.

Skardal, A., T. Shupe and A. Atala (2016). *Organoid-on-a-chip and body-on-a-chip systems for drug screening and disease modeling.* Drug Discov Today.

St-Pierre, M. V., M. A. Serrano, R. I. R. Macias, U. Dubs, M. Hoechli, et al. (2000). *Expression of members of the multidrug resistance protein family in human term placenta.* American Journal of Physiology-Regulatory Integrative and Comparative Physiology, 279(4): R1495-R1503.

Stark, W. J., P. R. Stoessel, W. Wohlleben and A. Hafner (2015). *Industrial applications of nanoparticles.* Chem Soc Rev, 44(16): 5793-5805.

Staud, F., L. Cerveny and M. Ceckova (2012). *Pharmacotherapy in pregnancy; effect of ABC and SLC transporters on drug transport across the placenta and fetal drug exposure.* J Drug Target, 20(9): 736-763.

Stern, S. T. and S. E. McNeil (2008). *Nanotechnology safety concerns revisited.* Toxicol Sci, 101(1): 4-21.

Stulc, J. (1997). *Placental transfer of inorganic ions and water.* Physiol Rev, 77(3): 805-836.

Tahara, K., T. Sakai, H. Yamamoto, H. Takeuchi, N. Hirashima, et al. (2009). *Improved cellular uptake of chitosan-modified PLGA nanospheres by A549 cells.* Int J Pharm, 382(1-2): 198-204.

Tawada, T., M. Kurabayashi, T. Okuyama and H. Furuya (1985). *Studies on the placental transport mechanism for iron.* Nihon Sanka Fujinka Gakkai Zasshi, 37(5): 735-742.

Tenenbaum-Katan, J., R. Fishler, B. Rothen-Rutishauser and J. Sznitman (2015). *Microfluidic in Vitro Platforms of Pulmonary Alveolar Physiology*. 6th European Conference of the International Federation for Medical and Biological Engineering, Springer.

Thery, M. (2010). *Micropatterning as a tool to decipher cell morphogenesis and functions.* Journal of Cell Science, 123(24): 4201-4213.

Tibbitt, M. W. and K. S. Anseth (2009). *Hydrogels as extracellular matrix mimics for 3D cell culture.* Biotechnol Bioeng, 103(4): 655-663.

Tinkle, S., S. E. McNeil, S. Muhlebach, R. Bawa, G. Borchard, et al. (2014). *Nanomedicines: addressing the scientific and regulatory gap.* Ann N Y Acad Sci, 1313: 35-56.

Tomson, T., D. Battino, E. Bonizzoni, J. Craig, D. Lindhout, et al. (2011). *Dose-dependent risk of malformations with antiepileptic drugs: an analysis of data from the EURAP epilepsy and pregnancy registry.* Lancet Neurol, 10(7): 609-617.

Tremblay, J., D. B. Hardy, L. E. Pereira and K. Yang (1999). *Retinoic acid stimulates the expression of 11beta-hydroxysteroid dehydrogenase type 2 in human choriocarcinoma JEG-3 cells.* Biol Reprod, 60(3): 541-545.

Tung, Y. C., A. Y. Hsiao, S. G. Allen, Y. S. Torisawa, M. Ho, et al. (2011). *High-throughput 3D spheroid culture and drug testing using a 384 hanging drop array.* Analyst, 136(3): 473-478.

Tzatzalos, E., O. J. Abilez, P. Shukla and J. C. Wu (2016). *Engineered heart tissues and induced pluripotent stem cells: Macro- and microstructures for disease modeling, drug screening, and translational studies.* Adv Drug Deliv Rev, 96: 234-244.

Vahakangas, K. and P. Myllynen (2009). *Drug transporters in the human blood-placental barrier.* British Journal of Pharmacology, 158(3): 665-678.

Van Calsteren, K., L. Heyns, F. De Smet, L. Van Eycken, M. M. Gziri, et al. (2010). *Cancer during pregnancy: an analysis of 215 patients emphasizing the obstetrical and the neonatal outcomes.* J Clin Oncol, 28(4): 683-689.

Vargas, A., J. Moreau, S. Landry, F. LeBellego, C. Toufaily, et al. (2009). *Syncytin-2 Plays an Important Role in the Fusion of Human Trophoblast Cells.* Journal of Molecular Biology, 392(2): 301-318.

Veiby, G., A. K. Daltveit, B. A. Engelsen and N. E. Gilhus (2014). *Fetal growth restriction and birth defects with newer and older antiepileptic drugs during pregnancy.* J Neurol, 261(3): 579-588.

Verma, U. and N. Verma (2013). An Overview of Development, Function and Diseases of the Placenta. *The Placenta: Development, Function and Diseases*. R. Nicholson. New York: Nova Science Publishers, Inc.

Volkov, Y. (2015). *Quantum dots in nanomedicine: recent trends, advances and unresolved issues.* Biochem Biophys Res Commun, 468(3): 419-427.

von Kleist, L. and V. Haucke (2012). *At the Crossroads of Chemistry and Cell Biology: Inhibiting Membrane Traffic by Small Molecules.* Traffic, 13(4): 495-504.

von Kleist, L., W. Stahlschmidt, H. Bulut, K. Gromova, D. Puchkov, et al. (2011). *Role of the clathrin terminal domain in regulating coated pit dynamics revealed by small molecule inhibition.* Cell, 146(3): 471-484.

Wang, L., G. Huang, B. Sha, S. Wang, Y. L. Han, et al. (2014). *Engineering three-dimensional cardiac microtissues for potential drug screening applications.* Curr Med Chem, 21(22): 2497-2509.

Wang, M., L. N. Zheng, B. Wang, H. Q. Chen, Y. L. Zhao, et al. (2014). *Quantitative Analysis of Gold Nanoparticles in Single Cells by Laser Ablation Inductively Coupled Plasma-Mass Spectrometry.* Analytical Chemistry, 86(20): 10252-10256.

Wang, T., J. Bai, X. Jiang and G. U. Nienhaus (2012). *Cellular uptake of nanoparticles by membrane penetration: a study combining confocal microscopy with FTIR spectroelectrochemistry.* ACS Nano, 6(2): 1251-1259.

Wanninayake, A. P., S. Gunashekar, S. Li, B. C. Church and N. Abu-Zahra (2015). *CuO Nanoparticles based bulk heterojunction solar cells: Investigations on morphology and performance.* Journal of Solar Energy Engineering, 137(3): 031016.

Weaver, V. M., S. Lelievre, J. N. Lakins, M. A. Chrenek, J. C. Jones, et al. (2002). *beta4 integrin-dependent formation of polarized three-dimensional architecture confers resistance to apoptosis in normal and malignant mammary epithelium.* Cancer Cell, 2(3): 205-216.

Wice, B., D. Menton, H. Geuze and A. L. Schwartz (1990). *Modulators of Cyclic-Amp Metabolism Induce Syncytiotrophoblast Formation Invitro.* Experimental Cell Research, 186(2): 306-316.

Wick, P., A. Malek, P. Manser, D. Meili, X. Maeder-Althaus, et al. (2010). *Barrier capacity of human placenta for nanosized materials.* Environ Health Perspect, 118(3): 432-436.

Wilson, R. (2008). *The use of gold nanoparticles in diagnostics and detection.* Chem Soc Rev, 37(9): 2028-2045.

Yamada, K. M. and E. Cukierman (2007). *Modeling tissue morphogenesis and cancer in 3D.* Cell, 130(4): 601-610.

Yamashita, K., Y. Yoshioka, K. Higashisaka, K. Mimura, Y. Morishita, et al. (2011). *Silica and titanium dioxide nanoparticles cause pregnancy complications in mice.* Nat Nanotechnol, 6(5): 321-328.

Yang, H., C. J. Sun, Z. L. Fan, X. Tian, L. Yan, et al. (2012). *Effects of gestational age and surface modification on materno-fetal transfer of nanoparticles in murine pregnancy.* Scientific Reports, 2.

Yang, M., Z. M. Lei and C. V. Rao (2003). *The central role of human chorionic gonadotropin in the formation of human placental syncytium.* Endocrinology, 144(3): 1108-1120.

Zerbo, O., Y. Qian, C. Yoshida, J. K. Grether, J. Van de Water, et al. (2015). *Maternal Infection During Pregnancy and Autism Spectrum Disorders.* J Autism Dev Disord, 45(12): 4015-4025.

Zhang, X., J. G. Teodoro and J. L. Nadeau (2015). *Intratumoral gold-doxorubicin is effective in treating melanoma in mice.* Nanomedicine, 11(6): 1365-1375.

Zhao, H. Y. and H. S. Hundal (2000). *Identification and biochemical localization of a Na-K-Cl cotransporter in the human placental cell line BeWo.* Biochemical and Biophysical Research Communications, 274(1): 43-48.

Zheng, M., Z. Li and X. Huang (2004). *Ethylene glycol monolayer protected nanoparticles: synthesis, characterization, and interactions with biological molecules.* Langmuir, 20(10): 4226-4235.

Zheng, M., S. Liu, J. Li, D. Qu, H. Zhao, et al. (2014). *Integrating oxaliplatin with highly luminescent carbon dots: an unprecedented theranostic agent for personalized medicine.* Adv Mater, 26(21): 3554-3560.

Zhou, F. F., M. Hong and G. F. You (2007). *Regulation of human organic anion transporter 4 by progesterone and protein kinase C in human placental BeWo cells.* American Journal of Physiology-Endocrinology and Metabolism, 293(1): E57-E61.

Zhu, M., G. Nie, H. Meng, T. Xia, A. Nel, et al. (2013). *Physicochemical properties determine nanomaterial cellular uptake, transport, and fate.* Acc Chem Res, 46(3): 622-631.

Zygmunt, M., F. Herr, S. Keller-Schoenwetter, K. Kunzi-Rapp, K. Munstedt, et al. (2002). *Characterization of human chorionic gonadotropin as a novel angiogenic factor.* Journal of Clinical Endocrinology & Metabolism, 87(11): 5290-5296.